

Radio synchrotron emission: electron energy spectrum, supernovae, microquasars, active nuclei, cluster relics and halos; X-ray halos

Nimisha G. Kantharia

Tata Institute of Fundamental Research
Post Bag 3, Ganeshkhind, Pune-411007, India

Email: nkprasadnetra@gmail.com

URL: <https://sites.google.com/view/ngkresearch/home>

April 2019

Abstract

In this paper, transient high energy events and their hosts are discussed with focus on signatures of radio synchrotron emission. There are numerous outstanding questions ranging from the origin of the two phases of radio emission in supernovae to the formation of conical jets launched at relativistic velocities in active nuclei to the formation of radio hotspots in FR II sources to the formation of radio relics and halos in clusters of galaxies to the origin of the relativistic electron population and its energy spectrum which is responsible for the synchrotron emission to the composition of the radio synchrotron-emitting plasma in these sources. Observations have helped build an empirical model of active nuclei but the origin of the narrow line regions, broad line regions, dust, accretion disk in active nuclei and their connection to radio jets and lobes remains largely unknown. This paper attempts to understand and resolve the above outstanding issues. The summary of a few inferences presented in the paper is:

- The matter before being ejected in a transient explosive event like a supernova has to be rapidly accelerated in situ to at least the escape velocity. The energy distribution of the ejected cosmic rays including electrons has to be a normal distribution since the energising process will be statistical in nature. The peak of the normal distribution has to be at or beyond the energy equivalent of the escape velocity for protons for a large fraction of matter to escape. This explains the ubiquitous curved+power law nature of the observed radio synchrotron spectra and the cosmic ray energy spectra which peaks near 1 GeV. The dispersion of the E/m i.e. energy/mass distribution for each species of particles will be different and will determine the range in their random velocity component so that for a constant energy imparted per particle, the light particles can acquire extremely high velocities.
- The prompt radio synchrotron emission detected soon after a supernova explosion is from light plasma composed of positrons and electrons which should escape the explosion site soon after the neutrinos and radiate in the ambient circumstellar magnetic field. The delayed radio emission from supernova remnants can be explained by synchrotron emission from the relativistic proton-electron plasma mixed with and radiating in the magnetic field frozen in the ejected thermal plasma. All matter has to be energised to escape velocities or more before expulsion. The main source of energy in both type I and II supernovae has to be a thermonuclear explosion and the ejected matter will consist of relativistic neutrinos, relativistic positron-electron plasma, non-thermal proton-electron plasma and thermal ionized plasma. Neutrinos and positrons can be generated in the thermonuclear reactions.
- The observable structure of an accreting rotating black hole has to consist of a quasi-spherical pseudosurface made of infalling matter which has been compressed to degenerate matter densities near the event horizon, a broad line region (BLR) accreted on the non-polar regions of the pseudosurface and accreted matter on the polar regions of the pseudosurface which is enriched and episodically ejected due to energy injection from a thermonuclear outburst which should occur when favourable physical conditions in the accreted matter are achieved. The ejected matter from the poles is observed as synchrotron jets and thermal narrow line region (NLR). Dust is generated in the metal-rich clumps formed in the NLR. An accretion disk is formed in the non-polar regions from the excess matter that col-

lects beyond the BLR due to latitude-dependent accretion rates on a rotating black hole which are minimum for the equatorial regions. The observed spectral lines appear at a redshift which is some combination of gravitational redshift, Doppler shift and galaxy redshift.

- The accreting black hole in all jetted sources is rotating and hosts an accretion disk in the equatorial regions.
- Observations support a positron-electron composition for the fast radio jets launched from the polar regions of microquasars and active nuclei. The light plasma will radiate in the magnetic field that is frozen in the ejected thermal gas i.e. in the narrow line region.
- The fast positron-electron jet is launched from near the event horizon of a fast spinning black hole and hence requires relativistic escape velocities. This explains the relativistic bulk expansion velocities observed for radio jets and their ballistic nature which persists upto long distances. The radial ejection of jet plasma is from the polar region of the quasi-spherical pseudosurface which is not influenced by the centrifugal potential i.e. is devoid of a broad line region and this region will be small in extent for a fast spinning black hole. This readily explains the observed range of jet opening angles, conical shapes of jets and their high collimation. The central black holes in FR II radio sources have to be the fastest spinning objects in the universe that we know.
- The positron-electron plasma has to emit annihilation line photons near 511 keV along the entire length of the jet. Compton scattering of these soft γ -ray photons to X-ray energies can explain the formation of the thick X-ray beams detected along radio jets in several radio galaxies (e.g. Cygnus A, Pictor A). The annihilation photons can also explain the formation of hotspots and backflow lobes in FR II sources due to the radiation pressure they exert back on the plasmas when the annihilation happens beyond the observable jet i.e. beyond the periphery of thermal gas. When the lobes flow back to the core in FR II sources, the large accretion disk around the black hole will deflect them by $\sim 90^\circ$ which explains the formation of winged radio structure.
- The radio plasma in cluster radio halos and relics is commensurate with the relativistic positron-electron plasma which was ejected from the su-

permissive black hole in the central galaxy during its active phase and which has since diffused over a large region. The relics can indicate the orientation of the jet axis of the black hole during its active phase indicating that a fraction of the plasma still retains its forward-directed motion. The formation of relics can be explained by radiation pressure exerted back on the plasmas by pair annihilation photons formed beyond the extent of the thermal X-ray halo.

Contents

| | | |
|----------|--|-----------|
| 1 | Introduction | 3 |
| 1.1 | Recap from Kantharia (2016a, 2017) | 3 |
| 1.1.1 | Formation of a pseudosurface | 3 |
| 1.1.2 | Origin of relativistic particles | 4 |
| 1.1.3 | Clump and dust formation | 4 |
| 1.1.4 | Formation of accretion disk and bipolar outflow | 4 |
| 1.2 | Known Emission Processes | 5 |
| 1.2.1 | Synchrotron emission | 5 |
| 1.2.2 | The Compton processes | 6 |
| 1.3 | This work | 7 |
| 2 | Cosmic rays | 7 |
| 2.1 | Background on particle acceleration | 7 |
| 2.2 | Observed cosmic ray energy spectrum | 8 |
| 2.3 | Normal distribution of cosmic ray energies or universal spectrum | 9 |
| 2.4 | Observed radio synchrotron spectrum | 11 |
| 3 | Supernovae and supernova remnants | 12 |
| 3.1 | Summary of observed features | 12 |
| 3.2 | A comprehensive explanation | 14 |
| 3.3 | Case Studies | 18 |
| 3.3.1 | Type II SNR: Cas A in Milky Way | 18 |
| 3.3.2 | Type II SN: SN1986J in NGC 891 | 21 |
| 3.3.3 | Type II SN: SN1987A in LMC | 23 |
| 3.3.4 | Type II SN: SN1993J in M 81 | 27 |
| 3.3.5 | Summary | 29 |
| 4 | Accreting rotating black holes | 29 |
| 4.1 | Microquasars | 30 |
| 4.1.1 | Summary of observed features | 31 |
| 4.1.2 | A comprehensive explanation | 33 |
| 4.1.3 | Case Studies | 35 |
| 4.1.3.1 | SS 433 in Milky Way | 35 |
| 4.1.3.2 | GRB 170817A in NGC 4993 | 38 |
| 4.2 | Active Galaxies | 40 |
| 4.2.1 | Summary of observed features | 42 |

| | | |
|---------|---|-----|
| 4.2.2 | A comprehensive explanation . | 50 |
| 4.2.2.1 | Recap: Quasar model | 51 |
| 4.2.2.2 | Model for active galaxies | 52 |
| 4.2.2.3 | Summary | 76 |
| 4.2.3 | Case Studies | 80 |
| 4.2.3.1 | FR II quasar - 3C 273 | 82 |
| 4.2.3.2 | FR II galaxy - Cygnus A | 84 |
| 4.2.3.3 | FR I galaxy - Virgo A | 89 |
| 4.2.3.4 | Seyfert 1.5 - NGC 4151 | 92 |
| 4.2.4 | A short summary | 96 |
| 4.3 | Radio relics and halos in galaxy clusters | 97 |
| 4.3.1 | Summary of observed features . | 98 |
| 4.3.2 | A comprehensive explanation . | 100 |
| 5 | Formation of soft X-ray halos | 105 |
| 6 | Resolving outstanding problems; creating new ones | 107 |
| 7 | Summary and Conclusions | 121 |

1 Introduction

Radio synchrotron emission which requires relativistic electrons and a magnetic field is detected from most high energy phenomena in the universe underlining the ubiquity of relativistic plasma and magnetic fields. Although the first extraterrestrial detection of such radiation was less than a century ago, it has since been extensively detected from a large range of astronomical objects and has become one of the important diagnostics available to us for the study of energetic phenomena. With the advent and development of multi-band telescopes, it has also become possible to study the same astrophysical object in different wavebands and hence obtain a complete observational picture which is a tremendous aid to the interpretation process. This has helped shed light on several intriguing astrophysical systems. However the large data quantities and involvement of many more scientists in research have also led to the emergence of several different interpretations of the same observational results which has caused confusion.

The paper discusses the strong radio synchrotron emitters namely supernovae, microquasars, active nuclei, cluster halos and relics. While extensive observations have led to solid observational results and have also allowed classification of these sources into different types, it has also led to multiple explanations put forward to explain parts of the object so that we still do not have a complete picture. Explanation for several key issues elude us so that we do

not know all the sources of energy in active nuclei the launch-site of jets, the origin of the relativistic plasma responsible for the radio synchrotron emission, the connection between the prompt short-lived radio emission from supernovae and long-lived radio emission from supernova remnants, the origin of radio halos and relics in clusters, the reason for spectral curvature at low radio frequencies in most radio sources and so on. Aiming to resolve these within the realm of known physics and respecting multiband observational results as inviolable boundary conditions, we research these problems in detail. The results of this effort are presented in the paper.

In the paper, black holes refer to compact objects with masses higher than neutron stars so that their densities have surpassed the values at which degeneracy pressure of neutrons can be counter gravitational collapse. Since a neutron star is surmised to be typically $3 - 4R_s$ in radius, further contraction can be surmised to lead to matter being squeezed within a sphere of radius R_s or smaller. Basically, all the mass is inside the event horizon and can be supported either by the degeneracy pressure of quarks or other particles. We have no way of knowing whether the mass is distributed in a sphere of radius R_s or $R_s/100$. To summarise, we refer to that object as a black hole wherein all the mass is compressed to within the event horizon - the mass could range from stellar mass to billions of solar masses. This is not to be confused with the mathematical black hole which is believed to be a singularity.

The rest of this section presents short summaries of a few relevant points which were made in the context of quasars and nova outbursts but are applicable to many other astrophysical energetic systems like supernovae and active nuclei and short summaries of known emission processes.

1.1 Recap from Kantharia (2016a, 2017)

Detailed physical models which could explain the ultraviolet characteristics of quasars was suggested in Kantharia (2016a) and the multiwavelength characteristics of novae in outburst and in quiescence was suggested in Kantharia (2017). Several aspects of these models are applicable to other astrophysical events like supernova explosions and other classes of active nuclei and hence a short summary of the relevant points from these papers is presented here.

1.1.1 Formation of a pseudosurface

All accreting black holes should form a layer of degenerate matter at or beyond its event horizon. As matter falls in towards the event horizon of the black

hole, its density will increase on being squeezed into an ever-decreasing volume as the radial separation from the black hole decreases. At some point outside the event horizon, the matter can exceed the densities at which normal matter can exist i.e. $> 10^5 \text{ gm cm}^{-3}$. Electrons will be stripped from the densely packed atoms and form the degenerate electron gas. At still higher densities, electrons and protons can fuse to form a neutron gas. This is suggested in analogy to the degenerate matter that has been shown to arrest further gravitational collapse in white dwarfs and neutron stars. The degenerate pressure of neutrons/electrons can then counter the gravitational pull of the black hole and a quasi-stable layer of matter of a certain thickness can deposit outside the event horizon of the black hole. This surface is referred to as the *pseudosurface* of the black hole. Further accretion will deposit matter on the pseudosurface. Since black hole physics is well understood, it might be possible to derive conditions under which such pseudosurfaces will form and their separation from the event horizon. The black body component of the observed continuum emission from quasars which peaks around blue/ultraviolet wavelengths is due to the hot pseudosurface.

1.1.2 Origin of relativistic particles

Radio synchrotron emission is detected from some novae especially recurrent novae. This means that a population of relativistic electrons can exist and whose origin is often attributed to post-ejection shock acceleration. In the shock acceleration scenario, one can then infer that the nova explosion only energises the heavy particles while the light charged particles are electrically dragged with the heavy particles and are not relativistic when they leave the parent system. In this scenario, electrons are accelerated by the forward shock set up by the explosion.

As was suggested, a plausible origin for the relativistic electrons is in the thermonuclear explosion by the same process that energises the heavy particles. Under the simple assumption that the released energy is equally divided amongst all particles (both light and heavy) in the ejecta can lead to electrons by virtue of their miniscule mass to acquire relativistic velocities in addition to an outward velocity equal to the escape velocity from the white dwarf. The efficacy of this process will depend on the available average energy per particle. This explanation does away with having to find an independent mechanism to accelerate electrons to relativistic velocities. There could exist a population of charged light particles which are bound to other light particles of opposite charge and which as a result might acquire higher

expansion velocities than the massive ejecta. This population could leave the system before the main ejecta.

1.1.3 Clump and dust formation

Novae outbursts lead to an expanding ejecta and are characterised by detection of absorption and emission lines in the optical bands with their velocity displacement and linewidths respectively, being determined by the expansion velocity of the line-forming gas. The velocity shift of the absorption lines have been observed to systematically change with the outburst phase so that at least four major spectral line systems are chronologically identifiable in a nova outburst: pre-maximum, principal, diffuse enhanced and Orion lines. The velocity displacement of the absorption lines increases from pre-maximum to Orion. Observations strongly support a single burst of explosion energy in novae and hence it has been difficult to explain the higher velocity lines by subsequent faster ejections. Dust is detected from the several nova ejecta but its origin has remained unclear.

These points were explained in Kantharia (2017). If similar energy is imparted to all particles in the ejecta, then the atoms of heavier elements would lag as compared to hydrogen and helium in the ejecta of finite thickness. The heavier atoms can then cluster due to mutual gravity and form clumps in the ejecta. These clumps, if optically thick, will be subject to the radiation pressure due to the white dwarf radiation and can hence acquire a higher velocity than the optically thin uniform density ejecta. Absorption lines forming in these clumps will, hence, show a larger velocity displacement compared to the lines forming in rest of the ejecta. This scenario explains the higher velocity displacements of the diffuse enhanced and Orion absorption lines which are often due to transitions in heavy elements.

Once clumps are formed as described above, it follows that the insides of the optically thick clumps would be ideal sites for dust formation since they consist of heavy elements and will be shielded from the harsh radiation field of the white dwarf. It was suggested that dust forms inside the clumps in the ejecta. The reasons for clump and subsequent dust formation in novae are sufficiently general to be applicable to other systems where matter is ejected.

1.1.4 Formation of accretion disk and bipolar outflow

While observations strongly support a connection between an accretion disk and bipolar outflows/jets in a system, the precise nature of the connection has re-

mained elusive. One of the theories that is commonly used to explain formation of an accretion disk is that the infalling particles carry angular momentum and hence form the disk to lose their angular momentum before accreting on the central object. One of the theories of jet launching supports its ejection from the accretion disk.

Distinct physical explanations pointed out in Kantharia (2017) are summarised here. In this explanation, the angular momentum carried by the infalling particle is considered inconsequential. Instead it is pointed out that the incoming particles should experience a latitude-dependent attractive force when falling onto a rotating spherical massive object due to the combined effect of the latitude-independent gravitational and latitude-dependent centrifugal forces. It was pointed out that a particle falling in at the poles of the rotating object will only be subject to the gravitational force whereas at the equator, it will be subject to the same gravitational force but maximum opposing centrifugal force so that the net attractive force at the equator will be lower than at the poles. The physical implication of this would be maximum accretion rates at the poles and minimum rates at the equator. In case of spherical accretion and uniform density of infalling matter, all the infalling matter would accumulate at the poles while only a fraction will accrete at the equators with the remaining matter accumulating outside and forming an accretion disk. The radial extent of the accretion disk will be largest at the equator and it will taper down towards the poles. Another outcome of the latitude-dependent accretion rates would be the formation of a prolate-shaped accreted envelope on the compact object which in the extreme case can lead to bipolar ejections i.e. outflows.

This explanation which follows from the nature of gravitational and centrifugal forces and spherical accretion of matter by a rotating compact object can account for several observations: (1) formation of an accretion disk in the equatorial plane of the accretor (2) formation of bipolar outflows/jets in several objects (3) the connection between the accretion disk and bipolar outflows/jets. The explanation also expects that (1) there should no accretion disk or bipolar outflows around a non-rotating object, (2) there should be a spherical ejection from a non-rotating object. Thus combining these with observations should help us better understand several accreting astrophysical systems.

We will use these explanations when encountering a similar situation in the systems under discussion in the paper.

1.2 Known Emission Processes

In this section, synchrotron and inverse Compton processes are briefly introduced since these frequently explain the observed radio, X-ray or γ -ray emission from many astrophysical systems.

1.2.1 Synchrotron emission

It was suggested by Alfvén & Herlofson (1950) that the main physical process responsible for the observed radio emission from active nuclei was synchrotron which has stood the test of time with observations having proved this origin beyond doubt.

Synchrotron emission refers to the radiation from relativistic electrons accelerated in a magnetic field under the influence of the Lorentz force. This is possible only when the magnetic field B and velocity v of the electron are not parallel so that Lorentz force $F = e(v \times B) \neq 0$ where e is the electronic charge. A large part of the energy spectrum of the radiating electrons is approximated by a power law with index p i.e. $N(E_e)dE_e = \kappa E_e^{-p}dE_e$ where $N(E_e)dE_e$ denotes the number of electrons per unit volume with energies between E_e to $E_e + dE_e$ and κ is an indicator of the total number of electrons. The observed synchrotron spectrum due to such an electron population will be a power law with an index $\alpha = (p-1)/2$ i.e. $S \propto \nu^{-\alpha}$.

Synchrotron emissivity at frequency ν is defined as

$$J_\nu = A \kappa B^{(p+1)/2} \nu^{-(p-1)/2} \quad (1)$$

where A is a constant. Thus, the emissivity depends on the total number of radiating electrons κ , magnetic field B and the electron energy spectrum index p . An interesting feature of synchrotron emission which is particularly useful in interpretation is that electrons of a given energy emit maximally at a particular characteristic frequency ν_c (which is related to the cyclotron frequency) in a given magnetic field. The simplified formula that quantifies this and is often used in literature is:

$$\nu_c \sim 0.016 B_\perp E_e^2 \quad (2)$$

where ν_c is in GHz, B_\perp is in μG and E_e is in GeV. This formula then allows us to calculate the energy of the electrons which principally emit at some ν_c , if the magnetic field can be estimated from polarisation studies and equipartition arguments. For example, the energy of the electrons which dominantly radiate between 0.1 to 10 GHz in a magnetic field of $10\mu\text{G}$ will be 0.8 to 8 GeV. If the magnetic field is stronger at $100\mu\text{G}$ then electrons of lower energy i.e. between 0.25 to 2.5 GeV will radiate within the

same band. Thus, Equation 2 allows us to generate the energy distribution of the parent population of electrons given a magnetic field. It also means that if the magnetic field strength is spatially varying in an object, then the synchrotron radiation at the same frequency will be from electrons of varying energies.

Similarly a simplified equation is used in literature to estimate the the synchrotron lifetime of a radiating electron:

$$t_s \sim 1.06 \times 10^9 B_{\perp}^{-3/2} \nu_c^{-1/2} \quad (3)$$

where B_{\perp} , ν_c are in μG and GHz whereas t_s is in years. The lifetime of electrons in a magnetic field of $10\mu\text{G}$ and $100\mu\text{G}$ emitting at a radio frequency of 10 GHz will be 1.06×10^7 years and $1.06 \times 10^{5.5}$ years respectively. Lifetime of electrons in the same fields emitting at a X-ray frequency of 10^8 GHz will be $1.06 \times 10^{3.5}$ years and 1.06×10^2 years respectively. This only showcases the shorter lifetimes of X-ray emitting electrons due to higher energy losses as compared to radio-emitting electrons. The estimated lifetimes of relativistic electrons then allows us to estimate the distances they can traverse before they stop radiating. Thus, for a bulk speed of $0.1c$, the X-ray emitting electron with a lifetime of 1.06×10^2 years can travel $1 \times 10^{14}\text{ km}$ i.e. 3 pc whereas the radio emitting electron with a lifetime of $1.06 \times 10^{5.5}$ years can travel 10 kpc . Obviously for larger bulk velocities the electrons will travel further from the core. Lower magnetic fields will cause lower energy losses and will also allow the electron to travel further from the core.

The bulk velocity of the emitting electron (mass m_e) is often expressed in form of the bulk Lorentz factor Γ as $E_e = (\Gamma - 1)m_e c^2$ where standard MKS units are used. If energy is specified in GeV , then $\Gamma = 1953.6E_e + 1$. The bulk velocity v_e is related to the bulk Lorentz factor Γ as $\Gamma = 1/\sqrt{1 - v_e^2/c^2}$ and is often expressed in terms of $v_e = \beta c$.

Synchrotron radiation is expected to be linearly polarised. The polarised emission can help estimate the intensity of the ordered magnetic field from equipartition arguments. While the total intensity measures the total magnetic field (random and ordered), measurement of linearly polarised emission allows the ordered component of the magnetic field to be estimated. Detailed treatment of synchrotron emission process can be obtained from textbooks.

1.2.2 The Compton processes

The mechanism wherein low energy (frequency) photons gain energy on being scattered off relativistic electrons which lose energy in the process is referred

to as the inverse Compton process. This process is inverse of the Compton process in which high energy photons lose energy on collision with electrons which in turn gain energy (Compton, 1923). Both the processes are important in astronomical systems given favourable conditions. In the Compton process, the high energy photon (generally effective with X-ray or γ -ray) loses energy to electron whereas in the inverse Compton process, the electron loses energy to a photon (any wavelength). Inverse Compton process is often found to be responsible for the formation of hard X-ray photons in active nuclei.

The change in the wavelength of the photon, Compton scattered by an electron depends mainly on the scattering angle θ . This Compton shift is estimated by the relation:

$$\lambda' - \lambda = h/(\gamma m_e c) (1 - \cos\theta) \quad (4)$$

where $h/m_e c = 2.43 \times 10^{-12}\text{ m}$ is the de Broglie wavelength of the electron. When $\theta = 90^\circ$, the shift in the wavelength of the high energy photon is equal to the de Broglie wavelength of the electron while when $\theta = 180^\circ$ the shift is twice the de Broglie wavelength which is the maximum value of the shift. This process is likely to be most effective in situations involving photons whose energy is close to the rest mass energy of electrons.

The mean frequency of the photon energies which are inverse Compton scattered by relativistic electrons can be estimated from the equation:

$$\langle \nu_{IC} \rangle = 4/3 \Gamma^2 \nu_0 \quad (5)$$

where ν_0 refers to the frequency of the low energy photon which is boosted to a higher frequency ν_{IC} due to collisions with relativistic electrons of energy Γ . For example, a photon of frequency $\nu_0 = 300\text{ GHz}$ when scattered by an electron of energy $\Gamma = 1000$ will result in a photon of frequency $\nu_{IC} = 4 \times 10^8\text{ GHz}$ which is an X-ray photon. This has been found to be an important process responsible for generation of X-ray photons in active galaxies. A special case of this process is when the radio photon generated by the synchrotron process is boosted to X-ray energies by collisions with the same synchrotron-emitting electrons. This is referred to as self synchrotron Compton (SSC) process. This process is found to be particularly active in bright synchrotron emitting regions where both radio photons and energetic electrons are available in plenty. For example, a $\nu_0 = 10\text{ GHz}$ radio photon will be radiated by an electron of energy 1.44 GeV ($\gamma = 2813$) gyrating in a magnetic field of strength $300\mu\text{G}$ through the synchrotron process. The 10 GHz photon can then collide with the electron

of $\gamma = 2813$ which can boost the radio photon to X-ray energies i.e. $\nu_{IC} = 10^8$ GHz. In SSC, the energy losses suffered by the relativistic electrons will be due to both synchrotron and inverse Compton processes which can lead to reduction in their lifetimes.

More detailed treatment of Compton processes can be obtained from textbooks.

1.3 This work

Keeping the above in mind, we study supernovae (and supernova remnants), microquasars, active nuclei and cluster relics, halos. The focus in this work is more on the synchrotron emitting sources and their properties although other wavebands are included when relevant to the discussion. Before we embark on study of these exotic objects, we discuss the origin of the observed spectrum of cosmic ray energies and connect it to the observed synchrotron radio spectra.

2 Cosmic rays

We start with a short summary of particle acceleration mechanisms from literature and then proceed to put forth a more likely scenario for particle acceleration that is supported by observations. This builds on the brief summary presented in the introduction.

2.1 Background on particle acceleration

One of the mechanisms is Fermi second order acceleration in which the proton component of cosmic rays is accelerated in the interstellar medium due to collisions with irregularities in the magnetic field (Fermi, 1949). While this mechanism results in a power law distribution for the energies of protons and has hence been widely used, it runs into difficulties in accelerating heavy nuclei and electrons and the acceleration is a rather slow process with energy increase being proportional to v^2/c^2 (Fermi, 1949). The mechanism requires a small pool of seed protons of energy ≥ 200 MeV and it was suggested that such protons could be produced in the vicinity of magnetically active stars (Fermi, 1949). It is important to keep in mind that this acceleration mechanism was suggested when the origin of nova outbursts and supernova explosions were not fully understood while active nuclei and black holes were yet to be identified and understood. Our knowledge, hence, about the immense energetics of such systems and its origin was fairly limited. In that situation, Fermi acceleration was revolutionary since it could explain the energies of the detected cosmic rays especially protons and the observed power law spectrum although the process was slow. Fermi's second order acceleration found it

difficult to explain the existence of relativistic electrons in cosmic rays because it was estimated that the losses incurred by electrons in a collision generally exceed the gain so that the electron does not gain energy (Fermi, 1949). It is interesting to note that at that time, the ubiquity of relativistic electrons in the interstellar medium was not yet known and hence this inability was not considered a drawback of the mechanism. It is to be noted that the first detection of radio synchrotron emission from outside the solar system (Jansky, 1933) had only been done in the early 1930s and systematic radio studies were only undertaken in the 1940s. The synchrotron origin for the low radio frequency emission was recognised in 1950 (Alfvén & Herlofson, 1950).

In analogy to acceleration of protons due to repeated collisions with magnetic irregularities, a mechanism which instead of magnetic irregularities uses repeated shock crossings by the particle has been found to more satisfactorily explain cosmic rays including electrons. Referred to as shock acceleration, it has been considered as a possible mechanism for accelerating cosmic rays since 1960s. Shock acceleration results in a power law distribution of energies of roughly the index observed in cosmic rays (Bell, 1978). The seed particle population was considered to be relativistic particles which were further accelerated by the shock front (Bell, 1978). In this process, acceleration is achieved by the fast particles making repeated shock crossings and the confinement of the charged particles to the shock front is achieved by scattering off Alfvén waves which are also generated by the particles (Bell, 1978). This mechanism has come to be known as first order Fermi acceleration due to the increase in energy being proportional to v/c which is faster than second order Fermi acceleration. The first order Fermi acceleration is also referred to as diffusive shock acceleration (DSA) especially when the shock is supersonic. DSA has been the favoured mechanism since strong shock waves are expected in several astrophysical systems like supernovae which are believed to be one of the major sites of particle acceleration. Supernova remnants are also believed to be an important source of cosmic rays with the energy being extracted from the expansion energy of the supernova remnant. DSA is believed to impart similar velocities to all particles so that lighter atoms/ions acquire lower energies than heavier atoms/ions. The seed particles to the DSA mechanism are considered to be the pool of thermal particles. Currently DSA is the favoured mechanism for explaining the existence of cosmic rays in the universe. Another acceleration mechanism which is often used to explain the relativistic electrons in cluster

halos is turbulence generated by a cluster merger. It appears that while shock or turbulence-driven acceleration might be able to accelerate particles over long timescales, the relativistic electrons and cosmic rays that are detected immediately after energetic outbursts like supernovae, novae etc has to be due to another, must faster physical process.

Now that we know about the huge energy output of events like supernova explosions and jet launching, it seems advisable to revisit the particle acceleration mechanism. The easiest and obvious alternative to DSA is the scenario wherein energetic events like nova outbursts and supernova explosions adiabatically impart comparable energy to all the available particles (heavy and light particles) before they are ejected from the explosion site as summarised in section 1.1.2 and Kantharia (2017). Since we already accept that heavy matter is energised by the explosion energy, it appears contrived to assume that light particles are left out. Although this explanation removes the need to require shocks for particle acceleration, the role of the blast wave and shocks set up by the explosion and fast ejecta remains important in compressing matter and hence enhancing matter densities and magnetic fields. This, then, leads to simplifying the discussion since there remains no need to invoke any extra physical process to accelerate electrons to relativistic energies or search for a seed population of particles. Observations support all particles leaving an explosion site with tremendous energy and expending it in radiation, kinetic motion etc over a long timescale. In fact, if we believe the energetic event is unable to accelerate electrons to relativistic energies then we have to explain why electrons are selectively excluded from being energised whereas heavier particles are energised.

In the following sections we discuss the observed cosmic ray spectrum.

2.2 Observed cosmic ray energy spectrum

The observed cosmic ray energy distribution is shown in Figure 1. Figure 1a shows the combined spectrum of all cosmic ray particles (also separately for electrons, protons, positrons) between energies of 1 GeV to a few times 10^{11} GeV. A few gross features are recognisable from the spectrum: a turnover at low energies, a power law-like behaviour at higher energies and a spectral break inbetween often referred in literature as the ‘knee’. The energy spectrum of most cosmic rays shows a turnover at energies ~ 1 GeV. Although the intensity of all species of cosmic rays is found to turnover at low energies, the origin of this turnover is not well understood. Some of it is at-

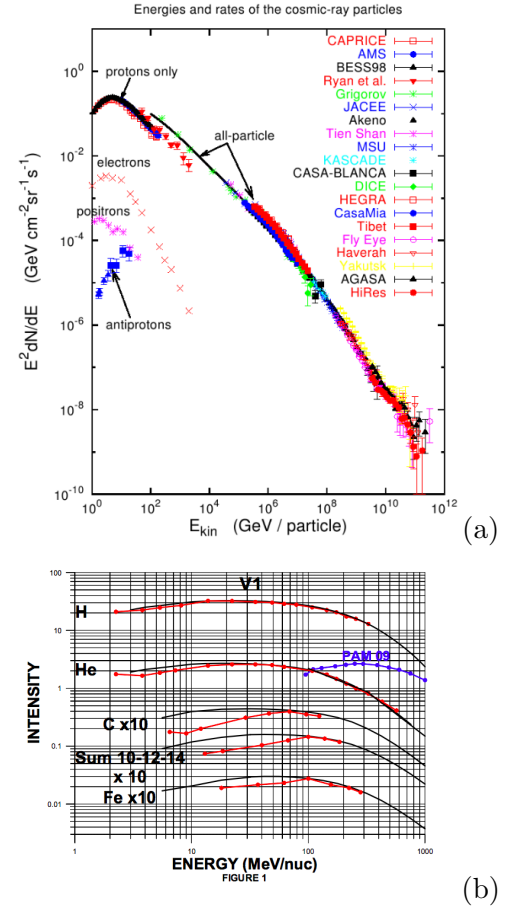


Figure 1: (a) Figure shows the distribution of cosmic ray intensity with energy. Figure downloaded from the internet. (b) Figure reproduced from Webber (2015). Figure shows the distribution of intensity of low energy cosmic rays of H, He, C, (Ne+Mg+Si), Fe measured by Voyager 1 beyond the heliopause. Notice the turnover observed in the energy spectra of cosmic rays.

tributed to solar influence but considering that the turnover was even noted by the Voyager spacecraft beyond the heliopause (Webber, 2015) as shown in Figure 1b indicates that the turnover has to be intrinsic to the distribution. It should be kept in mind that the global cosmic ray spectrum in Figure 1a contains contribution from several independent cosmic ray sources - different types of sources (e.g. supernovae and active nuclei) and several same type of sources (e.g. contribution from several supernovae and several active nuclei). The most intense sources will dominate the cosmic ray spectrum and depending on the energies of the cosmic rays generated by the different sources, they can dominate different energy ranges. The global integrated cosmic ray spectrum shown in Figure 1a is observed to show two breaks at high energies, which is interpreted in literature, to indicate two distinct dominant sources of contribution to the spectrum. The break referred to as the ‘knee’ occurs around few times 10^{15} eV and

it is believed that the cosmic rays below this energy are accelerated in supernova explosions. The cosmic rays of energies greater than the knee are believed to be accelerated by active nuclei. The second break referred to as the ‘ankle’ occurs between 10^{18} and 10^{19} eV. Overall, the higher energy cosmic ray spectrum can be approximated by a power law of index p between 2 and 3.

Figure 1b shows the energy spectrum for a few atomic species with particle energies ranging from 0.001 GeV to about a GeV that was recorded by the Voyager spacecraft beyond the heliopause (Webber, 2015). The figure is a blow-up of the part of the spectrum where the intensity of lower energy cosmic rays shows a turnover and it appears to be around 0.1 GeV which is comparable for primary cosmic rays of hydrogen and iron although the lighter atoms seem to show a flatter turnover than the heavier atoms (Webber, 2015). The peaks in Figures 1a and b differ and these could be attributed to solar effects.

A typical nova outburst ejects about $10^{-5}M_{\odot} \sim 2 \times 10^{25}$ kg of matter. If this entire mass was composed of hydrogen then it would mean about 1.25×10^{52} protons and at least that many electrons are ejected in the process. A typical nova outburst can release $\sim 10^{38}$ Joule of energy and if we assume that all of it is equally distributed amongst the particles, then it would impart an average energy of $\sim 0.25 \times 10^5$ eV to each particle. Similarly, we can make order of magnitude estimates for a supernova explosion of energy 10^{45} Joule which ejects half a solar mass of matter. If the ejected mass consists of protons then it would eject 0.6×10^{57} protons and an equal number of electrons. The energy acquired by each particle then would be 0.5×10^7 eV. This simple argument is included to show the lower limit for the energy imparted to particles in nova or supernova explosions. In practise the ejecta will contain heavier atoms also and hence the energy imparted to each particle will be higher. In the next section we discuss the origin of the observed energy distribution of cosmic rays.

2.3 Normal distribution of cosmic ray energies or universal spectrum

We keep in mind that the observed cosmic ray distribution shown in Figure 1(a) has a shape that can be approximated by a power law at high energies which peaks at low energies (0.1 to 1 GeV) and the spectrum turns over at still lower energies. In literature, two explanations exist for the origin of the observed nature of the cosmic ray/electron energy distribution: (1) the power law energy spectrum is due to the injection spectrum of electron energies expected from

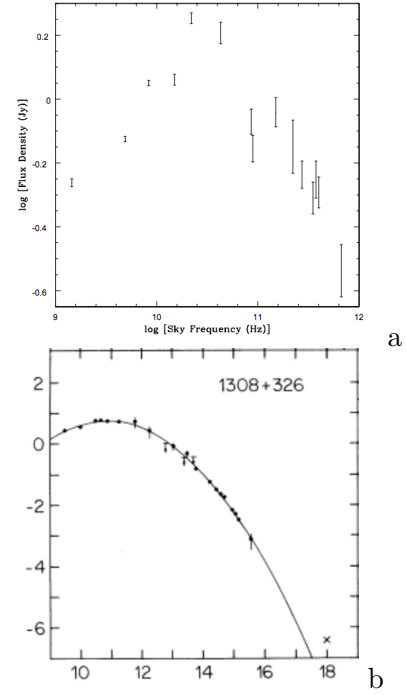


Figure 2: (a) The spectrum of the core of the radio galaxy Cygnus A. Figure copied from Carilli et al. (1999). Notice that the peak occurs near 30 GHz. (b) Wide-band spectrum of the active nucleus 1308+326 copied from Landau et al. (1986). X-axis is in units of log(frequency). Notice the log parabolic nature of the spectrum.

DSA and the low frequency turnover is due to solar modulation or a cutoff due to some appropriate process (2) the observed energy spectrum is intrinsic which is often referred to as the universal spectrum. Since no satisfactory theory to explain the origin of a universal spectrum has emerged, the first alternative has been favoured in literature. Here we explore the existence of processes that would support a universal spectrum. Motivation for this arises from strong observational evidence for energising of all particles before they are ejected. Fast neutrinos, which are amongst the first signatures of the explosion, are detected from supernovae and hence require the neutrinos to be energised at the site of the explosion before being expelled at relativistic velocities. It follows that the same should be true for all other particles which are ejected following the explosive event. It appears that this argument convincingly rules out shock acceleration of electrons beyond the explosion site and strongly supports the same physical mechanism being responsible for the acceleration of neutrinos, electrons and heavy particles.

The observed spectral energy distribution (SED) of blazars and the compact cores of radio galaxies, especially in the radio band, is generally peaked and curved (see Figure 2) so that the power law behaviour is found to be valid in a narrow radio frequency range.

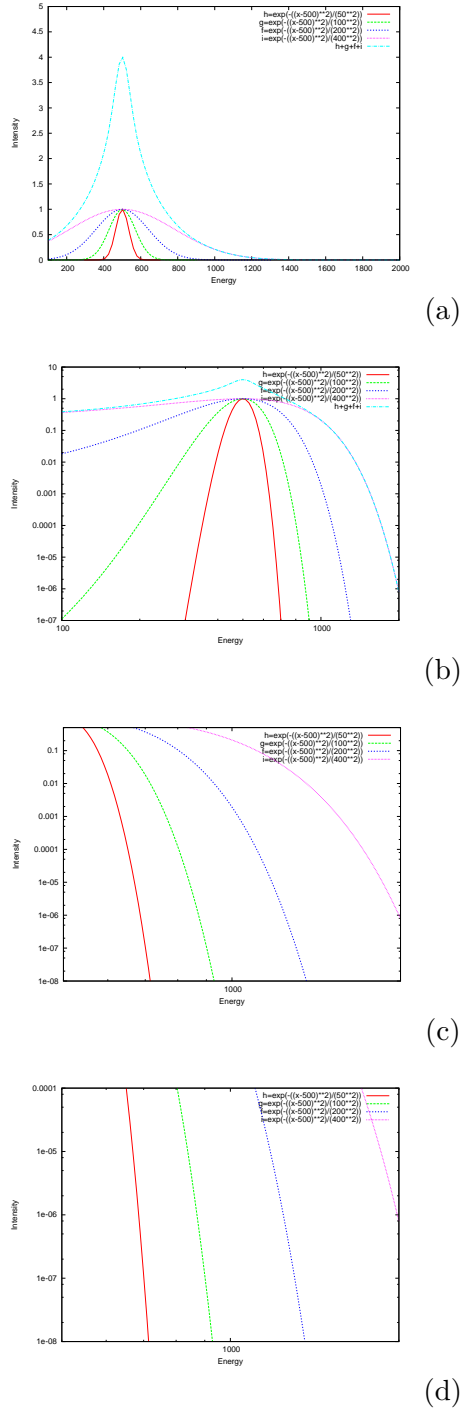


Figure 3: Indicative plots for the intensity of cosmic rays with their energy in arbitrary units assuming that the injected distribution of energies is normal/Gaussian. (a) Linear scale. (b) Logarithmic scale. (c) Logarithmic scale, the peak is omitted. The curves are power law for high energies and show a flattening at lower energies. These reproduce the observed curves fairly well. (d) Logarithmic scale, the peak is omitted and the range of on the y-axis is limited to four orders of magnitude. Notice how the curves are better approximated with a power law for the narrower energy range.

BL Lacs are classified as HBL (high frequency BL Lac) if the spectrum peaks in X-rays and as LBL (low frequency BL Lac) if the spectrum peaks at radio frequencies. The reasons used to explain the curved SED of blazars and compact radio cores range from an intrinsic curved injection spectrum of relativistic electrons (e.g. Massaro et al., 2004) to the effect of radiative losses and escape of high energy electrons (e.g. Krawczynski et al., 2002). The curved smooth nature of the observed spectrum from radio to ultra-violet bands of active nuclei especially blazars is well-approximated by a log-parabolic function (Howard et al., 1965; Landau et al., 1986). The spectra of BL Lac objects show a log-parabolic shape with a narrow range of curvature parameters (Giommi et al., 2002) which could indicate that this shape is a general characteristic of blazars (e.g. Massaro et al., 2004). Comparing Figures 1 and 2 reveals that the shapes of both the energy distribution of cosmic rays and radio spectra of radio cores/blazars can be approximated by a power law component and a curved component. In other words, since the parent electron energy spectrum is curved, the observed radio synchrotron spectrum will also be curved when radiating in an appropriate magnetic field.

Being convinced that electrons and other primary cosmic rays are instantaneously energised in explosive events before being ejected from the system, we think of the energy distribution that these particles would acquire in such an event. Since the number of particles that is being energised is very large, it is a statistical system for which the favoured distribution should be a normal (or log-normal) distribution which are maximum entropy distributions for a given mean and variance. Since the second law of thermodynamics tells us that all processes lead to an increase in entropy of the system, the process of instantaneous energising of the cosmic rays has to result in a normal (or log-normal) distribution of particle energies. Another way of looking at it is from Gibbs entropy formula, $S = -k \sum p_i \ln(p_i)$ where k is the Boltzmann constant and p_i is the probability that some microstate i takes up an energy E_i . Gibbs formula applies to both equilibrium and non-equilibrium systems. The most likely microstates (i.e. particle energies) are those which maximise S and hence the distribution, typically displayed by large statistical systems, is normal (or log-normal).

The particulate matter that acquires an outward component of velocity which exceeds the escape velocity from the object will be lost from the system. One can think about the centroid of the normal distribution to signify the escape velocity from the object and the dispersion to signify the magnitude of the

random velocity component i.e. the difference in energy between the total imparted energy per particle and the required escape energy. One can think about the escape velocity as the radially outward directed component which can range from sub-relativistic to relativistic whereas the random velocity component has to be relativistic if the plasma is to be capable of emitting synchrotron radiation else no synchrotron radiation will be emitted.

In Figure 3, four normal distributions having the same mean but different variance are shown along with the result of adding the four distributions. These can be taken to be indicative of the cosmic ray spectrum so that the x-axis is an indicator of the cosmic ray energy and the y-axis is an indicator of the intensity of the cosmic rays in arbitrary units. Figure 3a is in linear scale while rest of the panels are on the logarithmic scale. Figure 3b can be compared to the spectrum of the radio core of Cygnus A (Figure 2). The two lowermost panels are zoom-ins to demonstrate the peak and power-law parts of the gaussians. The observed radio spectra of synchrotron sources also show such shapes. Only the particles whose energy exceed the escape velocity from the object will be able to leave which means if the centroid is at the escape velocity then only the distribution at higher energies will be observable. The rest of the particulate matter will remain on the system. Interestingly, the slope of the curves, which can be approximated by power laws, for the four distributions within the narrow range which highlights their linear nature plotted in the lowermost panel of Figure 3b appear to be comparable. The distributions with the same centroid but varying variance, plotted in Figure 3 schematically depict the energy distributions which would be expected for different species of particles. The narrowest distribution should correspond to the heaviest element and the broadest distribution correspond to the lightest particle. This can be understood as follows: for comparable energy imparted to all particles, the heavier particle will use up a larger fraction of its energy in escaping from the system i.e. $mv_{esc}^2/2$ due to its large mass m while lighter particles like electrons will need to use only a small fraction of its energy $m_e v_{esc}^2/2$ to escape from the system and the remaining energy will be in the random component which can be relativistic, making them efficient synchrotron emitters.

As mentioned earlier, the global cosmic ray spectrum that we observe has to be a combination of multiple spectra from several different sources. In Figure 3a,b, the spectrum obtained by adding four distinct distributions with the same mean has also been shown. This spectrum closely follows the dis-

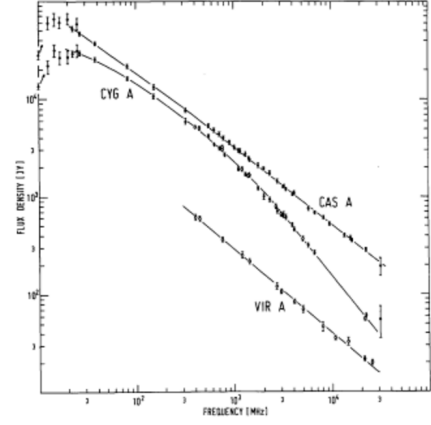


Figure 4: Figure shows the observed radio spectrum of Cas A and Cygnus A copied from Baars et al. (1977). Note the turnover at low radio frequencies and the convex-shaped spectrum of Cygnus A.

tribution with the largest dispersion except near the peak which is more pronounced compared to the individual distributions. The nature of the integrated spectrum can also account for ‘knee’-like features. This allows the inference that combination of multiple normal distributions can explain the nature of the low energy turnover, ‘knee’ and ‘ankle’ features of the global cosmic ray spectra and supports the existing hypothesis wherein the features delineate the distinct source of cosmic rays.

To summarize, it is suggested that the energy spectrum of relativistic electrons (and cosmic rays) that are energised in an explosive event like nova, supernova and other transient events will follow a normal (or log-normal) distribution of energy with a mean and variance determined by the energetics of the event. The distribution can be approximated by a power law at high energies and shows a smooth convex-shaped turnover at low energies. In the next section we discuss if the typical observed radio synchrotron spectrum of radio sources is consistent with the explanation given here.

2.4 Observed radio synchrotron spectrum

In Figure 4, the observed integrated radio spectra of three strong radio sources: the Galactic supernova remnant Cas A and the radio galaxies Cygnus A and Virgo A are shown. The spectra of Cas A and Cygnus A show a turnover at frequencies lower than about 30 MHz. The spectrum of Cas A at frequencies above 30 MHz and Virgo A are well-approximated by a power law whereas the spectrum of Cygnus A shows a convex shape beyond 30 MHz. The behaviour of the spectrum of Cygnus A is generally attributed to the effect of different components of the radio galaxy. It is interesting to note that the shape of the radio

spectrum of Cygnus A compares well with the global cosmic ray spectrum shown in Figure 1a. The low frequency turnover in Cas A is explained by free-free foreground absorption whereas it remains to be understood in the case of Cygnus A. In fact, the radio spectra of several (all?) radio sources show a turnover at low frequencies and these are generally attributed to free-free absorption, synchrotron self-absorption or a low energy cutoff. Moreover the different components of the radio source also show such turnover (see Figure 2).

From the discussion in the previous section, turnovers in the observed spectral energy distribution are expected due to the very nature of the injection spectrum of the electron energies i.e a normal distribution. The observed differences in the peak frequencies will depend on the details of the energy injection and ageing. Thus, the core spectrum of Cygnus A (Figure 2a) shows a peak around 30 GHz, whereas the integrated spectrum of Cygnus A which includes other radio components shows a peak around 30 MHz. If we assume that the turnover in the spectra of Cas A and Cygnus A are due to the underlying electron energy spectrum then we can estimate the energy of electrons that emit near 30 MHz given a magnetic field. For a magnetic field of $100\mu\text{G}$ which is typical in supernova remnants and radio galaxies, the electrons emitting at 30 MHz would have energies of ~ 140 MeV. Interestingly, from Figure 1b, it is seen that several cosmic ray species are detected with a flat energy spectrum near 100 MeV.

Since the effect of thermal free-free absorption, synchrotron self absorption and the turnover due to the energy spectrum are similarly manifested in the radio spectrum, it is difficult to disentangle the different contributions and verify the effect of the curved injection spectrum. Cases where the effect of free-free absorption and synchrotron self-absorption is expected to be minimal need to be studied.

3 Supernovae and supernova remnants

Supernova explosions are divided into two main types (type I and type II) based on the spectral lines that are detected during the phase of peak optical emission with type I lacking hydrogen lines and type II showing the presence of hydrogen lines (Minkowski, 1941). Type Ia explosions are associated with a white dwarf mass crossing the Chandrasekhar limit while type II explosion is associated with core-collapse in massive stars. The origin of the energy release in Type II supernova explosion is believed to be the

sudden gravitational contraction of the stellar core (implosion) when it runs out of fuel and ignition of matter outside the core which blows away the outer parts of the star i.e. explosion (Hoyle & Fowler, 1960). The energy released when light elements other than hydrogen ignite at a billion degrees K is about 5×10^{17} ergs gm^{-1} (Hoyle & Fowler, 1960). If $0.5 M_{\odot}$ of matter were ignited in a supernova explosion then it could lead to an instantaneous release of energy $\sim 10^{51}$ ergs which can be catastrophic for the star. This energy is released within 1-100 seconds (Hoyle & Fowler, 1960). In case of hydrogen fusion, the energy release can also be large but is much slower (Hoyle & Fowler, 1960). Long-lived supernova remnants are left behind by supernova explosions of both types. It has also been possible to identify the explosion type from the spectral composition of the supernova remnants.

In the next few sections, we summarise the observed properties of these objects, describe the model which emerges and present a few case studies to demonstrate the validity of the model.

3.1 Summary of observed features

Some of the observed properties of supernovae and supernova remnants are:

- The mean observed value of the peak B band absolute magnitude of supernovae of type Ia is -19.46 magnitudes while it ranges from -17 to -19.27 magnitudes for supernovae of type II (e.g. Richardson et al., 2002).
- Progenitors of type II supernovae suffer extensive mass loss before the explosion. The mass loss could be continuous at typical rates estimated to be 10^{-8} to $10^{-4} M_{\odot}\text{yr}^{-1}$ and typical outflow velocities of 10 to 40 km s^{-1} or the mass loss could be episodic. This matter forms the circumstellar medium around the star/supernova. Since there is no comparable mass loss prior to a type I supernova explosion, no circumstellar medium is expected.
- Typical energy of $\sim 10^{51}$ ergs is released in a supernova explosion.
- Type I supernovae are observed to occur in all types of galaxies whereas type II explosions are generally recorded in star forming galaxies.
- The peak luminosity of supernovae follows a direct relationship with t_2 which is the time taken by the peak luminosity to decline by 2 magnitudes. Longer t_2 is recorded for a higher peak

luminosity of the supernova. This behaviour is opposite to that seen in classical nova outbursts. Since the peak luminosity recorded for type Ia supernovae is confined to a small range, the t_2 is also recorded within the narrow range of 30 to 40 days.

- Absorption lines and emission bands are detected in the supernova spectrum. The spectrum eventually evolves to be pure nebular containing only emission lines. These lines are used to estimate the expansion velocities.
- Initial expansion velocities in supernovae are generally measured to be upwards of 20000 km s^{-1} which are observed to decline to a few thousand km s^{-1} (see Figure 5). The expansion velocities measured from Fe II lines are lower than those measured from hydrogen lines (see Figure 5 for SN 1987A). Expansion velocities ranging from a couple to a few thousand km s^{-1} are commonly recorded in supernova remnants.
- The prompt radio emission, detected soon after the supernova explosion, is due to the synchrotron process. Prompt radio emission is commonly detected from type II supernovae while it has never been detected from type Ia supernovae.
- Prompt X-ray emission is detected from type II supernovae but has never been detected from a type Ia supernovae.
- The radio emission from supernova remnants is mainly due to the synchrotron process.
- The radio light curves of the prompt emission show a frequency-dependent detection epoch such that emission at the higher frequencies is detected before the emission at the lower frequencies. The frequency-dependence is well-understood as being due to thermal free-free absorption by foreground or mixed thermal gas, since the free-free optical depth has a frequency dependence $\tau_\nu \propto \nu^{-2}$.
- The prompt radio emission from supernovae is, at best, weakly polarised. Strong linearly polarised radio emission is detected from supernova remnants.
- Polarisation studies detect radially aligned magnetic fields in young supernova remnants whereas older remnants tend to show a tangential magnetic field (e.g. Dickel & Milne, 1976).

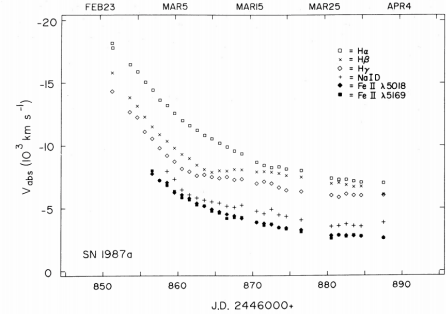


Figure 5: Figure showing the evolution of the spectral line velocity for SN 1987A copied from Blanco et al. (1987). Notice the rapid decline in the expansion velocity of the ejecta which is typical of several supernovae and the lower expansion velocities recorded at a given epoch for the heavier elements like Fe II. Even the higher level transitions in hydrogen ($H\beta$, $H\gamma$), show lower velocity shifts than $H\alpha$ especially at early times and then tend towards similar values at later epochs. A velocity of -18000 km s^{-1} was recorded for $H\alpha$ in the first observation conducted a day or so after discovery with the wings of the P Cygni profile extending upto $\pm 30000 \text{ km s}^{-1}$ (Blanco et al., 1987).

- The magnetic fields in supernova remnants are estimated to be between 0.1 mG to 1 mG.
- Many relatively young supernova remnant shells appear spherical supporting a predominantly spherically symmetric explosion in massive stars.
- Optical line emission is often confined to the filamentary structure distributed across the supernova remnant whereas the continuous emission is observed to arise from a smoothly distributed emitting component.
- Forbidden line emission is detected from fast moving knots in supernova remnants which are often devoid of hydrogen and helium lines. H, He lines are observed from streaks and wisps of lower expansion velocities, which are distributed in the remnant along with the knots (Osterbrock, 1989). *The spectral nature of knots and streaks is reminiscent of the behaviour of the Orion and principal spectral lines observed from the nova ejecta.*
- Asymmetric line profiles, such that the blue sides are stronger than the red parts, are commonly detected from supernova remnants. It is inferred that the red part of the line, which arises in the distant part of the object, is fainter due to obscuration by dust in the remnant (e.g. Milisavljevic & Fesen, 2017).
- In several supernova remnants, a thin hard X-ray (or optical) rim of synchrotron emission has been

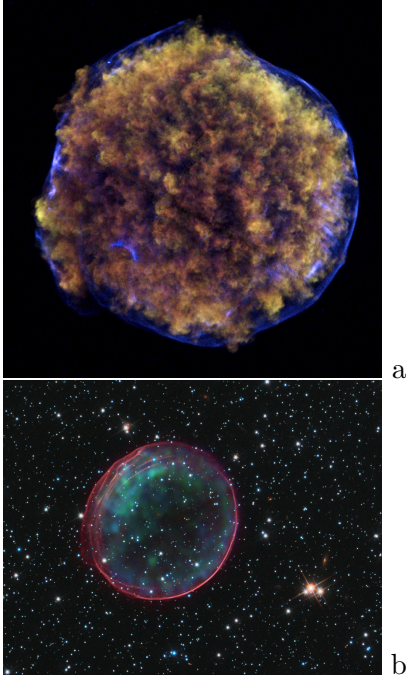


Figure 6: Images downloaded from <http://chandra.harvard.edu/photo/>. (a) The X-ray image of the type 1a Galactic supernova remnant Tycho. The outer thin ring in blue is hard X-ray emission whereas the cloudy emission in yellow is low energy X-rays. (b) Composite X-ray and optical image of the supernova remnant SNR 0509-67.5 in the Large Magellanic Cloud (LMC). The thin outer ring in red is optical emission while the X-ray emission is the diffuse emission within the ring. In most supernova remnants, the outer ring is observed in hard X-rays as shown for Tycho whereas in SNR 0509-67.5 the outer ring is detected in optical bands. The formation process is likely to be the same for both though.

observed encircling the main body of the remnant from which thermal X-ray and multiband emission are detected (e.g. see Figure 6 where the type 1a supernova remnants SNR 0509-67.5 in the Large Magellanic Cloud (LMC) and the Tycho remnant are shown). Such rims are predominantly detected around remnants of type 1a supernova explosions e.g. Kepler, Tycho, SN 1006, G1.9+0.3. One of the rare type II supernova remnant which shows such a rim is Cas A.

- The observed radio spectra of a large fraction of Galactic supernova remnants show a low frequency turnover (e.g. Kassim, 1989). The turnover is generally attributed to thermal free-free absorption in the foreground ionized gas.
- The 20cm flux density of a few Galactic supernova remnants are listed here. The flux density of Tycho (1572 AD) was ~ 40 Jy in 1997, Kepler (1604 AD) was ~ 17 Jy in 1988, Cas A (~ 1670 AD) was around 2700 Jy in 1980 and SN 1006

(1006 AD) was around 25 mJy in 2003.

- There exist supernova remnants from which the detected multiband emission especially X-rays is dominated by synchrotron emission. Faint thermal X-ray lines from small regions within the remnant are sometimes detected. Occasionally emission is detected at TeV energies which is believed to be due to the inverse Compton process. A few examples of such remnants are G347.3-0.5 (Slane et al., 1999), G266.2-1.2 (Slane et al., 2001), G1.9+0.3 (Reynolds et al., 2008; Borkowski et al., 2013).
- G1.9+0.3 is the remnant of the youngest Galactic type 1a supernova with an age less than 150 years and synchrotron radio and X-ray shells are detected (Green et al., 2008). This shell remnant is estimated to lie at a distance of about 8.5 kpc and the 100' diameter X-ray shell would correspond to about 2.2 pc in size (Reynolds et al., 2008).

3.2 A comprehensive explanation

We search for a comprehensive model which can coherently explain the observational results on supernovae and supernova remnants. The model includes already known aspects of these objects from literature. Since nova and supernova explosions share several similar features e.g. sudden optical brightening, expulsion and fast expansion of matter, dust formation, shell-like remnant, emission bands, the explanation also includes features of the nova model presented in Kantharia (2017). Since the behaviour of a range of multi-band features have already been explained for novae in the above paper, we focus on mainly understanding the behaviour of the detected synchrotron emission from supernovae and supernova remnants and use this with multiband explanations to derive a detailed explanation for the phenomena.

We start with the known aspects of a supernova explosion which have been consistently supported by observations. In a type II explosion, the core starts contracting to neutron star densities after running out of fuel and triggers a thermonuclear explosion in the surrounding gas which ignites and blows out matter. Typical energies of about 10^{51} ergs are inferred to have been released in the supernova explosion which can be explained by simultaneous ignition of about $0.5 M_{\odot}$ of fuel with the energy being released within 10-100 seconds (Hoyle & Fowler, 1960). The circumstellar medium around type II supernovae is dense due to extensive mass loss suffered by the massive progenitor star whereas it is tenuous or absent

around type 1a supernovae which is an explosion in a low mass star. The type 1a explosion occurs when a white dwarf crosses the Chandrasekhar mass limit which triggers a thermonuclear eruption which blows the star apart. The progenitor system for a type 1a explosion is always a binary. Following a supernova explosion, the exploded star rapidly brightens by 15 magnitudes or more in the optical bands and after reaching a maximum luminosity starts declining in brightness. Similar optical light curves are recorded for most type II supernovae which are generally double-humped and for type I supernovae which are generally single-peaked. There remain various unknowns such as the reason for this optical light curve behaviour, origin of dust, origin and composition of the relativistic plasma, the difference between prompt radio emission and remnant radio emission etc which we now discuss.

The explosion releases copious amount of energy which is imparted to the overlying matter - neutrinos, electrons, protons, ions, etc. The thermonuclear explosion and formation of neutron star releases neutrinos. Neutrinos constituted the first signal that reached us after the explosion in SN 1987A in the LMC, indicating their high velocities. The neutrinos had to be energised at the explosion site before being expelled with relativistic velocities which far exceeded the escape velocity to explain the immediacy with which neutrinos were detected. It has been implicitly accepted that the stellar matter (protons+ions) that is ejected at very high velocities is energised in the explosion which enables it to escape. However a distinct explanation for the acquisition of relativistic velocities by electrons such as DSA are invoked in literature without detailing why such a distinct treatment is required by electrons. Since there does not appear any reason for the special treatment of electrons, we accept that electrons acquire energy in the same process that imparts energy to protons and ions accelerating them beyond the escape velocity. Since large energy is pumped into matter made up of an extremely large number of particles, the aggregate energy distribution of all particles and separately for each particle species has to be gaussian-shaped with a mean and a dispersion as described earlier. Thus, in the most simple scenario, it can be assumed that the distribution for all particles is a gaussian centred on the escape velocity from the star with a dispersion determined by mass of the particles. In other words, the dispersion will quantify the random velocity component of the particles of a given species. Thus electrons by virtue of their smaller mass will have a larger random velocity component and hence can have a much wider gaussian

distribution as compared to protons. This holds for comparable energy allocation to all particles which are expelled. This explanation, as discussed earlier, is supported by the roughly similar energy spectra observed for all particles which turns over around 1 GeV. The gaussian-shape of the injected energy spectrum of electrons explains the observed curved radio spectra of many supernova remnants.

The supernova ejecta should also contain positrons generated by the thermonuclear explosion. It is possible that while a fraction might be annihilated close to the generation site, there could be a large number which are energised to relativistic velocities and escape alongwith an equal number of relativistic electrons, thus forming a light positron-electron plasma. There will also be a large number of electrons which will be tied to protons/ions in the ejecta and these will form the heavier proton(ion)-electron plasma. Thus a supernova explosion, can in principle energise and eject neutrinos, a positron-electron plasma and a proton(ion)-electron plasma with decreasing expansion velocities assuming comparable energy allocation to all particles. In all these cases, the energising of particles is completed before they are expelled from the star at velocities in excess of the escape velocity from the star. No significant acceleration occurs after the ejection. Since all this is expected from simple physical arguments, we assume that all explosions result in three energetic component ejecta. In reality, it is possible that the details of the explosion and type of progenitor will decide the ejected components. This means that observational signatures of all three components or any subset should be detectable from a supernova and which should be determinable from interpreting observational results on case-to-case basis.

The observational signature of the neutrino component are neutrinos as was detected in the case of SN 1987A in the LMC. Neutrinos are ultra-light, travel at ultra-relativistic velocities, are all ejected within seconds of the explosion and hence their detection depends heavily on having collected data at a critical juncture. Hence although neutrinos have long been expected from supernova explosions, till date they have only been detected from SN 1987A.

Both the positron-electron and proton(ion)-electron plasma are relativistic and hence can be a source of synchrotron radiation. There should be a single injection energy spectrum of the electrons, which are part of both plasma. The only difference in the energies of the electrons that are part of the two plasmas could be in the range of energies they encompass such that the positron-electron plasma which is lighter is constituted from the higher velocity section

of the parent distribution while the proton-electron plasma contains electrons of relatively lower velocity. However it would be difficult to confirm this observationally and this is only assumed since it sounds reasonable. The detectable signals which could help differentiate between the two plasma composition are as follows. The positron-electron plasma will be a source of the 511 keV annihilation line. In this process, a pair of positron-electron is expected to annihilate resulting in emission of two or three γ -ray photons of total energy of 1 MeV with the maximum energy of a photon being 511 keV. The proton(ion)-electron plasma will be at a high temperature and can emit soft X-rays if at a million degrees or optical continuum if around 10000 K. This plasma will also be the source for the several multiband absorption and emission lines that are detected in the supernova spectrum. Thus, in addition to synchrotron emission, the two plasmas should also result in independent observational signatures. While to the best of our knowledge, no annihilation line emission has been reported from a supernova/supernova remnant indicating that the presence of a positron-electron plasma is not conclusively established, the signatures of the proton(ion)-electron plasma are regularly detected from supernovae/supernova remnants proving its existence.

We, hence, examine observational results to search for any distinct signatures of the synchrotron emission from the two plasma of different compositions. This, then, brings into focus the two phases in which radio emission is detected from supernovae of type II namely prompt emission soon after the explosion and delayed emission in the remnant phase. This observation, then, strongly supports the existence of two components of relativistic plasma. We already know that the proton(ion)-electron plasma constitutes the massive ejecta of the explosion and as noted above is responsible for the thermal continuum and line emissions. This ejecta is very dense and hence synchrotron radio emission is not expected from this plasma in the early days after the explosion due to excessive free-free mixed thermal optical depths of the plasma itself. Synchrotron emission will become detectable at later dates when the ejecta has expanded sufficiently for the plasma to have become optically thin to radio emission. Thus, the proton(ion)-electron plasma is ruled out from being the source of the prompt synchrotron emission. This actually turns out to be convenient since it clearly points to the existence of the positron-electron plasma which has escaped from the explosion site before the proton-electron plasma and after the neutrinos and can be responsible for the prompt synchrotron emission

from type II explosions. Since the positron-electron plasma precedes the proton-electron plasma, the radio emission is only obscured by the free-free optical depth of the circumstellar medium which is much lower than that of the dense plasma expelled by the star. This, then, explains the frequency-dependent detection of prompt radio emission from the positron-electron plasma. It also explains the high expansion velocities ($\sim 30000 \text{ kms}^{-1}$) that have been inferred for the plasma giving rise to prompt radio emission from some supernovae such as SN 1987A. *This discussion then conclusively establishes the ejection and existence of positron-electron plasma which is responsible for the prompt radio emission from explosions of type II.* This raises the question of the existence of a positron-electron plasma in case of type Ia explosions since prompt radio emission has never been detected from this type. Since the generation of a large quantity of positrons is in a thermonuclear reaction and type Ia explosions also undergo this reaction, the positron-electron plasma is expected to have left the explosion site. However since the progenitor of type Ia are low mass stars which do lose mass and hence do not form a dense circumstellar medium, the lack of prompt radio emission can be attributed to lack of an appropriate magnetic field in the circumstellar region of the star. This means the fast positron-electron plasma should be ejected in type Ia supernova but which will keep expanding at high velocities suffering minor kinetic losses till it encounters an ambient magnetic field when it will start radiating synchrotron emission. This plasma should also keep annihilating at some rate even as it expands outwards. It might, hence, be possible to detect the annihilation line from supernova although it is possible that the lines might be too faint to be detectable. *To summarise: The prompt radio emission detected in supernovae of type II is from the positron-electron plasma radiating in the ambient magnetic field.* It is interesting that around several type Ia supernova remnants, a thin ring of hard X-ray emission (or optical) is detected. This well-defined rim of emission could be a signature of the positron-electron plasma and although this sounds speculative at first it is a well-founded inference. The rim is expanding ahead of the main remnant, is radiating in a distinct magnetic field and does not contain any thermal component of radiation - all signatures which support the positron-electron plasma which left the explosion site but could not radiate due to the lack of a magnetic field. The X-ray and optical rim emission could be synchrotron or could be the Compton-scattered positron-annihilation photons as the soft γ -ray photons interact with the dense inter-

stellar medium. The degeneracy in the origin needs to be further investigated. The radio emission that arises between the main remnant emission and the outer rim in the rare type II supernova with a X-ray rim i.e. Cas A is synchrotron in origin but with distinct magnetic field properties. The reason such rims should not be expected in type II supernova remnants is because the positron-electron plasma would have suffered large synchrotron losses soon after ejection as they emit the prompt synchrotron radiation detected at radio and X-ray bands. Unless this emission is quenched soon after, as was the case in SN 1987A, the plasma will continue to lose energy and hence might not be as potent as in type Ia supernova remnants. However this needs to be observationally confirmed. *To summarise: from the above discussion it can be surmised that the observational signatures of the positron-electron plasma are (1) prompt synchrotron emission following a supernova explosion (2) positron-electron annihilation lines (3) the X-ray or optical rims detected around supernova remnants.*

We now examine the signatures of proton(ion)-electron plasma. This as mentioned earlier contains most of mass that is ejected in a supernova explosion. In other words, this plasma is the supernova remnant which is detected in thermal continuum emission, spectral lines and radio synchrotron emission. It consists of ions of several elements, protons and relativistic electrons. This ejection of the outer parts of the star should have also carried along the stellar magnetic field which should be radially stretched as the remnant expands. In fact, the detection of a radial magnetic field in young supernova remnants as surmised from radio polarisation studies, gives strong evidence to the frozen-in magnetic field in the proton(ion)-electron plasma. The synchrotron radio emission from this plasma should also show a frequency-dependent detection due to the free-free optical depth of the thermal gas mixed with the relativistic plasma. This kind of behaviour was actually detected in SN 1986J i.e. a prompt radio emission episode and a delayed episode of radio synchrotron emission with both showing a frequency-dependent detection. The radio synchrotron emission is detectable in several remnants and easily resolved in nearby supernova remnants. *To summarise: the radio synchrotron emission from the proton(ion)-electron plasma gyrating in the magnetic field frozen in the plasma is detected when the thermal free-free optical depth of the remnant declines leading to a frequency-dependent detection. The remnant will keep shining till the relativistic electron population survives. The thermal continuum and spectral line emission also arise from the remnant.*

Polarisation studies show that the magnetic field which is radially oriented in young supernova remnants becomes tangential in older remnants. The radial behaviour is explained by field lines frozen in the radially expanding ejecta. As the remnant ages and slows down, its interaction with the environment increases. When the remnant runs into dense matter, it can be compressed and the magnetic field lines will also be quashed in the direction perpendicular to the radial vector i.e becoming tangential. Thus the behaviour of the field orientation in a supernova remnant is easily understood.

It has been inferred from observations that clumps and dust are formed in supernova remnants. Since a massive ejecta composed of a range of elements is expelled after the explosion, we examine the efficacy of the same clump and dust formation scenarios that were remarkably useful in case of nova outbursts and was summarised in the introduction. The expansion velocities inferred from the spectral lines observed soon after the explosion show higher values for lines of hydrogen and lower velocities values for iron lines (see Figure 5). This could be inferred to mean that in the supernova ejecta, the heavier elements lag behind the light elements like hydrogen and helium. The heavier atoms which are lagging behind can cluster together due to mutual gravity and form metal-rich clumps. The insides of the clumps can be shielded from the ultraviolet radiation field and hence provide favourable conditions for dust formation. Thus, dust detected in the supernova forms within these optically thick metal-rich clumps. Since a hot neutron star is expected in a type II supernova, its radiation field can exert radiation pressure on the optically thick clumps forcing them to move faster. This, then explains the high velocity metal-rich knots that are detected in type II supernova remnants like Cas A. Since the wispy hydrogen features are not optically thick, no radiation pressure acts on it explaining their lower velocities. Thus, the explanations for both dust formation and the excess velocity picked up by the optically thick clumps can be similar to the explanations that work for the same phenomena in nova ejecta. Since no central hot star is left behind in a type Ia supernova explosion, no difference in the expansion velocity of metal-rich knots and hydrogen wisps is expected. However the dust formation scenario in both types of supernovae can remain the same.

The discussion in this section can be summarised as:

- Relativistic electrons are energised alongwith the heavier matter before they are ejected in the supernova explosion. Assuming all particles are

imparted comparable energies, the energy spectrum of each species of particles will follow a normal (Gaussian) distribution with similar mean energies (greater or equal to the escape velocity) but a varying dispersion dependent on the mass of the particle. The heavy particle distribution will show a lower dispersion compared to the light particle distribution.

- Observations support three-component ejection from the explosion site in the listed order due to decreasing expansion velocities: neutrinos, a light particle ejecta consisting of positron-electron plasma and a heavy ejecta consisting of proton(ion)-electron ejecta.
- The prompt radio synchrotron emission detected soon after the explosion in type II supernovae is due to the positron-electron plasma radiating in the circumstellar magnetic field. The radio synchrotron emission detected in the supernova remnant phase is from electrons within the main remnant shell (i.e. proton(ion)-electron plasma) that are radiating in the magnetic field frozen in the remnant.
- X-ray/optical rims have been detected predominantly around remnants of type Ia supernovae and are suggested to be due to emission from the positron-electron plasma. The emission could either be due to the synchrotron process or could be the Compton scattering of the positron-electron annihilation photons as the plasma strikes the surrounding higher density thermal matter.
- The magnetic field is observed to be predominantly radial in young supernova remnants. This can be explained by stretching of the field lines frozen in the matter in the radially expanding ejecta. Older remnants show a predominantly tangential field which would be expected when the remnant interacts with the ambient dense medium leading to compression of the radial field.
- Clump formation in supernovae is supported by the detection of fast metal-rich knots devoid of hydrogen. These knots observing to be expanding faster than hydrogen/helium-rich streaks are formed due to clustering of heavy atoms which lag behind in the ejecta. The knots will be optically thick and hence accelerated to higher velocities by the radiation pressure exerted by the photons from the central hot star. The insides of the optically thick metal-rich knots will be

well-shielded from the hard radiation field and hence conducive to dust formation. This dust will eventually disperse and increase in the dust content of the galaxy.

- Since the formation scenario for type Ia supernova remnants indicate that it should not be hosting a central hot object, this means that metal-rich knots and the hydrogen-rich wisps in the remnant should be moving with similar velocities. In other words, the detection of faster metal-rich knots would mean there exists a hot compact object at the centre of the remnant.

We now discuss the observational results on a few supernovae and a supernova remnant in light of the above model.

3.3 Case Studies

We discuss the observational results on the Galactic supernova remnant Cassiopeia A and the extragalactic supernovae SN 1986J, SN 1987A and SN 1993J. As in the previous sections, the focus is on the synchrotron emission although other diagnostics are not excluded. Cas A has been traced to a type II supernova explosion. The other two well known Galactic supernova remnants namely Kepler and Tycho are believed to have been type Ia. All three remnants show the presence of a hard synchrotron X-ray rim which surrounds the main remnant and similar synchrotron radio characteristics. This supports the ejection of relativistic plasma in all the remnants - the positron-electron plasma which is responsible for the thin hard X-ray rim and proton(ion)-electron plasma which is responsible for the radio emission coincident with the multi-band emission from the remnant shell. While prompt radio emission is likely to have been detected from the Cas A explosion, it would not have been detected from the explosions which resulted in the Kepler and Tycho remnants.

3.3.1 Type II SNR: Cas A in Milky Way

Cas A is the remnant of a type II supernova explosion located in the Perseus arm at a distance of ~ 3.5 kpc that occurred about 350 years ago. The shell-like remnant of diameter $\sim 5'$ (linear size ~ 5 pc) left behind by the explosion is the brightest source in the radio sky. The observable remnant consists of three main parts: (1) a bright shell of radius $\sim 2'$ which emits thermal continuum emission, multiband spectral lines and radio synchrotron emission. This shell contains most of the mass ejected in the explosion and refers to the central bright region in Figure 7a; (2) faint radio synchrotron emission which surrounds

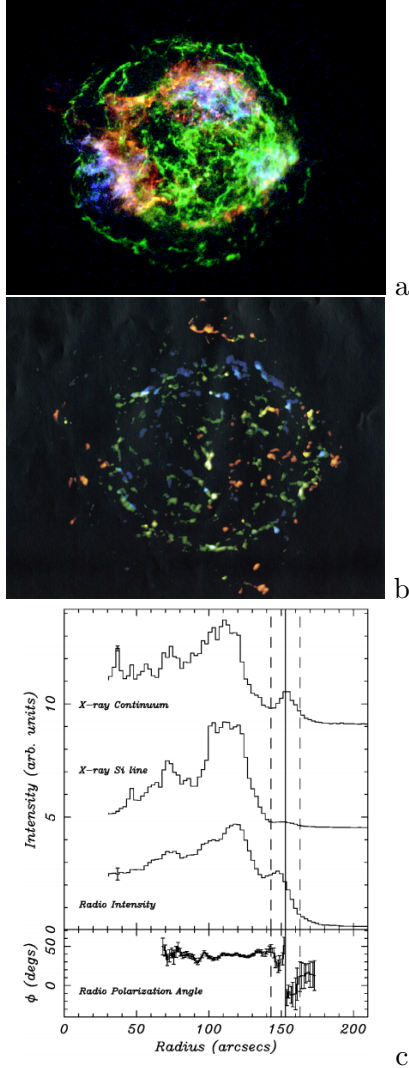


Figure 7: (a) X-ray three-colour image of the supernova remnant Cassiopeia A copied from Hwang et al. (2004). The colour coding is Si He α (1.78-2.0 keV; red); Fe K (6.52-6.95 keV; blue) and 4.2-6.4 keV continuum (green). Note the outer wispy ring in hard X-rays due to synchrotron emission. (b) Figure showing radio spectral index of knots in Cas A estimated in epoch 1985 reproduced from Anderson & Rudnick (1996). The red colour indicates a spectral index of -0.9 whereas blue indicates 0.75 and the steeper knots lie outside the main ring of Cas A. (c) This figure reproduced from Gotthelf et al. (2001) shows the radial variation in brightness in different bands and in the radio polarisation angle. Notice the outer parts are detected in radio synchrotron and X-rays and the radio polarisation angle also changes. In the main remnant, the polarisation angle is constant and the magnetic field has been inferred to be mainly radial.

the bright shell and is referred to as the radio plateau in literature; (3) a thin ring of wispy hard X-ray emission of radius $\sim 2.6'$ (Gotthelf et al., 2001) (green ring in Figure 7a) which is coincident with the outermost part of the radio plateau. The three top curves in Figure 7c, copied from Gotthelf et al. (2001), are the radial cut across the source in three tracers - X-ray continuum, Si line emission and radio synchrotron emission. The main remnant is detected in all three tracers. While the Si emission is confined to the main remnant, the X-ray and radio synchrotron emission show a second peak beyond the main remnant which corresponds to the X-ray rim and radio plateau respectively. Figure 7b, copied from Anderson & Rudnick (1996), shows the distribution of radio spectral index between 1.4 and 5 GHz of the knotty emission in Cas A. The couple of distinct characteristics of the radio synchrotron emission from the main remnant and from the radio plateau are: (1) the radio spectrum of knots in the radio plateau is steeper with $\alpha > 0.8$ ($S \propto \nu^{-\alpha}$) compared to knots within the remnant (Kassim et al., 1995; Anderson & Rudnick, 1996) (also see Figure 7b). Steeper radio spectrum is also detected from a small region in the western part of the main remnant which begs the inference that it is the foreground part of the radio plateau (see Figure 7b). (2) The radio polarisation angle which is fairly constant within the main remnant and indicative of a radial magnetic field starts varying in the radio plateau and then shows an abrupt jump which is coincident with the peak emission of the hard X-ray rim (lowermost curve in Figure 7c). This behaviour could be inferred to indicate the distinct nature of the magnetic field in the remnant and in the radio plateau. The equipartition magnetic field in the knots, estimated from radio data at 83 GHz ranges from 1 to 5 mG. (Wright et al., 1999). The average magnetic field in Cas A has been estimated to be > 0.5 mG from X-ray observations (Vink & Laming, 2003). Assuming the X-ray rim in Cas A is due to the synchrotron process magnetic field of 0.1 mG has been estimated in the rim (Vink & Laming, 2003).

We try to understand this behaviour in light of the model put forward here. The X-ray rim and the radio synchrotron emission from outside the main remnant lend support to their origin in the positron-electron ejecta which precedes the heavy proton(ion)-electron ejecta from the explosion. The light ejecta radiates radio synchrotron emission in the ambient magnetic field while the plasma in the main remnant emits in the magnetic field frozen in itself. This, then, explains the observed abrupt jump in the radio polarisation angle (see Figure 7c). However it should

be noted that the circumstellar magnetic field is also originally the stellar field which was carried away in the mass loss suffered by the progenitor. Since the wind velocities are much lower at $\sim 10 - 20 \text{ km s}^{-1}$ compared to the explosion ejecta velocities, the circumstellar field will not display the strictly radial behaviour that is exhibited by the remnant field. These, then explain the observed behaviour of the radio polarisation angle in Cas A shown in Figure 7c. The parent electron population within the main remnant and the outer radio plateau should be the same i.e. electrons accelerated by the thermonuclear explosion in the supernova. However different sections of the parent normal distribution can contribute to the remnant and plateau so that the radiating electrons can be of varying range of energies. These, when subject to distinct magnetic field strengths can result in electrons of different energies i.e. different parts of the energy spectrum radiating at a give frequency so that the observed radio spectral indices are also different. This means that emission at a given observing frequency can arise from high energy electrons in the plateau for which a magnetic field of 0.1 mG has been measured while it will arise from lower energy electrons in the remnant wherein a magnetic field around 0.5 mG has been measured (see Equation 2). Since the electrons of lower energy will lie closer to the peak energy and hence show a flatter energy spectrum than electrons of higher energy - this could contribute to the steeper radio spectrum detected in the radio plateau region outside the main remnant.

It is believed that cosmic rays upto energies $\sim 10^{15}$ eV (1000 TeV) i.e. the knee in the cosmic ray energy spectrum are accelerated in supernovae or supernova remnants. However detailed studies of supernova remnants have not been successful in supporting this conclusion. From a study of several supernova remnants, it was inferred that the high energy cut-off of synchrotron-emitting electrons was around 80 TeV (Reynolds & Keohane, 1999). MAGIC observations have suggested an even lower energy cutoff at ~ 3.5 TeV for the cosmic rays from Cas A (Guberman et al., 2017). This is not surprising in light of the explanation provided in the paper wherein the acceleration of the cosmic rays is mainly effected by the energy released in the thermonuclear explosion before matter is ejected. This means even if particles were accelerated to energies of 1000 TeV in the supernova explosion, these would have rapidly lost energy and moved to lower energies after 350 years so that a high energy cutoff near 3.5 TeV is observed by MAGIC in the cosmic ray spectrum from Cas A (Guberman et al., 2017). This demonstrates that the issue of the maximum energy of the particles accelerated by

the supernova explosion remains unresolved and we might be able to resolve this issue by targetting young powerful supernovae like SN 1986J for studies which aim at estimating the high energy cutoff of the cosmic ray spectrum studies instead of targetting supernova remnants where the cosmic ray spectrum has aged. Maybe such studies already exist which the author has missed, in which case, we might be able to readily be able to examine data on the same.

Electrons of energy ~ 80 TeV gyrating in a magnetic field of 0.1 mG should be able to emit hard X-rays ($\nu \sim 10^{19}$ Hz) as observed in the outer rim but would have a short synchrotron lifetime of only 10 years. If the magnetic field was much lower then, the electron energies required to explain the hard X-ray emission assuming it is synchrotron in origin would be higher and these could also survive longer. For example, if the magnetic field was $10 \mu\text{G}$, the electron energies emitting hard X-rays ($\nu \sim 10^{19}$ Hz) would need to be 250 TeV and their synchrotron lifetime would be ~ 3000 years. However, the two studies noted above seem to certainly rule out electrons of energy beyond 80 TeV. For electrons of energy 5 TeV to emit hard X-rays would require a magnetic field of 25 mG. This discussion is geared towards understanding the hard X-ray rim that is detected around the main remnant and the emission mechanism. The above discussion suggests that the only way the emission could be synchrotron is if the electrons did not suffer any synchrotron or inverse Compton losses during its expansion to the present location so that the electrons retained the high energies they acquired from the explosion energy. However since the recent observation have not detected any high energy electrons and the magnetic field is not observed to be so large as 25 mG, it appears that the X-ray rim might owe its origin to a different physical process. Since the X-ray rim and radio plateau can be associated with the positron-electron plasma, it is likely that the X-ray rim is the positron annihilation radiation at 511 keV that has been Compton-scattered to hard X-ray frequencies by thermal electrons when the plasma has encountered the ambient interstellar gas. The low energy positron-electron plasma continues to radiate by the synchrotron process in the radio plateau region.

The detection of the hard X-ray rim (which is more commonly detected in supernova remnants of type Ia explosion) in Cas A might suggest an episodic mass loss by its progenitor star - a scenario similar to the more recent type II supernova SN 1987A. As in SN 1987A, the prompt radio emission in Cas A might have been short-lived, allowing the high energy positron-electron plasma to survive longer due to their expansion causing only kinetic losses. This

is suggested due to predominant detection of X-ray rims around type Ia remnants wherein it is known that the circumstellar magnetic field is very weak and hence the synchrotron losses suffered by the positron-electron plasma are small and radiation from it is detected several hundred years after the explosion.

The observational results on Cas A can be briefly explained: following the explosion, a fast expanding positron-electron ejecta would have emitted prompt radio and X-ray synchrotron emission and is currently responsible for the thin rim of hard X-ray emission and radio plateau around the remnant. A proton(ion)-electron plasma which follows, is responsible for synchrotron emission detected from the entire remnant and the multi-band thermal emission including spectral lines. The magnetic field in the main remnant is radial indicating stretching of field lines due to radial expansion of the remnant while it includes a larger random component in the radio plateau which is indicative of the field in the circumstellar/interstellar medium.

3.3.2 Type II SN: SN1986J in NGC 891

SN 1986J was detected in the galaxy NGC 891 (distance ~ 10 Mpc) from radio continuum observations at 21 cm (van Gorkom et al., 1986). At 10 Mpc, $1''$ corresponds to about 50 pc. Although the supernova was identified in 1986, several observations pointed to the explosion having occurred in 1983.2. There existed a radio detection of the supernova in 1984 (Rupen et al., 1987), the fitting of post-discovery radio light curves indicated an earlier explosion date than 1986 (Chevalier, 1987) and the VLBI images taken in late 1986 (Bartel et al., 1989) resolved the radio emission also indicating an earlier date for the explosion (Bietenholz et al., 2002). After its identification, SN 1986J has been intensively observed at radio wavelengths both in integrated flux density and with the Very Long Baseline Interferometry (VLBI) which has resulted in images with a few milliarcsecond resolution. A peak radio emission of 128 mJy at 6 cm was recorded about 1200 days from the estimated date of explosion (Weiler et al., 2007).

The radio images of SN 1986J show a complex structure and the evolution of radio emission has been captured in detail by both VLBI images and radio light curves allowing us a rare glimpse into the early time behaviour of a supernova and its transition to a supernova remnant. In the VLBI images obtained in late 1986, the source was inferred to be extended along a position angle of around 150° (Bartel et al., 1989) which is similar to the major axis of the extended emission observed about 5.5 years after the explosion in late 1988 as shown in Figure

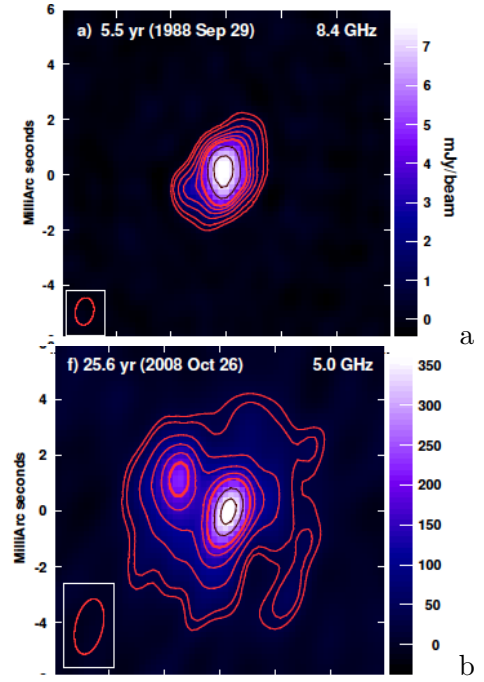


Figure 8: Figures showing SN 1986J at radio wavelengths and VLBI resolution are copied from Bietenholz & Bartel (2017a). The figures show SN 1986J at 8.4 GHz about 5.5 years (a) and at 5 GHz about 25.6 years (b) after the estimated date of explosion. The central component in (a) expands to the north-east and a new component emerges in the centre of the source and has exceeded the brightness of the old component by 25 years as seen in (b). Both the components show a frequency-dependent onset.

8a copied from Bietenholz & Bartel (2017a). An equipartition magnetic field of 70 mG was estimated from the detected radio emission in late 1988 (Bietenholz et al., 2002). Even while the emission kept expanding about this axis, the central peak of emission moved towards the north-east and was then referred to as the hotspot in the shell. Due to this, there was no central peak from 1999 to 2002 in the 5 GHz images. A new component had appeared in the centre of the shell at 5 GHz in the image taken in 2005 and which got brighter than the hotspot by 2008 (Bietenholz et al., 2010b). This component was first detected at higher radio frequencies which could be due to frequency-dependent delayed detection (Bietenholz et al., 2010b). As can be seen in Figure 8b, the radio emission from SN 1986J had evolved to a quasi-spherical shell-like structure after 25 years which hosted a hotspot in the north-east and the bright central component (Bietenholz et al., 2002; Bietenholz & Bartel, 2017a). The flux density of the new central component exceeded that of the shell hotspot about 25 years after the explosion (Bietenholz & Bartel, 2017a). The radio emission from the shell hotspot and the central component measured about 14 years after the explosion had spectral

indices ($S \propto \nu^{-\alpha}$) of 0.63 and 0.76 (Bietenholz & Bartel, 2017b). The new central source got progressively brighter while the shell hotspot got progressively fainter so that in images taken around 31.6 years after the explosion, the hotspot had faded and the central bright component was surrounded by a faint shell of radio emission (Bietenholz & Bartel, 2017a). Several possible origins for the new central radio component in SN 1986J have been examined and while it has been difficult to arrive at a conclusive origin, it has been possible to infer that the emission was arising in the physical centre of the supernova shell (Bietenholz & Bartel, 2017b).

It is estimated that the hotspot plasma was expanding at $\sim 20000 \text{ kms}^{-1}$ about 0.25 years after the explosion in 1983 which had slowed down to about 6000 kms^{-1} about 16 years later (Bietenholz et al., 2002). The expansion velocity of the central new component is estimated to be $680^{+80}_{-380} \text{ kms}^{-1}$ assuming its expansion since the explosion epoch of 1983.2 (Bietenholz & Bartel, 2017a).

The detection of two distinct radio components - the prompt component which was detected soon after the discovery of the supernova which showed a frequency-dependent detection with the peak emission at 5 and 1.4 GHz being detected about 3 and 5 years after explosion (Weiler et al., 1990) and the new central component which also showed a frequency-dependent detection (Bietenholz et al., 2010b) give strong support to the model suggested in the paper. The late peaks recorded for the radio emission from SN 1986J indicates the presence of extensive circumstellar medium and light curve fitting has indeed shown that clumpy thermal medium is required to explain the frequency-dependent behaviour of the observed multifrequency light curves (Weiler et al., 1990). The prompt emission was synchrotron emission from the positron-electron plasma which was free-free absorbed by the circumstellar medium. The new component which became detectable at a later date and was inferred to be located at the physical centre of the supernova was synchrotron emission from the proton(ion)-electron plasma in the massive remnant. This emission was free-free absorbed by the thermal plasma in the remnant which was several times denser than the circumstellar matter. The different velocities of the two components and the slightly different radio spectral indices also support the separate origin for the radio emission from the hotspot and the central source. Thus, the emission from the positron-electron plasma is what we refer to as the prompt radio emission from a supernova while the emission from the proton-electron plasma is what we refer to as the emission from the supernova rem-

nant. Thus, SN 1986J has provided us with valuable data that has helped elucidate the above.

The existence of the supernova remnant is verifiable from data at other bands and although the angular resolution is insufficient to locate this remnant, the most likely location is in the centre of the radio shell emitting synchrotron emission. The emission detected at wavelengths of 1.2 mm and 3 mm from SN 1986J in late 1986 was higher than the expected radio synchrotron emission as extrapolated from lower radio frequencies (Tuffs et al., 1989). An origin in a synchrotron nebula powered by a pulsar was suggested as a possible origin for this excess (Tuffs et al., 1989). The X-ray spectrum of SN 1986J taken in 2000 and 2003 show the presence of iron, silicon, sulphur, oxygen, neon and magnesium with the abundance of silicon and sulphur being super-solar (Houck, 2005). The X-ray luminosity in the energy range 0.5-2.5 keV is observed to decline rapidly (Houck, 2005). The optical spectrum of SN 1986J obtained in 1986 contained narrow $H\alpha$ lines of widths $\sim 700 \text{ kms}^{-1}$ (Rupen et al., 1987) whereas the forbidden lines of oxygen were detected with larger widths ranging from 1000 to 2000 kms^{-1} (Leibundgut et al., 1991). Narrow faint lines of neutral helium were also detected. In 1989, the narrow hydrogen lines became fainter while the forbidden lines of oxygen remained unchanged (Leibundgut et al., 1991). Further observations of the forbidden oxygen lines showed that all the profiles displayed a double-peaked structure and that both peaks were blue-shifted wrt to the galaxy redshift by -1000 and -3500 kms^{-1} (Milisavljevic et al., 2008). While the strengths of the $H\alpha$, [O II] and [O III] had declined considerably by 2007 with the change in the hydrogen line being maximum, the [O I] lines seemed to have evolved the least (Milisavljevic et al., 2008). While all this data is significant in enhancing our knowledge of the remnant, here, this information is mainly used to infer that the massive remnant which emits thermal continuum and spectral lines was emitting, expanding and evolving alongwith the radio synchrotron emission. Infrared emission inferred to be from warm dust at a temperature of a couple hundred degrees Kelvin is detectable after more than two decades (Tinyanont et al., 2016). Since dust is expected to form in the main remnant of the explosion which is rich in metals as discussed earlier, these observations also give evidence to the presence of the supernova remnant and which should be coincident with the central radio source. If we are able to resolve the emission from SN 1986J at several bands before it fades, then in future we should detect multiband thermal continuum emission including spectral lines coincident with the central radio

synchrotron emitting component. While this is obvious from the radio evolution of the source, obtaining independent evidence from multi-band data should put our understanding on a firm footing allowing us to explore further.

We can convert the radio flux densities measured for SN 1986J at a distance of 10 Mpc to a fictitious supernova located 10 kpc from us. This entails multiplying the observed flux densities by a factor of a million and can be useful in comparing with the order of magnitude flux densities of Galactic supernova remnants like Cas A, Kepler and Tycho remnants. The peak flux density of 128 mJy noted at 5 GHz around 1200 days after the explosion in SN 1986J would be recorded as a source of flux density of 128000 Jy if the supernova had exploded at a distance of 10 kpc. In 2012 i.e. 29.6 years after the explosion a flux density of 1.82 mJy was recorded at 5 GHz (Bietenholz & Bartel, 2017b). If the supernova was located at a distance of 10 kpc then we would have recorded a flux density of 1820 Jy. The flux density of the remnant is evolving and is comparable to that of Galactic remnants.

To summarise: The two distinct radio components sequentially detected in SN 1986J with both components showing a frequency-dependent delay in detection due to optical depth effects lends strong support to the existence of a fast light ejecta composed of positrons and electrons which is responsible for the prompt radio emission and a slower massive ejecta composed of protons/ions and electrons which is the radio component that makes a late appearance and is the supernova remnant. The optical depth of the circumstellar medium delays the detection of the prompt radio emission while the optical depth of the massive ejecta itself delays the detection of the radio emission from the remnant. SN 1986J is hence a useful example demonstrating the origin of the prompt and delayed radio emission from the supernova phase and the supernova remnant phase respectively.

3.3.3 Type II SN: SN1987A in LMC

A supernova explosion of type II was recorded on February 23, 1987 in the LMC, first surmised from the detection of neutrinos of energies a few tens of MeV in a span of 6-13 seconds (Hirata et al., 1987; Bionta et al., 1987) which preceded the detection of the explosion at electromagnetic bands. Till date, this appears to be the only supernova explosion from which neutrinos have been detected. Neutrinos are expected in supernova explosions since they are released in nuclear fusion reactions and when protons combine with electrons to form the degenerate neutron core. Being one of the nearest explosions, since

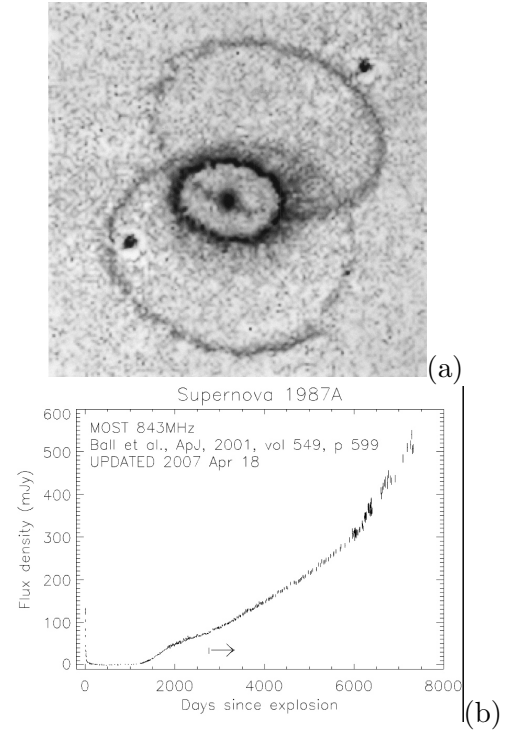


Figure 9: (a) Figure copied from Burrows et al. (1995) showing the triple ring system around the SN 1987A. The semi-major axis of the inner equatorial ring is $0.81''$ (0.19 pc) and semi-minor axis is $0.57''$ (0.14 pc) while the semi-major axes of the northern outer ring and southern outer rings are $1.77''$ (0.43 pc) and $1.84''$ (0.45 pc) (Burrows et al., 1995). (b) Figure downloaded from <http://www.physics.usyd.edu.au/astrop/SN1987A> and presented in Ball et al (2001). The radio light curve shows the prompt radio emission which was rapidly quenched and the second longer-lasting phase of radio emission detected from SN 1987A at 843 MHz.

LMC is at a distance of ~ 50 kpc, this supernova has since been extensively observed with high linear resolution. At this distance, $1''$ corresponds to about 0.25 pc. SN 1987A has allowed us to study several evolutionary aspects of type II supernova explosions and also provided important input to nature of mass loss in the progenitor star. Some of the peculiar observed characteristics of SN 1987A are summarised below with comments included in italics:

- Prompt radio emission was detected at frequencies between 840 MHz and 2.4 GHz with the MOST telescope with the first detection on 25 February 1987 i.e. 2 days after the detection of neutrinos (Turtle et al., 1987). The frequency-dependent delayed detection and peaks in the multi-frequency light curve were observed within a week even for the lowest observed frequency (Turtle et al., 1987) and the emission at all observed frequencies had disappeared by September 1987 (Ball et al., 1995). A light curve at 843 MHz which includes the prompt emission soon

after the detection and the more persistent radio emission detected later is shown in Figure 9b. Generally it takes the order of 100 days or more for the prompt radio emission near GHz frequencies from type II supernovae to become detectable - for example the light curve of SN 1993J in Figure 12 - and it takes a few years for the emission to fade. Thus, by type II standards, the prompt radio emission from SN 1987A was extremely prompt, fainter and faded very quickly.

- Narrow ultraviolet and optical lines were detected from SN 1987A when it was observed soon after the explosion. These lines were believed to be forming in the circumstellar medium (Fransson et al., 1989; Wampler & Richichi, 1989).
- An unexpected result from optical imaging was the detection of a triple ring system (see Figure 9) within $\sim 5''$ of SN 1987A (Crotts et al., 1989; Wampler et al., 1990; Burrows et al., 1995). The rings had to be due to mass loss by the progenitor system prior to the explosion otherwise they would require superluminal expansion, if ejected in the explosion. *The equatorial nature of the three rings indicates that the progenitor suffered extensive mass loss from its equatorial regions.*
- The inner ring is likely expanding at a rate of $\leq 50 \text{ km s}^{-1}$ as surmised from optical emission lines of [O III] detected in December 1987 (Wampler & Richichi, 1989).
- The radio emission in the second brightening phase was first detected at the low frequency of 843 MHz (Ball et al., 1995) and then at 4.8 GHz (Staveley-Smith et al., 1992) indicating that the radio detection in this second phase of the radio emission was not governed by free-free absorption. *This contrasts with the case in SN 1986J wherein the emergence of both radio components (shell hotspot and central source) was delayed due to free-free absorption. The observed behaviour of the radio emission in SN 1987A helps one infer that the second phase was not from the proton-electron plasma in the remnant which then means that the emission was still from the positron-electron plasma.*
- The second brightening at 4.8 GHz was detected in July 1990, between days 1140 and 1200 after the explosion (Staveley-Smith et al., 1992, 1993; Ball et al., 1995). This radio emission when resolved in images taken in 1992 (Gaensler et al., 1997) was along a ring located towards the inner

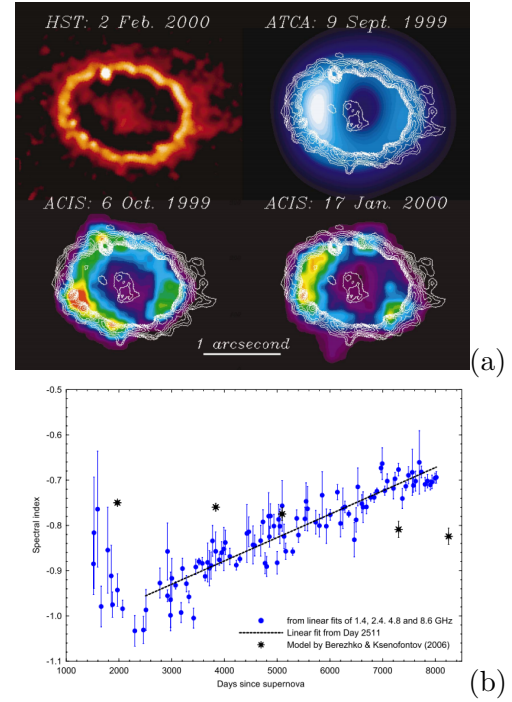


Figure 10: (a) Figure showing multi-band emission from SN 1987A reproduced from Burrows et al. (2000). The bulk ejecta (which we refer to as the supernova remnant) from the supernova explosion has to be the compact emission located in the central part of the ring. The positron-electron ejecta moving with much larger velocities has reached the optical ring when it begins to radiate radio and X-ray synchrotron emission in the magnetic field of the ring. (b) Figure reproduced from Zanardo et al. (2010) showing the spectral index variation in SN 1987A from day 2511. Notice how the spectrum gets flatter with time.

edge of the equatorial optical ring (see Figure 10a). X-ray emission was also detected from the same region (Beuermann et al., 1994) (see Figure 10a). Both radio and X-ray emission have been since been rising (Staveley-Smith et al., 2014; Frank et al., 2016). Optical hotspots started appearing in the inner equatorial ring from around 1996 (Garnavich & Kirshner, 1996).

- Assuming the second phase of radio emission was associated with the forward shock which had reached the optical ring, an expansion velocity of 29200 km s^{-1} was estimated for the shock (Staveley-Smith et al., 1993). From the expansion of the radio ring it was then surmised that the shock had slowed down to about 3500 km s^{-1} after entering the inner equatorial ring (Staveley-Smith et al., 2005). *We need to replace the shock by the presence of relativistic positron-electron plasma which by virtue of being light can expand with high velocities and retain the same till it encounters dense matter.*
- Wide P Cygni profiles were detected for the

Balmer lines of hydrogen with the velocity shift of the H α absorption line being -18000 km s^{-1} in the first observation taken on 25 February 1987 (see Figure 5) while the wings of the P Cygni profile extended to $\pm 30000 \text{ km s}^{-1}$ (Blanco et al., 1987; Phillips et al., 1988). Fe II 5169Å was detected at a velocity shift of -11355 km s^{-1} around day 4 (Phillips et al., 1988). The velocity shift of the Balmer lines of hydrogen stabilised around -4000 to -5000 km s^{-1} around day 80 while those of Fe II stabilised around -2000 km s^{-1} (Phillips et al., 1988) (see Figure 5). *Since these high velocity lines have to emerge from the massive remnant of the explosion, their velocities signify the expansion velocity of the massive remnant. The initially recorded expansion velocities of 18000 km s^{-1} or more had slowed down to $4000\text{-}5000 \text{ km s}^{-1}$ in 80 days. This alongwith similar behaviour recorded in other supernovae inform us of the rapid slowing down of the expansion of the massive remnant unlike the light positron-electron plasma.*

- The HST optical image of the inner equatorial ring in Figure 10a shows a bright ring with hotspots and a blob in the central regions. The optical hotspots progressively move outwards (Fransson et al., 2015) as the diameter of the radio and X-ray emission rings increase. The central blob of emission is not detected at low radio frequencies or X-rays. *The central blob is the massive remnant of the explosion which is the source of the broad absorption and emission lines and which is optically thick to radio synchrotron emission.*
- The central blob detected in SN 1987A is expanding as can be seen in Figure 11. This nebula has evolved to a structure stretched along north-south with a similarly elongated cavity in its centre. The nebula which was fairly compact in early days has expanded and encountered the southern part of the inner equatorial ring. The central blob as seen in the optical image given in Figure 10a, shows wispy extensions stretching out in the north-east and south-west which appear to be along the segments of the northern ring that intersects the inner equatorial ring (see Figure 9a). The wispy extensions are not detected in later images shown in Figure 11b. *The central blob is the massive metal-rich remnant of the explosion which is also expanding. The wispy extensions to the central blob seem to be the gas excited in the northern ring when the positron-electron plasma passed through it lead-*

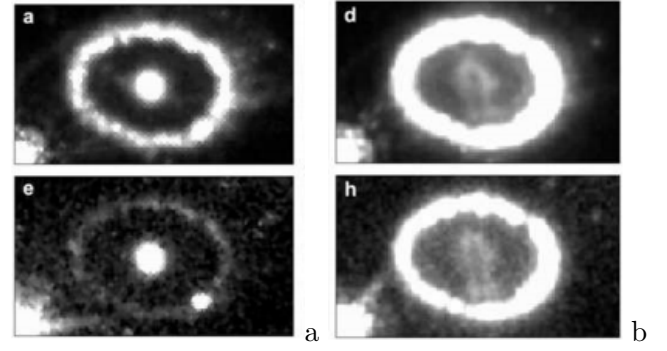


Figure 11: From Larsson et al. (2011). Figures show the R (top panels) and B band (lower panels) evolution of SN 1987A. The left panels show SN 1987A on 24 September 1994 (day 2770) and the right side panels are from 9 April 2009 (day 8101). Notice how the circumstellar ring brightens with time and the central ejecta increases in size and evolves to an elliptical ring. It is suggested that the electron-positron plasma is the cause of the synchrotron emission from the ring while in future radio synchrotron emission might be detectable from the non-thermal electron-proton plasma in the central component.

ing to its temporary brightening. This emission has since faded. Since all the rings are equatorial, the progenitor has suffered excess mass loss in the equatorial planes which might explain the prolate-shaped remnant assuming projection effects are not misleading.

- Synchrotron emission from the ring is detected at a short wavelength of 0.87 mm while only the central blob is detected at still shorter wavelengths and which has been inferred to be emission due to dust in the blob (Indebetouw et al., 2014). *This observation lends further support to the central blob being the metal-rich remnant of the explosion where dust is being formed and which is still optically thick to radio synchrotron from mixed relativistic plasma.*
- The radio spectral index measured in 1992 was 0.97 which in 2000 had reduced to 0.88 ($S \propto \nu^{-\alpha}$) (Manchester et al., 2002). The spectral index has continued to decrease as seen in Figure 10b taken from Zanardo et al. (2010). *Note that this behaviour, which is opposite of what is expected from an ageing electron energy spectrum, is exhibited by the radio emission coincident with the inner equatorial ring. No new radio component from the central remnant has yet appeared.*
- No central compact object has been detected from SN 1987A.

The triple ring structure around SN 1987A indicates that the progenitor lost mass through episodic

ejections instead of undergoing continuous mass loss. These two types of mass loss by massive stars before they explode as supernovae has been confirmed from studies of massive supergiant stars. For example, it was inferred from the study of two massive red supergiant stars that Betelgeuse was undergoing a steady mass loss whereas VY CMa was experiencing episodic mass loss (Smith et al., 2009).

While it is difficult to explain the equatorial nature of the triple ring system, its structure can be trivially explained if the progenitor of SN 1987A was in a loose binary with an orbital radius of the order of half a parsec or so. In this case, the distinct centres of the three rings detected around SN1987A would be due to three episodes of mass loss suffered by the progenitor when it was at three different locations in the orbit. The centres of the three rings then outline the orbital path of SN 1987A. From the observed structure, (assuming the orbital motion was not affected by the explosion) it appears that the star is moving northwards towards the centre of the northern ring. The rings are fairly symmetric indicating mass loss from a single object in the centre of the rings. The southern ring is observed to be the largest and can be inferred to indicate the first episode of mass loss. Since the size of the northern ring is similar, one can infer that both the mass loss episodes happened in the same orbit. The separation between the centres of the two large rings is about 0.4 parsec which means that if the star was moving with a velocity of 100 km/s (this value has no observational basis from data on SN 1987A), it would have taken about 3900 years to traverse that distance. In the 3900 years that the star took between the two mass loss episodes, the southern ring would be 0.04 parsecs in size if it was expanding at a rate of 10 km/s (the rings are likely to have been ejected with a higher velocity and also probably expanding at a higher velocity). The star has then completed its orbit in which both the rings have expanded to a radius of ~ 0.4 parsecs. During another orbit when the progenitor is between the two rings, it suffers another mass loss episode which results in the inner ring of diameter 0.19 pc. No further mass loss seems to have occurred before the progenitor exploded as a supernova. The supernova still appears to be at the centre of the last mass loss episode which suggests that the expansion velocities of matter ejected in the last episode of mass loss is much larger than the space motion of the star. If a companion star to SN 1987A forming a loose binary can be identified then it would give a boost to this explanation. Such large orbits are not exceptional since orbital periods have been observed to range from less than an hour to hundreds

of thousands years. For example, while cataclysmic variables have short orbital periods, there exist long period double (or triple) binaries like Alpha Centauri AB and Proxima Centauri. Proxima Centauri has an orbital period of 550000 years around Alpha Centauri AB with the major axis being about 0.2 light years. Alpha Centauri A and B form a tight binary with an orbital period of about 80 years and a separation of about 11 AU.

The triple ring system around SN 1987A are not spherical shells but equatorial rings with the supernova being located at the centre of the inner ring. The reasons for the mass loss being confined to equatorial rings and not spherical are not clear and require further investigation. The rings have to have been ejected with high radial velocity larger than the orbital motion of the star, so that the rings continued to expand around the ejection position of the star and were not affected by the motion of the stars. All the three rings since due to equatorial mass loss should lie in the same plane. This can then account for the enhanced optical emission which is detected in the overlap region between the inner ring and northern part of the southern ring (see Figure 9a). *To summarise - the triple equatorial ring system around SN 1987A, due to episodic mass loss from the progenitor, can be explained if the star was in a loose binary and underwent three distinct episodes of mass loss from the equatorial regions, at much higher ejection velocities than the orbital motion and from three different positions in its orbit. The reason for equatorial mass loss instead of spherical mass loss from the progenitor star is not clear and needs to be investigated.*

The radio properties of SN 1987A can be easily explained by the fast ejection of a positron-electron plasma which is responsible for the short-lived prompt radio emission which was detected with a frequency-dependent delay and the second phase of radio emission coincident with the inner equatorial ring but detected with a frequency-dependent delay. That the prompt radio emission from SN 1987A was detected almost immediately after the explosion indicating low free-free thermal optical depths and was also extinguished much sooner than is generally observed in type II supernovae probably due to the lack of an appropriate magnetic field, argue for the lack of a distributed circumstellar medium around the supernova. As has been inferred from the triple ring structure, the progenitor lost mass predominantly in episodic ejections so that the distributed circumstellar matter around SN 1987A could be absent. However the detection of prompt emission soon after the explosion indicates that there does exist some distributed circumstellar medium in the immediate

vicinity of the star.

Since the progenitor star, for some inexplicable reason, lost mass in episodic ejections only from the equatorial regions, it is intriguing on what happened to the outer parts of the star in the non-equatorial regions. The detection of a central nebula which has evolved to be elongated perpendicular to the equator suggests that the star did retain more mass in the non-equatorial regions which was blasted away in the supernova explosion. The nebula seems to have expanded to 0.14 pc from the explosion site around day 8101 (Figure 11b) which means that the remnant has been expanding with a mean velocity of about 6200 km s^{-1} since the explosion. However before drawing any firm conclusions it will be useful to wait for more observational results on the central remnant to become available.

No radio synchrotron emission has been detected from the central nebula. This could indicate that the nebula is still optically thick to radio frequencies. Since this supernova is continuously being monitored, we should be able to detect the frequency-dependent switching on of the radio synchrotron emission from the central remnant in the future.

To summarise - all the synchrotron signatures of SN 1987A from the time of explosion to the bright radio ring are due to the fast positron-electron plasma set forth by the explosion. This means the synchrotron radiating plasma should also be radiating the positron annihilation line at 511 keV as it expands away from the explosion site. Deep observations of this line immediately after the explosion and when the prompt radio emission becomes detectable might help confirm this. The central nebula which contains most of the mass ejected in the explosion i.e. is the supernova remnant. No radio synchrotron emission has been detected from the proton(ion)-electron plasma in the main remnant. This is likely due to the large optical thickness of the thermal material to radio emission and one can expect it to become transparent in the near future allowing detection of radio synchrotron emission from the remnant.

3.3.4 Type II SN: SN1993J in M 81

SN 1993J was a supernova of type II which was recorded on 28 March 1993 in the galaxy M 81 located at a distance of about 4 Mpc (Ripero et al., 1993). At this distance, 1 arcsec corresponds to about 20 pc. The optical (BVRI) light curves of SN 1993J showed a double-peaked structure (van Driel et al., 1993) which is commonly observed in type II supernovae. This supernova has been extensively observed at radio wavelengths including high resolution VLBI imaging. The prompt radio emission near 25 GHz

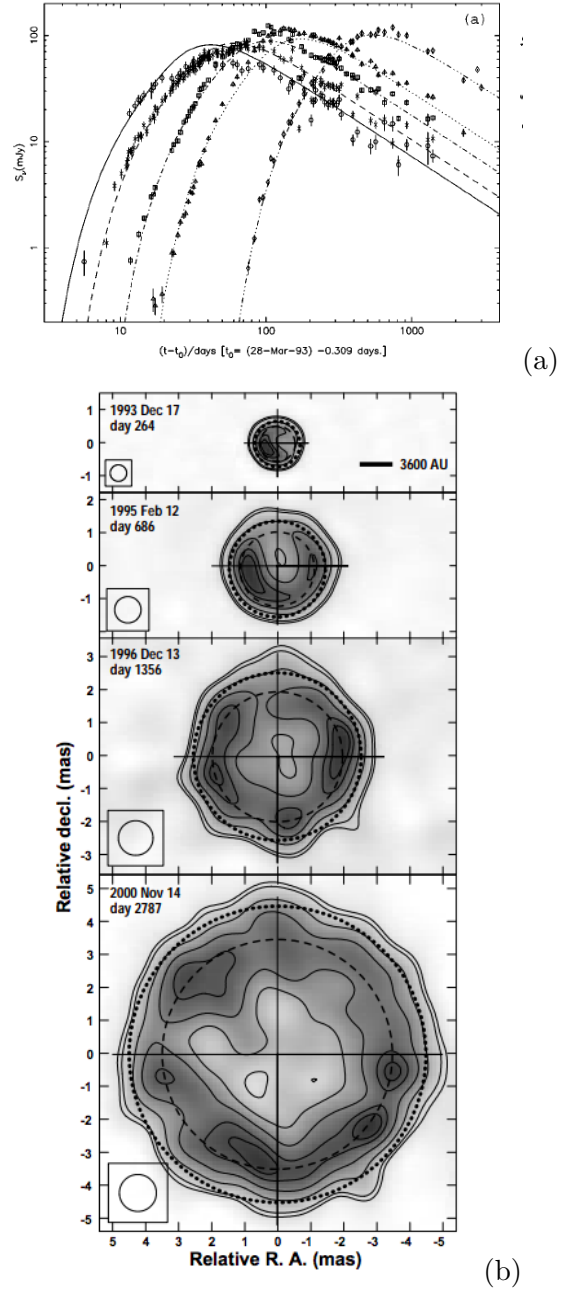


Figure 12: (a) The figure showing the radio light curves of SN 1993J is reproduced from Weiler et al. (2002). Light curves at 22.5 GHz (open circles), 14.9 GHz (stars), 8.4 GHz (open squares), 4.9 GHz (open triangles), 1.5 GHz (open diamonds) are shown. The onset of the highest frequency emission precedes the lower frequencies. (b) The figure showing a few VLBI images at 8.4 GHz of SN 1993J for different epochs is reproduced from Bartel et al. (2002). Notice the shell which should be composed of only positron-electron plasma is similar to a supernova remnant and no central radio component has been detected yet. The image epochs shown in (b) are included in the light curve in (a).

was detected around day 5 while it was detected at 1.4 GHz around day 75 (Weiler et al., 2007). The prompt radio emission from SN 1993J has persisted for more than a decade after its frequency-dependent detection at radio bands (see Figure 12a). The radio emission of SN 1993J at 6 cm peaked around day 132 at ~ 117 mJy whereas it peaked at 20 cm around day 739 at 119 mJy (Weiler et al., 2007). The flux density of SN 1993J at 1.7 GHz measured with the VLBI in 2010 had reduced to 1.7 mJy (Bietenholz et al., 2010a). If the supernova had exploded at a distance of 10 kpc from us, then the recorded peak flux density at 1.4 GHz would have been 19000 Jy while the flux density at 1.7 GHz in 2010 would have been 270 Jy. The radio emission at 8.4 GHz was resolved with VLBI into a shell-like structure on day 175 (Bietenholz et al., 2003). Since then the radio shell has been showing near-symmetrical expansion (see Figure 12b) and its radio synchrotron structure is similar to relatively older shell supernova remnants like Cas A and Tycho. This is not surprising since the spherical radio shell indicates that these supernova explosions have been spherically symmetric and ejected a spherical shell of relativistic plasma which has evolved to the observed symmetric radio shell. The synchrotron radio emission from the older supernova remnants should be emitted by the proton-electron plasma while in SN 1993J, the positron-electron plasma should be emitting. The symmetric shell in SN 1993J also helps us infer that the progenitor star suffered mass loss in the form of a uniform continuous wind so that the circumstellar medium and magnetic field are fairly uniform around SN 1993J. In fact, if one visualises the positron-electron plasma being incapable of sweeping up matter, then the detailed structure of the prompt radio emission in the shell should trace the structure of the underlying circumstellar magnetic field. Interestingly, the rate of decline of radio emission increases from $t^{-0.7}$ to $t^{-2.7}$ beyond about day 3100 with little change in the radio spectral index which remains around ~ -0.8 (Weiler et al., 2007). However (Bartel et al., 2002) find that the radio spectral index flattens from a mean value of ~ 0.85 upto day 1000 to ~ 0.63 observed upto 3164 days (Bartel et al., 2002). More recent data on this supernova, if available, should be able to resolve this issue. Interestingly it was found that the behaviour of the X-ray light curve was similar to the radio light curve so that the X-ray emission also showed a faster decline after day 3100 (Weiler et al., 2007). The shell in SN 1993J was estimated to be expanding with velocities ~ 22500 kms^{-1} early on which reduced to 17200 kms^{-1} around day 30, further slowed down to ~ 8900 kms^{-1} around day 1600 and

to 8700 kms^{-1} around day 3164 (Bartel et al., 2002). Only faintly polarised radio signal is detected from SN 1993J (Bietenholz et al., 2003). *To summarise: prompt radio emission from SN 1993J is resolved into a spherical shell indicating the ejection of a positron-electron plasma radiating in a uniform circumstellar magnetic field. The fast expanding plasma has slowed down to expansion velocities less than 8700 kms^{-1} .*

A radio source due to synchrotron radiation from a proton-electron plasma, coincident with the massive remnant of the explosion is expected at the centre of the radio shell. Unlike SN 1986J, no new synchrotron radio source in the centre of the shell in SN 1993J has been detected (Bietenholz et al., 2003, 2010a). This does not seem to be abnormal since while a radio source has emerged in the centre of SN 1986J, it is yet to emerge in SN 1987A. The detection of the central radio source depends sensitively on the properties of the ejected mass especially the drop in the free-free optical depth which can follow different evolutionary timescales for different supernovae. Since the radio shell in SN 1993J has an extent of only a few milliarcsecs, it has not been possible to ascertain the presence or otherwise of a central optical nebula i.e. a remnant as was possible in SN 1987A. The existence of the remnant has to be surmised from lower angular resolution spectral observations at optical, X-ray and infrared bands. The evolution of the optical spectral features of SN 1993J in the first few years ranged from detection of broad hydrogen lines which weakened over time and the eventual appearance of the nebular spectrum (Matheson et al., 2000). It is noted that from around day 300 or so, a box-like profile was recorded for $\text{H}\alpha$ and a few other elements (Matheson et al., 2000). After day 670 or so, it was noticed that a narrow emission feature had appeared on top of the box-like profiles (Matheson et al., 2000). While the nature of the optical features is intriguing and hence have been difficult to interpret, we can certainly infer that the broad optical features arose in the massive remnant. Infrared emission from warm dust is detected from SN 1993J more than two decades after the explosion (Tinyanont et al., 2016). The formation of dust in SN 1993J is also deduced from the dimming of the red part of the spectral lines of [O III] and from which dust of mass 0.08 to $0.15 M_{\odot}$ was inferred to have formed by 2009 (Bevan et al., 2017). It was found that the dust mass associated with supernova remnants of type II increases as they evolve and that Cas A had formed dust of mass $\sim 1.1 M_{\odot}$ about 330 years after explosion (Bevan et al., 2017). *To summarise: In SN 1993J, the positron-electron plasma that the explosion set forth has been radiating radio synchrotron emission in a spherically symmet-*

ric shell-like structure supporting both a spherical explosion and a uniform density circumstellar medium. Detection of wide optical lines and dust in SN 1993J supports the existence of a supernova remnant which in analogy to SN 1986J and SN 1987A should be in the centre of the observed radio shell. No radio synchrotron source is detected in the centre of the shell indicating that the massive remnant of the explosion is still optically thick to radio frequencies.

3.3.5 Summary

Most type II supernovae are observed to peak at 6 cm within a few hundred days after the explosion whereas type Ib and Ic are observed to peak within 50 days with typical observed peak radio luminosity being between 10^{26} to 10^{29} erg s⁻¹ Hz⁻¹. (see Table 3 in Weiler et al., 2002).

In literature, a supernova explosion is explained by the scenario in which the core starts contracting into a degenerate neutron star and triggers a thermonuclear explosion in the gas outside the core which energises and expels matter from the star. This scenario has been strongly supported by observations. The first signature of the explosion has been observed to be fast neutrinos. We sketch the further evolution of the supernova especially from the radio signatures. We point out that that observations support the ejection of a fast positron-electron plasma followed by a relatively slower proton(ion)-electron plasma in addition to the neutrinos. In fact, most of the radio observations and several multi-band features are easily explained once the inevitability of both the plasma being ejected following the explosion and the expected observational implications of the same are appreciated. It is also possible that both the plasmas are expelled at comparable velocities but the latter suffers larger kinetic losses and quickly slows down. The positron-electron plasma gyrates and radiates in the circumstellar magnetic field and is responsible for the prompt radio emission from a supernova which becomes detectable once the foreground densities in the circumstellar gas have sufficiently declined. The absence of a circumstellar field will lead to absence of prompt radio emission. Although the relativistic electrons in the massive remnant will be radiating in the field frozen in the remnant, we detect this only when the initially large free-free optical depths of the thermal gas mixed with the radio plasma have sufficiently declined. This emission should be what we refer to as the supernova remnant. The frequency-dependent detection of radio synchrotron emission from both the plasma, as was observed in SN 1986J, unequivocally supports the above interpretation. The existence of a faster

positron-electron plasma and a slower remnant is also supported by the observations of SN 1987A wherein an expanding central remnant is detected in dust and in optical bands while the fast plasma is responsible for the prompt radio emission and the currently detectable emission from the inner equatorial ring. The central remnant in SN 1987A continues to be optically thick to radio frequencies but eventually radio synchrotron emission should become detectable from it. In fact, frequency-dependent detection of radio emission from a central component in SN 1987A, SN 1993J and other such supernovae should conclusively support this explanation. The existence of the two types of plasma ejected by a supernova explosion is also supported by the detection of a thin outer rim in X-rays (or optical) and radio synchrotron emission around several old supernova remnants like Cas A, Kepler etc in addition to radio synchrotron emission from the massive remnant. The rim emission is from the positron-electron plasma while the radio emission from the remnant is from proton-electron plasma radiating in the field frozen in the remnant. The rim emission appears to be due to Compton scattering of the annihilation photons to lower energies.

The above discussion also highlights some testable inferences regarding the differences in the supernovae of type Ia and type II: (1) The optical light curves of type II supernovae are generally observed to be double-peaked whereas those of type Ia are single-peaked. This behaviour can be inferred to indicate that the second peak in type II supernovae is due to the central hot star left behind by the explosion. Since no central star is expected in type Ia supernovae, the second peak is also missing. (2) The detected higher expansion velocities of metal-rich knots as compared to the hydrogen/helium-rich wisps in supernova remnants are due to the effect of the radiation pressure exerted on the optically thick metal-rich knots by photons from the central hot star. This feature should, hence, only be detected in remnants which do host a hot object at its centre. Since no central star is expected to be left behind in a type Ia supernova explosion, all the compact features in the remnant should be expanding with similar velocities. This, then also provides an observational method to identify the existence of a central hot object in a remnant.

4 Accreting rotating black holes

In this section we discuss objects which owe several of their characteristics to energy input from phenomena near black holes. Black holes are objects wherein matter densities are so large (larger than in

neutron stars and white dwarfs) that matter is compressed into a volume much smaller than a sphere of Schwarzschild radius (R_s) defined by the mass of the object. The fictitious surface of a black hole is referred to as the event horizon. Since the velocity required by matter or light to escape from the region inside the event horizon is greater than the velocity of light, nothing can escape from the black hole and anything which falls through the event horizon of the black hole is trapped forever. For a static black hole, the event horizon is the sphere of radius R_s . For a rotating black hole, the event horizon is prolate-shaped and the sphere of radius R_s is referred to as the ergosurface with the region between the event horizon and ergosurface referred to as the ergosphere. The escape velocity from the ergosphere is equal to velocity of light and hence electromagnetic radiation can escape from it as is observationally supported by the spectral lines showing a gravitational redshift greater than 0.5 which are regularly detected in the quasar spectra and which have to necessarily arise from a region with a separation less than R_s from the black hole (Kantharia, 2016a). The gravitational potential ($\phi = GmM_{BH}/R_s$) experienced by a particle of mass m at the Schwarzschild radius R_s will be same for a stellar mass or a supermassive black hole - this is because the ratio $M_{BH}/R_s = 1/3 M_\odot \text{ km}^{-1}$ is the same for black holes of all masses. In other words, as the mass of the black hole increases, its Schwarzschild radius also increases so that the ratio M_{BH}/R_s is a constant. An important physical implication of this is that it should lead to similarity and uniformity in the physical properties of phenomena in the immediate vicinity of the black hole irrespective of its mass and the observed differences will be due to the differing linear dimensions of the systems.

Some of the well known black hole-powered objects are microquasars and active galactic nuclei (active galaxies). Microquasars are stellar mass black hole binaries and are mostly detectable in the near universe while phenomena associated with supermassive black holes can be probed to cosmological distances. Microquasars should exist in distant galaxies but their small size and hence lower energy phenomena might not allow their detection from the distant universe except occasionally during high energy transient flares. A supermassive black hole e.g. $\sim 10^8 M_\odot$ will have $R_s \sim 3 \times 10^8 \text{ km}$, whereas a stellar mass black hole e.g. $\sim 20 M_\odot$ will have $R_s \sim 60 \text{ km}$. Such widely different linear scales will lead to differences in global accretion rate, total energy budget, angular sizes and hence detectability. The phenomena associated with black holes emit over almost the entire electromagnetic spectrum from γ -rays to

radio bands. Synchrotron emission is detected in many such high energy phenomena indicating that such processes always generate relativistic electrons and that magnetic fields are ubiquitous. Radio synchrotron emission is commonly detected from many active nuclei, microquasars and is the only diagnostic, currently available to us, for studying relics and halos in clusters. These strong synchrotron radio emitters are discussed in this section. We follow the inferences from (Kantharia, 2016a) and (Kantharia, 2017) especially regarding the origin of (1) relativistic particles, (2) accretion disk and bipolar jets and (3) degenerate matter surface around the event horizon of a black hole. These were summarised in the introduction.

We begin the discussion with microquasars. Although these were identified much later than active nuclei, the extensive and unique observational results that exist on microquasars shed significant insight on the physical processes that occur near accreting black holes. We follow it up with a discussion on active nuclei and on the origin of radio relics and lobes in clusters of galaxies. A physical model that derives from observational results is included for the aforementioned objects and is used in understanding particular examples. As in earlier papers, the aim throughout has been to look for consistent and cohesive explanations of observational results within the framework of known physics instead of contrived and exotic ones in unknown physics. It should be added that it has been possible to conduct this study due to the careful observational results and inferences by several scientists.

4.1 Microquasars

Microquasars are binary stellar systems consisting of an accreting compact object like a black hole and a gaseous companion. The name seems to capture the essence of their observational properties in the sense that these are stellar-size versions of a quasar or a radio-loud active nucleus. Microquasars display stellar-like compact appearance but are much brighter in the optical and X-ray bands, are variable, host radio jets and are not located at the centres of galaxies. Another category of such point-like sources which are extremely bright in X-rays ($L_X > 10^{39} \text{ erg s}^{-1}$ in a band like $0.3 - 8 \text{ keV}$) and are not located at the centres of galaxies are the ultraluminous X-ray sources (ULX). It is believed that ULX are binaries which either host an accreting intermediate mass black hole ($10^2 - 10^5 M_\odot$) or an accreting stellar mass black hole. Since the known microquasars are fainter than ULX in the X-rays, these have been considered as different class of objects. ULX are rare

with none having been detected in the Milky Way and generally only one ULX being detected in most galaxies. There do exist exceptions such as the ring galaxies Cartwheel and NGC 922 which host several ULX sources mostly located in the star forming ring or other star forming regions in the galaxy (Wolter & Trinchieri, 2004; Prestwich et al., 2012).

Microquasars were identified and named as such when radio jets and lobes were detected around the Galactic source 1E1740.7-2942 (Mirabel et al., 1992). Astrophysicists have long appreciated the fact that if we can better understand the physical mechanisms active in these nearby objects, we might be able to improve our understanding of extragalactic quasars and active nuclei. More than 40 microquasars have been identified in our Galaxy (Mirabel, 2012). A few notable Galactic microquasars are SS 433, GRS 1915+105, Cygnus X-3 and Scorpius X-1. We briefly include a few interesting observational results on these microquasars and then discuss the results on SS 433 in detail. Several microquasars have been monitored at radio bands (e.g. Trushkin et al., 2017a) and other wavebands over long periods which has resulted in a database of simultaneous multi-frequency observations. Radio jet blobs are observed to expand at relativistic velocities ranging from superluminal in GRS 1915+105 (Mirabel & Rodríguez, 1994) to $0.45c$ in Scorpius X-1 (Fomalont et al., 2001) to $0.25c$ in SS 433 (Margon et al., 1979a) and which if interpreted as the escape velocity of the blob from the compact object ($v_{esc} = c/\sqrt{n}$ where n indicates the radial separation of the launching region from the black hole in units of R_s) would mean that these were launched from regions separated by less than $16R_s$ from the compact object. In Table 1, the separation from the black hole for different jet velocities (assuming they represent the escape velocity from the black hole) and the gravitational redshift that should be shown by a line photon ejected from that separation are listed.

4.1.1 Summary of observed features

The observed features of microquasars can be summarised as follows:

- A bright star-like object displaced from the centre of the galaxy which is bright in multiple wavelengths including radio.
- Multi-band variability observed on timescales of minutes to hours.
- Presence of a radio core, relativistically expanding radio jets, fast radio variability and radio flares often showing some form of correlation with X-ray and γ -ray emission.

Table 1: The connected nature of the separation from the black hole $R = nR_s$, escape velocity required by matter to overcome the gravity of the black hole $V_{esc} = c/\sqrt{n}$, the gravitational redshift $z_g = 1/(2n)$ that line photons will suffer when emitted from R is shown here. In the last column the intrinsic redshift that will be shown by the line photon emerging at R is listed. Within the ergosphere, $V_{esc} = c$.

| V_{esc} | R | z_g | z_{in} |
|-----------|-----------|---------|----------|
| 0.1c | $100R_s$ | 0.005 | 0.005 |
| 0.25c | $16R_s$ | 0.03125 | 0.03226 |
| 0.5c | $4R_s$ | 0.125 | 0.143 |
| 0.75c | $1.78R_s$ | 0.281 | 0.391 |
| 0.9c | $1.23R_s$ | 0.4065 | 0.6849 |
| 0.99c | $1.02R_s$ | 0.49 | 0.9608 |

- Microquasars are seen to be either in a radio quiescent state wherein they maintain a constant flux density or a radio flare state wherein they rapidly brighten. Such flaring is also observed in other bands.
- Microquasars display a hard spectral state in which hard X-rays due to non-thermal processes dominate and a soft spectral state wherein soft X-rays due to a thermal process dominate the X-ray emission.
- Most microquasars show a correlation between the radio and X-ray states. A microquasar in a hard X-ray state shows persistent radio synchrotron emission from the jets which seem to be disrupted in the soft X-ray state e.g. Cygnus X-1. However the opposite is also at times observed to occur.
- High resolution milliarcsec radio images of microquasars show a sequence of events - the core gets brighter and increases in size, a component detaches from the core and the core gets fainter, the component starts expanding away from the core at relativistic velocities, sometimes such a phenomenon is also noted on the opposite side of the core either simultaneously or with a delay, the component(s) expand, diffuse out over some timescale and eventually become undetectable. The sequence of events is not periodic but is often observed to repeat on timescales ranging from hours to days to years.
- The range of observed properties of microquasars: jet sizes range from 10 to 5×10^5 astronomical units, the jet radio luminosity ranges from 10^{24} to 10^{26} W (e.g. Spencer et al., 2001), the jet bulk velocities appear to range from

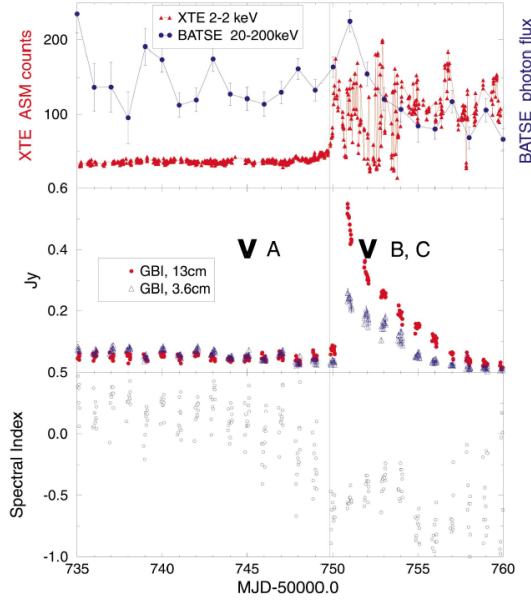


Figure 13: Figure showing light curves of the microquasar GRS1915+105 reproduced from Dhawan et al. (2000). The X-ray (top) and radio (middle) light curves range from 14 October to 8 November 1997 during which a flare was recorded. The variation in the radio spectral index is shown in the bottom panel and the change from a flat spectrum to a steep spectrum during the flare can be seen.

0.25 c to superluminal. While the radio jets in some microquasars are long-lived, in others they rapidly fade.

- The flat radio spectrum of the core in GRS 1915+105 is always resolved into a compact jet in high resolution observations and the radio emission consists of a compact jet (AU-scale) and a large scale jet (several 100 AU-scale) with superluminal motion being registered in the large scale jet (Dhawan et al., 2000). Coeval radio and X-ray observations of GRS 1915+105 have provided some interesting results as noted in Dhawan et al. (2000) such as (a) a plateau/quiescent state is observed in which the radio spectrum is flat and the radio source is compact (few AU) with typical radio flux densities 10-100 mJy and a constant flux of X-ray emission in the 2-12 keV band and (b) a flare state is observed in which the radio emission brightens upto a Jansky at a wavelength of 13 cm within a day, the flat spectrum transitions to an optically thin synchrotron spectrum and the X-rays between 2-12 keV brighten and show fast variability (see Figure 13). The source in the flare state reverts to the radio plateau phase in a few days (see Figure 13). Their study of GRS 1915+105 prompted Dhawan et al. (2000) to suggest that the unresolved flat spectrum core

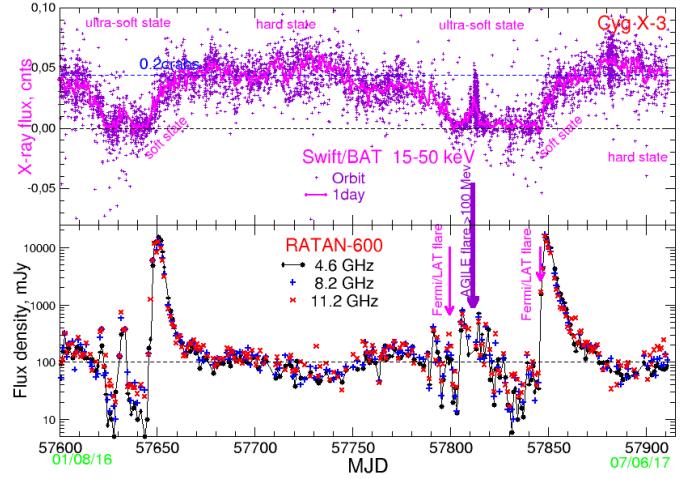


Figure 14: Figure, showing the evolution of radio and X-ray emission of the microquasar Cygnus X-3, reproduced from Trushkin et al. (2017b). A giant radio flare is often seen to occur at the end of the ultra-soft X-ray phase which is characterised by weak hard X-ray emission and constant soft X-ray emission. In the radio flares, the mean quiescent flux density of ~ 100 mJy increases to ~ 20 Jy. The excellent coincidence of a giant radio flare and the γ -ray flare is also marked in the figure.

is a compact, quasi-continuous synchrotron jet and that both a steady jet and episodic ejections are observed from GRS 1915+105.

- From VLBI observations of Cygnus X-3, it is inferred that the microquasar has milliarcsecond jets expanding at 0.25 c with an opening angle of 80° and is radio variable (Molnar et al., 1988). In Cygnus X-3, the correlation of radio flares (Trushkin et al., 2016b,c) with γ -ray flares (Cheung & Loh, 2016) have been well established (see Figure 14) with the γ -ray flares preceding the radio flares by a few days. It has been noted that the radio emission dips below the mean value just before a radio flare occurs so that the radio dip is a precursor of a flare (Waltman et al., 1994) (see Figure 14). Frequent radio flares are also recorded from SS 433 (e.g. Trushkin et al., 2016a) although these are fainter than in Cygnus X-3.
- The microquasar Circinus X-1 displays curved radio jets (Stewart et al., 1993).
- Scorpius X-1 shows ejection of blobs on opposite sides of the radio core which then move out and disappear over a day or so and another pair emerges from the core with the north-east component generally being brighter (Fomalont et al., 2001). The ejected blobs move outwards with constant but distinct velocities ranging from 0.31 c to 0.57 c (Fomalont et al., 2001).

Radio variability on timescales of hours is noted which is explained by the VLBI images which show the blobs forming in the core as can be surmised by its brightening, the blob being detached and moving away from the core and eventually disappearing (Fomalont et al., 2001).

- The electron-positron annihilation line at 511 keV has been observed from the microquasars - 1E 1740.7-2942 (Bouchet et al., 1991; Sunyaev et al., 1991), Cyg X-1 (Ling & Wheaton, 1989), V404 Cygni (Siebert et al., 2016) and Nova Muscae in which the annihilation line persisted for at least 10h (Sunyaev et al., 1992; Goldwurm et al., 1992).
- The microquasars 1E1740.7-2942 and GRS 1758-258 located close to the Galactic centre, are persistent soft γ -ray (30 – 500 keV) sources and host double-sided radio jets extending upto a few parsecs but no optical or near-infrared counterparts have been detected (e.g. Mirabel, 1994).

4.1.2 A comprehensive explanation

Here we use the inferences that can be drawn from multi-band observational data on microquasars and existing laws of physics to present a simple physical model for microquasars. The model builds on the already known aspects of microquasars so that a consistent explanation for the myriad observed phenomena emerges.

The most likely compact object which would be responsible for microquasars appears to be black holes as in active nuclei. One of the most important reasons for this is the mass and hence size of the system. A neutron star is generally expected to be less than $2\text{--}3 M_{\odot}$ in mass with a radius of about 10 km i.e. around $3R_s$. However if it is a stellar black hole, it can be $10\text{--}30 M_{\odot}$ or maybe more and R_s will range from 30 to 90 km or more. The larger surface area in the higher gravitational potential at R_s as compared to neutron stars can lead to more energetic and hence detectable phenomena. The detection of radio jets expanding with velocities in excess of $0.45c$ which is equal to the escape velocity from the compact object could mean that the ejection happens from within $5R_s$ of the compact object. If the compact object was a neutron star which are known to have an extremely large magnetic field, it is likely that either the field or some effect of the magnetic field would have been detectable on the core and jet emission. However no such effect seems to be present as seen from the uncanny similarity between the microquasar jets and jets in active nuclei. Hence it appears more likely

that the compact object in all microquasars is a massive stellar-mass accreting black hole and we assume the same. The companion is a gas-rich star from which the black hole is spherically accreting matter.

The jets in microquasars are bipolar indicating the presence of an accretion disk in the equatorial regions of the black hole. This then indicates a rotating black hole which has led to a latitude-dependent accretion rate so that over time an accretion disk has formed. A bright soft X-ray and optical core is often detected in microquasars indicating the presence of a hot degenerate matter surface, emitting black body radiation, which has formed outside the event horizon of the black hole from the infalling matter. We refer to this surface as the pseudosurface of the black hole as was done for the supermassive black hole in quasars. Thermal emission is generally detected in soft X-ray to infrared wavelengths. Any form of instability in the pseudosurface of the black hole should be detectable as variability in the thermal continuum from X-rays to infrared wavelengths. This instability would not lead to variability in the radio bands. The relatively high accretion rates in the polar regions of the rotating black hole should lead to accumulation, compression and heating of matter in a small circular polar region. The process is similar to the accreting white dwarf in novae except the accretion on white dwarfs appears to be predominantly over the entire surface due to their slower rotation. Taking cue from novae, when temperatures of 100 million degrees or higher are achieved in the lower layers of the accreted fuel in the polar regions of the pseudosurface, these should ignite in an explosive thermonuclear reaction. If hydrogen ignites, then energy released is expected to be 6×10^{18} ergs gm^{-1} and if elements heavier than hydrogen like carbon and oxygen ignite when temperatures beyond billion degrees K are reached, then energy released is expected to be 5×10^{17} ergs gm^{-1} (Hoyle & Fowler, 1960). While the energy release in the fusion of heavier elements can be achieved within 1-100 seconds, it takes longer for hydrogen fusion (Hoyle & Fowler, 1960). Thermonuclear explosions have long been identified as a process which can instantaneously release huge quantities of energy (Bethe, 1939; Hoyle & Fowler, 1960; Mestel, 1965) and has successfully explained the outbursts in classical, recurrent novae and supernovae. When physical conditions of temperatures and densities in the accreted matter on the pseudosurface of a black hole which has been accreting normal matter from its companion become similar to that on the accreting white dwarf in a nova then a thermonuclear explosion has to be the most likely physical process that should occur. We suggest that is pre-

cisely what occurs in the polar regions of the accreting black hole. The thermonuclear process can instantaneously inject energy on very short timescales and hence energise and eject matter at high velocities. This, then, is similar to the ejecta that erupts from the nova following the thermonuclear explosion and eventually forms a shell around the star. The difference in the rotation speeds of the compact object i.e. the fast rotation of the black hole leads to extreme bipolarity of the ejected matter in form of collimated jets in microquasars. This is due to the variation in the accretion rates across the pseudosurface and the presence of an accretion disk. This process then trivially explains the formation of relativistic synchrotron jets and optical line forming regions both of which are directed outwards along the polar axis and observed in SS 433 to be expanding with velocities of $0.25c$. The ejected matter moves away from the compact object along jets. As long as the black hole keeps accreting matter, thermonuclear explosions will keep occurring which will release energy and propel matter outwards along the jet. The local conditions should determine the frequency of explosions and eruptions from the polar regions for a given system and which explains the continuing ejection of blobs/knots of radio emission which is observable with VLBI in several microquasars (e.g. Scorpius X-1, GRS 1915+105). On formation, these knots of emission might be obscured due to free-free absorption or synchrotron self-absorption which eventually decreases as it is ejected and expands leading to frequency-dependent detection with higher radio frequencies being detected earlier as is often observed (see Figure 15b). It also explains the behaviour shown by GRS 1915+105 wherein in quiescence the radio emission shows faint emission with a flat spectrum which evolves to bright optically thin synchrotron emission with a steep spectrum during a flare (see Figure 13). Similar frequency-dependent behaviour is regularly observed in supernovae and novae. From similar arguments, the accreted matter in the non-polar regions should also ignite although the lower accretion rates might lead to infrequent eruptions. This might explain the occasionally observed extended radio emission in the equatorial regions of SS 433. *To summarise, the energy source of jets and optical line forming gas observed in the polar regions of a microquasar is a thermonuclear outburst in the accreted matter on the pseudosurface of the black hole.* Variability in the radio synchrotron emission will result from the varying jet characteristics such as a new knot/blob being energised and ejected. This can also explain variability in the hard synchrotron X-rays and γ -rays when the latter are generated by

the inverse Compton process.

The axis of the rotating black hole often shows precession, so that the jet direction changes (e.g SS 433), which can be understood as being due to the gravitational torque exerted by the companion star as they orbit each other.

The separation of the line forming matter from the black hole will determine the gravitational redshift (z_g) component in the spectral line redshift. If it is located several hundred R_s away, then there will be a negligible contribution of gravitational redshift to the observed redshift of the line. However if the photon emerges very close to the black hole then the contribution can be significant. The expansion velocities when estimated from the proper motion of blobs in the jets of microquasars are found to be relativistic. Assuming these are comparable to the escape velocity from the black hole, it would mean that the observed redshift of the line photons emitted from the jet launching site should include a gravitational redshift component. In Table 1, the z_g (and the intrinsic redshift z_{in}) of a line forming at different separations from the black hole are listed. As listed in Table 1, a jet which is launched from a separation of $4R_s$ will need to be ejected with at least $0.5c$ to be able to escape the black hole while a spectral line forming at $4R_s$ will experience a gravitational redshift of 0.125 (intrinsic redshift = 0.143) due to the strong gravitational potential of the black hole. This means that the spectral line from the microquasar would be observed at a redshift of about 0.7.

The frequent recurrence of radio blob/knot ejection in microquasars over hours/days indicates frequently recurring thermonuclear outbursts in the accreted matter on the black hole in the X-ray binary. The behaviour is reminiscent of dwarf nova outbursts which recur over timescales of days and last over timescales of days so that the optical brightening is short-lived. It was suggested that these small amplitude outbursts in dwarf novae are also caused by thermonuclear explosions which are not sufficiently energetic to expel matter and only succeed in expanding the accreted envelope which eventually contracts (Kantharia, 2017). This is expected since the accreted matter on the white dwarf (or black hole) which is already heated to high temperatures can be repeatedly ignited leading to an inflation of the outer envelope till nucleosynthesis leads to formation of iron or a sufficiently energetic explosion occurs which succeeds in ejecting the envelope. This also means that for the few microquasars that we observe with radio jets and cores, there might exist many more which are like dwarf novae in that the thermonuclear outburst is not sufficiently energetic to expel matter

and the thermonuclear reaction enriches the accreted matter but seldom expels it.

This discussion then concludes that (1) the main source of black body continuum emission from the microquasar is the hot pseudosurface of the black hole. This is mainly detected at wavelengths ranging from soft X-rays to infrared, (2) the main transient source of energy in microquasars is a thermonuclear outburst which leads to jet launching consisting of relativistic plasma and optical line emitting gas, (3) the main source of synchrotron continuum emission is the relativistic plasma ejected from the pseudosurface following the thermonuclear explosion. This emission dominates at hard X-ray and radio wavelengths, (4) the redshift of the line photons emerging from the jet launching location should also include a gravitational redshift component, (5) in some microquasars, frequent thermonuclear explosions can enrich the accreted matter instead of ejecting it.

In the next section we use this model to understand the detailed observational results on SS 433.

4.1.3 Case Studies

We discuss, in detail, the case of SS 433 which is very well observed and has provided us important insight into phenomena that occur close to accreting black holes. We then discuss the case of the short γ -ray burst GRB 170817A which was detected in the galaxy NGC 4993 on 17 August 2017 and sparked off wide-ranging observations, simulations and interpretation. It was interpreted to be a signal from the merger of two neutron stars - we investigate if the observational results can also be explained by a better understood physical process since GRBs are fairly common in the universe. In an earlier paper (Kantharia, 2016a), the similarity between quasar spectra and the afterglow spectra of several GRBs was pointed out and it was suggested that GRBs are energetic transient events on quasars. We continue this line of argument which can be generalised to suggest that GRBs are transient events on a black hole and examine if GRB 170817A could have occurred on a microquasar in NGC 4993. It is to be noted that the only fast source of huge quantities of energy that has been well established from theory and observations, is a thermonuclear outburst when a large quantity of matter is simultaneously ignited.

4.1.3.1 SS 433 in Milky Way : SS 433 is a microquasar at a distance of about 5 kpc, is luminous in the optical ($V=14.2$ magnitudes) and has been estimated to have a large line-of-sight extinction of $A_v = 8$ magnitudes (Margon, 1984). The star-like

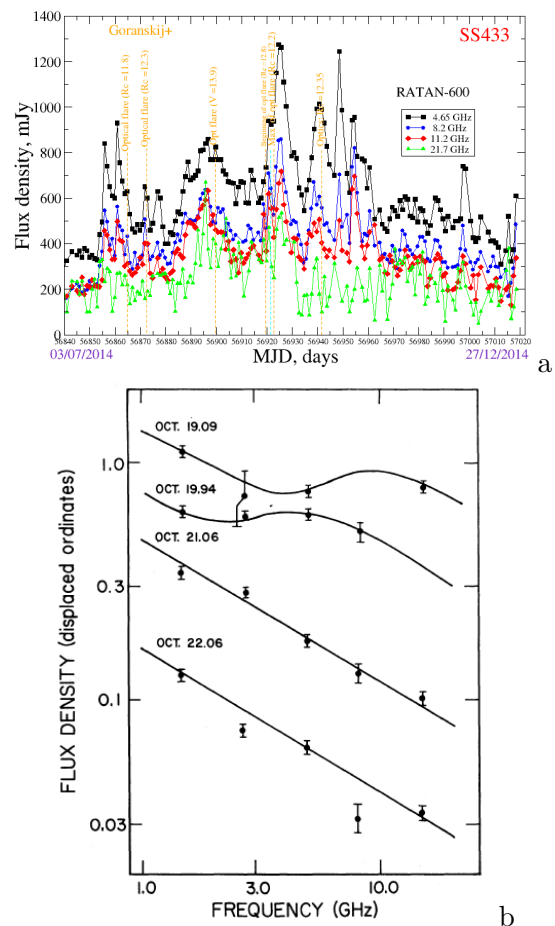


Figure 15: (a) The evolution of radio flux density of SS 433 shows the occurrence of multiple radio flares and coincident optical flares. Figure reproduced from Trushkin et al. (2014). (b) Figure copied from Seaquist et al. (1982) showing the varying radio spectrum of SS 433 during a flare with changes recorded within a day.

object which had been independently detected in the optical, radio and X-ray bands was shown to correspond to the same system and it was suggested that it might be connected to the supernova remnant W 50 (Clark & Murdin, 1978). The similarity of SS 433 to Circinus X-1 was pointed out (Clark & Murdin, 1978).

Some of the other observed properties of SS 433 can be summarised to be:

- Multi-band variability is recorded in SS 433.
- The orbital period of the binary is measured to be around 13 days (Crampton et al., 1980).
- It was noted that three optical spectral features from SS 433 were found to move in velocity space by about 25000 km s^{-1} in 28 days (Margon et al., 1979b). Further observations showed that there existed two sets of hydrogen Balmer lines and He I lines with one pair showing large and changing redshift and the other pair showing large

and changing blueshift with the variations being periodic over a 164 day duration such that the maximum positive and negative velocities were 50000 km s^{-1} and -35000 km s^{-1} respectively and these were symmetric about a red-shift of ~ 0.04 ($\sim 12000 \text{ km s}^{-1}$) (Margon et al., 1979a). These were explained by Doppler shifted lines arising in oppositely directed precessing jets/clouds expanding at velocities of $\sim 0.26c$ oriented at an angle of about 65 degrees to the line of sight with this being referred to as the kinematic model for SS 433 (Abell & Margon, 1979; Fabian & Rees, 1979; Milgrom, 1979; Margon et al., 1979a).

- Broad emission lines of widths $\sim 4000 \text{ km s}^{-1}$ were detected from SS 433 (Clark & Murdin, 1978). The spectrum consisted of unshifted wide Balmer lines of hydrogen whose equivalent widths are variable, He I, He II and several other lines (Margon, 1984).
- Occasionally the shifted features are absent from the spectra for several days and they also undergo fast intensity changes with the changes in the blue and red-shifted components being quasi-simultaneous (Margon, 1984). It was observed in data from 1983 that the moving line velocities increased to $0.3c$ and then disappeared from the spectrum for some time (Margon et al., 1984).
- Radio emission is detected from SS 433 (Ryle et al., 1978; Seaquist et al., 1979) and is variable (see Figure 15). The radio spectrum of SS433 between 1 and 10 GHz changes within a day during a radio flare (Seaquist et al., 1982) (see Figure 15b). On many days the spectrum is a power law, on other days it is absorbed at the lowest frequencies and on still other days it shows enhanced emission at the higher frequencies so that the spectrum becomes flatter (see Figure 15b).
- The radio source consists of double-sided milliarcsec jets (see Figure 16a) which are observed to precess (Hjellming & Johnston, 1981). The entire source is located at the centre of the large supernova remnant W 50 and is believed to be the compact object formed in the supernova explosion whose remnant is W 50. Extended radio lobe-like structures are seen surrounding a spherically symmetric W 50 along the jet axis of SS 433 and are often referred to as the radio ears of W 50 (see Figure 16b).
- Combining the data from radio synchrotron and optical line emitting gas has helped constrain

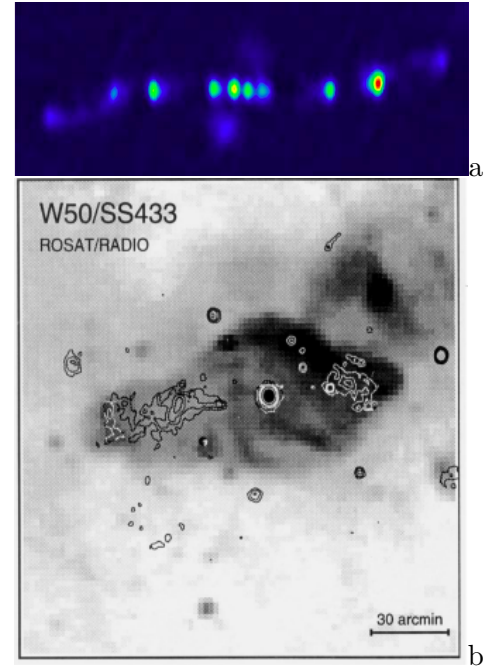


Figure 16: (a) VLBA image of SS 433 (Credit: Mioduszewski et al., NRAO/AUI/NSF). Knots in the precessing jet are noticeable as is the emission extending outwards from the equatorial regions. (b) The ROSAT X-ray contours superposed on radio emission at 11 cm in grey scale copied from Brinkmann et al. (1996). The entire structure hosting radio jets shown in (a) is contained within the central bright X-ray core in (b).

most of the parameters of the system. The jets precess on a cone of half-angle 20° over a period of about 163 days and the central axis of this cone is inclined by 79° to our sightline *Since both the relativistic plasma and optical line emitting gas support this, it tells us that the thermal gas in which the lines form and the relativistic plasma which is observed as the radio jet have to part of the same relativistic ejection from the microquasar.* From the width of the emission lines and assuming a conical geometry, the optical jets are found to be highly collimated with an opening angle of $1^\circ - 1.4^\circ$ (Borisov & Fabrika, 1987).

- The optical line emitting regions occupies a smaller volume than the radio emitting region. The relative narrowness of the moving optical lines indicate highly collimated jets.
- The first X-ray imaging observations indicated that 90% of the soft X-ray (1-3 keV) emission was coincident with the optical object while the rest arose in two extended jet/lobe-like regions about $\sim 30'$ long and aligned along the major axis of W 50 and which established the connection between SS 433 and W 50 (Seward et al.,

1980; Watson et al., 1983). The X-ray emission in the jets/lobes is much softer than from the central source (Watson et al., 1983). The position angle of the radio jets on arcsecond scales (e.g. Hjellming & Johnston, 1981), of the X-ray lobes on several arcminute scales (e.g. Watson et al., 1983) and the major axis of W 50 on several arcminute scales are all measured to be around 100° (see Figure 16). The east-west extend of the radio source in W50 is about 2 degrees which at a distance of 5 kpc is about 175 pc.

- Variability of short timescales $\sim 2 - 8$ minutes are detected at radio, infrared and X-ray band (Chakrabarti et al., 2005).
- Radio and optical flares in SS 433 are observed to be coincident (e.g. Trushkin et al., 2014) as shown in Figure 15a.
- The evolution of the radio knots in the two jets are independent (Schilizzi et al., 1984). It was suggested that the knotty radio emission in jets is related to flare activity in SS 433 (Schilizzi et al., 1984).
- The radio spectrum of SS 433 shows a turnover at low frequencies ~ 150 MHz (e.g. Broderick et al., 2018).
- No radio emission is detected from the core of SS 433 in high resolution images which has been inferred to be due to synchrotron self-absorption and free-free absorption (Paragi et al., 1999).
- Spatially resolved γ -ray photons upto 25 TeV have been detected from the lobes of SS 433 near the X-ray peaks (HAWC Collaboration et al., 2018). The emission from radio bands to TeV energies are all compatible with the same population of electrons in a magnetic field of about $16 \mu\text{G}$ (HAWC Collaboration et al., 2018).

SS 433 is the only source wherein the discrete plasma blobs emitting radio synchrotron and ionized gas emitting moving optical lines have been observed to be moving outwards with the same relativistic velocity i.e. $0.26c$. In most other microquasars, only the radio blobs in the jet are observed to be expanding relativistically. The black hole in the SS 433 will accrete matter which rapidly accumulates on the poles of its pseudosurface due to the highest possible accretion rates. When favourable physical conditions are achieved, a thermonuclear explosion in the accreted matter on the poles of the pseudosurface will

occur, energising and ejecting matter. Since the radio blobs are seen to expand away from the black hole, it tells us that the matter has been ejected with velocities equal to or exceeding the escape velocity. For simplicity, we assume that the matter is ejected at the escape velocity which implies ejection from a region separated by about $14.8R_s$ from the black hole. The detection of both radio synchrotron blobs and optical lines expanding at $0.26c$ gives a rare insight into the properties of matter that is launched from the polar regions in the vicinity of the black hole. Such ejections consisting of both relativistic plasma and thermal ionized matter are commonly observed in supernova explosions whereas ionized matter is always ejected in classical nova outbursts. As was pointed out in the discussion on supernovae, the energetic ejection of matter following the thermonuclear explosion consists of three components - neutrinos, a fast positron-electron ejecta and a slower proton(ion)-electron ejecta and observational results strongly supported the existence of the two plasma with different compositions. The same should be expected as a result of the thermonuclear explosion on the black hole pseudosurface. SS 433 has provided crucial evidence on the ejection of the proton(ion)-electron plasma in which the optical lines form. Since the optical line forming gas in SS 433 is observed only close to the black hole and not along the entire length of the radio jet, it could signal its rapid slowing down after ejection at $0.26c$. This, then would indicate that the knotty radio emission that travels at $0.26c$ a long way from the core of SS 433 is due to the fast positron-electron plasma that was also ejected. Although the annihilation line has not been detected in SS 433, its detection from other microquasars (e.g. 1E1740.7-2942) lends strong support to the presence of positrons in microquasars. The few microquasars which are detected as persistent soft γ -ray sources also support this inference. *To summarise, the accreting black hole in SS 433 undergoes repeated thermonuclear outbursts which expels a proton(ion)-electron and positron-electron plasma at $0.26c$. The proton(ion)-electron plasma from which optical lines emerge rapidly slows down whereas the positron-electron plasma continues at high velocities over long distances.*

The expected gravitational redshift that a photon emerging from a region separated from the black hole by $14.8R_s$ should show is 0.034. The moving optical lines from SS 433 are observed to be varying about a constant redshift of about 0.04 i.e. $\sim 12000 \text{ kms}^{-1}$. If we assume this is the intrinsic redshift due to a gravitational redshift component, then it translates to a gravitational redshift of 0.0384. The compara-

ble values of the observed redshift (0.0384) and the expected gravitational redshift (0.034) from escape velocity arguments give independent support to ejection of matter from a separation $\leq 14.8R_s$ in addition to explaining the origin of the observed redshift of 0.04 over which the moving optical lines are observed to be symmetric. This region located close to the black hole will have a finite thickness in which the gravitational redshift will change. Even small changes in the properties of this region can lead to detectable changes in the gravitational redshift component and escape velocity of the matter. For example, if the launching region moved closer to the black hole, the escape velocity required would increase. If at this location, the explosion energy is unable to accelerate matter to the escape velocity, then the ejection would not occur which can explain the occasional disappearance of the optical lines. If ejection does happen from this region then it explains the occasional appearance of the moving lines at velocities in excess of $0.26c$. Thus a gravitational redshift origin for the excess redshift of 0.04 is able to explain several observations of SS 433. Interestingly soon after the detection of the shifting optical lines, there were suggestions that the observed velocities of the shifting lines are a combination of Doppler shifts and gravitational redshift (e.g. Milgrom, 1979). However this proposed gravitational redshift component was not connected to the redshift over which the lines are symmetric i.e. 0.04.

The coincidence of radio flares with X-ray and/or γ -rays can be expected if the emission is due to processes involving relativistic electrons. No correlation would be observed if the emissions involve completely independent processes. For example, the radio flares and soft X-ray will not show any correlation if the former is due to synchrotron process at the poles and the latter is due to thermal emission from the pseudosurface unless there was a connection between the two, say through the thermonuclear explosion which heats up the entire pseudosurface and also accelerates the electrons to relativistic energies.

The two poles are separated by the accretion disk and will hence not undergo simultaneous ejection events. Since both poles will have high accretion rates compared to other parts of the pseudosurface, the thermonuclear blasts and ejections will be frequent but quasi-simultaneous. This explains the independent behaviour of the jets that has been observed in SS 433. The similar shifts in the velocity of the optical lines indicate that the ejection from both poles happen from a launching region separated from the black hole by about $14.8R_s$.

To summarise: The ejected proton(ion)-electron

plasma is detected in SS 433 in the form of Doppler shifted optical lines. These lines and radio synchrotron blobs are observed to expand with a relativistic velocity of $0.26c$ which is shown to be the escape velocity at a separation of $14.8R_s$ from the black hole. It can be inferred that matter is launched from this separation. The line photons emerging at this distance would show a gravitational redshift of about 0.034 (intrinsic redshift will be 0.035) which is close to the observed value of about 0.04 lending strong support to this explanation. The observed flares are when a new component of relativistic plasma is ejected.

4.1.3.2 GRB 170817A in NGC 4993 : GRB 170817A which was detected by Fermi-GBM on 17 August 2017 became one of the most famous short γ -ray burst (GRB) due to its linking to a source of gravitational waves GW 170817 which had been recorded a couple seconds prior to it by LIGO (Abbott et al., 2017a). The GRB became more famous when a bright optical transient source AT 2017go was detected in the S0 galaxy NGC 4993 within 11 hours of the GRB within the angular region defined by the large observing beams of the two instruments (Coulter et al., 2017). It was suggested that all these were signals from the same source and since the source of gravitational waves which was localised to a region of area 31 square degrees, was linked to merging of two neutron stars at a luminosity distance of 40 Mpc as deduced from templates of gravitational wave signals, the electromagnetic signals also got linked to the same source (Abbott et al., 2017b).

The electromagnetic signals associated with GRB 170817A consisted of three components - (1) a relatively faint short γ -ray burst, (2) bright thermal emission at ultraviolet, optical, and infrared bands which is detected a few days after the GRB and fades by day 110. This emission component is known in literature as a kilonova and (3) a synchrotron component which dominates radio and X-ray bands at all epochs from around day 9, peaks in both bands around day 160 and then declines. A constant spectral index of ~ 0.585 fits the synchrotron spectrum from X-ray to radio bands at all epochs (Margutti et al., 2018a). Figure 1 in Margutti et al. (2018a) shows the wide band spectral energy distribution between day 9 and day 160 where the distinct nature of the kilonova and the synchrotron emission are identifiable. The X-ray luminosity on day 160 was estimated to be $\sim 5 \times 10^{39}$ ergs $^{-1}$ (Troja et al., 2018) which is similar to ULX sources. A fit to only the post-peak X-ray data i.e. > 160 days results in a spectral index of 0.8 ± 0.4 , a fit to only the radio data results in a spectral index of 0.4 ± 0.3 while the

fit to the entire spectrum results in a spectral index 0.585 ± 0.005 (Troja et al., 2018). No further γ -ray signals were detected from this source after the initial GRB which was about 2 – 6 order of magnitudes fainter than other short GRB at known redshifts (Abbott et al., 2017a). The luminosity of most GRBs upto $z = 4.5$ in the energy range 1 keV to 10 MeV is observed to be between 10^{51} and 10^{54} erg s $^{-1}$ while the luminosity of GRB 170817A was only $\sim 10^{47}$ erg s $^{-1}$.

Since the γ -ray pulse of GRBs is frequently observed to be followed by multiband emission referred to as the afterglow which ranges from strong thermal continuum to wide multi-redshifted absorption lines to radio synchrotron emission, the association of the GRB with the optical transient in NGC 4993 has a sound basis. Since the observed spectra of GRBs show similarity to quasar spectra in terms of the presence of wide emission and multi-redshifted absorption lines, it was suggested that GRBs can be explosive events on quasars (Kantharia, 2016a). We pursue this line of reasoning and further investigate if the connection of GRBs to active nuclei or more generally to events near black holes can be conclusively established from observational results.

A quasar consists of a black hole with the infalling matter forming its pseudo-surface around which a broad line region forms in the non-polar regions - all of this very close to the event horizon of the black hole. Quasars are generally bright in the ultraviolet and optical bands and are the most luminous of active nuclei. However it is possible that a quasar with its structure intact has evolved to dimness. If a transient energetic event occurs on the dim quasar then it can brighten the system for some time. This can, then, explain a GRB as an energetic event on a dim quasar. One possible origin of this energetic event was suggested as a thermonuclear outburst on the pseudosurface of a dim quasar which will emit γ -rays till it lasts. If a large mass is ignited simultaneously then huge quantities of energy can be injected into the system in a short time and this can heat the pseudosurface which starts emitting as a black body especially in the X-ray to infrared bands. This can also lead to ejecting overlying matter. Thus explosions on dark quasars are a strong contender as a possible origin site of GRBs and are backed by observational evidence in form of the broad lines and extremely high energy outputs. This argument can be extended to accreting black holes of lower masses - intermediate mass black holes or stellar mass black holes. The surface area involved in the explosion and luminosity of the system will depend on the mass of the black hole so that it will be largest in case of a su-

permassive black hole and smallest in a stellar mass black hole.

We test the validity of the above explanation to observations of GRB 170817A. The short GRB in NGC 4993 was localised to a region displaced from the centre of the galaxy. This then leaves the option of the explosion having been on a microquasar hosting a stellar mass black hole in the galaxy or on an intermediate mass black hole. Since very little is known about intermediate mass black holes in galaxy disks, we confine this discussion to investigating the origin of the GRB on a dim microquasar by finding viable explanations for the three emission components that were detected from GRB 170817A. A burst of γ -rays is expected from a thermonuclear outburst and should exist for the duration of the burst. Whether we detect the γ -rays of energy released in the explosion or enhanced energies depends on whether the photons reach us directly or are inverse Compton scattered to higher energies. This can vary from case to case. Anyway the burst of γ -ray photons from GRBs can be explained in this origin. The thermonuclear outburst which happens on the pseudosurface can impart some of the released energy to the highly conducting electrons in the pseudosurface, and hence enhance its temperature. The thermal emission that followed the γ -rays i.e. the kilonova emission from GRB 170817A can be explained by emission from the hot pseudosurface which was heated by the thermonuclear explosion. The emission lasted till the pseudosurface cooled down. The relativistic plasma responsible for the synchrotron emission would have been accelerated by the thermonuclear energy before being ejected. For a rotating black hole, matter would be accreted directly at the poles whereas an accretion disk would have formed in the non-polar regions. Thus the explosion would be able to easily eject energised matter from the poles, thus explaining the long-lived synchrotron afterglow from GRB 170817A along jets. In short, the short GRB being due to a thermonuclear explosion on the pseudosurface of a black hole is able to explain all the observed features of GRB 170817A and hence supports the origin of GRB 170817A on a microquasar.

The radio emission of the microquasar in quiescence is likely to be undetectable at a distance of 40 Mpc. For example, the quiescence radio emission of SS 433 which is estimated to be at a distance of 5 kpc is around 300 mJy at 5 GHz. Emission of similar strength from the microquasar in which GRB 170817A appears to have occurred at a distance of 40 Mpc would be 0.005 μ Jy. If radio flares of 5 Jy occurred in this source then these would be recorded by us as signals of strength 0.08 μ Jy. Thus, it is not sur-

prising that the source became detectable only during a major energy outburst.

To summarise: All the three observationally recorded electromagnetic components of GRB 170817A can be explained by a thermonuclear outburst in the accreted matter on the pseudosurface of the black hole in a microquasar. This provides strong reasons to believe that the GRB 170817A and the afterglow occurred on a microquasar.

4.2 Active Galaxies

Active galaxies are those galaxies which host an accreting supermassive black hole in their centres and exhibit multi-band features whose origin can be traced to the active nucleus. Active galactic nuclei generally show the following observable characteristics: (1) bright non-stellar multi-component continuum emission detectable in all wavebands (2) a non-stellar line spectrum often consisting of broad permitted emission lines and/or narrow permitted and forbidden emission lines (3) single-sided or double-sided radio and/or multi-band jets extending out from the nuclear region (4) radio lobes and/or hotspots located on either side of the nucleus and (5) multi-band variability. The general picture of an active nucleus in literature comprises of a central accreting supermassive black hole hosting an accretion disk from which jets are launched that form the radio lobes and hotspots. However the detailed physical processes responsible for energy production, injection, jet ejection, broad line forming region, variability etc are not known with certainty. In this section, we search for explanations for all these processes within the purview of known physics so that the working of the entire physical system becomes apparent. Radio galaxies extend over regions ranging in size from kpc to hundreds of kpc to Mpc while the radio structure in Seyferts, gigahertz-peaked sources (GPS) and compact steep spectrum (CSS) sources are generally comparable or smaller than galactic dimensions. The host galaxies of radio galaxies, GPS, CSS sources are ellipticals whereas those of Seyferts are generally disk galaxies. There remains ambiguity regarding the host galaxy of quasars and existing observations indicate the prevalence of both elliptical and disk galaxies.

In the early studies, many elliptical galaxies were found to emit nuclear radio emission of lower luminosity than radio galaxies but stronger than the radio emission detected from the nuclei of spiral galaxies (Rogstad & Ekers, 1969). Moreover it was noted that radio emission was predominantly detected from elliptical galaxies whose absolute photographic magnitudes were brighter than -20 magnitudes and a

correlation between the presence of radio emission and presence of optical emission lines was noticed (Rogstad & Ekers, 1969). It was noted that the probability of nuclear activity increased when the galaxy was a member of a group or cluster (e.g. Slingo, 1974) with the probability being maximum for galaxies in pairs (Hummel, 1981). The central source in interacting spiral galaxies was observed to be stronger by a factor of 2 to 3 than in isolated spiral galaxies (Hummel, 1980). It was shown that the nuclear emission in spiral galaxies was more extended and displayed a steeper spectrum ($\alpha \sim 0.7$; $S \propto \nu^{-\alpha}$) compared to the nuclear source in lenticulars and ellipticals ($\alpha \sim 0.1$) (Ekers, 1974; Condon & Dressel, 1978; Hummel, 1981). A good correlation between the presence of a strong nuclear radio source and extended radio emission in elliptical galaxies was measured which was inferred to indicate that the nucleus played a role in the extended emission (Ekers, 1974). Enhanced nuclear activity in galaxies was attributed to increased gas accretion by the nuclear black hole (Condon & Dressel, 1978).

Active nuclei have been classified based on observational features such as (1) radio morphology/power e.g. FR I and FR II classes or (2) observed widths of spectral lines e.g. Narrow Line Radio Galaxy (NLRG)/Seyfert 2 and Broad Line Radio Galaxy (BLRG)/Seyfert 1 or (3) on the type of host galaxy e.g. Seyfert if disk galaxy host and radio galaxy if an elliptical host or (4) on the radio detectability e.g. radio-quiet and radio-loud galaxy or (5) on the light output from the central core e.g. quasars, BLRG, Seyfert 1 which have bright cores and NLRG, Seyfert 2 which have a faint core or (6) size of the radio source e.g. radio galaxy for extended radio structures and Gigahertz Peaked Sources (GPS), Compact Steep Spectrum sources (CSS) for small powerful radio sources. It has been useful to have all these results derived from meticulous observations which have enhanced our understanding of active galaxies and also added to their complexity. Several studies have been aimed at unifying these active galaxies based on attributing many of the observed differences to the orientation parameter. The schematic in Figure 17 by Urry & Padovani (1995) summarises the widely accepted unification model for active nuclei as surmised from observations. This orientation model (see Figure 17) explains a host of observations indicating that the different parts of the active nucleus have been appropriately located wrt to the black hole and sightline. In the orientation model shown in Figure 17, the supermassive black hole is surrounded by an equatorial accretion disk which in turn is surrounded by a dust torus. The

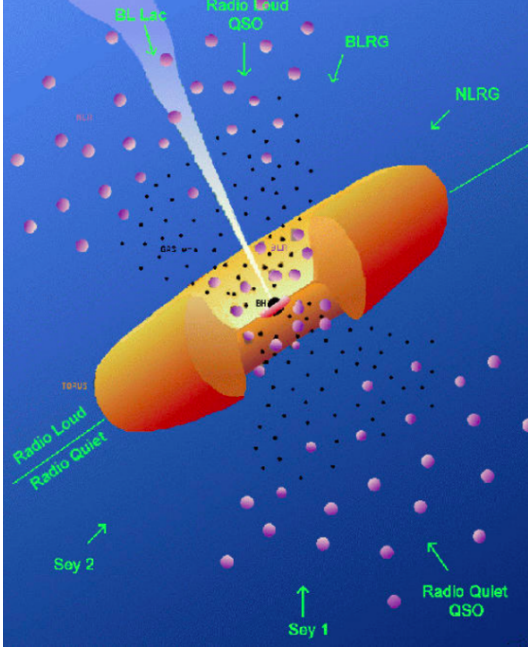


Figure 17: Unification of active galaxies summarised in a schematic by Urry & Padovani (1995). Figure copied from <http://pulsar.sternwarte.uni-erlangen.de/wilms/teach/xray2.old/xray20233.html>.

The pink filled circles represent narrow line regions whereas the black dots represent broad line regions. The orange structure is the dust torus whereas the white coloured outflow from the black hole is the radio jet. The dark pink band which cuts across the black hole is the accretion disk. The orientation-based unification model for the different types of active galaxies is labelled.

broad and narrow lines are believed to arise in clouds distributed within biconical polar regions around the black hole with the narrow line clouds being extended to larger separations from the black hole. The narrow lines form in the narrow line region (NLR) while the broad lines form in the broad line region (BLR). In this model, the active nuclei observed close to the polar axis of the black hole are classed as radio-loud blazars if radio-bright and radio-quiet quasars if radio-faint while rest of the objects are explained by increasing polar angles with NLRG and Seyfert 2 being observed through the torus. Although this observational model has been able to explain several observables, there remain outstanding questions like the origin and reasons for the surmised location of the various line forming regions around the black hole, origin of the intense photoionizing continuum, and whether orientation is the only varying parameter between the different active nuclei.

The continuum light output from the central parts of active galaxies especially in case of quasars, BLRG and Seyfert 1 galaxies, is a significant fraction of the galaxy luminosity and at times as in case of quasars, can render the light from the extended galaxy unde-

tectable. The wideband continuum spectrum of the nuclear emission of active galaxies and even normal elliptical galaxies tend to show an ‘ultraviolet/blue bump’. In many cases, it is found that the wideband nuclear spectral energy distribution can be approximated by a combination of a power law, a black body spectrum and a thermal spectrum.

It was estimated that $10^3 - 10^6 M_{\odot}$ of warm ionized gas detected in [O II] 3727A is present in the central few hundred parsecs of elliptical and lenticular galaxies and many times this gas appeared to be arranged in the form of a rotating disk (e.g. Osterbrock, 1960; Caldwell, 1984; Phillips et al., 1986). The rotating disk is found to show varying orientation with the minor axis which has prompted an external origin explanation for the gas (e.g. Caldwell, 1984). More recent observations of large samples of elliptical and S0 galaxies collectively referred to as early type galaxies (ETG) in literature find that this gas is often kinematically misaligned wrt to the stars (e.g. Davis et al., 2011) for which a gravitational torque as the cause has been suggested (Kantharia, 2016b). About $\sim 50\%$ of ETGs show the presence of ionized gas in the central parts. Dust has been detected in ellipticals from which mass of $10^7 - 10^8 M_{\odot}$ have been estimated for the cold interstellar gas in the central parts of elliptical galaxies (e.g. Jura et al., 1987). More recent studies estimate even larger gas masses in centres of elliptical galaxies. These studies have conclusively established the existence of a significant quantity of gas in the centres of ETGs.

It is interesting to note that the existence of a supermassive black hole at centres of galaxies was not hypothesized till 1960s. In 1950s, it was believed that the centres of strong radio sources like Cygnus A and Virgo A, which were just being optically identified, could be due to colliding nebulae of gas or colliding galaxies (e.g. Baade & Minkowski, 1954b). The existence of a very massive object at the centres of galaxies was slowly being appreciated and it was speculated that the strengths and multiple redshifts of lines observed in a quasar spectrum could be explained due to a gravitational redshift component if the line photons arose very close to a supermassive object (Greenstein & Schmidt, 1964). The existence of supermassive black holes/dead quasars at centres of galaxies was discussed by Lynden-Bell (1969) whereas Lynden-Bell & Rees (1971) discussed the existence of a supermassive black hole in the centre of our Galaxy. Backed by several observations, it is now widely accepted that there exists a supermassive accreting black hole at the centre of active galaxies and which hosts an accretion disk in the equatorial regions. Several studies have discussed the struc-

ture, accretion rates, physical conditions, viscosity, angular momentum transfer, jet formation, corona, outflows etc in accretion disks near black holes (e.g. Lynden-Bell, 1969; Shakura & Sunyaev, 1973; Blandford, 1976; Paczynski, 1978; Pringle, 1981; Subramanian et al., 1996, 1999).

We start by summarising observational results on active galaxies which includes quasars, BLRG, NLRG, FR I, FR II, GPS, CSS, Seyfert 1 and 2 and follow it with a discussion on the physical model which emerges from the observations and present a few case studies to demonstrate the validity of the model. While efforts have been made to keep the discussion concise and succinct, the volume of observational results in literature and our understanding of these intriguing and amazing objects is so vast, evolving and wide-ranging as reflected in literature that it is a formidable task. It is hoped that the discussion is sufficiently clear and tight that the inferences are obvious.

4.2.1 Summary of observed features

- An active galactic nucleus is generally detectable in all wavebands. The brightest nuclear emission is detected from quasars, BLRG and Seyfert 1 galaxies. The spectral energy distribution (SED) follows a power law in infrared and optical wavelengths, becomes flat in blue and ultraviolet wavelengths and then starts declining around 2500 Å with the decline becomes steeper at wavelengths lower than 1200 Å so that at X-ray bands, the same power law appears to be applicable (e.g. Malkan & Sargent, 1982). The spectra of most nuclei show an excess in the blue or ultraviolet emission which is referred to as the blue bump in literature. Several normal elliptical galaxies also show this blue bump in their SED.
- The multi-band continuum emission from the active nucleus is often variable. Variability in the X-ray, ultraviolet and optical bands is often found to be either simultaneous or the lower frequency emission follows the higher frequency emission (e.g. NGC 5548; Clavel et al. 1992) and this has been well studied in Seyfert galaxies. However occasionally a flare confined to the ultraviolet band is also recorded from these galaxies (e.g. NGC 5548; Clavel et al. 1992). Similar phenomena are noted in NGC 4151 (e.g. Perola et al. 1986).
- Optical/ultraviolet emission lines of a wide range of excitation are generally detected from the active nucleus suggesting a non-stellar hard exciting source. Narrow (FWHM of few hundred kms^{-1}) emission lines are detectable from almost all active nuclei. These consist of low and high ionization lines. Many narrow lines are asymmetric with a wider wing on the blue side compared to the red side. Broad (FWHM of thousands of kms^{-1}) permitted emission lines are detected from quasars, BLRG and Seyfert 1 galaxies. No broad forbidden lines are detected. Broad lines are often variable in both amplitude and width which is correlated with the variability in the thermal continuum emission whereas no variability is detected in the narrow lines (e.g. Osterbrock, 1989). This property has been used in reverberation studies of Seyfert 1 galaxies wherein the delay in correlated variability in the continuum and broad lines are used to determine the size of the BLR and the separation of the BLR from the continuum emitting region. This method has resulted in deriving a size of a few light days for the BLR in Seyfert 1 galaxies (e.g. Gaskell & Sparke, 1986).
- The radio structure associated with the active nucleus in Seyferts is fainter and more compact than radio galaxies and is generally confined within the optical galaxy.
- Extended Lyman α emission coincident with the extended radio structure has been detected towards several radio galaxies (e.g. 3C 294 McCarthy et al., 1990). Also the velocities recorded for the Lyman α on either side of the core are observed to be blueshifted and redshifted - for example in 3C 294, the Lyman α emission coincident with the northern lobe is blueshifted by about 900 kms^{-1} whereas the emission coincident with the southern lobe is redshifted by about 500 kms^{-1} (McCarthy et al., 1990). The Lyman α emission often shows asymmetric distribution on the two sides of the core. *These observations wherein the radio emission and line emission are of similar extents and the latter show expansion on either side of the core support the ejection of both the ionized gas and radio plasma from the vicinity of the black hole.*
- An approximate linear correlation exists between the radio power at 1.4 GHz and the luminosity of the [O III]5007Å line for Seyfert galaxies (de Bruyn & Wilson, 1978). A correlation between the radio power and optical continuum luminosity is also observed for Seyfert galaxies (e.g. Edelson, 1987). Wilson & Willis (1980)

noted that radio emission showed remarkable similarity with the distribution of the optical line emitting gas in a few Seyfert galaxies and suggested that these galaxies also hosted a double radio source.

- In the Seyfert 2 galaxy NGC 5929, double-peaked [O III] profiles are detected in addition to a double-lobed radio structure both separated by 200-300 pc from the nucleus (Whittle et al., 1986). Correlation between discrete components in [O III] and radio emission are detectable with both diagnostics extended along similar position angles (Whittle et al., 1986). Such double-peaked optical emission lines are often detected from Seyfert galaxies with the peaks displaced by a few hundred kms^{-1} on either side of the rest frequency i.e. consisting of blue and redshifted components.
- The typical widths of high excitation forbidden lines like [O III] from the NLR close to the nucleus is around $300\text{-}500 \text{ kms}^{-1}$. Such high excitation lines are also detected at distances of several kpc from the nucleus but are fainter, significantly narrower at $< 45 \text{ kms}^{-1}$ and the velocity gradient within the region is small. Such a region has been referred to as the extended NLR i.e. ENLR (Unger et al., 1987).
- The range of excitation observed in the emission lines from an active nucleus is much larger than that from a HII region or a planetary nebula and which appears to have a photoionization origin (e.g. Osterbrock, 1989).
- Soft X-ray emission especially upto 2 keV is seen to show good correlation with the narrow line region traced by forbidden lines of oxygen [O III]5007Å and $\text{H}\alpha + [\text{N II}]6548, 6583$ in terms of morphology and extension with the extension being along the radio jet axis in the Seyfert galaxy NGC 1068 (Young et al., 2001).
- Radio continuum emission is detected from several components of active galaxies - compact core, collimated jets, extended lobes and compact hotspots and the emission is due to the synchrotron process.
- Collimated narrow single-sided jets and symmetric two-sided lobes and hotspots are commonly detected in radio images of powerful quasars and FR II galaxies (Fanaroff & Riley, 1974). The central core, symmetric and often bent jets and lobes are commonly detected from FR I galaxies.

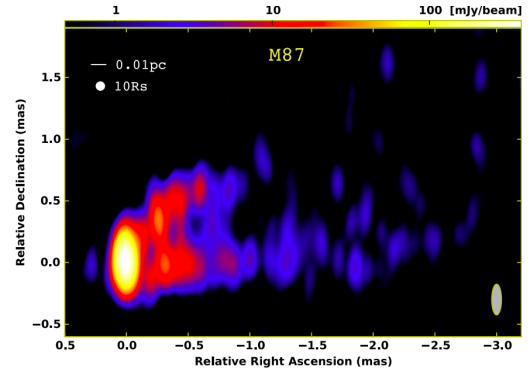


Figure 18: The central region of M 87 at 86 GHz and high resolution. Figure copied from Hada et al. (2016). Notice the limb-brightening in the jet and the presence of a faint counter-jet close to the core.

- Narrow single-sided X-ray jets are detected close to the core and the emission process has been found to be synchrotron. However X-ray beams which are extended from the nucleus till the hotspots but laterally more diffuse than radio jets have been detected in a few FR II radio galaxies like Cygnus A and Pictor A. The emission process for these X-rays remains unknown.
- The radio power of the active galaxies in the 3CR catalogue of strong radio sources is a strong function of redshift such that it increases with redshift.
- Radio jet collimation has been found to be inversely correlated with luminosity such that most radio luminous (FR II) sources host highly collimated jets (jet opening angles $\leq 3^\circ$) whereas lower luminosity (FR I) sources show larger jet opening angles ($\sim 5^\circ - 15^\circ$). The bulk velocity of the jet in FR II is measured to be higher than in FR I sources.
- Some jets show a limb-brightened morphology starting from close to the black hole as seen for M 87 in Figure 18. The jet in M87 was the first jet to be discovered (Curtis 1918) and is detected across the electromagnetic spectrum - radio to TeV γ -rays VLBI images at 1.3 mm have spatially resolved the base of the jet in M 87 indicating that it has been launched from a region separated from the black hole by $\leq 5.5 R_s$ (Doeleman et al., 2012).
- Optical emission extended along the radio jets was detected beyond the host galaxy in Centaurus A, Fornax A and NGC 7720 (Matthews et al., 1964).
- The narrow line emission in many radio galaxies

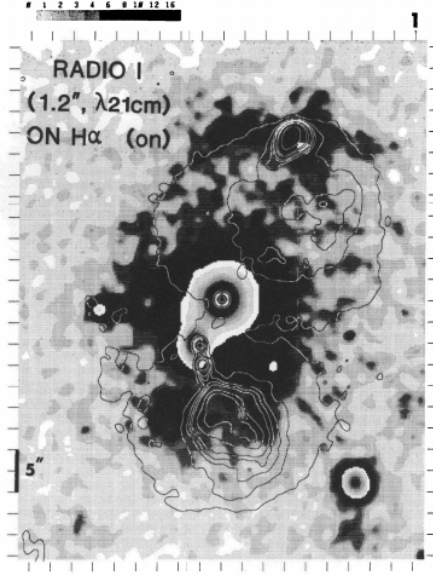


Figure 19: Figure reproduced from van Breugel et al. (1985), showing the radio continuum emission in contours and optical H α emission in grey scale for the central galaxy in Coma cluster - 3C 277.3. Notice the co-extensive nature of the two diagnostics.

has been mapped and found to extend over a region comparable to the radio structure as shown in Figure 19 for the radio galaxy 3C 277.3 located at the centre of the Coma cluster (Miley et al., 1981; van Breugel et al., 1985). The optical line brightness was observed to be correlated with radio continuum intensity in 3C 277.3 and the optical lines were red-shifted in the north and blue-shifted in the south of the nuclear source indicating expansion (Miley et al., 1981). From such studies, an interaction between the radio plasma and the optical emission line gas has been inferred. Additionally, it has also been inferred that a common energy source is responsible for the optical lines and radio continuum (Baum & Heckman, 1989b). A tighter correlation between radio jets and narrow emission lines is found in steep spectrum extended radio galaxies (Baum & Heckman, 1989b). Extended emission line gas has more commonly been observed in steep spectrum radio-loud quasars as compared to flat spectrum radio loud or radio-quiet quasars (Boroson et al., 1985; Stockton & MacKenty, 1987). The median size of the optical line emitting region in radio galaxies is found to be about 10 kpc (Baum & Heckman, 1989a). The extent of the emission line region is found to be smaller for radio-quiet active galaxies.

- From studies of a large sample of radio galaxies, it is found that extended optical emission line gas

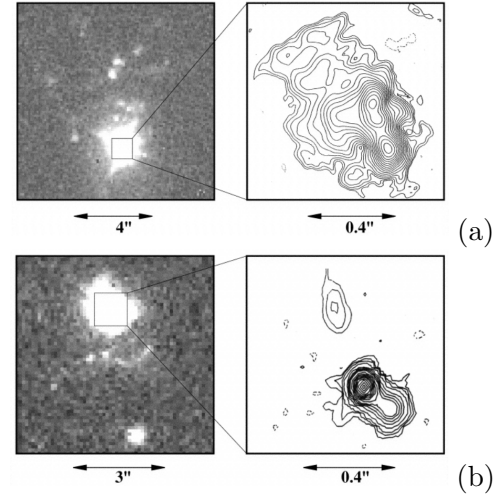


Figure 20: Figures showing the distribution of red-shifted narrow band forbidden line emission (left) and radio continuum emission (right) of compact steep spectrum sources, reproduced from Axon et al. (2000). (a) 3C 48 (b) 3C 147. Notice that [O III] emission is extended along the radio axis and is more extended than the radio continuum emission for both the sources.

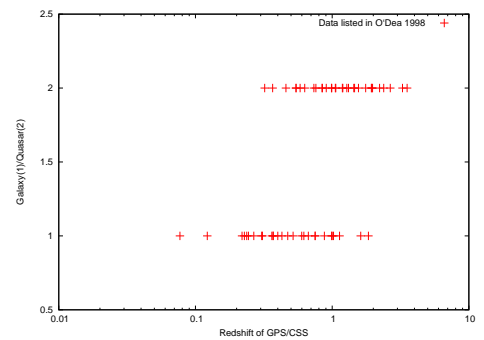


Figure 21: Figure showing the redshift distribution of GPS, CSS galaxies and quasars. 1 refers to a source classified as a galaxy and 2 to a quasar classification.

on scales of 40-100 kpc is commonly associated with powerful radio galaxies (Baum et al., 1988). No correlation is observed between broad line emission and radio power (Baum & Heckman, 1989b).

- Optical line emitting gas is detected in about 90% of the 53 observed 3CR radio galaxies with $0.05 < z < 2$ and is distributed over scales ranging from sub-parsec to about 300 kpc (McCarthy et al., 1995). The emission line regions are found to be aligned with the radio jets/lobes for sources located at $z > 0.3$ while for sources at $z > 0.6$ the optical/ultraviolet continuum emission also shows an alignment with the radio axis (McCarthy et al., 1995).
- Emission lines are detected near the radio jets especially at the outer edges of bends in radio jets and near knots and hotspots with the spectrum resembling the higher excitation spectrum of Seyfert 2 nuclei and not HII regions (e.g. Bridle & Perley, 1984). Typical electron densities estimated from the optical emission lines are $\sim 10^2 - 10^3 \text{ cm}^{-3}$ for temperatures of $\sim 20000 \text{ K}$ (e.g. Bridle & Perley, 1984). The typical bulk velocities are estimated to be a few hundred kms^{-1} with detected line widths typically being less than 1000 kms^{-1} .
- The observed forbidden line ratios ($[\text{O II}]/[\text{O III}]$) detected from the nuclear region and the extended region along the radio jet in radio galaxies appear to be well explained by the same ionizing source. The ionizing source is inferred to be a black body of temperature around $1.3 \times 10^5 \text{ K}$ i.e. an ionizing radiation field consisting of mean photon energies of 30-40 eV which rules out a stellar continuum origin (Robinson et al., 1987).
- Optical line emitting gas is also detected along the radio axis in GPS and CSS sources (see Figure 20). The radio emission in GPS and CSS sources shows relatively lower linear polarisation and higher rotation measures. The optical brightness of the central source in GPS and CSS sources is dominated by emission lines (Axon et al., 2000). Broad ($\sim 2000 \text{ kms}^{-1}$) and flat-topped $[\text{O III}]$ profiles are observed from CSS nuclei (Gelderman & Whittle, 1994). A correlation between the narrow line luminosity and the total radio power is also noted in GPS and CSS sources (e.g. Gelderman & Whittle, 1994; Gelderman, 1995).
- GPS and CSS constitute about 10% and 30% respectively of the radio source population and their host galaxies resemble the elliptical hosts of radio galaxies (e.g. O'Dea, 1998).
- The emission line redshifts of GPS and CSS are ≥ 0.1 as shown in Figure 21.
- Jets are observed to be one-sided close to the core in both FR I and FR II galaxies. Double-sided jets are detected on kpc scales in FR I galaxies but continue to be single-sided along their entire length in FR II sources so that the jet-counterjet brightness ratios are large (e.g. Bridle et al., 1994; Laing, 1995). The non-detection of a counter-jet is attributed to Doppler beaming owing to relativistic bulk jet speeds indicating that such speeds continue till the hotspot in FR II sources. The jet-counterjet asymmetry can be explained by relativistic jet velocities β between 0.65 and 0.8 for jet viewing angle between 45° and 75° (Wardle & Aaron, 1997). These studies do not support significant intrinsic asymmetry in the jets.
- Many jets show the same opening angle at parsec and kiloparsec scales (e.g. NGC 6251 in Figure 22) which would be indicative of a free jet (Miley, 1980). However larger opening angles are noted in milliarcsec jets imaged with VLBA/VLBI e.g. Virgo A, (Junor et al., 1999) and Cygnus A (Boccardi et al., 2016) as compared to the opening angles measured at parsec/kiloparsec scales.
- FR I radio galaxies and radio-quiet active galaxies with similar host optical magnitude show similar narrow emission line luminosities (Baum et al., 1995). It is also found that the host galaxy and nuclear properties of the class of radio sources which are known as FR 0 in literature are comparable to FR I except that extended radio structure is only associated with FR I (Baldi et al., 2019). The ultraviolet continuum from the active nucleus in FR I sources is fainter than in FR II sources. *shift this to explanation: These observational results would argue for a decrease in both bulk velocity and the random relativistic velocities of the electrons going from FR I to FR 0 to radio-quiet active galaxies which in turn could argue for an increasing separation of the launching region from the black hole and hence decreasing escape velocity i.e. lower energy thermonuclear bursts which lead to lower energy ejections.*
- Optical and X-ray synchrotron emission from several jets close to the core have been observed.

Additionally optical emission with polarisation properties similar to the radio synchrotron emission has been found to be coincident with radio hotspots and radio lobes in a few sources e.g. 3C 285 (Tyson et al., 1977), 3C 33 (Simkin, 1978; Meisenheimer & Roeser, 1986).

- Excess soft X-ray emission (0.1 - 2 keV) over a power law is detected in most Seyfert 1 galaxies which is also found to be variable (Turner & Pounds, 1989). This excess is well-fit by a multi-temperature black body with temperatures ranging from 40 to 150 eV which indicates that the emitting region is closer than $3R_s$ (La Parola et al., 1999; Piro et al., 1997). These galaxies also show a ultraviolet excess. The hard X-ray emission (2-10 keV) is well described by a power law so that the entire X-ray spectra for many Seyfert 1 is well described by the combination of a power law and a black body spectrum.
- In some FR I sources, the X-ray jet is bright close to the core and which coincides with a faint radio jet whereas further from the core, the X-ray jet fades and the radio jet brightens (e.g. 3C 31 Laing et al., 2008).
- An anti-correlation is observed between the hot spot prominence and jet bending such that when the hot spot is more prominent, the jet is straight and vice versa (Bridle et al., 1994).
- Radio polarisation studies find that the magnetic field lines are along the jet in luminous sources such as FR II galaxies. In fainter sources like FR I galaxies, the magnetic field lines are along the jet close to the central active nucleus but perpendicular to the jet at larger distances from the nucleus (see Figure 22). It is observed that the fraction of the jet length over which the magnetic field is parallel to the jet is determined by the radio core luminosity such that a stronger radio core shows a parallel field over a longer jet length than a fainter radio core (Bridle, 1982). Moreover jet-counterjet brightness asymmetry is more pronounced in the radio sources with a powerful core i.e. ones which show a parallel magnetic field configuration (Bridle, 1982).
- Quasars, BLRG and Seyfert 1 galaxies show the presence of wide emission lines in their nuclear spectra. The ratio of the strengths of nuclear broad $H\alpha$ to $H\beta$ is around 3.5 in Seyfert 1 whereas it is around 6 in BLRG (Osterbrock, 1989). It is also observed that the emission lines of Fe II are absent or significantly fainter in

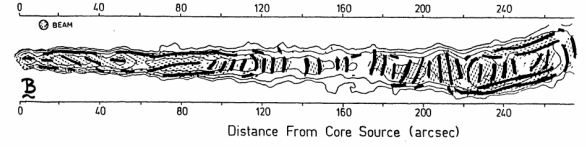


Figure 22: Figure showing the typical magnetic field orientation in a FR I galaxy. The figure showing NGC 6251 is reproduced from Bridle (1982). Note how the magnetic field is along the jet in the inner parts and flips to being transverse to the jet at larger distances when the jet starts flaring up.

the nuclear spectrum of BLRG than in Seyfert 1 galaxies (Osterbrock, 1989). It is also observed that lobe-dominated radio sources show weaker [Fe II] emission in their core spectrum compared to core-dominated sources (Bridle & Perley, 1984).

- The spectra of some Seyfert 2 galaxies show the presence of broad lines in polarised light (e.g. NGC 1068; Antonucci & Miller, 1985) while the spectra of narrow lined Seyfert 2 nuclei are observed to transform to an intermediate 1.5 type or type 1 spectrum and then revert back to type 2 over time. The galaxy NGC 1566 has been observed to transit from a Seyfert 2 to a Seyfert 1 type i.e. its core brightens and broad permitted lines of hydrogen appear with no change in the narrow lines over a period of about 1300 days (Alloin et al., 1985, 1986). Energy of the order of $\sim 10^{51}$ ergs has been estimated to be released but an origin in supernova explosions have been ruled out (Alloin et al., 1986). Radio emission and narrow line [O III] emission have been detected from NGC 1566.
- The broad lines of higher ionization are observed to be wider and more variable than the broad lines of low ionization in Seyfert 1 and quasars. This has been understood in terms of stratification in the BLR with the high ionization region lying closer to the ionizing source and hence directly subject to variations in the ionizing source (e.g. Peterson & Horne, 2006).
- It was inferred that the radial extent of the BLR in the Seyfert galaxy Arp 151 increased by a factor of two between 2008 and 2011 when the continuum varied (Pancoast et al., 2018). It was inferred that the inner boundary of the BLR remained the same as measured from reverberation mapping in data taken over seven years (Pancoast et al., 2018).
- Quasar spectra show broad emission lines at the

highest detected redshift and absorption features at several lower redshifts. The presence of multiple redshifts in the quasar spectra has been explained by a varying gravitational redshift component in radially distributed line forming zones in the BLR (Kantharia, 2016a). Similar behaviour but of much smaller redshift magnitude has also been observed in other active nuclei.

- Broad emission lines like C IV from the BLR are often observed to be asymmetric with a steeper profile on the red side compared to the blue side. The velocity of the high ionization lines like C IV in quasars is systematically blue-shifted by $\sim 600 \text{ km s}^{-1}$ wrt to the lower ionization lines like Mg II (Gaskell, 1982). *These two observations might be connected if the strong gravitational potential in which the C IV line is formed is responsible for the line asymmetry which in turn leads to the measured centroid being biased towards the blue.*
- The radio and γ -ray emission especially between 0.1 and 100 GeV show a tight correlation in active nuclei especially blazars. The correlation which is observed to be strongest for BL Lac objects declines at energies $> 100 \text{ GeV}$ (Lico et al., 2017). Recently a high-energy neutrino IceCube-170922A with energy surmised to be about 290 TeV has been detected from a flaring blazar TXS 0506+056 (IceCube et al., 2018). While neutrinos of lower energy have been detected from the sun and the supernova SN 1987A, this is the first detection of neutrinos associated with an active nucleus which is in the active phase and also emitting γ -rays.
- Quasars could be divided into two groups based on the detection of Fe II emission lines: (1) when Fe II emission lines are not detected, narrow lines are stronger, [O III]/H β ratio is large, hydrogen lines are broad and complex and the radio emission is extended with a double-lobed structure and a steep spectrum. (2) When Fe II emission is strong, narrow lines are weak, the hydrogen lines are narrower and smoother with relatively lower ratios of [O III]/H β and the radio structure is compact with a flat spectrum (Miley & Miller, 1979; Boroson & Oke, 1984).
- The optical continuum of quasars (also Seyfert 1 and 'N' type radio galaxies) was observed to be either variable (change by ≤ 0.5 magnitude within a year or so) or violently variable (change by a magnitude or so even within a night), with the latter being referred to as optically violently variable (OVV) quasars (e.g. Penston & Cannon, 1969; Cannon et al., 1971). The OVV quasars are also characterised by flat radio spectra and radio variability at high frequencies. The variability of these sources is not periodic. In more recent terminology, the OVV quasars are referred to as flat spectrum radio quasars (FSRQ).
- Quasar host galaxies range from disk galaxies to elliptical galaxies with typical sizes between 2 kpc and 15 kpc and absolute R band magnitudes within -21 and -24 magnitudes (Kotilainen et al., 2013). Majority of quasars are radio-quiet.
- The spectra of several active compact sources like blazars show a smooth log parabolic/convex shape from 1.4 GHz to about 1400 A with peaks occurring between 10 and 1000 GHz (e.g. Landau et al., 1986) (also see Figure 2).
- Multi-phase interstellar mediums is detected in almost all elliptical and lenticular galaxies and dust has also been detected (Goudfrooij et al., 1994).
- The infrared emission in Seyfert 1 galaxies is observed to be confined to a core source ($< 0.1 \text{ pc}$) whereas the radio emission is detected from a core source and an extended source of several hundred pcs to a few kpcs (de Bruyn & Wilson, 1978). The typical radio power of Seyfert galaxies at 21 cm is $10^{21} - 10^{22} \text{ W Hz}^{-1}$ (de Bruyn & Wilson, 1978). A small fraction of Seyferts host a flat spectrum compact radio source while some Seyferts show the presence of a radio halo of several tens of kpc (de Bruyn & Wilson, 1978).
- The sequence of active nuclei in terms of increasing emission line redshifts is Seyfert 2, Seyfert 1, FR I/NLRG, FR II/BLRG galaxies, GPS/CSS, quasars. For this sequence, there is a rise in the minimum redshift that an object in the specific class is detected such that it is lowest for Seyferts and highest for quasars as shown in Figure 23.
- H α and [N II] emission lines of varying relative intensities are detected from the central regions of all spiral galaxies which has helped classify them into LINERs (Heckman, 1980) and HII nuclei. It is found that 80% Sa, Sb galaxies are LINERs while 20% of Sc galaxies are LINERs (Osterbrock, 1989). LINER gas is also detected in a large fraction of early type galaxies (e.g. Annibali et al., 2010; Davis et al., 2011).

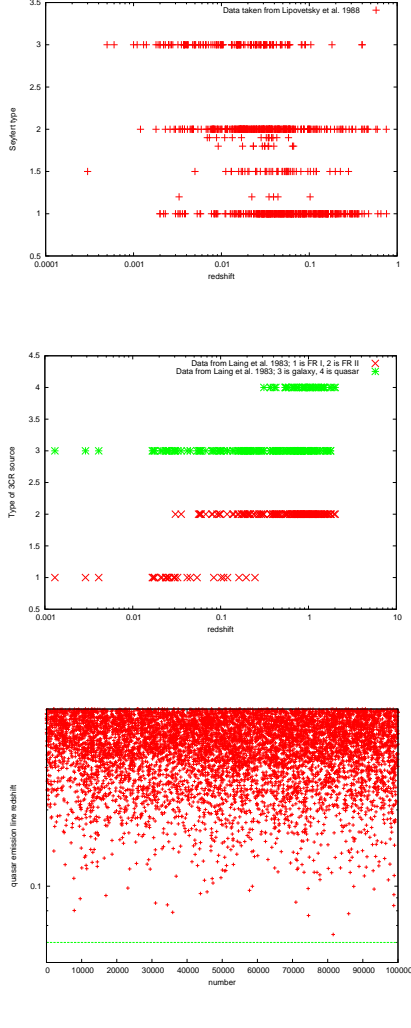


Figure 23: (a) Redshift distribution of Seyfert galaxies from the catalogue compiled by Lipovetsky et al. (1988). The number on the y-axis between 1 and 2 denotes the type of the active nucleus. Ignore 3. (b) The redshift distribution of more than 100 3CR radio sources classified into FR I (1) and FR II (2) (red crosses) and classified into galaxy (3) and quasars (4) (green stars) as listed in Laing et al. (1983). FR II galaxies are not detected at low redshifts unlike FR I galaxies. Also quasars are detected at much higher redshifts than galaxies. Such a gradation is indicative of the increasing influence of a gravitational redshift component which is maximum for quasars. (c) Distribution of the smallest redshifts ($z \leq 0.5$) detected for the quasars in the seventh data release of the SDSS quasar catalogue (Schneider et al., 2010).

- The angle between the radio jet axis and optical polarisation angle is found to be different for Seyfert 1 and Seyfert 2 galaxies such that the two are predominantly parallel in Seyfert 1 galaxies and predominantly perpendicular in Seyfert 2 galaxies (Antonucci, 1983).
- Similar polarisation fraction and angle are detected for permitted emission lines and continuum emission from the nucleus of the Seyfert 2 galaxy NGC 1068 whereas the forbidden lines are weakly polarised with a different position angle (Angel et al., 1976). It is inferred that the continuum and allowed emission lines formed in the nuclear region and hence were similarly scattered by dust in a cloud of size $\sim 1''$ leading to similar polarisation properties whereas the forbidden lines formed outside the nuclear region and hence were not scattered by the dust (Angel et al., 1976).
- In NGC 1068, broad permitted lines ($\text{FWZI} \sim 7500 \text{ km s}^{-1}$) were detected in polarised light (Antonucci & Miller, 1985). The broad lines were redshifted by $\sim 600 \text{ km s}^{-1}$ wrt the narrow lines (Antonucci & Miller, 1985). Such behaviour is not detected in all Seyfert 2 type galaxies.
- A few inferences from HI absorption studies of radio-loud nuclei Morganti & Oosterloo (2018): (1) HI absorption has been detected from several active nuclei (2) HI absorption is detected from the radio core and/or jets and/or lobes. (3) Blueshifted HI absorption features are more widely detected than redshifted features. Blueshifted features are interpreted as outflows whereas redshifted features are interpreted as gas flows from the accretion disk into the nucleus. (4) The HI detected in the central regions of active nuclei is deduced to be in form of a circumnuclear disk. It is found to form a thick disk of small radial extent in high power sources and a thin, extended disk in low power sources. (5) The circumnuclear HI disk merges with the galactic disks in Seyfert galaxies.
- Some of the main inferences from reverberation mapping (Bahcall et al., 1972; Blandford & McKee, 1982) of the BLR in Seyfert 1 galaxies as summarised by Peterson & Horne (2006) are that (1) The variability in the continuum emission in the ultraviolet to optical bands are in phase to within a day or so. (2) Variability in the continuum first induces variability in the highest ionization lines - He II 1640Å, C IV 1549Å,

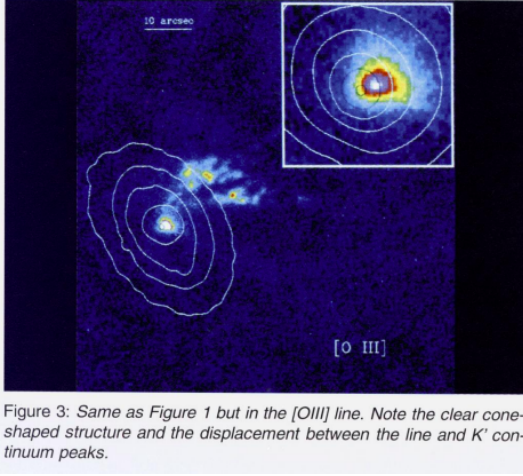


Figure 24: [O III] image of the Seyfert 2 galaxy Circinus copied from Marconi et al. (1994). The conical clumpy outflow in [O III] which defines the NLR of the active nucleus is clearly seen. The inset shows a zoom-in into the central regions of the image where the cone is even better defined. The contours indicate the optical continuum morphology of the galaxy. Radio jets and lobes are detected along the [O III] cone and extend out to several kpc from the nucleus.

$\text{Ly}\alpha$ and then in lower ionization lines - $\text{H}\beta$, C III] 1909A lines. The lags increase with the luminosity of the nuclear source in Seyfert 1.

- The NLR is distributed in a conical region with the black hole at the apex as seen in the [O III] image of Circinus in Figure 24 copied from Marconi et al. (1994). The conical region is often referred to as the ionization cone. The radio jets and lobes are also extended along the same axis. This Seyfert 2 galaxy is gas-rich and hosts a large warped HI disk and a starburst. The radio jets are spread over a smaller conical angle than the NLR.
- Broad Balmer lines have been detected in the polarised spectra of a few NLRGs and are also detected in total flux when deep spectra are obtained (e.g. Ogle et al., 1997; Cohen et al., 1999). These observations indicate that some NLRG also host a BLR. When resolved, the broad lines in NLRG appear to be arising in a polar biconical region around the core like in Figure 24. The biconical region has been inferred to be a reflection nebula around the core which scatters the broad lines from the BLR into the sightline (e.g. Cohen et al., 1999).
- The highest emission line redshift at which Seyfert 1 galaxies are detected is larger than Seyfert 2 galaxies (Khachikian & Weedman, 1974). The highest emission line redshift at

which FR II radio galaxies are detected is higher than FR I radio sources.

- The spectrum of the NLR consist of emission lines ranging from neutral atoms to multiply-ionized ions. There exists a correlation between the lines from neutral and singly-ionized ions indicating their origin in a common zone and between the different high ionization lines which indicate their origin in a common zone - this then suggests the existence of at least two separate ionization zones in the NLR (Koski, 1978). Similar line widths are recorded for the narrow emission lines from Seyfert 2 and NLRG. Moreover it has been noted that the velocities of the low and high ionization narrow lines from Seyfert 2 nuclei differ by a few hundred kms^{-1} (Koski, 1978).
- Continuum emission of Seyfert 2 galaxies contain a significant contribution from stellar light in addition to the active nucleus (Koski, 1978).
- Strong multiple permitted Fe II lines of widths \leq Balmer lines of hydrogen are frequently detected in Seyfert 1 galaxies but rarely in Seyfert 2 galaxies (Osterbrock, 1977; Koski, 1978). The forbidden [Fe II] lines are generally weak (Phillips, 1978). The intensity ratio [O III]/ $\text{H}\beta$ is generally smaller in Seyfert 1 compared to Seyfert 2 galaxies (Khachikian & Weedman, 1974). Forbidden lines of widths $300\text{-}800 \text{ kms}^{-1}$ are detected in both Seyfert 1 and 2 galaxies (Osterbrock, 1977) but appear to be stronger in Seyfert 2 (Koski, 1978). Iron lines are generally strong in radio-quiet quasars but absent or weak in radio galaxies.
- Using statistical arguments, it was shown that the origin of the large line widths in Seyfert 1 galaxies was not rotation (Osterbrock, 1977).
- In a sample of 55 Seyfert galaxies (19 Sy 1 and 36 Sy 2) observed in the radio continuum at 3.6 cm only one was not detected (Schmitt et al., 2001). Radio emission from the active core is commonly detected from Seyfert galaxies and in a few Seyferts, the radio emission is extended with double-sided conical jets. It is noticed that the position angle of the radio axis of the Seyfert is seldom perpendicular to the galaxy major axis (Kinney et al., 2000) *This could indicate large conical angles of ejection due to a low spin the black hole.*
- The nuclear radio power in Seyferts ranges from 10^{38} to $10^{40} \text{ ergs}^{-1}$, in normal spirals with strong

nuclear emission from 10^{36} to 10^{38} ergs $^{-1}$ and in other spirals is $< 10^{36}$ ergs $^{-1}$ (van der Kruit, 1973). The nuclear/core radio power in several early type galaxies including LINERs is in the range 10^{36} to 10^{38} ergs $^{-1}$, for FR 0 sources ranges from 10^{38} to 10^{40} ergs $^{-1}$ and for the core of FR I sources ranges from 10^{38} to 10^{42} ergs $^{-1}$. The X-ray luminosity of active nuclei are generally estimated to range from 10^{42} to 10^{46} erg s $^{-1}$. The bolometric luminosities of active nuclei are estimated to be in the range 10^{44} to 10^{48} erg s $^{-1}$ (e.g. Woo & Urry, 2002).

- The properties of some Seyfert nuclei have been observed to switch between type 1 and type 2 in terms of the high nuclear continuum luminosity and presence of broad lines in the spectrum transition to a fainter nuclear continuum luminosity and disappearance of the broad lines e.g. NGC 1566, Mrk 590.
- The jet opening angle in blazars is estimated to be $1^\circ - 2^\circ$ (Pushkarev et al., 2009). The jet opening angle in Cygnus A is measured to be 1.6° far from the core and about 10° close to the core (Boccardi et al., 2016). The jet opening angles are modified by the angle made by the jet with the sightline.
- In the FR II BLRG, Pictor A, a single radio jet is detected whereas double-sided X-ray beams which are thicker than the radio jet extend from the core to the hotspots (Hardcastle et al., 2016) (see Figure 34). The X-ray beam in the east terminates in a X-ray hotspot which is distinct from the bright radio hotspot. The opening angle of the jet is $\sim 3^\circ$ (Hardcastle et al., 2016). The radio spectrum of Pictor A turns over around 100 MHz (Perley et al., 1997). X-ray beams are also detected in the FR II galaxy Cygnus A.
- A large fraction of the extragalactic γ -ray sources detected by the Fermi LAT are blazars with only $\sim 3\%$ not being associated with blazars but with nearby FR I galaxies (Grandi et al., 2012a).
- The γ -ray flares detected in radio galaxies by Fermi LAT have generally been associated with the detection of a new radio component e.g. FR II BLRG 3C 111 (Grandi et al., 2012b) and and FR I BLRG 3C 120 (Casadio et al., 2015). In both the sources, the γ -ray flaring is observed to be associated with the brightening of the radio core followed by the ejection of a new radio blob along the jet and subsequent dimming of

the core (Grandi et al., 2012b; Casadio et al., 2015). This kind of behaviour has been observed in microquasars. However all radio flaring events do not seem to result in γ -ray flares as observed from the periodic radio flaring in 3C 120 (Casadio et al., 2015).

- Hard X-rays have been detected from radio lobes of Fornax A which have been attributed to inverse Compton scattering of the CMB photons by relativistic electrons (Feigelson et al., 1995; Kaneda et al., 1995). Soft to hard X-rays have been detected from the radio lobes of several other galaxies like 3C 219 (Brunetti et al., 1999), 3C 452 (Isobe et al., 2002), Pictor A (Grandi et al., 2003; Hardcastle & Croston, 2005), 3C 98 (Isobe et al., 2005) with most of these galaxies showing a FR II radio morphology and the coincident X-ray emission being attributed to inverse Compton scattering of the CMB photons. X-ray emission is observed to be coincident with at least one of the radio lobes in most of the FR II radio sources.
- The soft X-ray emission which is coincident with radio lobes in FR I galaxies and especially those located in groups and clusters of galaxies is often observed to be fainter than the rest of the diffuse X-ray emission that forms a halo around the radio galaxy. These regions are referred to as X-ray cavities in literature and are believed to have formed due to the radio plasma in the lobes pushing out the thermal plasma. The X-ray cavities are often surrounded by denser and cooler gas.

4.2.2 A comprehensive explanation

We derive a model for active nuclei which well explains their wide-ranging observed properties. We begin with a summary of the physical model for a quasar as described by Kantharia (2016a) which was mainly derived from results at ultraviolet bands and then expand and refine it to encompass the observed multi-band features (especially radio) of active galaxies. The similarity in the observed radio features of a microquasar and a radio galaxy is remarkable and underlines the uniformity of physical processes near an accreting black hole irrespective of its mass. It then means that the model put forward for microquasars should be applicable to active nuclei in its entirety with observed differences being confined to effects of the very different linear dimensions associated with the two systems which will lead to wide differences in the energy budget, variability amplitudes

and timescales, mass ejected and linear scales. Since microquasars showcase significant properties of active black holes, discussion on the same was included before active nuclei. We begin the section by a short recap of the unique model that had emerged from the behaviour of quasar spectra and then expand it. The results which are relevant to active nuclei and which have already been justified in case of novae in Kantharia (2017) and the effect of gravitational torques on gas distribution and rotation in galaxies justified in Kantharia (2016b) are referred to where required. This is followed by a few case studies which highlights the efficacy of the model.

4.2.2.1 Recap: Quasar model The ultraviolet spectra of quasars consist of wide high-redshift permitted emission lines and a host of multi-redshifted absorption lines blueshifted wrt to the emission lines. Most of the redshifts involved are significantly higher than other active galaxies. Since this sort of spectrum is unique to quasars and observed in quasars at all redshifts, Kantharia (2016a) explored an intrinsic origin for the multiple redshifts. The physical process that was predicted by the general theory of relativity wherein the line photon suffers a redshift when arising in a strong gravitational potential was found to well explain the observed behaviour of the redshifts. It was reasoned that if an intrinsic redshift component contributed to the redshift of the observed lines then the lowest redshift instead of the highest redshift detected in the quasar spectrum would indicate the cosmological redshift and the difference redshift would quantify the largest value of the intrinsic component. Data also showed that the lowest redshift detected in a quasar spectrum increased with quasar redshift (emission line redshift) which is exactly what would be expected if the quasar redshift included an intrinsic component in addition to the increasing cosmological component. The gravitational redshifts of the emission lines for the sample of quasars listed in Seyffert et al. (2013) were determined to be between 0.016 (photon emitted from $31.25R_s$) and 0.5535 (photon emitted from $0.9R_s$) with a median of 0.25 (the photon would be emitted from $2R_s$). Gravitational redshift is always ≤ 1 and gravitational redshift larger than 0.5 would mean that the photon arises within the ergosphere and gives irrefutable evidence to the existence of rotating black holes and escaping of a photon from within the ergosphere i.e. escape velocity being equal to velocity of light. When the intrinsic redshift component due to the gravitational redshift is removed from the observed emission line redshift, quasar redshifts are significantly reduced. In fact, since the absorption lines of Mg II

and Fe II occur at the lowest redshifts detected in a quasar spectrum, these provide the distribution of the quasar redshifts. The existence of gravitational redshift component in the quasar spectral lines has motivated a unique model for the active nucleus in quasars as was shown in Kantharia (2016a) which we summarise below. This also begs a critical revisit to our understanding based on the existence of quasars at high redshifts and their extreme luminosities in addition to the existence of superluminal motions.

It was reasoned that matter falling in towards the supermassive black hole should progressively increase in densities as it approaches the black hole (or any other compact object) and this can lead to significant consequences. If the infalling densities became $> 10^5$ gm/cc outside the event horizon of the black hole than matter could enter the degenerate state. This was briefly explained in Section 1.1. A more detailed explanation is presented here due to its importance in active nuclei. In analogy to white dwarfs and neutron stars, it was suggested that the degenerate pressure of electrons or neutrons (or other particles) would prevent the collapse of these layers of matter into the black hole. Thus, layers of degenerate matter can be expected to deposit outside the event horizon of the black hole whose outer surface would then constitute the pseudosurface of the black hole which forms a quasi-stable configuration close to the black hole. Emission from this hot pseudosurface would then be the electromagnetic signal that arises closest to the black hole that we can detect. For simplicity, the pseudosurface can be assumed to be spherical - however an uneven asymmetric latitude-dependent surface cannot be ruled out and hence it is probably more appropriate to describe it as quasi-spherical. This pseudosurface can form anywhere outside the event horizon of the black hole. Observations show that it is formed close to the event horizon in quasars. Since this layer is formed in the strong gravitational potential of the black hole it can be gravitationally heated to high temperatures with the high conductivity of the degenerate matter ensuring that it quickly uniformises through the layer. This hot pseudosurface can be a source of continuum emission contributing black body radiation to the spectral energy distribution of the active nucleus and explaining the blue bump or ultraviolet excess which is observed from active nuclei and nuclei of quiescent elliptical galaxies. Further accretion will lead to the infalling normal matter collecting on this degenerate pseudosurface. The matter accreted immediately outside the pseudosurface of the rotating black hole in the non-polar regions gives rise to the broad emission lines. The dense matter layers beyond the emission line layer

give rise to the absorption lines detected in the quasar spectrum. Such stratification, very close to the black hole, leads to line photons arising in a rapidly varying strong gravitational potential and hence appearing at a range of redshifts in the quasar spectrum. Thus, the continuum emission and multi-redshifted spectral lines in quasar spectra dictate a unique model for the distribution of matter around the supermassive black hole as was pointed out in Kantharia (2016a).

It was also suggested that the structure of nuclei of active galaxies other than quasars are also likely to be similar with the observational differences likely due to some differing parameters like the separation of the line forming matter from the supermassive black holes since the gravitational redshift critically depends on it and the quanta of this component in the spectral lines other active nuclei is lower than in quasars.

4.2.2.2 Model for active galaxies With the basic model for an active nucleus being determined from the data on the most extreme of the active nuclei i.e. quasars, we elaborate on this further by studying multifrequency (especially radio) data on all types of active galaxies and examining the myriad of physical processes that can be active in these. Moreover the explanation for microquasars will apply to active nuclei and hence the model discussed in Section 4.1.2 is also relevant to this discussion. We begin by outlining and describing the expected physical processes and their observational implications, followed by a description of the model that can explain an active nucleus of a galaxy and then elaborate on the effect of varying physical parameters of the black hole/accretion on the observed properties. We then describe the match between observations and the model structure of the active galaxy and end with case studies to demonstrate the comprehensive nature of the model. We hope to have convinced readers of the validity of the model by then and the experts will notice that this has raised many other interesting research problems.

Expected physical structure & processes: The physical system that we are trying to understand consists of a rotating supermassive black hole immersed in a gaseous medium i.e. the interstellar medium of the host galaxy. Since the black hole dimensions are very small compared to the scale height of the galaxy, it is reasonable to assume spherical gas inflow. The black hole accretes matter with volume densities increasing as $1/r^3$ where r indicates the separation of the infalling matter from the black hole. Outside the event horizon, it can be postulated that the mass densities become so large that matter transforms to

the degenerate state and its degeneracy pressure provides support against collapse into the black hole. A quasi-stable layer of degenerate matter accumulates outside the event horizon forming the pseudosurface of the black hole. The local accretion rates vary with latitude due to latitude-dependent centrifugal force which leads to a prolate-shaped event horizon of a rotating black hole and could lead to the formation of a prolate-shaped pseudosurface. Subsequent to the formation of the pseudosurface, infalling matter deposits on it and does not fall into the black hole. All the infalling matter in the polar region deposits directly onto the pseudosurface. In the non-polar regions, rotation leads to relatively lower accretion rates so that some matter will deposit onto the pseudosurface and the remaining infalling matter will accumulate outside in the form of an accretion disk. Eventually, the infalling matter will collect in the accretion disk with the same accretion rate as at the poles and then flow onto the pseudosurface at a lower rate. Thus in rotating black holes, an accretion disk will always be present beyond the layer of normal matter that accumulates on the pseudosurface in the non-polar regions. The layer of matter deposited on the non-polar pseudosurface and the accretion disk is likely to be dragged along by the rotating black hole. The detection of molecular gas arranged in a rotating disk morphology whose axis is coincident with the radio jet axis in Centaurus A (<https://www.eso.org/public/news/eso1222/>), Hydra A and Abell 262 (Olivares et al., 2019) could be signatures of an accretion disk around the supermassive black hole. The linear extent molecular gas disk is few kiloparsecs in both the cases. Such disks should be present in all accreting rotating black holes and they should be detectable in molecular lines and dust emission. The distinct environment of the collected matter in the polar regions and the non-polar regions is to be noted. In the polar regions, matter accumulates at the highest possible accretion rates for the system on the pseudosurface and is confined on the inner side by the pseudosurface but free on the outer side. In the non-polar regions, matter accumulation is slower and the layer of normal matter which accumulates on the pseudosurface is sandwiched between the accretion disk on the outer side and pseudosurface on the inner side. *Thus the structure of all rotating accreting black holes is expected to consist of (1) a quasi-spherical pseudosurface composed of degenerate matter (2) normal matter collected on the pseudosurface (3) a non-polar accretion disk.* The detailed physical properties of such a structure will depend on the specifics of the system e.g. a supermassive black hole will form an accretion disk which

is larger in linear dimensions than a stellar mass black hole.

Further reflection on the differences in the accumulation of matter at the poles and in the non-polar regions allows us to understand the evolution of the accreted matter. The rotating matter accumulated in the non-polar parts on the pseudosurface are blocked on both sides and hence a likely evolutionary path is conversion to the degenerate state as densities increase due to compression and hence thickening of the degenerate matter layer. This accreted matter can be ejected from the system only if sufficient energy is pumped into it so that it can overcome rotation and shatter the accretion disk which if not impossible should have a lower probability than retention of all the accreted matter. Thus, the evolution of infalling matter in non-polar regions can be summarised to be: accumulation in the accretion disk, flowing onto the pseudosurface, getting compressed to higher densities and thickening of the non-polar pseudosurface or occasional ejections. In contrast to this, the matter accreted in the polar regions of the pseudosurface is likely to follow a different evolutionary path wherein some of the accreted matter is ejected following an energy pulse. In this case, the only condition to be met is that the injected energy is sufficient to eject the matter at escape velocities. This then boils down to the following scenario which has already been shown to be valid in the case of the accreting white dwarf in a nova binary and on the accreting black hole in X-ray binaries. Continuous accretion of normal matter at the poles will lead to compression of the lower accumulated layers and hence their heating. Once the temperature of the lower layers exceeds 10^8 K, an explosive thermonuclear reaction can occur which can inject a pulse of energy to the accreted matter. We already know from other astrophysical systems and physics that this type of energy release is huge (depending on the quantity of matter that is ignited) and fast. This energy can accelerate the matter to escape velocities and since the matter is not confined on the outside, matter can explode out of the system. Thus, the polar regions can be envisaged to be frequently going through a cycle of matter accretion, compression, ignition and ejection. This ensures that the infalling matter in the polar region always forms a thin layer on the pseudosurface before being expelled and hence the degenerate matter layer would not thicken with time. However there are likely to be a fraction of the explosions which are not of sufficient energy to accelerate matter to escape velocities and hence this matter will accumulate on the polar region till the next explosion occurs. Another outcome of the thermonu-

clear explosions will be enrichment of the accreted matter. Thermonuclear explosions can be expected to occur over the entire pseudosurface since the only requirement is that matter is compressed and heated to high temperatures which is expected in matter accreted by a compact object. Although the explosions might not be energetic enough to eject matter in the non-polar regions, these will lead to enrichment of matter. Thus all matter that has experienced a thermonuclear reaction will be enriched till iron is formed after which the exothermic nature of the thermonuclear reaction will cease. This means that the matter in the non-polar regions which is rarely ejected will be continuously enriched with time while in the polar regions, the matter that is not ejected will be enriched. The enriched matter can accumulate on the pseudosurface at the poles and thicken the pseudosurface. *The expected physical processes in the accreted matter on the pseudosurface, which underline the quasi-stable nature of structure close to the black hole, will be (1) existence of a layer of normal matter on the non-polar pseudosurface accreted through the accretion disk. Repeated thermonuclear explosions in the accreted matter in the non-polar regions which enrich the accreted matter and hasten its eventual evolution to the degenerate state which thickens the non-polar pseudosurface. The accumulated matter in the non-polar regions forms the broad line region (BLR). (2) Repeated thermonuclear explosions in the accreted matter at the poles powering episodic outbursts of matter. The matter ejected from the poles forms the narrow line regions (NLR). In some cases, the explosions lead to enrichment of matter and thickening of the polar pseudosurface.*

The above discussion has already led to a model for the active nucleus/galaxy which we summarise below.

Summarising the model: Now that the basic physical structure of a rotating accreting black hole and physical processes in the accreted matter have been outlined, we can describe the physical model for an active nucleus/galaxy and connect it to observational results before elaborating on the different parts.

We recall the main observable signatures of an active nucleus: (1) luminous multiband continuum emission from an unresolved core, (2) occasional presence of broad permitted emission lines arising in the BLR, (3) ubiquitous narrow permitted and forbidden emission lines arising in the distributed NLR, (4) occasional presence of radio core, jets, lobes, hotspots (5) multi-band variability.

In literature, the origin of the black body component that is required to explain the observed SED

of the core has been attributed to the accretion disk since black holes do not have a surface and observations require a hot emitting body. Now with the inevitable formation of a hot dense pseudosurface around the black hole as described above, it has to be the source of the black body component. The hot pseudosurface will also be the source of hard ionizing photons required to explain the high excitation line spectra observed from active nuclei. The line spectra will be formed in the accreted gas either in the matter accumulated on the non-polar pseudosurface or in the matter ejected from the polar regions. These points mean that the existence of a hot pseudosurface which is expected from physical arguments outlined above, is well supported by observational results. Continuum emission can also be contributed by the hot normal matter accreted onto the non-polar pseudosurface. The nature of the observed line emission from the BLR and NLR are expected to be different. The matter in the polar regions is accreted, heated, enriched, ejected and will be eventually spread over a large region whereas in the non-polar regions, the matter is confined to a small region near the black hole, compressed, heated, enriched but seldom ejected. The polar line forming region will be the NLR which has been surmised from observations to exist from near the core to large distances along the polar direction whereas the non-polar line forming region will be the BLR which has been surmised from observations to be compact. The co-existence of the extended NLR and radio jet/lobes/hotspots along the polar axis (generally the minor axis of the galaxy which is generally the rotation axis of the black hole) supports their origin in matter ejected from the poles of the black hole following energy injection from a thermonuclear explosion in the accreted matter. The accreted matter in the non-polar regions which is sandwiched between the pseudosurface and the accretion disk is compact and rotates with the black hole. Since this region lies close to the black hole, it is responsible for the broad emission lines with the large widths being due to the large and varying gravitational potential within the BLR. The large gravitational potential in which the photon is formed leads to a shift in its wavelength (gravitational redshift component) and the finite thickness of the line forming region leads to broadening of the lines. Both the factors depend critically on the separation of this region i.e. BLR from the black hole. If the BLR forms very far from the black hole then the spectral lines will not show a gravitational redshift component nor will they be gravitationally broadened. This helps us infer that all the active nuclei which show the presence of a broad line in their

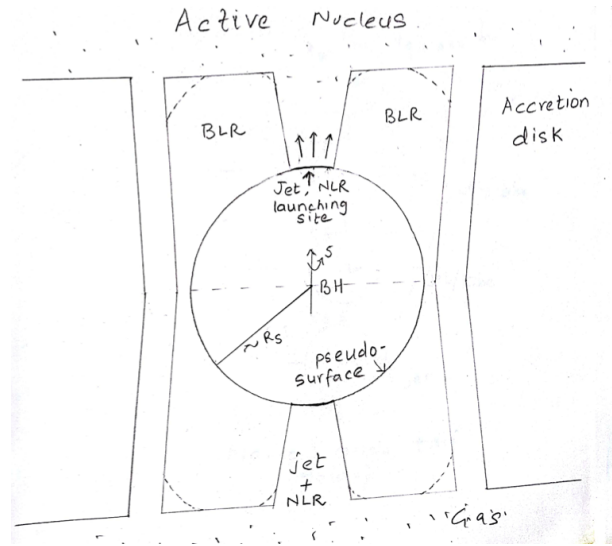


Figure 25: A zoom-in of the nuclear region of an accreting black hole, showing the structure as supported by observations and physics. The BLR is hour-glass shaped with a hole in the polar regions from where the jet and NLR are launched. The accretion disk contains the excess matter which accumulates outside the pseudosurface due to the reduced non-polar accretion rates in a rotating black hole. The pseudosurface can also be prolate-shaped for a fast rotating black hole.

spectra, have formed a BLR sufficiently close to the black hole for the line photons to include a contribution from a gravitational redshift. The active nuclei from which only narrow lines are detected can indicate that the BLR is located far from the black hole so that the influence of the gravitational potential is negligible. However it is also possible that the sight-line has missed intercepting the BLR in these cases. Careful examination of observational results should help us disentangle the two types of cases which can lead to non-detection of broad lines.

Thus the structure of the active nucleus or more generally the distribution of matter around an accreting rotating black hole is illustrated in the schematic in Figure 25 as expected from known physics and known physical processes. This structure trivially explains several observed properties of an active nucleus. *To summarise: (1) a layer of hot dense degenerate matter accumulates around the black hole forming its pseudosurface. The pseudosurface emits black body radiation which is the photoionizing radiation field exciting the line forming regions, (2) matter accreted in the non-polar regions of the pseudosurface forms a BLR from which broad emission and absorption lines emerge, (3) episodic thermonuclear explosions in the accreted matter at the poles launch bipolar radio synchrotron jets and NLR from which narrow forbidden lines emerge.*

Spin, mass, pseudosurface of black hole: In

general relativity, the concept of an innermost stable circular orbit (ISCO) has been introduced. Matter located inside the ISCO is unstable and plunges into the black hole. The radius of the ISCO for a non-rotating black hole has been estimated to be $3R_s$ whereas for a rotating black hole, the ISCO is the equatorial radius of the event horizon which can be as small as $R_s/2$ for a maximally rotating black hole. In the quasar sample that was examined in Kantharia (2016), the median gravitational redshift shown by quasars was $z_g = 0.25$ indicating that the emission line photon in half the quasars arises at a separation $< 2R_s$ from the black hole which then provides another unambiguous piece of evidence to spinning black holes in quasars. The bipolar radio jets and NLR detected in many active galaxies also argue for a spinning black hole and hence it appears safe to assume that all active galaxies host a supermassive rotating accreting black hole. To recap, at least three different observations support the existence of spinning black holes in active nuclei: (1) a gravitational redshift that is > 0.5 which indicates the existence of an ergosphere (2) existence of matter within the ISCO of a non-rotating black hole as surmised from the gravitational redshift component in spectral lines (3) presence of bipolar radio jets and NLR in active nuclei.

For an accreting spinning supermassive black hole, the fundamental variables are mass (or Schwarzschild radius) and spin rate of the black hole and the infalling matter densities. Table 2 shows the nature of dependence of the observed properties of active nuclei on the spin and mass of the black hole for the same infalling matter densities. The black hole spin emerges as the single-most important parameter which can account for a range of observed properties of active nuclei. Higher spin rate of a black hole should lead to lower accretion rates in the non-polar regions due to the larger magnitude of the centrifugal force ($F_c \propto r_i \omega^2$ where ω is the angular velocity of the black hole and r_i is the separation of the surface at latitude i from the polar axis) which reduces the effective gravitational force acting on the infalling matter. It will also lead to the BLR & accretion disk enclosing almost the entire pseudosurface due to the modified gravitational force being effective to larger latitudes so that broad lines from the BLR should be detectable from such nuclei over most sightlines. The pseudosurface and BLR can be radially thinner, hotter and more variable - all due to their proximity to the black hole. On the other hand, the accretion disk around such black holes will be radially extended due to the lower accretion rates on the pseudosurface. The higher spin of the black hole will lead to reduc-

ing the extent of the polar region (while the BLR encloses most of the pseudosurface) wherein the effect of the centrifugal force ($r_i \rightarrow 0$ in the polar region) is negligible so that the infalling matter is subject to the highest possible gravitational force. Infalling matter will accumulate directly in this region instead through an accretion disk and can be compressed and heated. When the temperature exceeds 100 million degrees K, a thermonuclear outburst can eject the accreted matter i.e. jets and NLR from this polar region. Since the extent of this region will determine the jet opening angle, faster rotating black holes will have smaller jet opening angles. This ejection can happen from close to the black hole since matter accumulates in a small region and matter has to be ejected with relativistic velocities to be able to leave the system. In a faster spinning black hole, energy will be focussed within a smaller opening angle thus explaining the highly relativistic velocities observed for narrow jets. *To summarise, black hole spin is responsible for the latitude-extent of the non-polar BLR, accretion disk and opening angle of polar jets amongst other features. A range in the spin rate of black holes explains the range of radio jet opening angles that are observed in active nuclei and the detectability of broad lines.*

The main effect of a larger mass, given other parameters are the same, is to increase the linear dimensions of the system with one of the important outcomes being increased detectability of the system. Mass differences can lead to black hole powered objects being classed into different types e.g. microquasars host stellar mass black holes and quasars host supermassive black holes with the former being randomly distributed in a galaxy while the latter always located at the centre of the galaxy. The main effect of larger infalling densities given other parameters are the same, would be to enhance the accretion rates and hence thicken the pseudosurface and/or the BLR in the non-polar regions and lead to more frequent thermonuclear outbursts in the polar regions. In such a case, the photons from the BLR will progressively arise from an increasing distance from the black hole as the pseudosurface thickens. The frequent thermonuclear explosions in the polar regions, if not energetic enough to expel matter, can lead to a radio-quiet active nucleus and if energetic enough to expel matter, can lead to frequent episodes of matter ejection and hence a radio-loud nucleus with distributed optical line emitting gas i.e. NLR. We now examine in detail, the properties listed in Table 2 starting with the non-polar regions.

It can be inferred from the highly luminous nuclear continuum (e.g. quasars) and broad emission

Table 2: The expected behaviour of physical parameters for a spinning, accreting black hole which can be surmised from physics are listed in this table. All cases assume the same infalling matter densities. A black hole of the same mass is considered for examining the spin-dependent properties and a black hole of the same spin is considered for examining the mass-dependent properties. L refers to 'largest' of the property while S means the smallest and O means that there is no effect on that parameter. Accretion rate is considered in terms of total mass accreted so that around a more massive black hole the accretion rate will be larger by virtue of a larger surface area (i.e. larger R_s).

| Region | Physical parameter | BH of same mass | | BH of same spin | |
|---|------------------------------------|---|------------------------|---|------------------------------|
| | | High spin BH | Low spin BH | High M_{BH} | Low M_{BH} |
| Non-Polar region properties | | | | | |
| Pseudosurface (degenerate matter layer) | Global accretion rate ¹ | S | L | O | O |
| | Radial thickness | S | L | S | L |
| | Latitude thickness | L | S | O | O |
| | Separation from BH | S | L | O | O |
| | Temperature | L | S | O | O |
| | UV luminosity | L | S | L | S |
| | Variability | L | S | | |
| Broad line Region | Radial extent | S | L | S ² | L ² |
| | Latitude thickness | L | S | O | O |
| | Ionization,excitation | L | S | L | S |
| | Variability | L | S | | |
| Accretion disk | Radial extent | L | S | S | L |
| | Latitude thickness | L | S | O | O |
| Examples ³ | | quasar BLRG Seyfert 1 | - NLRG Seyfert 2 | quasar BLRG Seyfert 1 | - NLRG Seyfert 2 |
| Polar region properties | | | | | |
| Pseudosurface (degenerate matter layer) | Global accretion rate ⁴ | S | L | L | S |
| | Thickness ⁵ | S | L | O | O |
| | Separation from BH ⁵ | S | L | O | O |
| | Emitting region | S | L | O | O |
| Accreted matter layer | Thickness | L | S | O | O |
| | Circular size | S | L | L | S |
| | Separation from BH ⁵ | S | L | O | O |
| Thermonuclear outburst ⁶ in accreted matter | Frequency | L | S | O | O |
| | Energy directivity | L | S | O | O |
| Expulsion of matter ⁶ | Recurrence rate | L | S | O | O |
| | Ejection speeds | L | S | O | O |
| | Jet opening angle | S | L | O | O |
| | Jet lengths | L | S | O | O |
| | NLR length | L | S | O | O |
| | Random relativistic speeds | L | S | O | O |
| | Radio synchrotron | L | S | L | S |
| Examples ³ | | FR II ^{7,8} GPS, CSS ^{7,8} | FR I Seyferts | Radio galaxy ⁸ Radio qsr ⁸ | Sy,LINERs Radio-faint qsr |
| Host galaxy ⁹ | | Elliptical | Spiral | Elliptical | Spiral |

¹ Varying accretion rates due to latitude dependent centrifugal potential; largest at poles. ² Larger mass of the black hole increases the surface area of the outer event horizon leading to the listed outcomes. ³ The examples are compared in pairs. ⁴ Varying accretion rates caused by different linear sizes of the polar region involved. ⁵ This follows from the frequent outbursts so that most accreted matter is ejected. ⁶ Achieving conditions conducive to thermonuclear explosion should be easier in a small region with high accretion rates. ⁷ FR II and FR I are comparable in size and GPS, CSS are comparable in size to the radio structure in Seyferts ⁸ These examples are made on basis of the radio loudness property. ⁹ This is based on observational results.

lines of high ionization and a significant gravitational redshift component (e.g. quasars) that the pseudosurface and BLR in that active nucleus have formed in close proximity to a fast spinning black hole. Similarly we can infer from the radio jets observed to be expanding with highly relativistic velocities and launched within small opening angles (e.g. FR II sources) that the ballistic ejection in that active nucleus has happened from close proximity to a fast spinning black hole where the escape velocity is relativistic. The main observable attributes of the non-polar regions are the black body radiation from the pseudosurface and continuum and broad lines from the BLR whereas that of the polar regions are the radio jets and optical line forming NLR. The polar region involved in the thermonuclear explosion gets larger and the latitude extent of the BLR smaller for black holes of lower spin rates. The jet is launched within a larger opening angle and the efficiency of energy transfer, collimation and subsequent processes decline so that the jet is relativistic close to the core from where it is launched but quickly becomes sub-relativistic (e.g. FR I). Since the radio structure in FR II and FR I sources extend upto several hundred kiloparsecs but show distinct jet behaviour (opening angle and persistence of ballistic nature), they represent the high and low spin cases respectively in high mass black holes. The dimensions of the radio structure of GPS, CSS sources is comparable to Seyferts although the radio strengths are very different. These, then, might represent the high and low spin systems of a lower mass black hole with other parameters contributing to rest of their observed differences.

The ejection of matter occurs from the polar region of the quasi-spherical pseudosurface which will have a finite curvature. For simplicity if we assume that the pseudosurface is a spherical surface then radial ejection of matter from the poles of such a surface, irrespective of the black hole spin and mass, will always lead to a conical outflow. This means that the observed conical radio jets and NLR are expected when the ejection is from the pseudosurface and no other explanation is necessary. In other words, the conical outflows provide independent evidence to the ejection of jets and NLR from the polar pseudosurface. The spin of the black hole will vary the cone angle such that a fast spinning black hole will launch the jet within a small conical angle while a slower black hole will launch the jet in a larger conical angle. Thus the conical angle which is viewed in two dimensions and which we refer to as the jet opening angle is a function of the black hole spin. The observed conical angle will be enhanced by effects like a precessing spin axis of the black hole.

The synchrotron emission from radio jets in several cases is observed to consist of a discrete clumpy component and a uniform component. While the bulk expansion of the clumpy component is measured to be relativistic from proper motion measurements, it is difficult to ascertain the expansion speed of the uniform emission component. One can speculate that while the clumpy component is accelerated by the thermonuclear outburst, the uniform component consists of the infalling matter which has been pushed out by the action of radiation pressure of the photons from the pseudosurface. However this would require that the observed radio spectrum of the clumpy and uniform component are different as is possibly the source of the magnetic field. This is a speculation which needs to be investigated further with observational data.

The variety of observed features of the different active nuclei has prompted their classification into several types. Quasars are characterised by a luminous star-like nucleus which overwhelms the galaxy emission, wide and highly redshifted emission lines of permitted high ionization transitions and wide absorption lines at redshifts lower than the wide emission lines. BLRG are radio galaxies characterised by a bright nucleus (fainter than quasars), wide emission lines of permitted transitions and narrow forbidden lines. BLRG show a FR II radio morphology. NLRG are radio galaxies characterised by faint nuclear emission and narrow lines of both permitted and forbidden transitions. NLRG show a FR I radio morphology. Seyfert 1 host a bright nucleus, wide permitted emission lines and narrow forbidden emission lines while Seyfert 2 show a faint nucleus and only narrow emission lines. A radio core is commonly detected in Seyferts. While radio galaxies are radio bright, a large fraction of quasars and Seyferts are radio faint. Blazars are radio bright compact active nuclei and comprises BL Lac objects and flat spectrum radio quasars (FSRQ). While BL Lac objects generally show a featureless continuum, FSRQ show broad emission lines superposed on the continuum.

It appears that the observed range of properties of active nuclei arise due to a combination of important physical differences and orientation to the sight-line. We try to identify the differences here. The higher continuum luminosity and quanta of gravitational redshifts in quasars are signatures of the proximity of the pseudosurface, BLR to the black hole as compared to other active nuclei. This property has a physical origin in the non-polar regions which differentiates quasars from other active nuclei. Considering that the radio structure of quasars, when detected, is similar to FR II radio galaxies, it in-

icates similarity of physical processes in the polar regions of quasars and the active nucleus in FR II galaxies but differences in the non-polar regions. It means that the polar ejections happen close to a fast spinning black hole in quasars and FR II galaxies but the non-polar BLR in quasars is located closer to the black hole than in the latter. Many quasars are radio-quiet like Seyferts and show the presence of Fe II lines as do several Seyfert 1. On the other hand, BLRG are radio bright but notoriously deficient in Fe II lines. This aspect argues for the same physical process being responsible for iron enrichment in active nuclei which could be nucleosynthesis in thermonuclear reactions. This could occur in the BLR and/or in the accreted matter in the polar regions which is not expelled. The lack of iron lines in BLRG argues for their production in the polar region in that in BLRG, the thermonuclear energy always expels matter so that iron is seldom synthesised from the hydrogen-rich fuel whereas in the radio-quiet quasars and Seyferts, ejection is infrequent and hence iron could be ultimately synthesised at the poles. However the prevalence of iron lines in Seyfert 1 as compared to Seyfert 2 argues for its synthesis in the BLR. Thus the ambiguity on where the iron lines are formed - in the BLR or the polar region or both. This needs further investigation. Currently we can infer that the observations provide strong independent support to the occurrence of thermonuclear explosions in the accreted matter near the supermassive black hole. The orientation-based unification theory and radio observations have long suggested that quasars and blazars are the same objects observed from different angles. The broad lines from blazars contain a large gravitational redshift component like quasars (Kantharia, 2016a) which lends independent support to their unification. The orientation-dependent unification works for quasars and blazars with BL Lac objects being viewed exactly pole-on so that the sightline misses the BLR explaining the lack of broad lines and FSRQ being viewed at a small angle to the jet axis so that the broad lines from the BLR are detectable. Quasars viewed from any other sightline will always detect the BLR explaining the ubiquitous presence of broad lines in their spectra. The ubiquity of radio emission from blazars which are observed along the jet axis and its rarity in most quasars might be due to the combination of Doppler beaming and inherent faintness due to extremely narrow opening angles. Only quasars (includes blazars) amongst active nuclei show large gravitational redshift components in their spectral lines highlighting the important physical difference between quasars and other active nuclei of differing separation of the BLR from

the black hole. Since most FR II are BLRG while most FR I are NLRG, these highlight the differences in the spin of the black hole, covering factor of the BLR and its separation from the black hole and the jet opening angle. The classes ranging from Seyfert 1 to 2 seem to signify the increasing separation of the BLR from the black hole and only a subset of Seyfert 2 might host a hidden BLR close to the black hole. Since the radio properties of Seyfert 1 and 2 are similar, it would indicate that their spins are comparable. It appears that the radio galaxies referred to as FR I and NLRG are the same as are FR II and BLRG. The classification of FR I/FR II has been made from polar properties (radio synchrotron) whereas NLRG/BLRG is from non-polar (spectral lines from BLR) properties of the same objects. This means that in FR II/BLRG, the BLR is located close to the black hole and its covering factor is large whereas in FR I/NLRG, the BLR is located relatively far from the black hole and its covering factor is smaller.

To summarize: The black hole spin is the single-most important physical parameter responsible for several observed properties of active nuclei. Only rotating black holes can launch ballistic relativistically expanding bipolar jets and optical line forming NLR and higher the spin rate, smaller is the jet opening angle. Rotating black holes form a BLR in the non-polar regions from which gravitationally redshifted and broadened lines arise in addition to an accretion disk beyond the BLR. Infalling matter densities determine the maximum possible accretion rates while mass of the black hole determines the linear size of the region over which the black hole exerts its gravitational influence.

Since the nuclei of all active galaxies are observed to be a multi-band compact source, it supports the formation of a hot pseudosurface in all active nuclei. The simplest scenario for the location of the pseudosurface is at the event horizon of the rotating black hole. Since the event horizon of a rotating black hole is prolate-shaped, this means that the pseudosurface of rotating black holes will be prolate-shaped if a thin layer is deposited at the event horizon. The main condition for the formation of a pseudosurface is that matter enters a degenerate state and the degeneracy pressure is sufficient to prevent the gravitational collapse of matter into the black hole. Matter can enter the degenerate state when densities exceed 10^5 gm cm^{-3} . Since volume matter densities will increase as $1/r^3$, it is possible that in dense environs where the infalling matter densities are high, such densities are reached at a larger separation r from the black hole compared to when the infalling matter densities are

small. This means that the pseudosurface need not always form at the event horizon and instead its separation from the black hole can be a variable which depends on the global infalling matter densities such that when the density is low, the pseudosurface (and BLR) forms close to the black hole and when the density is high, the pseudosurface (and BLR) forms far from the black hole. The same argument will also hold in the polar regions so that the pseudosurface and hence matter ejection will happen far from the black hole if the infalling matter density is high and from closer to the black hole if the infalling matter density is low. This means that the radial separation of the pseudosurface from the black hole is likely to be dependent on the infalling matter densities.

We can understand this further by using the gravitational redshift z_g of the broad emission line to quantify the separation of the non-polar pseudosurface from the black hole and the bulk relativistic velocity of the polar jet v_{bulk} equated to the escape velocity to quantify the separation of the pseudosurface from the black hole in the polar regions. We consider the example of the quasar 3C 273 which is discussed later on wherein its distance has been revised to 20 Mpc. For this case, the broad emission line from the BLR appears to include a component $z_g \leq 0.131$ which indicates that the pseudosurface is located at a separation $\sim 3.8R_s$ while the jet bulk velocity of $0.16c$ is derived from the proper motion of the blobs which corresponds to a launch site being separated from the black hole by about $39R_s$. These values indicate a prolate-shaped pseudosurface in 3C 273. The varying separation of the BLR and jet launch site from the black hole can be explained either by a prolate-shaped thin pseudosurface which has formed far from the event horizon or an asymmetric pseudosurface of varying thickness at the event horizon such that it is thick at the poles and thin at the equator which is expected from the latitude-dependent accretion rates. Although we refer to the two parts as polar and non-polar for simplicity, we are cognisant that there will be variation of properties within the non-polar parts of the pseudosurface as a function of latitude. This simplified reference is resorted to keeping in mind that only if we can fully grasp the distinction in properties between the polar and non-polar parts can we hope to understand the variation within the non-polar parts. The range of large gravitational redshifts that are detected in the quasar spectra indicate that the BLR is radially extended and consists of emission line and multiple absorption line zones located in close proximity to the black hole supporting the formation of the non-polar pseudosurface at the event horizon. In fact, observations show that the

emission line zone of the BLR in quasars is located at a separation $\leq 32R_s$. Thus, it can be inferred that the pseudosurface forms close to the event horizon in quasars. From the above discussion it might be possible to infer that the non-polar accretion rates are low owing to lower infalling matter densities and/or high spin of the black hole in quasars. Only a small contribution of z_g appears included in the broad line redshifts of BLRG and Seyfert 1 nuclei indicating a large separation of the line forming zone in the BLR and the black hole. Since in BLRG/FR II, relativistically expanding jets are launched from close to the black hole, the low observed values of gravitational redshifts would mean that the BLR is located far from the black hole while the jet launching site is close to the black hole. This can be translated to indicate a oblate-shaped pseudosurface. The pseudosurface of the black hole in BLRG could show a latitude-dependent thickness with the first layer of degenerate matter having deposited close to the event horizon. Gradually the non-polar pseudosurface has thickened as an increasing quantity of matter has been accreted, compressed, heavier elements synthesised and finally compressed to degenerate matter densities. In Seyfert 1 nuclei, the radio emission is generally compact and faint and jets are seldom observed to be expanding relativistically. Since gravitational redshifts are also negligible, it appears that both the BLR and the jet launching site in Seyfert 1 are located far from the black hole. The infalling matter densities in Seyfert nuclei can be large as their spiral hosts are gas-rich and it is likely that the large infalling matter densities have led to the formation of a pseudosurface far from the event horizon. However it is likely to be closer to the black hole and hotter in Seyfert 1 than in Seyfert 2 galaxies as can be surmised from the luminous core and broadening of the lines in the former.

It was pointed out by Fowler (1926) that matter can exist in the degenerate state if it has sufficient energy so that the electrons are not bound to any atom but free. These electrons have energy to escape from any nucleus that they happen to venture close to during their journeys. Thus when matter enters the degenerate state, its energy content will be high which will be reflected in the high temperature which will radiatively decline if there is no further energy input. As Fowler (1926) also pointed out, the radiative losses will lead the temperature of the degenerate matter to gradually approach 0°K while the energy content will continue to remain finite which naturally emerges from quantum statistical mechanics. To quote from Fowler (1926) - "Temperature then ceases to have any meaning, for the star is strictly analogous to one gi-

gantic molecule in its lowest quantum state. We may call the temperature then zero.” This giant molecule will continue to have its ground state energy but will stop radiating since its temperature will be zero.

The hot pseudosurface formed around the black hole provides the ionizing photons for the non-polar BLR and polar NLR. The degenerate matter will cool as it radiates and unless there is continuous energy input or formation of a new degenerate matter layer, the pseudosurface will cool. The lower temperature of the pseudosurface would lead to a softer radiation field which will reduce the quanta of hard photons that can excite high-ionization lines in the BLR and/or NLR. This would eventually lead to the quenching of broad emission lines from the BLR so that the existence of a BLR in systems with a low temperature pseudosurface is ambiguous. It is to be noted that in Seyfert 1, a luminous nucleus and wide lines are observed whereas the Seyfert 2 nucleus is fainter and wide lines are absent. Range of line widths and nuclear continuum are observed for Seyfert nuclei which are then placed between types 1 and 2. These observations tend to support the scenario in which the pseudosurface in Seyfert 1 and 2 are of different temperatures which lead to varying nuclear strengths and different physical conditions in the BLR. Since the temperature of the pseudosurface can vary it could also lead to varying physical conditions in the BLR. For example, if the pseudosurface was heated and brightened then the BLR will also suddenly be heated and ionized and start emitting wide lines. This, then, can explain the changing look active nuclei (e.g. quasars and Seyferts) in which the properties flip-flop between the two types. This hypothesis appears highly plausible since it explains both the changes in the continuum and line properties that occur when a type 2 transforms to a type 1 nucleus or vice versa. Additionally, the above can also explain the existence of the intermediate types between 1 and 2 as simply a result of the range in the temperature of the pseudosurface.

To summarise: A hot pseudosurface composed of degenerate matter is formed around all black holes in active nuclei. This quasi-spherical surface is formed near the event horizon in quasars but much further in Seyfert nuclei. The radiating pseudosurface will cool and the temperature changes can explain the range of properties observed for type 1 and 2 Seyferts and quasars. A hotter pseudosurface will ionize the BLR so that wide lines arise from it whereas the BLR near a cooler pseudosurface will be undetectable. Thus, the bright nucleus and broad lines observed from quasars, Seyfert 1 and BLRG indicate the presence of a hot pseudosurface whereas the faint nucleus and absence

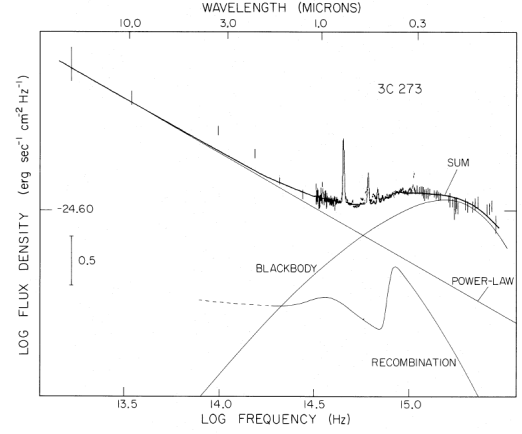


Figure 26: Figure copied from (Malkan & Sargent, 1982) showing the three component fit to the SED of 3C 273 from infrared to ultraviolet bands. The three components are black body of temperature 26000 K, a Balmer continuum of temperature between 13000-15000 K and a power law of index 1.1.

of broad lines in Seyfert 2 and NLRG can be explained by a cooler pseudosurface. The changing look active nuclei can be explained by a change in the temperature of the pseudosurface.

In the remaining part of the section, we discuss the wideband SED; BLR; thermonuclear explosions and variability; redshift components; jets, lobes, hotspots; magnetic field around a black hole; dust formation in NLR; gas for accretion and radio faint active nuclei.

Wideband SED: The wideband spectral energy distribution of several active nuclei are often well-fit with three components - a black body component, a power law component and a Balmer continuum component (such as thermal free-free) as was demonstrated for Seyfert 1 and quasar nuclei by Malkan & Sargent (1982) (see Figure 26). In the framework of the model presented here, the origin of all three components is explained. The black body component should arise from the hot pseudosurface of the black hole, the power law component should arise from the synchrotron emitting relativistic plasma in the polar regions that is energised in a thermonuclear explosion and the Balmer continuum should arise in the photoionized BLR around the hot pseudosurface in the non-polar regions. The contribution of the three components can vary amongst active nuclei as also their dominance at different wavelengths. For example, the black body component often dominates at soft X-rays, ultraviolet, optical wavelengths while the synchrotron component dominates at hard X-rays, radio and infrared wavelengths.

We first discuss the black body component and start with the example of the quasar 3C 273. An emitting area of about $3 \times 10^{33} \text{ cm}^2$ was required

to explain the 26000 K black body component that was surmised for 3C 273 from observations (Malkan & Sargent, 1982). As suggested here, the emitting area should indicate the area of the quasi-spherical pseudosurface which for simplicity we consider to be spherical and located at the event horizon of the black hole. The radius of this pseudosurface would be 1.5×10^{16} cm which if equal to the Schwarzschild radius of a black hole would require its mass to be close to $10^{11} M_{\odot}$. However it is to be noted that the distance to the quasar 3C 273 has been overestimated due to the presence of the z_g component in the broad emission line redshift and this is discussed more in the next section. 3C 273 is more likely to be located at ~ 20 Mpc (instead of ~ 650 Mpc) which will reduce its emitting area by the factor $(20/650)^2$ i.e. the area will be 2.8×10^{30} cm². This corresponds to a spherical surface of radius 4.7×10^{14} cm which is equal to the Schwarzschild radius of a black hole of mass $1.6 \times 10^9 M_{\odot}$. The mass of the black hole in 3C 273 has been estimated to be around a billion solar masses which then justifies the origin of the black body component in the (quasi)spherical pseudosurface formed near the event horizon. The physical parameters have emerged from observations without requiring any contrived explanations.

It was found that a single temperature black body provided a good fit to the observed SED and the best fit temperatures for several nuclei were estimated to lie between 20000 and 30000 K (Malkan & Sargent, 1982). The pseudosurface is composed of degenerate matter e.g. degenerate electrons which have high conductivity. The high conductivity ensures that the temperature is rapidly uniformised in the degenerate matter and hence the single temperature fit that is observationally found to be the best fit, is actually expected if the emission was from degenerate matter. From their fitting, Malkan & Sargent (1982) found that the Balmer continuum had a temperature ≤ 15000 K. This then supports its origin in the BLR which is photoionized by the much hotter black body radiating pseudosurface. This physical system bears resemblance to the photoionized HII region around a hot star although the detailed physical parameters such as size, temperatures, hardness of the radiation field etc are widely different.

If we assume that the pseudosurface forms at the event horizon, is a spherical surface and the entire surface radiates then we can estimate the expected black body luminosity for a few different black hole masses and temperatures as listed in Table 3. The estimates demonstrate the steep dependence of the absolute magnitude/luminosity on the black hole mass and temperature such that an order of magnitude

Table 3: The table lists the expected bolometric and V band magnitudes estimated from the Stephen-Boltzmann law for different mass black holes assuming that the black body radiation is from a spherical pseudosurface at the event horizon of the black hole. The estimates are shown for two values of temperature and the bolometric correction (BC) for $T = 16000$ K is -1.3 and for $T = 40000$ K is -3.8 . $M_V = M_b - BC$. Bolometric absolute magnitude of the sun is taken as -4.75 magnitudes and solar luminosity as 3.828×10^{26} Watts.

| M_{BH} M_{\odot} | $R_{s,BH}$ m | T = 16000K | | T = 40000K | |
|-------------------------|--------------------|-------------------|--------------|-------------------|--------------|
| | | M_b mag | M_V mag | M_b mag | M_V mag |
| 10^{10} | 3×10^{13} | -22.5 | -21.2 | -26.8 | -23 |
| 10^9 | 3×10^{12} | -17.5 | -16.2 | -21.8 | -18 |
| 10^8 | 3×10^{11} | -12.5 | -11.2 | -16.8 | -13 |
| 10^6 | 3×10^9 | -2.5 | 1.2 | -6.8 | -3 |
| 100 | 3×10^5 | 17.5 | 18.8 | 13.2 | 17 |
| 10 | 3×10^4 | 22.5 | 23.8 | 18.2 | 22 |

change in the black hole mass (and hence R_s) will lead to a change of 5 magnitudes in the luminosity while a change in the temperature by a factor of 2.5 leads to a change of 4.3 magnitudes in the bolometric luminosity. Importantly, the estimated values cover the range of luminosities that are normally recorded for active nuclei with M_{BH} ranging from 10^6 to $10^{10} M_{\odot}$. While all these values are determined assuming the entire pseudosurface emits, it is possible that at times the emission we record is from part of the pseudosurface because of obscuration and hence could be dimmer. These estimates also show that quasars which are the most luminous objects, host the most massive black holes with the hottest pseudosurfaces. Seyfert 1 and BLRG/‘N’ type galaxies although less luminous than quasars, are also likely to host massive black holes and/or hot pseudosurfaces explaining their bright nuclear continuum. The relatively faint nucleus in Seyfert 2 and FR I galaxies is likely due to a smaller radiating surface owing to a low mass black hole and/or a cooler pseudosurface. The temperature of the pseudosurface can be estimated from the bump in the wideband nuclear spectra since the black body peak should move to longer wavelengths in a cooler black body. The measured temperature alongwith the luminosity can then be used to estimate the area of the emitting surface and hence the mass of the black hole assuming the entire pseudosurface emits black body radiation. The effectiveness of such a method has already been demonstrated by Malkan & Sargent (1982) and others who have determined the emitting surface area and temperature

of the black body component. In literature, the origin of this black body component is often attributed to a hot accretion disk. This appears to be the case since a black hole does not have a surface unlike white dwarfs and neutron stars. However with the formation of a hot pseudosurface composed of degenerate matter around all accreting black holes, it has to be the source of black body radiation. It rules out the origin in an accretion disk which is much further from the black hole and saves us the trouble of having to hunt for models to explain the heating of the radially extended accretion disk.

The remaining two continuum emission components are also expected from the structure around an accreting rotating black hole. The Balmer continuum component of the SED arises in the hot photoionized non-polar BLR as mentioned earlier. In addition to the hot pseudosurface and BLR, there also exists the polar region where matter is accreted, ignited and ejected at relativistic velocities. Synchrotron emission which shows a power law spectrum is observed from the ejected jets. This would suggest that the power law component of the SED would be due to synchrotron emission radiated by the population of relativistic electrons that is energised in the thermonuclear explosions frequently occurring at the poles of an accreting black hole. The electron energies will follow a normal distribution (see Section 2) which readily explains the flatter or curved low radio frequency spectrum (due to lower energy electrons) as compared to the higher frequency emission (due to higher energy electrons) which is approximated by a power law. *To summarise: the origin of the three components which comprise the continuum emission from active nuclei are (1) black body emission from the hot (quasi)spherical pseudosurface around the black hole (2) Balmer continuum from the hot emitting zone of the non-polar BLR (3) power law synchrotron from the relativistic plasma energised and ejected from the poles.* These origins imply that the SED of an active nucleus viewed pole-on should not include any contribution from the Balmer component arising in the BLR while the SED of an object viewed edge-on will not include any contribution from the synchrotron emission at the poles.

The three radiation components responsible for the wideband continuum spectrum that are described above, will contribute varying amounts to emission at different wavelengths. Soft X-rays and ultraviolet bands will contain a significant contribution from the black body emission while emission at radio and hard X-rays will be dominated by synchrotron emission from the radio jets. The emission at optical and infrared wavelengths are likely to contain signif-

icant contributions from black body radiation, synchrotron emission and Balmer continuum. The energetic γ -rays that are often detected from flaring active nuclei can be due to inverse Compton scattering of γ -ray photons that are released in thermonuclear outbursts by relativistic electrons. It follows then that the variability detected in the continuum emission at optical, ultraviolet, soft X-ray band will be due to changes in the physical properties of the pseudosurface of the black hole, whereas the variability in the radio bands, hard X-rays, infrared bands will be associated with the polar changes such as new relativistic ejections, magnetic field inhomogeneities etc.

Broad line region (BLR): The BLR, observationally characterised by broad permitted spectral lines, is formed on the pseudosurface in the non-polar regions from matter that flows in from the accretion disk. It consists of emission and absorption zones and is photoionized by the radiation field of the pseudosurface. The matter in the BLR which is located next to the pseudosurface composed of dense degenerate matter will also be of high densities. Densities of $10^8 - 10^{10} \text{ cm}^{-3}$ have been derived for the BLR from photoionization arguments and lack of wide forbidden lines. The recombination (Balmer) component of the continuum emission has to arise in the emission zone of the BLR as discussed above. The BLR is formed so close to the black hole that the spectral lines arising in it are often shifted by a measurable gravitational redshift. The main difference in the gravitational redshift component present in the wide emission and absorption lines that are detected in the core spectra of quasars, BLRG, and Seyfert 1 galaxies is in the quantum of z_g . Moreover for a given active nucleus, the emission line redshifts are always greater than the absorption line redshifts indicating that the emission line zone forms closer to the black hole than the absorption line zone. It then follows that the photoionizing source lies between the black hole and the BLR. This gives further evidence to the existence of the hot pseudosurface of the black hole. In fact, noting that the emission line z_g measured for some quasars is as large as 0.5 i.e. the line photons arise at a distance of R_s from the black hole, conclusively rules out the accretion disk as the photoionizing source. If the accretion disk was the ionizing source, it would have to be located within R_s which is impossible. In literature the BLR is often considered to be located between the accretion disk and the dust torus since the accretion disk is believed to be the photoionizing source. This is now conclusively ruled out as discussed here. *The BLR lies between the pseudosurface i.e. black hole and the accretion disk and is photoionized by the radiation field of the hot*

pseudosurface. Most FR II radio galaxies are BLRG and it is found that even the FR II cores which show the presence of only narrow lines in total flux show strong wide lines in polarised flux revealing the existence of a BLR (e.g. Cohen et al., 1999). Broad lines are generally not detected from the nuclei of Seyfert 2 and FR I galaxies. However the existence of Seyferts with types between 1 and 2 in addition to changing look Seyfert galaxies which dynamically transition between the two types in addition to existence of the rare FR I galaxy which show broad Balmer emission lines in their nuclear spectrum indicate that there has to exist a continuum of properties for the BLR, and that a BLR exists in all active nuclei. The rarity of Seyfert 2 and FR I with wide lines prompts an interpretation that a fraction of the detected narrow lines in these cores can arise in a BLR which is located so far from the black hole that there is a negligible contribution from z_g . Observations do find a range of excitations in the narrow lines detected from Seyfert 2 which could be indicative of origin of a fraction of these high excitation lines in the BLR but with widths which are similar to the lines arising in the NLR making it difficult to differentiate the two origins.

If we assume that the many classes of active objects share the same space distribution since there appears no a priori reason to assume distinct distributions, then the observed variation in the emission line redshifts of the different classes of active nuclei can be attributed to the varying contribution of the intrinsic component of the redshift i.e. gravitational redshift. This is expected from the differing separation of the emission line zone in the BLR from the black hole in the different types of active nuclei. We can, hence, use the observed emission line redshift which contains a measurable component of gravitational redshift to estimate the separation of the emission zone of the BLR from the black hole. The BLR is located at a separation $\leq 30R_s$ in quasars (as deduced from the lowest gravitational redshift being ~ 0.016) and is within $2R_s$ for half the quasars (as deduced from the median gravitational redshift of 0.25). Since the gravitational redshift component in other active nuclei is generally smaller, it is assumed that the observed lowest redshift for a given class of active nuclei is dominated by gravitational redshift so that a rough estimate of the separation of the BLR from the black hole can be obtained. The observed emission line redshifts of FR II/BLRG are generally greater than 0.003 (see Figure 23) indicating that the BLR is separated from the black hole by $\leq 170R_s$ while those of FR I and Seyferts is around 0.001 (see Figure 23) indicating that the BLR is located $\leq 500R_s$

from the black hole. The GPS and CSS radio sources are detected at redshifts greater than 0.1 (see Figure 21) which would mean that the BLR is located at a separation $\leq 5R_s$. These GPS, CSS sources include objects classified as quasars and galaxies. When an entire class of objects systematically occur at high redshifts (e.g. quasars, GPS/CSS), it is important to first exhaustively explore intrinsic reasons before searching for exotic cosmological models which try to explain their absence in the local universe. This could prevent us from embarking on a wild goose chase.

The lines that are attributed to the BLR are very wide with FWZM ranging from 5000 to 30000 kms^{-1} or so. The BLR is located close to the event horizon of the black hole as conclusively demonstrated by the measurable gravitational redshift component in the broad spectral lines. In this case, the large widths of the lines from the BLR have to include a significant component due to the radially changing gravitational potential within the line forming zones of finite thickness. In other words, line photons arising from a range of radial separations from the black hole will be shifted by different gravitational redshifts with the net effect being a broadened line. Additionally the higher ionization emission lines appear from the innermost zones of the BLR and show larger gravitational redshifts and broadening while the lower ionization emission lines and absorption lines appear from the outer parts of the BLR and hence show lower gravitational redshifts and broadening. Thus the width of the broad lines and their gravitational redshift carries information on the radial extent and location of the line forming zone. The gravitational width ($\Delta\lambda$ expressed in the same units as wavelength λ) is related to the fractional thickness of the line zone $\Delta R/R = \Delta\lambda/\lambda$ (Greenstein & Schmidt, 1964). The high ionization line C IV 1550 Å is typically observed with widths $\geq 50\text{Å}$ (i.e. a velocity width $\geq 10000 \text{ kms}^{-1}$) from the BLR in quasars, Seyfert 1, BLRG. To make some quantitative estimates, we assume that the pseudosurface and BLR in these three classes of active nuclei typically form at a separation $\sim R$ from the black hole such that $R = 2R_s$ ($z_g = 0.25$) in quasars, $R = 50R_s$ ($z_g = 0.01$) in BLRG and $R = 250R_s$ ($z_g = 0.002$) for Seyfert 1. For a linewidth of 50 Å, the thickness of the C IV emitting zones in the BLR will be $\Delta R = 0.0322R$ i.e. $0.0644R_s$, $1.6R_s$ and $8R_s$ respectively for quasars, BLRG and Seyfert 1. This tells us that for the comparable line widths that are observed, the emission zone in the BLR is much more radially compact in quasars than in Seyfert 1 for a given black hole mass. For a black hole of mass $10^9 M_\odot$, the thickness of the C IV zone will be 1.9×10^8

km, 4.8×10^9 km and 2.4×10^{10} km - all within a light day (2.59×10^{10} km) for the three cases. For a $10^8 M_\odot$ black hole, the thickness of the C IV zone will be 1.9×10^7 km, 4.8×10^8 km and 2.4×10^9 km. All these explain the linewidth of 10000 km s^{-1} . If broader lines are detected, then the thickness of the region will be larger. For example, C IV lines of width 30000 km s^{-1} ($\sim 150 \text{ \AA}$) have been detected from NGC 4151 which gives $\Delta R/R = 150/1550 = 0.0968$. For this Seyfert galaxy for which the black hole mass has been estimated to be $\sim 10^8 M_\odot$, the thickness of the C IV zone would be about $24R_s = 7.2 \times 10^9$ km. High ionization lines of such widths are commonly detected in quasars where black hole masses are commonly estimated to be $\sim 10^9 M_\odot$. This would result in the thickness of the C IV zone being $7.2 \times 10^{10} \text{ km}$ i.e. about 3 light days. Similar exercise can be done on emission and absorption lines of different elements and different ionizations. This method, then, allows us to unravel the radial structure of the BLR from the observed gravitationally redshifted and broadened lines. The results should be comparable to those obtained from reverberation studies since the BLR spectral line variations are triggered by the photoionizing continuum of the pseudosurface.

BLR is formed from the matter that is accreted through the accretion disk onto the pseudosurface of the rotating black hole. To recall, the event horizon around a rotating black hole will be prolate-shaped whose semi-major axis (polar axis) is always equal to R_s whereas the semi-minor axis (equatorial extent) is $< R_s$ with its exact value depending on the spin. Noting that the local accretion rates are the lowest at the equator and gradually increase towards the poles means that the radial extent of the BLR will be minimum at the equator and will increase towards the poles (see Figure 25). The poles are devoid of an accretion disk and a BLR. Thus, the BLR can be visualised to be arranged in the form of an equatorially pinched, hourglass-shaped structure with small openings at the poles whose extent is determined by the spin of the black hole (see Figure 25). On the other hand, the accretion disk will accumulate maximum matter at the equator and matter accumulation will decrease with latitude. Hence the maximum radial extent of the accretion disk will be at the equator. The latitude coverage of the accretion disk will be similar to the BLR and its inner contour will be similar to the outer contour of the BLR so that if the accretion disk was to move in towards the BLR, the two surfaces would fit into each other (see Figure 25).

The BLR of a high spin black hole will have a larger covering factor by which we refer to the fraction of the event horizon/pseudosurface covered by

the BLR as compared to low spin black holes. The larger covering factor of the BLR of high spin black holes should make them detectable over most sightlines except maybe directly polar. Since the BLR around a low spin black hole will have a smaller covering factor and be confined to a smaller range of latitudes about the equator, detection of wide lines from these BLR will be more sightline-dependent.

The emission from a latitude-thin BLR which is not in our sightline, can be scattered by dust formed in the NLR or accretion disk into the sightline making it detectable. The distribution of dust in the accretion disk should be constant over long timescales while the distribution of the dust formed in the polar regions can be dynamic over shorter timescales. If the main scatterers are polar dust grains, then it provides another reason for the changing look active nuclei. The changing distribution of dust can change the properties of the scattered radiation and the BLR can alternate between detection and non-detection. All this supports the existence of a BLR in all active black holes with a spin-dependent covering factor. The covering factor of the BLR will approach unity in quasars and BLRG which will also explain a small opening angle for the jet and NLR while it should be small in Seyferts explaining the large jet angles when detected.

Spectral observations of Seyfert 1 nuclei have found that broad emission lines generally respond immediately or within a few days to any change in the optical/ultraviolet continuum emission. It is also noted that the higher ionization lines vary more and respond to the continuum changes before the lower ionization lines. The above is expected from the model presented here since the photoionizing is by the photons from the hot pseudosurface which lies between the black hole and the BLR.

To summarise: The matter accreted on the pseudosurface through the accretion disk forms the dense BLR consisting of emitting and absorbing zones. Observationally, this region is characterised by gravitationally redshifted and widened permitted spectral lines and Balmer continuum. The BLR should be arranged in a hourglass-like shape with conical openings at the poles whose opening angle is determined by the spin of the black hole.

Thermonuclear explosions and variability: In literature, the possible sources of the vast energy released in active nuclei are believed to be gravitational and/or rotational and/or magnetic in origin. The above three sources of energy are, no doubt, very important in the evolution of the active nucleus - gravitational contributing to the attraction and arrangement of matter around the black hole,

rotational contributing to the arrangement and rotation of accreted matter and magnetic contributing to providing a magnetic field for synchrotron processes. These demonstrate that the above three energy sources feed persistent processes. However it is difficult to envisage these energy sources being responsible for energetic transient events which lead to rapid acceleration of electrons and launching of relativistic jets. These perplexing issues have been extensively explored in literature and processes that might be active far from the black hole are promoted such as shock acceleration of electrons and magnetic collimation of jets. However, a water-tight physical explanation for basic jet-related issues like launching and collimation remain elusive and hence continue to perplex us with explanations in literature ranging from launching by the accretion disk to magnetic launching. We point out a simple physical process, that should be active close to the accreting black hole but has somehow been overlooked. This mechanism can provide energy to launch jets, accelerate electrons to relativistic velocities and consistently explain several observational results on active nuclei. This physical process is widely observed in the universe and hence requires no validation. In fact, it is the most obvious solution to the energy problem considering the physical conditions that should prevail in the accreted matter on the black hole and it is somewhat of a surprise that it has not been a favoured mechanism.

This important transient source of the vast energy released in active nuclei has to be catastrophic thermonuclear reactions. This follows from the fact that active nuclei consist of an accreting black hole wherein matter accumulates on the hot pseudosurface and should be progressively compressed and heated setting up physical conditions conducive to thermonuclear reactions. That such reactions can be highly explosive was convincingly demonstrated when it was shown that simultaneous ignition of $0.1 M_{\odot}$ of accreted matter will release $\sim 10^{50}$ ergs of energy in 1 – 100 seconds (Hoyle & Fowler, 1960). Such an explosion can be expected to occur in the accreted matter on the pseudosurface - leading to acceleration of matter and launching of jets from the poles and nucleosynthesis which enriches the matter and variability in the non-polar BLR. Observations have reported higher metallicity in the BLR which also supports nucleosynthesis in thermonuclear reactions. The ejected matter at the poles should consist of accelerated atoms/ions and relativistic electrons and observationally these are identified as the narrow line region (NLR) and radio synchrotron jets respectively. Since the energy source for the entire ejecta is the same thermonuclear outburst, this explains the

observational results which have long inferred a common energy source powering jets and NLR. There might also be explosive episodes at the poles wherein the energy released is insufficient for matter to escape so that the enriched matter accumulates on the pseudosurface at the poles. In such active nuclei, the accumulated matter can show higher metallicity and the pseudosurface at the poles can thicken as more matter is retained.

Correlated variability is noted in the ultraviolet/optical continuum strengths and amplitude/linewidths of broad emission lines such that when the continuum emission increases, the amplitude and linewidths of the broad lines also increase either instantaneously or with a delay. We explore if a thermonuclear explosion in the accreted matter in the non-polar regions i.e. in the BLR can explain such behaviour. Energy released in the thermonuclear explosion in the BLR should heat the BLR and/or the pseudosurface which should increase the continuum emission - Balmer continuum or black body radiation. Such changes in the continuum should trigger physical changes in the BLR which can consist of exciting a larger number of atoms of high ionization lines thus increasing the amplitude of the observed lines. Such a change can also increase the radial extent of the line forming zone in the BLR which can widen the line as the change in gravitational potential within the line forming zone increases. Thus, the energy input from the thermonuclear outburst can explain both the observables. This means that the source of the correlated continuum and line variability in the BLR can be the energy released in a thermonuclear explosion in the BLR.

The origin of the observed multi-band variability whether in polar or non-polar regions of the active black hole lies in thermonuclear energy - this could be either by direct heating or through acceleration of relativistic electrons. It needs to be appreciated that in the currently hydrogen-dominated universe, thermonuclear energy has to be one of the most important driving forces of transient energetic events especially in systems where there is ongoing accretion of normal matter. It will cease to be an energy injection mechanism when all the light elements have fused to form iron and the universe has become iron-dominated. The nature of the universe would then change and if transient events are seen to persist then we would be forced to look for an alternative energy source. *To summarise, thermonuclear explosions provide energy to fuel transient events in active black holes - launching of jets and NLR from the poles; variability and enrichment in the BLR.*

Redshift components: The polar matter which is

energised in a thermonuclear explosion has to be accelerated to at least the escape velocity to enable it to leave the system. The escape velocity that is required will depend on the separation of the ejection site from the black hole. For example, if matter is ejected from a site separated from the black hole by $2R_s$, then it has to have a bulk velocity of $0.707c$ i.e. bulk Lorentz factor $\gamma_{bulk} = 1/\sqrt{1-v^2/c^2} = 1.414$ to escape the black hole. The frequently deduced relativistic bulk velocities from knot expansion in the jets and Doppler boosting leading to detection of solitary jets in powerful radio sources, support ejection from regions located close to the black hole. It appears reasonable to assume that matter is efficiently expelled from the system when the energy distribution of the particles, which will be normal (Gaussian) as discussed earlier, is centred at least on the escape velocity. If the distribution is centred at a lower velocity, the matter ejection is likely to be inefficient.

If any spectral line was detectable just as the matter was ejected as it has been possible in the case of the Galactic microquasar SS 433, then this line should contain three distinct redshift components: (1) Lorentz factor for bulk expansion (2) gravitational redshift and (3) cosmological redshift. The emission lines detected with varying redshift from SS 433 contains contributions from (1) and (2) as discussed in the section on microquasars. Since SS 433 is a Galactic source there was no contribution from (3). Moreover as was observed in SS 433, the bipolar expansion of the NLR will be observed as a blueshifted and a redshifted component about the cosmological redshift. If the bipolar ejections occur from sites of comparable separation from the black hole then the gravitational redshifts that the blue and redshifted lines show will be similar. This means that both the redshifted and blueshifted components have to sit on a common redshift pedestal which will be a combination of the gravitational redshift and the cosmological redshift. This behaviour has also been demonstrated by the emission lines from SS 433.

Both the bulk Lorentz factor i.e. escape velocity and the gravitational redshift depend on the separation of the launch site from the black hole and contribute independent redshift components to the spectral line. The bulk velocity is actual motion of the line forming region to escape the gravity of the black hole whereas the gravitational redshift is the wavelength shift a photon suffers due to its formation in a deep gravitational potential. For example, a line photon that is emitted from $2R_s$ will be subject to a gravitational potential of $z_g = 0.25$ which will contribute an intrinsic redshift $z_{in} = 0.333$ while the redshift due to the bulk velocity (escape veloc-

ity) will be 1.414. Excluding the contribution due to cosmological redshift, the redshifted emission line from the poles should be detected at a redshift of $(1+z) = (1+z_{in})(1+z_{bulk}) = 2.218$ i.e. $z = 1.218$ whereas the blueshifted component will appear at a widely different velocity. As the ejected matter expands away from the black hole it forms the distributed NLR. If the bulk expansion velocity of the ejecta remains constant over sub-parsec scales, then the contribution of z_{bulk} to the spectral line velocity will remain unchanged for lines arising from that region. However z_{in} will rapidly decrease as the photon in the expanding NLR emerges progressively farther from the black hole. z_{in} would have declined to 0.005 for a line photon emerging at $100R_s$. The observational implication for this is that the spectral line should appear at progressively smaller velocity shifts along the jet as z_g approaches zero. Once the contribution of z_g has disappeared then the emission lines from NLR should show two components centred at $\pm z_{bulk} = 1.414$ about the cosmological redshift i.e. a blueshifted and redshifted component for the bipolar NLR. If the bulk velocity of the NLR declines over parsec scales then z_{bulk} will accordingly decrease and eventually approach the commonly observed few hundred kms^{-1} about the systemic velocity of the galaxy on parsec and kpc scales. Decrease in the velocity of the NLR decreases as it expands away from the black hole is expected. This can also be deduced from the observational results on supernovae explosions which tell us that the initially recorded Balmer line velocities of $30000\text{--}40000 \text{ kms}^{-1}$ decline over several weeks to $\sim 5000 \text{ kms}^{-1}$. Since these velocities signify the expansion rates of the supernova ejecta, it shows that the expansion slows down as the ejecta expands. A similar evolution is likely followed by the NLR so that it is ejected from the poles at relativistic velocities required to escape the gravity of the black hole but decelerates over parsec scales to a few hundred to thousand kms^{-1} which is the commonly detected expansion speeds in the NLR as surmised from the blueshifted and redshifted components of the narrow lines. Since no spectral lines attributed to the NLR have ever been detected with relativistic expansion velocities from an active nucleus; it tends to bias us towards their non-existence while the detection of high velocity lines in SS 433 supports the model suggested here wherein the NLR should always contain such lines. There remains the strong possibility that observations have missed the relativistically expanding NLR close to the core. This could be due an observational bias in that we have not really probed the NLR at such high redshifts or that the emission line gas rapidly slows down after ejec-

tion. It is interesting to note that in quasars, wide permitted emission lines and narrow forbidden lines are observed at similar redshifts. Since it was established that the wide lines contain a non-trivial contribution from gravitational redshift and arise close to the black hole, the narrow forbidden lines were suggested to be arising in small low density pockets in the same region (Kantharia 2016). However it now appears that the possibility of these forbidden lines arising in the matter that has just been ejected from the poles i.e. NLR cannot be ruled out and hence their origin requires further investigation using observational data. It is also important to note that the number of quasars which show the presence of forbidden lines decreases as the emission line redshift of the quasar increases. The reason for this needs to be investigated. One can expect the forbidden lines from the NLR to show extremely large redshifts when at the launch site (even larger than shown by lines from the BLR) and then consistently decrease along the radio jet direction as both the gravitational redshift and bulk velocity components decline. Considering that in several broad line galaxies, a narrow feature is seen riding the broad emission line prompts the question if the narrow feature can arise in the polar NLR. This point also requires further investigation since its validity hinges on the similar net redshift of the lines arising at the poles and in the BLR in some quasars which, as explained above can happen since the lines from the NLR can also appear at a range of redshifts except these can also include forbidden lines and will be narrower than those from the BLR and dependent on how often matter is ejected from the poles.

There exists some evidence regarding the presence of high velocity narrow line gas in compact steep spectrum sources. GPS and CSS are compact radio sources with typical sizes of GPS sources being a kpc or so and CSS extending to ≤ 20 kpc. Broad lines are detected from these sources. The lowest redshifts at which these objects are detected is fairly high ~ 0.1 (see Figure 21). Since there seems to be no compelling reason to believe that GPS and CSS sources should avoid the local universe, we go with the assumption that these sources share the same distribution as other active galaxies and the absence of lower redshift objects is because the lower redshift limit is dictated by z_g which is large. This indicates that the BLR in GPS/CSS sources lies within $5R_s$ of the black hole. What is of interest here is that spectral lines from the NLR, extended along the radio jets, are detected at the relatively large emission line redshifts of these sources and in several cases is observed to extend beyond the radio jet (Axon et al., 2000) (see

Figure 20). This is significant, since the observed emission line redshifts of these sources contain a sizeable contribution from z_g which the extended NLR should not include. The large redshift of the NLR lines then indicate gas expanding at high velocities i.e. the origin of the large redshift of the lines from the NLR and of the broad lines are distinct but can be comparable at some stage. The optical line emission distribution from the NLR is abruptly cut off and hence appears boxy in a few CSS (see Figure 21) e.g. 3C 147, 3C 48 (Axon et al., 2000). Such a morphology makes one wonder if the NLR does extend beyond the boxy boundary but at a lower redshift and hence has been missed. In other words, if the NLR gas is slowing down along its length then it will show a gradient in expansion velocity till it is close to the cosmological redshift of the host galaxy and the observations centred at high redshifts will miss the lower redshift extended components of the NLR. Further observational studies for quantifying gravitational redshift components and bulk velocities for these sources are required. The spectrum of the host galaxy, when detected, should appear at a much lower redshift - devoid of both gravitational redshift and bulk polar motions.

To summarise, the spectral lines from the BLR should contain two main redshift components: (1) cosmological redshift (2) gravitational redshift. The lines from the compact NLR can contain three redshift components: (1) cosmological redshift (2) gravitational redshift (3) redshift due to expansion. The distributed NLR will only contain two components i.e. 1 and 3. The lines from the NLR in CSS sources seem to show very high expansion velocities.

Radio jets, lobes, hotspots: As mentioned above, following the thermonuclear explosion in the small polar region of the pseudosurface close to the black hole, matter is energised to escape velocities and then ballistically shot out at relativistic velocities. The radially ejected matter is observed in the form of synchrotron emitting jets and the optical line emitting NLR extended in the general direction of the jet. The large forward momentum of the synchrotron jet propels it and since it is launched from a small polar region, it is highly collimated. Only when the forward momentum starts declining that the jet starts decelerating and losing its collimation. The deceleration should set in sooner if the ambient medium is dense or if the ejection velocities are low. The jets in FR I sources lose their collimation sooner than in FR II sources which sometimes show collimated jets upto Mpc scales. As the forward momentum declines, the synchrotron jet diffuses and thickens into a lobe. This explanation is generally accepted as the lobe

formation mechanism in FR I radio sources. However in FR II radio sources, a narrow collimated jet is detected all the way to the hotspot which is generally the extremum point of the entire radio structure. This would mean that the forward momentum of the jet dominates upto the hotspot. The lobe in FR II sources forms between the core and the hotspot and literature attributes its formation to a backflow from the hotspot due to the formation of a reverse shock at the hotspot. The hotspots are generally formed at the edge of the soft X-ray distribution in the radio galaxy (e.g. Figure 33). The hotspots typically subtend angles of a degree or less at the core which supports small jet opening angles and collimation of the jet upto hotspots in FR II sources (e.g. Bridle & Perley, 1984). Magnetic field in lobes is observed to be circumferential for both FR I and FR II galaxies. A circumferential field can be understood since the jet diffuses to form the lobe so that the frozen-in field is stretched and eventually becomes circumferential.

In some FR I sources, the jet appears to be abruptly halted at some distance from the core so that the radio lobe emission at all radio frequencies is confined within a well defined boundary (e.g. NGC 193 in Figure 27). The spectrum of emission from this interface region is observed to be similar to the jet i.e. a relatively flat spectrum as compared to the lobe emission (e.g. NGC 193 in Figure 27). East-west directed jets are observed in NGC 193 while radio emission is observed from a cylindrical region centred on the core. The radio jet in NGC 193 is likely to be precessing which explains the nature of the lobe emission and the series of flat spectrum hotspots that are identifiable in the interface region in the lower panel of Figure 27(a). The radio emission in the north-south of the core in NGC 193 is faint and is not confined within a well defined boundary. Such behaviour although not typical of FR I sources, is noticed in several FR I sources. Such sources appear to be confined due to some external force. The X-ray emitting thermal gas is of comparable extent as the diffuse radio emission in NGC 193 except in the western part (see Figure 27b).

While double-sided jets are detected in FR I sources with the jet-counterjet intensity ratios varying along the jet, only single-sided jets are detected in FR II sources. Literature attributes this behaviour in FR II sources to Doppler boosting of the jet directed towards us and Doppler fading of the jet directed away from us and observations have amply justified this reason. Studies determine that the jet-counterjet asymmetry can be explained by Doppler boosting for relativistic jet velocities between $0.65c$ and $0.8c$ and jet viewing angles between 45° and 75° (e.g. Wardle &

Aaron, 1997). This means that the jet bulk velocities in FR II sources are $\geq 0.65c$ indicating the jet launch site is separated from the black hole by $\leq 2.4R_s$. Although a single jet is detectable, the existence of double-sided jets in FR II sources, is surmised from the existence of symmetric lobes and hotspots located on either side of the core and from the detection of both jets in the rare closeby FR II galaxy like Cygnus A. In FR I sources, the jet-counterjet ratio is large near the core i.e. the counterjet is faint and the ratio decreases along the jet i.e. the counterjet gets brighter. This is explained in literature by the Doppler beaming argument and interpreted to mean that the jets in FR I galaxies are relativistic close to the core but soon slow down so that the Doppler beaming effects are maximum near the core but decline along the jet (e.g. Laing et al., 2011). Using the Doppler beaming argument on the non-detection of the counterjet in FR II galaxies leads to the inference that the jets remain relativistic over their entire length i.e. upto the hotspot (Laing, 1989). These explanations have remained well-supported by observations.

In FR II sources, a pair of hotspots can always be identified which are collinear with the core. In literature, the hotspots are often considered as sites of electron acceleration. In many FR II sources, multiple pairs of hotspots are detected with all pairs showing collinearity with the core. The presence of multiple pairs of hotspots provide evidence to the existence of a precessing jet with the separation between the farthest hotspots on the same side giving a measure of the precession angle which is generally rather small. In FR I sources, the precession angle appears to be larger than in FR II sources. Since no hotspots are detected in FR I sources, the precession angle in several FR I sources is surmised from the thick lobes which straddle the jet such that the radio structure forms an halo around the source e.g. M 87 and NGC 193 (Figure 27) and from wiggles in the jets. Thus both the jet opening angle and precession angle in FR I sources appear to be larger than in FR II sources. Till the magnetic field is observed to be aligned along the radio jet, the electrons whose relativistic random velocity is predominantly along the radio jet will not radiate but travel freely (Spangler, 1979) which should lead to lower energy losses and hence lengthen their lifetimes. We can extrapolate this argument so that, at the hotspots where the magnetic field is oriented perpendicular to the radio jet, all the electrons with the relativistic velocity component along the jet will furiously begin to radiate synchrotron emission. This can be an additional reason for the bright multi-band nature of hotspots where

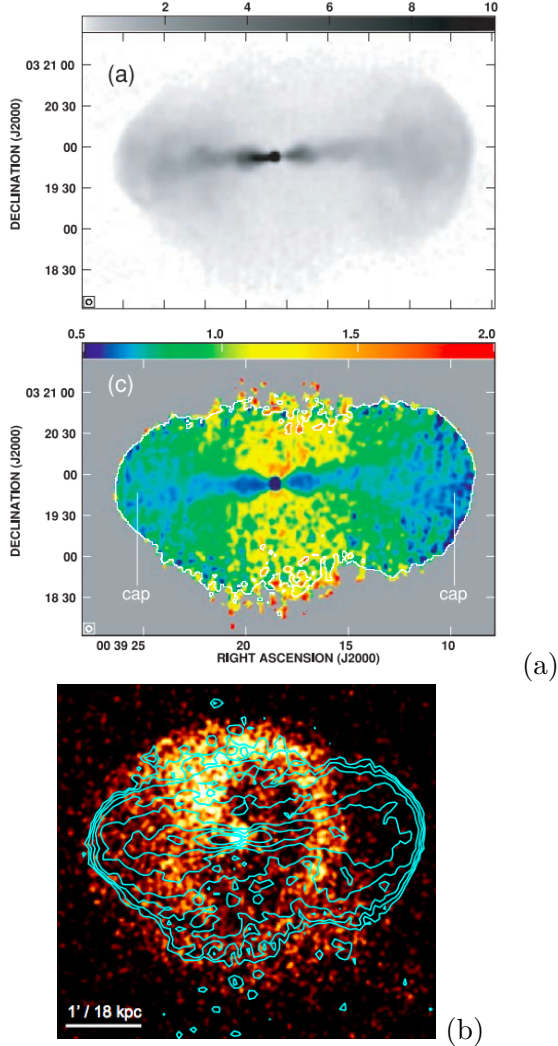


Figure 27: (a) Radio image of the FR I galaxy NGC 193 at 4.9 GHz (top) and spectral index between 4.9 and 1.4 GHz at 4'' resolution reproduced from Laing et al. (2011). Notice the flaring jets and the halo-like radio emission surrounding the active nucleus. The spectral index is flattest for the core and jets and is steeper in the lobes. The emission in the north-south of the core shows the steepest spectrum. Fragments of flat spectrum emission are detected at the boundary of the lobes. (b) Figure showing X-ray emission in colour superposed on the radio contours around NGC 193 reproduced from O'Sullivan et al. (2014). The radio extent of the galaxy at 60 Mpc is about 80 kpc. Notice that the radio and X-ray extents are comparable except in the west.

the magnetic field is enhanced compared to the jets and lobes. The higher magnetic field will also favour emission from lower energy electrons which should be larger in number and have longer lifetimes. Basically there does not appear to be a compelling reason for attributing electron acceleration at hotspots. For example, if the hotspots are formed about 100 kpc from the core, this means that the electrons accelerated at the core and travelling outwards at say a velocity of $0.8c$ should have sufficient energy to radiate at the hotspots. For a mean magnetic field of $\sim 30\mu\text{G}$ from the core to the hotspots, the electrons radiating at 1.4 GHz will have a lifetime of 5.45 million years. At a velocity of $0.8c$, these electrons in the jet can survive upto a distance of about 450 kpc while at a velocity of $0.5c$, the jet can survive upto about 250 kpc. Thus, the electrons accelerated at the core can explain the hotspots and there is no compelling reason to require reacceleration of electrons at the hotspots.

X-ray synchrotron jets are often detected close to the core in active galaxies and which indicates the existence of electrons with TeV energies in the jet. We can infer from this that the central thermonuclear engine is capable of accelerating particles to these energies before they are ejected. This also provides direct evidence to the origin of high energy cosmic rays from active nuclei. The early dousing of X-ray emission i.e. the shorter X-ray jet compared to radio jets is expected since the TeV electrons should quickly lose energy in magnetic fields of few tens of μG in the jets. In literature, the physical mechanism that is surmised for the X-ray emission from hotspots in FR II sources is inverse Compton emission or Self-Synchrotron Compton process. Synchrotron emission at X-rays, which requires exceptionally high energy electrons, is seldom cited as the process for the X-ray emission from hotspots which also supports the inference that we arrive at namely that all the major electron acceleration is completed in the core and hotspots are not sites of reacceleration.

The radio spectra of the different components of a radio galaxy show distinct behaviours. The core spectrum is generally flat or peaked at high radio frequencies, the jet spectrum is a power law with typical spectral index ~ 0.6 , the lobe spectrum is also a power law but generally steeper than jets while the hotspot spectrum peaks at low radio frequencies and shows a gentle break at a higher radio frequency like 10 GHz beyond which the spectrum steepens to a spectral index ~ 1 . As noted earlier in the paper, the explosion will result in a normal distribution of electron energies and the peak of the distribution should move to lower energies and the dispersion of the distribution should reduce as the population ages.

Depending on the magnetic field, electrons in a particular range of energies will radiate within a given range of frequencies. Since the magnetic field in the hotspots is enhanced, the electron energies which give rise to the radio emission in a given band of frequencies are lower than in regions with lower magnetic field. The curved low radio frequency spectrum can be understood if we visualise the lower energy electrons close to the peak of the aged distribution radiating in the higher magnetic fields. The steeper spectrum at higher radio frequencies would indicate enhanced losses due to both synchrotron and synchrotron self-Compton which is often the physical process invoked to explain the observed X-ray emission from hotspots. Although literature suggests electron reacceleration in the hotspots, it does not seem to be warranted by observations. There could be some reacceleration due to the Compton process but is trivial compared to the acceleration in the core.

Several radio jets are observed to show small wiggles along their length. These wiggles in jets can be explained by precession of the spin axis of the black hole as was conclusively shown for the microquasar SS 433. The presence of symmetric wiggles in jets on either side of the core in active nuclei lend strong support to their origin being related to the central object and not the ambient medium. The easiest model to explain a precessing spin axis is the presence of a companion in a binary system. However while this readily explains the precession in microquasars, it is difficult to imagine a quasi-stable binary system of two supermassive black holes. A binary of a supermassive black hole with a stellar mass black hole is unlikely to result in a detectable precession of the spin axis of the supermassive black hole and hence can be ruled out. Since formation of supermassive black holes remains an ill understood topic, we avoid supporting binary supermassive black holes. Instead other possible scenarios need to be examined using our current knowledge of the environment of the supermassive black hole. Precession of the spin axis can be triggered due to the effect of a gravitational torque. In Table 1 of Kantharia (2016b), the effect of a gravitational torque that is exerted on the matter in two galaxies due to their close approach has been quantified in a simple way. The close approach of the two galaxies enhances the gravitational force between them which is not symmetric and hence results in a torque i.e. induces a change in the angular momentum of the galaxy. The two components of angular momentum are the moment of inertia and angular velocity and the change can be reflected in either component as was described in Kantharia (2016b). From Table 1 in that paper, we note that when two massive

galaxies of mass $10^{11} M_{\odot}$ approach within 100 kpc, then a mass of $10^9 M_{\odot}$ within one of the galaxies can be torqued such that it results in an equivalent velocity of about 200 km s^{-1} . In this simplified calculation, no adjustment for the finite sizes of the galaxies or the fact that matter is distributed over a region comparable to the separation was made. The aim of that paper was to demonstrate that a gravitational torque due to the approach of another galaxy can disturb the kinematics and spatial distribution of gas in a galaxy even for a closest approach which was as large as a Mpc. A lower mass packet can experience a stronger torque. If we assume that the central black hole is also subject to the torque then it can result in precession of the spin axis i.e. change in the angular velocity of the black hole. Change in moment of inertia of the black hole is much more difficult to implement due to its enormous gravity. However the distribution of gas in the galaxy can change. The detailed mechanism of how the black hole spin is changed remains a mystery as does the mechanism which actually implements the changed angular momentum in the gas in a torqued galaxy. Moreover it should be mentioned that the gravitational torque which was successful in explaining the velocity or spatial displacement of the stellar and gaseous components, is observed to mostly affect the gaseous component and not the stellar component. So how does it affect the central black hole which hosts the highest concentration of matter in the entire galaxy? Maybe when we discuss the effect of the torque, it has to be on the central object which is then transmitted to the gaseous component through viscosity. This needs to be further investigated. From existing data and knowledge, it appears that the precession of the spin axis of the black hole is likely to be connected to the passage of a massive galaxy in the vicinity. That several active galaxies are observed to have companion galaxies lends support to the significant role played by gravitational torque in the evolution of the central black hole and the galaxy.

Many low power radio sources show bent jets and such radio sources are referred to as head-tail, narrow-angle tail (see Figure 31), wide-angle tail or S-shaped sources depending on their observed morphology. Such sources commonly occur in cluster environments and hence their origin has been attributed to the action of ram pressure exerted by the intracluster medium on the jets launched from the galaxy moving in the cluster medium (Begelman et al., 1979). While this explanation is likely, it is noteworthy that the observed morphologies can be explained simply by motion of the galaxy in the cluster. The schematic in Figure 28 summarises the picture. The nucleus of

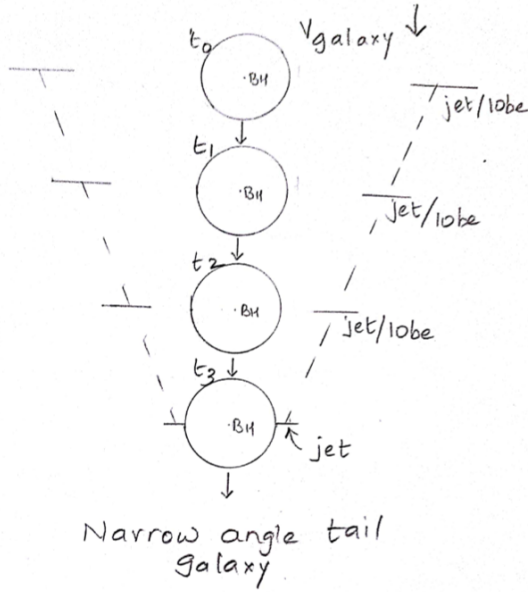


Figure 28: The schematic explains the formation of the radio structure of a narrow angle tail (NAT) galaxy. The galaxy is moving at high spatial velocity from the top to the bottom. At each position, the galaxy ejects plasma which ballistically expands away from the nucleus while the galaxy continues its downward motion. At time t_3 , the plasma from the previous outbursts has expanded away from the position of the black hole at times t_1 and t_2 , so that the radio structure shows a V-shaped or U-shaped structure. The older plasma loses its ballistic nature and diffuses. If the central galaxy is moving slowly or sideways then it would lead to different radio structures explaining the formation of NATs and WATs. This schematic shows that enhanced space motion of the galaxy under the influence of the gravitational potential of the cluster can explain the observed structures.

the moving galaxy ejects matter from different positions in space at different instants t_0, t_1, \dots as shown in Figure 28. The jet knot that is ballistically ejected from the black hole at t_0 will keep expanding radially away from the position of the nucleus at t_0 . The same will be true for later times t_1, t_2, \dots . The jet keeps expanding away from the spatial position of the core when it was ejected and will be oblivious to the changed position of the core at later times. Assuming all knots are ejected with comparable velocities, the matter ejected at an earlier epoch will have expanded further out than the later eruptions (see Figure 31). The earlier eruptions will also lose their ballistic nature and form lobes. The overall effect will be to lend a curved structure to the jets. The detailed morphology will depend on the velocity of the galaxy and the angle made by the sightline to the galaxy trajectory. A fast moving galaxy in the sky plane would result in a head-tail or narrow angle tail morphology as in Figure 28 (e.g. NGC

1265 shown in Figure 31) whereas a galaxy with a larger component of motion along the sightline and smaller component in the sky plane would result in a wide-angle tail radio structure. Thus a moving radio galaxy will show bent jets since the jet launching position is moving in space although the ejections are ballistic when launched. On the other hand, a stationary galaxy will always show straight jets since the jet launching position is constant in space. This suggests that the straight jets of FR II sources indicate very small space motion of the galaxy, if at all. Most FR II are field objects and hence lack of space motion is expected since most of the space motion of FR I is because they are members of clusters and hence moving under the influence of the cluster potential. In fact, the larger frequency of cluster membership in case of FR I can explain a number of the differences between them and FR II radio sources. For example, since FR I radio sources are located in a crowded environment, the larger precession angle is expected from a gravitational torque induced by the passage of another massive galaxy; moreover it is also possible that the crowded environment has led to the slowing down of the black hole and hence the active nucleus has evolved to a FR I radio source instead of a FR II source.

Composition of jets: In literature, several studies are devoted to unravelling the composition of the synchrotron jet - whether it is proton-electron or positron-electron. In other words, whether the radio jet is heavy or light. Neither origin has garnered convincing evidence from observations and the debate continues.

Observations have provided ample evidence to the ejection of both a synchrotron-emitting jet and emission line gas from the active nucleus - both components are distributed along the same axis, synchrotron blobs are observed to be expanding away at relativistic velocities from the nucleus, emission line gas has been observed to be expanding away from the nucleus but with much lower velocities. Such eruptions are expected from a thermonuclear explosion in the accreted matter at the poles. This means that the synchrotron emission can arise from the relativistic electrons that are coincident with protons/ions that give rise to the emission lines i.e. a proton-electron plasma or it could also be that the synchrotron emission arises in a separate component comprised of electrons and positrons. Thus while the thermonuclear explosion can explain the energising and ejection of matter from the black hole and also provide an intense source of positrons, it does not provide a water-tight resolution to the jet composition problem. It should be mentioned that in case

of stars, the positrons generated in thermonuclear reactions are assumed to be immediately destroyed releasing the annihilation photons around 511 keV. However countering this assumption are the observations which have detected the annihilation photons from the sun indicating that all positrons are not destroyed on formation but some fraction does make it to the solar surface. Here we suggest that a large fraction of the energetic positrons generated in the thermonuclear explosion are ejected alongwith relativistic electrons instead of being destroyed. At this point it is useful to mention that the annihilation line at 511 keV has been detected from microquasars e.g. 1E 1740.7-2942 (Bouchet et al., 1991; Sunyaev et al., 1991) which lends support to the positron-electron plasma component of the ejecta. It is important to appreciate that the fate of positrons i.e. destruction or survival is a studied assumption and we need to use observations to validate the assumption. In fact the annihilation line was observed from the sun during solar flares in 2002 and 2003 (i.e. near solar maximum) (Share et al., 2004). A possible origin for the positrons involved in this could be those generated in the thermonuclear fusion in the solar core which have managed to reach the solar surface. It is generally believed that the positrons generated in the core are immediately absorbed - however no empirical evidence for the same exists and hence a fraction of these emerging on the solar surface cannot be ruled out.

We might be able to obtain inputs on jet composition from observations of supernova explosions which are also thermonuclear eruptions and where the observed radiation also consists of synchrotron and line emission. Two separate radio synchrotron emission components from supernovae are recorded - the prompt radio emission following the supernova explosion which has to be from a fast light ejecta i.e. positron-electron plasma facilitating high forward velocities and the delayed radio synchrotron emission from the supernova remnant which is coincident with the slower moving line emitting matter and hence arising in a proton-electron plasma. In the microquasar SS 433, both the radio jet and the emission line gas are observed to be expanding at a velocity of 0.26c - if in analogy to supernovae, we assume that the radio jet is composed of fast positron-electron plasma then the observations of SS 433 indicate that both the plasma are ejected with high velocities which is expected since they are ejected from close to the black hole where the escape velocities are relativistic. As in supernovae, it is likely that the heavy ejecta (i.e. line forming gas) from active nuclei rapidly slow down after ejection. One would

expect the situation in active nuclei to be similar to SS 433 i.e. both the synchrotron emitting plasma and line emitting gas ejected at relativistic velocities especially since the matter is launched from a few R_s from the black hole. However it needs to be investigated since there could be a range of possible outcomes especially since no emission lines expanding with relativistic velocities have been identified from an active nucleus. While there exists a strong likelihood of all matter being ejected simultaneously, it could be that a fraction of the lighter plasma acquires an energy distribution centred on higher velocities than the heavier matter and hence shoots out with higher expansion velocities while the heavy matter fails to escape or it could be that all matter is ejected at relativistic velocities but the lighter plasma keeps ballistically expanding at the same velocity while the proton-electron plasma quickly decelerates. In some active nuclei, it could be that the electron-proton plasma is the main synchrotron emitter. With the range in physical properties of the active nuclei that are possible, it is likely that all the above scenarios are possible and manifested in different active nuclei. The lack of any relativistic line velocities from the NLR in active nuclei support a distinct origin for the radio synchrotron emission. If the synchrotron plasma and NLR were associated then the latter should have exhibited the large expansion velocities that are observed for the radio blobs. This, then, strongly supports the origin of the radio synchrotron emission in active nuclei especially in jets from a positron-electron plasma. *To summarise, the composition of the radio synchrotron jet in active nuclei is positron-electron plasma with a large pool of positrons being generated in the thermonuclear explosion.*

Formation of hotspots and lobes in FR II: In FR II radio sources, the jet seems to be stopped at the hotspots although the ballistic nature of the narrow jet indicates that the bulk velocity had continued to be relativistic till the hotspot before the jet at all radio frequencies suddenly lost its identity. It appears as if the forward propagation of the jet was suddenly braked at the hotspot where the relativistic plasma accumulated and radiated before being pushed backwards towards the core and forming the lobe. Since the medium beyond the hotspots is tenuous compared to the medium closer to the host galaxy which consists of X-ray emitting gas, emission line gas and radio plasma, the jet should have continued unhindered in the low density medium. What, then, stops the relativistic jet at the hotspots which is the interface between the dense medium around the active galaxy and the tenuous medium beyond ? In

literature, the abrupt nature of the jet termination, formation of hotspots and lobes is attributed to the effect of a reverse or termination shock travelling towards the core from the interface. This explanation is vague and riddled with difficulty leaving it open to individual interpretation. We, hence, revisit the problem in light of the increased understanding of active nuclei. All features at the hotspots point towards the influence of an external pressure i.e. the jet is halted and the plasma starts to flow back towards the core. The halting mechanism cannot be ram pressure since there is paucity of matter beyond the hotspots. The other known halting mechanism which is found to be active in several astrophysical systems is radiation pressure. For this mechanism, there needs to be a source of hard photons beyond the jets which can halt the jets and form hotspots, lobes. Keeping in mind that the jet has a positron-electron composition, we investigate if there can be a source of photons beyond the detectable radio jet. In the electron-positron jet, pair annihilation at some rate should be ongoing so that γ -ray photons of energy ~ 511 keV are continuously generated along the entire radio jet. Thus there should be soft γ -ray photons along the entire length of the radio jet. Since the jet is ploughing through a relatively dense medium as can be surmised from the soft X-ray emission and the optical emission lines, these γ -ray photons are likely to be scattered to lower energies making detection of the annihilation photons difficult. However when the jet propagates beyond the boundary of the dense medium i.e. beyond hotspots and into rarified ambient densities, the γ -ray photons generated in the pair annihilation will no longer be immediately absorbed and can instead retain their identity over a longer period due to longer mean free paths. This, then, provides a source of hard photons beyond the hotspots, which can exert a radiation pressure on the jet! A positron-electron pair which annihilates will give rise to at least two γ -ray photons of energy 511 keV moving in opposite directions. The photons which move back towards the radio jet can exert radiation pressure on the jet and halt their forward motion so that the plasma starts diffusing backwards and forms the lobes. The radiation pressure can also compress the matter at the interface with the intergalactic medium so that the plasma densities and magnetic field are enhanced leading to brighter radio emission i.e. hotspots. This process can explain the formation of hotspots, lobes in FR II and relics in clusters which form at the edge of the X-ray source. A fraction of positron-electron plasma that continues to escape along the jet to the near-vacuum beyond the hotspots will produce γ -rays of energy 511

keV which will continue providing the radiation pressure till the jet changes direction due to precession of the spin axis of the black hole. The old hotspot will gradually fade and a new hotspot will form. This explains the formation of multiple hotspots, their short lifetimes, gradual formation and shift in their position alongwith the precessing jet. The annihilation photon can also provide the seed photons for inverse Compton process so that much higher energy photons can also be generated. These photons can also lose energy to relativistic electrons through the Compton process.

The above strongly reiterates that there occurs no reacceleration of electrons except through the Compton process at the hotspots. The above explanation comprehensively describes the observed nature of FR II radio sources without requiring any further assumptions and lends convincing support to the positron-electron composition of the jet and the implications thereof. *To summarise: Radiation pressure due to the positron-electron annihilation photons is responsible for halting the jet and forming hotspots, lobes in FR II radio sources.*

Formation of X-ray beams along radio jets: In several FR II sources, two-sided thick X-ray beams coincident with the finer radio jet(s) have been observed e.g. Cygnus A and Pictor A (see Figures 33, 34). Even if the FR II galaxies show a single-sided radio jet, the X-ray beams are observed to be double-sided. We find that these X-ray beams can be understood as the Compton-scattered annihilation photons that are continuously generated along and around the radio jet thus leading to the thickening of the X-ray emission beams. Since the X-ray beams are not moving outwards at the rate at which the radio jet is expanding, no Doppler effect is expected and hence X-ray beams are observed on both sides of the core.

To demonstrate the feasibility of the above, we estimate the change in the wavelength of the 511 keV photon expected from Compton scattering by electrons using Equation 4. If the scattering angle is 90° then the wavelength shift expected in the 511 keV photon (i.e. photon of frequency $= 1.2 \times 10^{20}$ Hz or wavelength $= 2.4 \times 10^{-12}$ m) by collision with an electron of $\gamma = 10$ is 0.243×10^{-12} m whereas scattering by an electron of $\gamma = 1$ will result in a wavelength shift of 2.43×10^{-12} m. If the scattering angle is 180° then the shift will be twice the above. The wavelength of a 2 keV X-ray photon is 6.2×10^{-10} m. Few Compton scatterings of the 511 keV photon are required to downconvert the γ -ray photons to X-ray energies. This physical explanation can hence explain the X-ray beams coincident with the radio jet without having to resort to any contrived arguments.

Since 511 keV corresponds to the rest mass energy of an electron, Compton scattering by electrons is likely to be an important physical process that drain photons of this energy and in turn accelerate the electrons. If each Compton scattering event removes 50 keV from the photon then it means that the involved electron gains this energy which although small is non-zero. This happens throughout the jet length. This then has some observable implications: (1) deep observations might detect a faint 511 keV annihilation line along the jet unless all photons are Compton scattered to X-ray wavelengths (2) X-ray photons should be detectable along the jet which will not suffer Doppler beaming effects unlike synchrotron radiation since these are produced by Compton scattering of the pair annihilation photon. This has already been demonstrated by the X-ray beams detected in a few FR II sources all the way from the core to the hotspots.

Magnetic field around a black hole: In a star, a magnetic field that exists within the star can be ejected along with matter as in a supernova explosion. However a magnetic field generated within a black hole will never be detectable. However a magnetic field whose source is located outside the black hole can thread the accreted matter on the pseudosurface. If we assume that the BLR is the source of the polar magnetic field, then this field can be frozen in the accreted matter at the poles and ejected along with matter following episodic explosions. Since the ejecta is expanding away from the black hole, the magnetic field lines should also be stretched along the jet. This, then explains the observed magnetic field in radio jets which is always observed to be aligned along the jet near the core in FR I and along its entire length in FR II radio sources. In other words, the magnetic field observed to be parallel to the jet strongly supports ejection of matter with a frozen-in magnetic field from the poles of the black hole. Since the ejection from the poles consists of both positron-electron plasma which forms the radio jet and a proton-electron plasma (line forming gas) which is the bulk of the accreted matter that is ejected, the question that arises is whether the magnetic field is frozen in both plasma or predominantly in the proton-electron plasma. In supernova explosions, observations support the frozen magnetic field in the massive ejecta and not in the positron-electron ejecta. It is likely that the same exists for active nuclei so that the field is frozen in the proton-electron plasma. This would then require both the plasma to be expanding at relativistic velocities as long as the field is detected along the jet. However if the proton-electron plasma slows down soon after ejection, then

the field has to be frozen in the positron-electron jet. If lack of high velocity emission line gas is taken as proof of its absence along the jet then clearly the field has to be frozen in the positron-electron jet. However the entire velocity space has not been investigated for the emission line gas and hence it is premature to accept its absence along the radio jet. These are all possible, physically allowed situations and although not presented here, it might be possible to obtain convincing arguments one way or other from observations.

Literature often suggests the presence of a helical field around the jet and which is also used as a collimating agent. If the magnetic field was not frozen in the ejected material then it can be generated by a net current flow in the jet. Such a current should lead to a helical field around the jet.

The magnetic field is seen to become circumferential in the lobes and perpendicular to the jet in the hotspots. All this can also be explained by the diffusion of matter and hence the frozen magnetic field.

To summarise: the magnetic field is observed along the radio jet and suggests that it is frozen in the matter that was ballistically ejected from the poles of the pseudosurface of the black hole. Till further observations provide another explanation, it appears that the field is frozen in the positron-electron jet in active nuclei.

Dust formation in NLR: Fast ejection of normal matter from the poles of the pseudosurface of the black hole should lead to atomic mass-based segregation in the ejecta with the lighter elements leading and the heavier elements lagging, in analogy with novae and supernovae. Since the line forming gas ejected from the poles forms the NLR, the atomic mass-based segregation should lead to the formation of metal-rich dense clumps in the NLR. The inner parts of these optically thick metal-rich clumps will be shielded from the hard radiation field of the hot pseudosurface of the black hole thus facilitating dust formation. The dust formed in this process will be distributed along the polar axis. High resolution interferometric studies of active nuclei at mid-infrared wavelengths have indeed shown that dust emission elongated along the polar axis dominates the total mid-IR emission e.g. NGC 424 (Hönig et al., 2012), NGC 3783 (Hönig et al., 2013), Circinus (Tristram et al., 2014), NGC 1068 (López-Gonzaga et al., 2014). These results are expected in the model suggested here but were surprising when first obtained since in the existing model of an active nucleus, dust is expected to be distributed in an equatorial torus around the black hole. Broad lines from some Seyfert 2 nuclei are often detected in polarised light from a biconical

region about the core and are explained as being the nuclear spectrum scattered into our sightline by dust in the biconical reflection nebula. These observations lend strong support to the formation of dust in the polar biconical ejecta which then acts as a reflection nebula.

Atomic mass-based segregation in the polar ejecta which forms the NLR, leads to formation of metal-rich optically thick clumps within which dust forms. This process succeeds in explaining the observed biconical dust distribution and properties in active nuclei.

Dust could also form in the mid-to-outer parts of the accretion disk if densities are sufficiently large, metallicity is large and the radiation field of the pseudosurface is not able to penetrate far into the accretion disk. This could lead to the presence of dust in the parts of the accretion disk which are shielded from the radiation field of the pseudosurface.

Gas for accretion: The cycle of accretion, compression, heating, explosion, ejection from the poles of the supermassive black hole of the active nucleus will continue as long as there is matter for the black hole to accrete. This will lead to the formation of extended radio jets and NLR with the furthestmost parts of the jet and NLR having been ejected in the early days of the active nucleus. Since radio galaxies show the largest and hence oldest structures along the polar axis, it means that they have been going through the cycle much longer and more efficiently than Seyfert galaxies which show faint and compact radio emission. For the cycle to continue, the most important condition seems to be the existence of a pool of gas from which the supermassive black hole can accrete onto its pseudosurface. Once the black hole can accrete gas, rest of the steps in the polar cycle have to follow with differences being reflected in the strengths of the processes. If accretion is halted, the cycle stops due to lack of matter on the poles. The prolonged active nature of the nucleus in elliptical hosts of radio galaxies means that the required pool of gas has always existed in their central parts. While early shallow observations had failed to detect interstellar medium in early type galaxies, later observations have detected gas and dust in the central parts of a large fraction of early type galaxies with masses being estimated to be upto $10^8 M_{\odot}$ or so. This gas is the fuel that powers the active nucleus. If the black hole accretes at a rate of $1 M_{\odot}$ per year then it means that the nucleus can remain active for another 100 million years when the ambient gas will be exhausted. It is also interesting to note that several of the galaxies classified as LINERs (Heckman, 1980) show distribution of ionized gas in their cen-

tral few kpcs with excitation properties between the NLR and HII regions. It is possible that the LINER signatures mark the gas that is falling in towards the black hole. The galaxies which have exhausted this pool of gas will stop ejecting matter from the poles and only fossil lobes and NLR will be left behind. The core will become radio-faint i.e. the synchrotron continuum at the jet base will be extinguished. The non-polar pseudosurface can possibly keep radiating black body emission and the BLR can keep forming wide lines long after the galaxy has lost all accretable gas since once formed, these regions do not have a critical connection to accretion unlike the polar processes. In fact the hot pseudosurface can keep shining till the degenerate matter is cooled to the ground state quantum energy. Moreover accretion in the non-polar regions through the accretion disk can continue long after matter has stopped falling in i.e. the polar accretion has stopped. Thus by all counts, the non-polar regions of the active nucleus will remain active long after accretion has stopped i.e. the black body + recombination continuum of the active nucleus will be present long after the synchrotron component has disappeared. In other words, the core of the active galaxy will remain bright in X-ray to optical bands but will become undetectable at radio bands. This, then, provides one possible explanation for the large fraction of active nuclei which are not detected in radio bands but are bright in higher frequency bands. Spiral galaxies host a large mass of interstellar matter ($10^9 M_{\odot}$ or more) distributed throughout the galaxy. If finite gas mass in the spiral galaxy keeps tunnelling inwards and feeding the black hole then the polar activity can continue over a long timescale which will eventually deplete the interstellar medium of the galaxy. It can be speculated that the central black hole has been an important sink for the interstellar medium in elliptical and lenticular galaxies. If the black hole has been active for a billion years and if it has been accreting at a rate of a M_{\odot} per year then it would have accreted about a billion solar mass of the interstellar medium of the elliptical galaxy - some of this mass would have fallen into the black hole, some arranged in a pseudosurface, some used up in a BLR and accretion disk and some of it returned back as the NLR and jet plasma. No wonder elliptical galaxies have lost most of their gas!

To summarise: Gas accretion is a very important step in the cyclic process that signifies the radio-active black hole or nucleus. The polar explosions and ejections are exclusively dependent on gas accretion and stop soon after accretion is halted. The non-polar activity of a radiating pseudosurface and BLR,

although initiated by accretion, can continue a long time after accretion has stopped. These results can be interpreted to mean that the active core stops being a radio core once accretion stops but continues to radiate in higher frequency bands. In other words, the fraction of active cores which have stopped accreting will be radio-quiet but not ultraviolet-quiet or X-ray quiet.

4.2.2.3 Summary In this section, we present schematics (Figure 29) which summarise the model and list a pointwise summary which encompasses it.

The core: The core of an active galaxy consists of an accreting rotating supermassive black hole. In-falling matter on approaching the event horizon will be compressed to extremely high densities so that layers of degenerate matter deposit around the event horizon and which are supported from collapse into the black hole by degeneracy pressure. These layers form the pseudosurface of the black hole and subsequent to its formation, the infalling matter instead of falling into the black hole, deposits on its pseudosurface. In the polar regions which are free of any centrifugal influence, the accretion rate is the largest and the infalling matter accumulates directly on the pseudosurface. This matter will be compressed and heated so that it will undergo repeated thermonuclear outbursts which can energise and hurl matter outwards forming the synchrotron jets and the NLR. The accretion rates decrease on moving from the poles to the equator and while some matter accumulates on the pseudosurface and forms the BLR, the excess matter collects beyond and forms the accretion disk. The BLR, heated and ionized by the hard radiation field of the pseudosurface, is confined between the pseudosurface and the accretion disk. It is dense and consists of emitting and absorbing zones from which gravitationally redshifted and broadened spectral lines are observed. Both these zones are stratified with properties like varying ionization, temperatures and densities with distance from the black hole. This configuration of the black hole, pseudosurface, BLR and accreted matter at the poles would then define the structure of a compact core of the active nucleus or more generally an accreting black hole.

Wideband continuum emission from the core: The active core has a bright star-like appearance in quasars, Seyfert 1, 'N' type radio galaxies/BLRG/FR II. The observed spectral energy distribution is generally well accounted by the combination of a black body spectrum, a Balmer continuum spectrum and a power law spectrum. The hot pseudosurface contributes the black body component - this is similar to a hot star but much larger and hotter. The continuum emis-

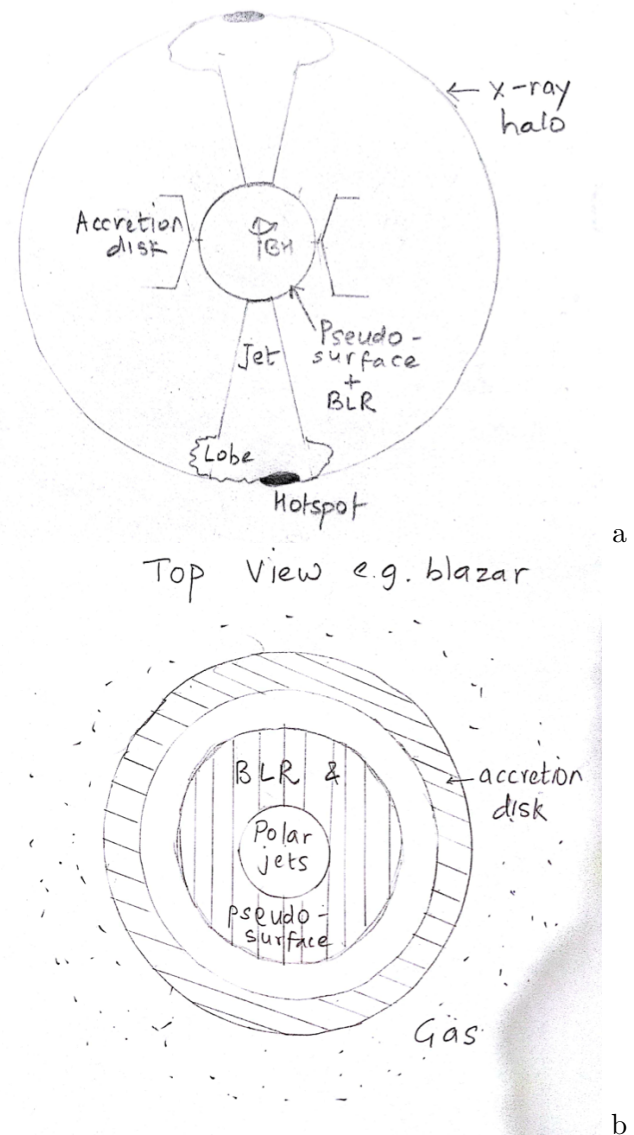


Figure 29: Schematic of the different components associated with an active nucleus/radio galaxy as described in the paper. The figures are not to scale. (a) The observed structure of a radio galaxy - the hotspots are a feature of FR II sources. The pseudosurface and BLR are approximated by the circle but in fact as shown earlier, the BLR will be an hourglass-shaped structure between the pseudosurface and accretion disk. The X-ray halo is approximated by a circle here. (b) Top view of an active nucleus (e.g. blazar) showing the polar region surrounded by a BLR which, after a gap, is surrounded by an accretion disk from which matter is accreted onto the BLR.

sion component of the BLR which can be taken to be similar to a HII region around a star would contribute a Balmer continuum spectrum. Relativistic electrons ejected from the poles and spiralling in a magnetic field will contribute a synchrotron component to the spectrum. The active core in Seyfert 2, NLRG and FR I galaxies is fainter and the peak of the black body emission occurs at relatively longer wavelengths. The SED of all active nuclei is due to the combined contribution of the three components.

Jet and narrow line gas launching from the core: In-falling matter deposits at the poles at a faster rate than at the equator. The situation at the polar region is similar to the accreting white dwarf in a nova so that when favourable physical conditions of density and temperature are reached, a thermonuclear reaction can ignite with rapid release of energy which instantly accelerates the overlying matter particles which are launched if their forward velocity exceeds the escape velocity. These episodic ejections will form the radio jet and the narrow line emitting region composed of matter with a range of excitation due to the photoionizing flux from the hot pseudosurface. The ejection episodes will keep recurring as long as the black hole keeps accreting matter and this explains continuing injection of cosmic rays along the jets. Detection of X-ray jets requiring electron energies of TeV indicate the high efficiency of the thermonuclear explosion in accelerating particles to such energies. The longer collinear jets in FR II sources argue for a larger ejection velocity which ensures the ballistic nature of the jet to larger separations from the black hole than in FR I sources.

Opening angles of conical jets: The jets (and NLR) are ejected from the polar region of the pseudosurface. The circular extent of the polar region that determines the jet opening angle is dependent on the spin of the black hole. A fast spinning black hole hosts a BLR with a large covering factor so that the jet opening angle is very small (see Figure 29). Since the pseudosurface is a quasi-spheroidal structure, the radial ejection from the poles will happen from a convex-shaped surface and hence the ejected matter will necessarily be confined to within a conical region whose apex will be the black hole (see Figure 30). As long as the ejected matter retains its ballistic nature, the jet will propagate within the conical region. Thus, the observed conical jets are expected from this model. In other words, the ubiquity and persistence of the conical nature of the observed jets and NLR in active nuclei provide irrefutable evidence to their ejection from a spherical pseudosurface while their ballistic nature gives evidence to their energy budget being mainly determined at ejection.

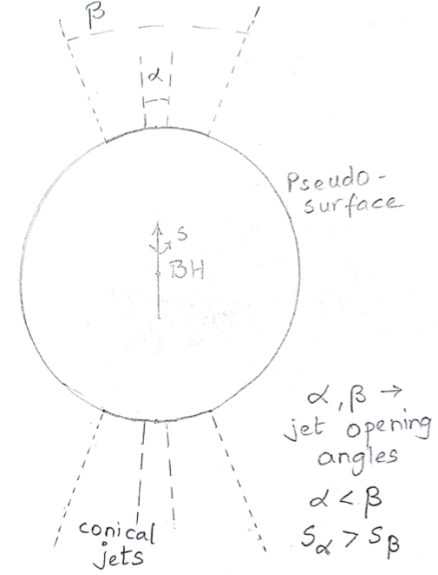


Figure 30: Schematic representation of the jets radially launched from the polar region of the spherical pseudo-surface which has to lead to conical jets. A faster spinning black hole as in FR II sources will have a smaller opening angle (α) while a slower spinning black hole as in FR I sources will have a larger opening angle (β). The schematic can also be used to understand the effect of a precessing spin axis of the black hole so that at any instant, α can be taken to be the angle in which the jet and NLR are launched and if the spin axis precesses in a cone of angle β then over time the entire region within β will contain radio plasma and NLR as was the case for NGC 193 (Figure 27).

The conical angle recorded for the NLR, especially in Seyferts, is generally larger than that of the radio jet. The above can be explained to be due to precession which increases the net conical angle over which persisting emission will be distributed. The narrow opening angle of the radio jet traces the current position of the jet whereas the NLR traces the entire precession region and hence is distributed over a larger conical angle. Thus, it can be inferred that in most cases, the jet opening angle gives a measure of the spin of the black hole while the opening angle of the NLR gives a measure of the precession angle.

Edge-dimmed jets: The radio emission from jets which are resolved along their widths are observed to exhibit either uniform brightness or edge-brightened structure or edge-dimmed structure. Some of this could be projection effects since we observe jets in the sky plane or these could have a physical origin. The edge-dimmed jets which have been noted in active nuclei with one of the first active galaxies in which it was noticed being NGC 1265 (O'Dea & Owen, 1986). The faint emission generally has a steeper radio spectrum and encloses the bright ra-

dio jet which has a flatter radio spectrum (e.g. Figure 27b). The faint envelope, often referred to as the sheath, is detected around jets at several linear scales (e.g. O’Dea & Owen, 1986; Katz-Stone et al., 1999). A possible origin for the sheath could be as follows. The collimated conical nature of the radio jet around which the sheath is observed indicates dominance of the forward momentum i.e. the component of the bulk velocity in the forward direction is much higher than in any other direction so that the jet retains its structure. However, the boundary layers of the ballistic jet might undergo some erosion due to physical processes like turbulent viscous stripping (Nulsen, 1982). This process can lead to stripping of the plasma from the edges of the jet which can then form a faint radio synchrotron sheath around the jet given an ambient magnetic field. The sheath is from the same electron population that is ejected from the pseudosurface but the steeper spectrum and larger polarisation fraction that are recorded for the sheath (e.g. Katz-Stone et al., 1999) are suggestive of a distinct magnetic field. The differing magnetic fields in the jet and sheath could lead to electrons of different energies emitting at the same radio frequency and hence explain the differing radio spectral index. The differing orientation and strength of the ordered magnetic fields could be due to the sheath shining in the ambient magnetic field left behind by previous polar ejections while the dense jet shines in the magnetic field frozen in itself. The variations in the magnetic field and spectral index could be specific to the radio source so that a range of plausible combinations can result. Such sheaths have been observed around jets in both FR I and FR II type sources including Cygnus A (Katz-Stone & Rudnick, 1994; Rudnick & Katz-Stone, 1996; Young et al., 2000). It would be difficult to explain the existence of such sheaths if jets were confined by an external medium which is often cited in literature as a reason for their confinement and collimation. In other words, the existence of sheaths indicate that jets are not confined by any external medium. Sheaths support confinement of jets due to their ballistic nature, after being ejected with relativistic velocities from the polar pseudosurface, so that their lateral expansion is prevented although they are highly overpressured with respect to the ambient medium.

Edge-brightened jets are detected when high resolution radio images which can resolve emission close to the core in FR I radio sources like Virgo A (3C 274) and Perseus A (3C 84) are made. Such edge-brightening might be because the thermal gas in which the magnetic field is frozen is compressed by the walls of the BLR which form a funnel at the

poles enhancing the magnetic field at the interface which enhances the radio emission at the cone edges close to the launch site.

Dust formation: In the narrow optical line gas ejected from the poles, the heavier atoms will lag while the lighter atoms will lead in the ejecta. This will lead to segregation of heavier atoms due to enhanced mutual gravity which will form dense metal-rich clumps whose insides will be shielded from the hot pseudosurface. Dust will, hence, form inside these clumps and will eventually be distributed along the polar axis. Observations predominantly detect dust along the jet axis validating this origin scenario.

Magnetic field: The magnetic field lines near the core in all radio galaxies, are aligned with the jet. The structure of the magnetic field provides strong support to their being frozen in the jet which is radially expanding away from the black hole so that the lines are stretched. That the field lines change direction when the jets start forming lobes in FR I galaxies but continue to be aligned along the jet upto the hotspots in FR II sources also argue for an origin in the jet plasma. In other words, the magnetic field lines are along the jet as long as the jet retains its ballistic forward motion.

Wiggles and bending of jets: The wiggles, observed to be symmetrically located on either side of the core in the jets are readily explained by precession of the spin axis of the black hole. Even the changing locations of hotspots on either side of the core in FR II sources such that all pairs remain collinear with the core are easiest to explain with a precessing jet axis. This reason suffices to explain these observed features since matter is radially ejected from the polar regions and when the polar axis precesses, the direction of radial ejection of matter varies which results in symmetric wiggles commonly observed in FR I jets and moving hotspot pairs in FR II jets.

In addition to wiggles, several FR I jets show large scale symmetric or asymmetric bending in the two jets. There are cases wherein one of the jets shows a sharp bend while the other continues uninterrupted in addition to cases wherein both the jets change direction. These features are difficult to attribute to precession. While the likely cause of asymmetric bending is inhomogeneities in the ambient densities, symmetric bending of jets which give rise to NAT and WAT morphologies are best explained by rapid motion of the galaxy (i.e. of the launching site). For example, the radio morphology of the NAT source, NGC 1265 (Figure 31) can be explained by motion of the galaxy from the north-east to the south-west and a non-trivial velocity component along the sightline. A fast moving galaxy in the sky plane will be viewed

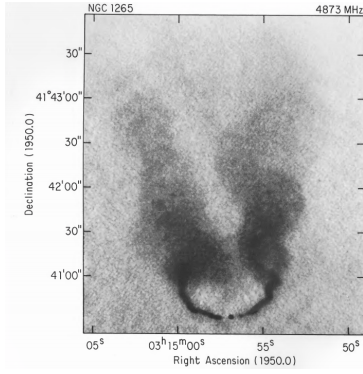


Figure 31: A radio intensity map at 6 cm of the galaxy NGC 1265 copied from O’Dea & Owen (1986). The observed morphology of this narrow-angle tail galaxy can be explained simply by motion of the galaxy in the sky as shown in the schematic in Figure 28. Ram pressure might aid in its formation but it does not appear to be crucial.

as a head-tail or narrow angle tail galaxy while a slow moving galaxy in the sky plane will be viewed as a wide-angle tail radio structure. A stationary galaxy would show straight, oppositely directed jets as the jet launching position is constant.

Composition of jets: Radio jets in active nuclei are composed of positron-electron plasma. Several observations like highly relativistic propagation of the jet to large distances, detection of the annihilation line from a few microquasars, X-ray emission coincident with the radio jets, abrupt halting of jets where hotspots are formed etc provide convincing evidence to this composition. A ready source of copious positrons is the thermonuclear explosion at the poles which precedes an episode of mass ejection in the form of a synchrotron jet and line forming gas. The positron-electron annihilation photons should be generated along the entire radio jet and scattered by the thermal plasma.

Radio lobes and hotspots: The process of lobe formation is distinct in FR I and FR II radio sources as has been highlighted in literature. In FR I sources, the jet loses its ballistic nature on kpc scales and subsequently diffuses out to form lobes. In case of FR II sources, the jet retains its ballistic nature upto the hotspots. As explained here, the forward motion of the jet is halted by radiation pressure exerted by the positron-electron annihilation photons near energies of 511 keV produced beyond the detectable radio jet. This results in hotspots where the plasma is halted which then diffuses back towards the core forming the lobes in FR II sources.

Halo-like lobes in FR I: The radio emission forms a halo around the active nucleus in FR I galaxies like NGC 193 (see Figure 27), 0206+35, 0755+37 (Laing et al., 2011) and M87 where the halo-like structure

has been explained by a precessing jet (Rao, 1987). Such structures in all FR I sources appears traceable to a precessing jet which sweeps over a large region about the core so that over time, a halo-like structure seems to form around the core. Moreover the radio plasma appears to be confined within a well-defined boundary around the active nucleus which is of similar extent as the thermal X-ray emission. The nature of the radio and X-ray structures are similar to those in centres of clusters of galaxies except for the different linear sizes.

Gravitational redshifts: The broad emission lines from quasars, BLRG and Seyfert 1 include an intrinsic redshift component due to gravitational redshifts. Any line which contains a gravitational redshift component will also be gravitationally broadened due to the finite thickness of the line forming region. By determining the gravitational redshift of the broad emission lines, we can locate the BLR wrt to the black hole in terms of the Schwarzschild radius and understand the structure of an active nucleus. The lines forming in the NLR should also show a gravitational redshift component if detected from close to the black hole as is seen in the case of SS 433. The synchrotron jet and NLR are launched from within a few R_s of the black hole in radio sources so that any line photons emerging from there should show a significant gravitational redshift component.

Thermonuclear source of variability: Variability is observed in the wide-band continuum emission at all wavebands. The soft X-ray/ultraviolet/optical variability has to be associated with the black body component while radio variability will be related to the synchrotron component. The former will be predominantly in the non-polar regions whereas the latter will be associated with activity in the polar regions. It is interesting that the variability in both regions can be powered by thermonuclear explosions which are expected when matter is compressed to high densities and temperatures. The variability in the non-polar continuum is also seen to trigger variability in the properties of the broad lines.

LINER gas as the infalling gas: The low ionization lines which are often detected in active nuclei and from the central regions of normal galaxies are believed to arise in the low ionization narrow emission line region (LINER) (Heckman, 1980). This region whose excitation properties lie between HII regions and the NLR is likely to be the pool of gas from which the black hole accretes. Many early type galaxies have been observed to show LINER behaviour and the observed line strengths occupy a distinct place in the diagnostic diagram. If the LINER gas is indeed the infalling gas then once it is exhausted, the super-

Table 4: The observed properties of FR I and FR II radio sources are summarised in the first part of the table while the lower part lists a few inferences that can be drawn from the model discussed in the paper.

| Parameter | FR I | FR II |
|--|---------------------------|--------------------------|
| Bright nucleus | no | yes ¹ |
| Broad emission lines from BLR | no ² | yes ¹ |
| Broad absorption lines from BLR | no | yes ¹ |
| Emission lines from NLR | yes | yes |
| Radio power | lower | higher |
| Radio jets | double-sided | single-sided |
| Jet launching speeds (relativistic) | lower | higher |
| Radio jet opening angle | $\leq 15^\circ$ | $\leq 2^\circ$ |
| Jet magnetic field | \parallel, \perp to jet | \parallel to jet |
| X-ray jet | single-sided | single-sided |
| Radio lobes | double-sided | double-sided |
| Radio lobe magnetic field | circumferential | circumferential |
| Radio hotspots | none | double-sided |
| Hotspot magnetic field | - | \perp to jet |
| X-ray from lobes | faint or none | inverse Compton enhanced |
| Diffuse X-ray halo | yes | no |
| Some Inferences | | |
| Black hole mass ³ | high | high |
| Black hole spin ³ | low | high |
| Accretion disk thickness ³ | thin | thick |
| BLR latitude coverage ³ | small | large |
| Jet opening angle ³ | large | small |
| Jet launching speed ⁴ | $\leq 0.65c$ | $\geq 0.65c$ |
| Jet launching region ⁵ | $> 2.4R_s$ | $< 2.4R_s$ |
| Gravitational redshift ⁵ at launch site | < 0.21 | > 0.21 |

¹ There do exist FR II galaxies where the nucleus is not bright nor is there a BLR. There also exist FR II wherein the BLR is detected mainly in polarised light. ² In a few FR I galaxies, broad lines from a BLR are detected in polarised light. ³ These are comparisons between FR I and FR II. ⁴ These numbers are based on studies in literature which give ballpark numbers for relativistic speeds when Doppler beaming can explain the single-sidedness of the jets in FR II sources. ⁵ These are estimated assuming the jet launching speed is equal to the escape velocity from the black hole.

massive black hole will lose its source of infalling gas and stop accreting, thus entering a quiescent state especially in case of its polar activity.

Final state of an active nucleus: When the galaxy runs out of gas, the black hole will stop accreting and the processes, especially at the poles, which are put in action by accretion will be halted. In particular, once accretion stops, the thermonuclear outbursts at the poles will stop, no further cosmic ray acceleration or ejection will occur and the already ejected radio plasma will keep emitting till it synchrotron ages into oblivion. Same will happen with the narrow line gas which will diffuse into oblivion. The hot pseudosurface and BLR will exist around the black hole and keep accreting from the accretion disk and radiating. If an instability leads to the black hole gobbling up the pseudosurface and the BLR then the black hole will enter a dark stage which can be forever unless

gas becomes available to the black hole and a fresh episode of accretion starts which reactivates the dormant nucleus.

FR I and FR II radio sources: Lastly we compare and contrast the properties of FR I and FR II radio sources in Table 4 and also summarise the inferences that can be derived from the model discussed in the paper.

4.2.3 Case Studies

In this section, we present a few case studies of active galaxies.

In several galaxies hosting an active nucleus, the luminosity is dominated by the central source. There remain uncertainties regarding the morphology of the host galaxy of most quasars due to the extremely bright nature of the central source. However when a host galaxy is discerned, its morphology is surmised

to be either elliptical or spiral. The absolute magnitude of quasars which show a star-like appearance with excess ultraviolet emission is generally found to be $M < -23$ magnitudes whereas for Seyfert 1 and 'N' type radio galaxies the central luminosities are generally ≥ -23 magnitudes and it is much lower for Seyfert 2 and FR I where the integrated luminosity is often dominated by the host galaxy. There appears to be a continuity in the ultraviolet/optical continuum properties of the nuclei in quasars, radio and Seyfert galaxies. However a word of caution, that the distances estimated from the emission line redshifts of quasars are grossly overestimated due to the large intrinsic redshift component that contributes to enhancing their emission line redshifts. This would mean that the actual distances to quasars are lower and hence their luminosity will also be lower when the correct distances are used. We follow the terminology in literature so that radio galaxies refer to radio doubles whose host is an elliptical galaxy whereas Seyferts refer to spiral galaxies hosting an active nucleus.

A large fraction of the narrow emission lines detected in the spectra of most active nuclei are likely to arise in the optical line forming gas that is ejected from the poles which then indicates the presence of an ejected NLR in most active nuclei. However in a fraction of active nuclei, the narrow emission lines could arise in a non-polar BLR that is far from the black hole so that the reduced gravitational broadening leads to narrower lines. It might be possible to differentiate the emission lines of the two distinct origin from the presence of radio jet emission i.e. if the narrow emission lines arise in the NLR then these active nuclei should also host a radio jet which can be compact or distributed whereas if the narrow emission lines arise in a distant BLR then it would be missing a NLR and hence should also be radio-quiet. Broad emission lines arising in the non-polar BLR are observed from quasars, BLRG and Seyfert 1 nuclei which also show the presence of narrow emission lines. The similar morphology of radio-loud double sources consisting of bipolar radio jets, lobes (and hotspots in FR II) and NLR around the jets indicates that the physical processes occurring in the polar regions of all active nuclei are similar. This is not surprising since all active nuclei host an accreting supermassive rotating black hole and hence should also lead to similar physical processes.

There do exist interesting observational differences between active nuclei which should give us important insight into the range of implications of the physical processes. Some of these differences are (1) iron lines are more frequently detected in radio-quiet quasars

and Seyferts while rarely observed in radio galaxies and radio-loud quasars. (2) The observed emission line redshifts of quasars are larger than radio galaxies and Seyferts (see Figure 23). The emission line redshifts of FR II quasars are higher than FR II galaxies which in turn are higher than FR I galaxies. Seyferts show the lowest emission line redshifts amongst active nuclei. (3) The spectra of the majority of quasars and a few radio galaxies and Seyferts contain emission lines and absorption lines with the absorption lines blueshifted wrt to the emission lines. While numerous multi-redshifted absorption lines are detected in quasars, only a few such lines are discernible in the spectra of other active nuclei. In light of the model presented here, we can now understand these points. The first point indicates that iron is more abundant in radio-quiet active nuclei. Since the radio emission in an active nucleus is confined near the polar axis, this correlation indicates that these iron lines arise in the matter accreted and/or ejected from the poles. Such a correlation between the radio emitting plasma and the iron lines arising in the BLR is not expected. A thermonuclear blast which supplies the energy for energising the NLR and radio plasma also forms heavier elements. If the energy released in the explosion is sufficient to accelerate and eject the accreted matter then this will lead to formation of a NLR and radio jets i.e. a radio-loud active nucleus. Assuming the infalling matter is hydrogen-rich, the thermonuclear reaction will also synthesise helium so that the ejected matter will consist of helium, hydrogen and other metals of say solar composition. The NLR of this active nucleus will not be rich in iron lines. However, if the energy released in the polar thermonuclear explosion in an active nucleus is insufficient to accelerate the accreted matter to escape velocities, then only nucleosynthesis will occur in the accreted matter at the poles with successive explosions leading to formation of increasing atomic mass elements till iron is formed. In this case, there will be no NLR or radio jets - in other words, the active nucleus will be radio-quiet but the accreted matter at the poles will be enriched in iron. The observed correlation between the radio loudness and presence of iron lines can thus be explained. The second point regarding the range of observed emission line redshifts of the different types of active nuclei can be explained by the larger component of gravitational redshift in the observed emission line redshift of quasars, followed by FR II nuclei and then by FR I and Seyfert nuclei. If it is assumed that the emission line redshifts are derived from the lines arising in the BLR, then the range of observed redshifts indicates the range of separations of the BLR from the black hole. The third

point can be understood from the proximity of the BLR to the black hole and hence the range of intrinsic redshifts that can distinguishable. In quasars the BLR is very close to the black hole so that the range of intrinsic redshifts for lines forming in the BLR of finite extent is large so that the emission and absorption lines of different redshifts can be discerned. As the separation of the BLR from the black hole increases, the intrinsic contribution to the line redshifts decline. All BLR are likely to host an emission line and absorption line zone but the intrinsic redshift component decreases from quasars to Seyferts so that the lines from the BLR appear close to the systemic velocity of the host galaxy.

We discuss the cases of radio-loud active nuclei namely 3C 273 (quasar), Cygnus A (FR II), Virgo A (FR I), NGC 4151 (Sy 1) in light of the model presented in the paper.

4.2.3.1 FR II quasar - 3C 273 : 3C 273 was the first quasar which was identified (Schmidt, 1963) and is also identified as the quasar with the lowest emission line redshift in the 3CR sample. The source consists of a bright core (see Figure 32) detected at multiple wavelengths, a one-sided jet detected from X-ray to radio wavelengths and a radio hot spot in which the radio jet terminates. Its V band magnitude is measured to be about 12.8, its emission line redshift is measured to be $z_{em} = 0.158$ and the knots in the jet are observed to expand at a rate of 0.76 mas/year. These observed parameters have been interpreted to indicate that the quasar is located at a distance of ~ 650 Mpc so that its absolute V band magnitude is -26.3 magnitudes and the knots are expanding with superluminal velocities $\sim 8c$ (e.g. Krichbaum et al., 1990). The radio spectrum of 3C 273 is observed to be variable over timescales ranging from days to years (Pauliny-Toth & Kellermann, 1966) with the behaviour being qualitatively similar to microquasar in that the variability is first detected at the higher radio frequencies. At the large distances that have been inferred for 3C 273, the energy requirements to explain such repeated variability are huge but would be modest if the source was nearby (Pauliny-Toth & Kellermann, 1966). Radio polarisation studies show the magnetic field to be aligned with the radio jet except in the hotspot where it becomes perpendicular to the jet (e.g. Perley & Meisenheimer, 2017). The jet is about $25''$ long which for a distance of ~ 650 Mpc (corresponding to $z = 0.158$) to the quasar would correspond to a length of about 79 kpc. An optical jet is also observed with comparable length but with a narrower transverse width than the radio jet (Thomson et al., 1993). No counter-jet has been detected

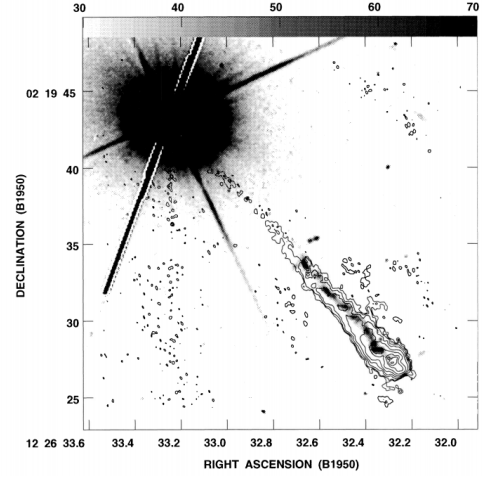


Figure 32: Figure showing the radio (contours) and optical (grey) emission with a resolution of about $0.16''$ and $0.1''$ for 3C 273 reproduced from Bahcall et al. (1995). Notice that the active nucleus is so optically bright that the host galaxy is not detected.

in any band. Broad emission lines at $z \sim 0.158$ and multi-redshifted absorption lines at redshifts < 0.158 have been detected in the spectrum of 3C 273 which is a property common to quasars.

The lowest redshifts at which absorption lines have been detected in the spectrum of 3C 273 are $z = 0.0053$ ($v \sim 1600$ kms $^{-1}$) and $z = 0.00337$ (Tripp et al., 2002). We follow the reasoning in Kantharia (2016) and assume that one of these is the actual cosmological redshift of the quasar which means the quasar is closer and the observed emission line redshift contains a gravitational redshift z_g component. We assume that $z_c = 0.0053$ is the cosmological redshift of 3C 273 (it could be 0.00337 which would only make the arguments presented here stronger). Since $(1 + z_{in}) = (1 + z_{em})/(1 + z_c)$, the intrinsic redshift suffered by the emission line will be $z_{in} = 0.1519$. The gravitational redshift will be $z_g = z_{in}/(1 + z_{in}) = 0.131$. The separation of the line forming zone from the black hole, R can be estimated from $z_g = R_s/(2R) = R_s/(2nR_s)$ where $R = nR_s$. The lines from the BLR which include a shift $z_g = 0.131$ will be located at $R \sim 3.8R_s$ and the non-polar pseudosurface in 3C 273 will be formed within $3.8R_s$ of the black hole.

Considering 3C 273 is at $z_c = 0.0053$ means it is located at a distance of about 20 Mpc so that $1'' \sim 0.1$ kpc. The length of the observed $25''$ jet would then be 2.5 kpc indicating that 3C 273 is a compact object similar to GPS and CSS sources. The central bright source in 3C 273 (Figure 32) which is the active nucleus is smaller than 50 pc. Radio knots in the jet of 3C 273 are observed to expand with angular rates of ~ 0.76 mas/year which translates to

an apparent velocity of about 8-10 times the speed of light at a redshift of 0.158 (Pearson et al., 1981, 1982). However if 3C 273 is at $z_c = 0.0053$, then 0.76 mas/year would correspond to 0.076 parsec/year = 0.24 light year/year. This velocity indicates the radial component of knot expansion along the sightline i.e. $v_{knot} * \cos\theta$ so that it approaches the actual knot expansion velocity v_{knot} for small angles between jet and sightline θ . If we ignore the inclination of the jet with the sightline for now then the knots are ejected at a velocity $0.24c$ which will in the least be equal to the escape velocity of the polar jet. This, then translates to ejection of matter from a region separated from the black hole by about $17R_s$. If the jet is oriented at an angle of 30° to the sightline, then the knots will be expanding at a velocity of $0.277c$ and would have been ejected from $13R_s$. Since Doppler boosting has led to the detection only a one-sided jet, the inclination of the jet to the sightline cannot be too large. This discussion indicates that the inference of superluminal motions appears to be wrong and has been misleading due to the incorrectly estimated cosmological redshifts of quasars and other active nuclei. As is shown here for 3C 273, once we estimate and remove the intrinsic redshift component, the active nucleus is found to be located close to us, thus reducing the linear motion of the knots estimated from their angular expansion.

At a distance of 650 Mpc, the V band absolute magnitude of 3C 273 is $M_V = -26.3$ magnitudes while if 3C 273 was separated by 20 Mpc, $M_V = -18.7$ magnitudes. The latter luminosity is typical of bright normal galaxies except that while in those galaxies, light from the entire galaxy contributes to the luminosity, in 3C 273 (and other quasars) the observed luminosity is from the compact active nucleus. This, then, demonstrates that our understanding of quasars can be flawed due to overestimated distances. Once the gravitational redshift component is removed from the quasar redshift, the distances to quasars will become comparable to other active nuclei i.e. located much closer. This will, amongst other properties, reduce the exceptionally large bolometric luminosities that have been attributed to quasars and make superluminal motions unnecessary.

A temperature of 26000 K has been estimated for the black body component in 3C 273 (Malkan & Sargent, 1982). The emitting area required to explain the observed luminosity, if the source was closeby at 20 Mpc, is $2.8 \times 10^{30} \text{ cm}^2$ as discussed in Section 4.2.2.2. If the emitting surface is spherical, then this area corresponds to a radius of $4.7 \times 10^{14} \text{ cm}$ which is equal to the Schwarzschild radius of a black hole of mass $1.6 \times 10^9 M_\odot$ which is comparable to the mass

Table 5: The table lists the change in properties of 3C 273 when the gravitational redshift component is removed from the observed emission line redshift (0.158) which leads to a revision in the distance estimate to the quasar (0.0053).

| Property | $z_c = 0.158$ | $z_c = 0.0053$ |
|---------------------------------|------------------------|-----------------------|
| Distance | $\sim 650 \text{ Mpc}$ | $\sim 20 \text{ Mpc}$ |
| M_V magnitudes | -26.3 | -18.7 |
| Emission line z_g | none | 0.131 |
| Distance bet BLR, BH | ? | $\sim 3.8R_s$ |
| v_{esc} at BLR | ? | $\sim 0.5c$ |
| Length of $25''$ radio jet | 79 kpc | 2.5 kpc |
| Knot expan 0.76 mas/yr | $\sim 8c$ | $\geq 0.24c$ |
| Knot expansion rate | superluminal | subluminal |
| Jet launching site ¹ | ? | $\leq 17R_s$ |

¹ Assuming that the proper motion of the knot (i.e. $0.24c$) indicates the escape velocity from the black hole.

that has been estimated for the black hole in 3C 273. For these values, the black body luminosity due to a spherical emitting pseudosurface will be -20.93 magnitudes and the V band magnitude will be -18.43 magnitudes. Recall that the observed V band luminosity, if 3C 273 was 20 Mpc away, is ~ -18.7 magnitudes. The matching of the estimates derived from distinct observed parameters tends to support the model presented here, in particular, the shorter distance to 3C 273 and the black body component being from the hot quasi-spherical pseudosurface of radius $\sim R_s$.

The properties of 3C 273 determined for redshifts 0.158 and 0.0053 are summarised in Table 5. The changes listed in Table 5 underline the importance of correctly estimating the cosmological redshift and hence distance to quasars since several important properties of quasars depend on the distance. Obtaining correct estimates of physical properties of quasars is crucial to improving our overall understanding else the discrepancy between observational results and our understanding will keep increasing.

To summarise: (1) The corrected distance to 3C 273, as estimated from one of the lowest redshift absorption lines in its spectrum is 20 Mpc. The V band absolute magnitude estimated from the observed apparent magnitude for the corrected distance is $M_V = -18.7$ magnitudes (For a distance of 650 Mpc, $M_V = -26.3$ magnitudes). The V band absolute magnitude expected for black body radiation at 26000 K, as estimated from the Stefan-Boltzmann law using parameters derived from observations (R_s and $T_{blackbody}$) is -18.43 magnitudes. The comparable values of M_V strongly justify the reasoning. Some difference in the observed V band luminosity with that

estimated from black body luminosity is expected due to non-zero contribution by synchrotron emission at V band and the quasi-spherical nature of the pseudo-surface. (2) The emitting zone in the non-polar BLR is located at a separation of $3.8R_s$ from the black hole. (3) The radio jet is about 2.5 kpc long and the radio dimensions of 3C 273 are similar to CSS/GPS quasars. (4) The polar knots are ejected from a region separated from the black hole by $\leq 17R_s$ at a velocity of $\geq 0.24c$.

4.2.3.2 FR II galaxy - Cygnus A : Cygnus A is a powerful FR II type radio galaxy at a redshift of 0.056 (distance ~ 230 Mpc) located in a nearby cluster of galaxies (Owen et al., 1997). Baade & Minkowski (1954a) detected narrow emission lines in the spectrum of Cygnus A and identified the optical host galaxy of Cygnus A. Broad lines were not immediately detected which prompted its classification as an NLRG FR II source which is rare. Generally FR II radio sources are hosted by BLRG nuclei while FR I are hosted by NLRG nuclei. An angle of 2 mas at the distance of Cygnus A corresponds to a linear distance of 2.2 pc. Some of the observed properties of Cygnus A are listed below with comments in italics.

- The host galaxy is a faint but large cD galaxy. The radio structure extends out to about 70 kpc on either side of the optical galaxy.
- Early observations detected faint optical nuclear continuum and emission from strong forbidden lines ([O II],[O III]) at the galaxy redshift of $\sim 16800 \text{ km s}^{-1}$ with widths $\sim 400 \text{ km s}^{-1}$ with the forbidden line emission extending beyond the nucleus (Baade & Minkowski, 1954a). More recent observations have found the [O III] emission to be spread over the central $\sim 10''$ (~ 11 kpc at the distance of Cygnus A) and elongated along the radio axis (Baum et al., 1988). The emission line spectrum consists of recombination lines and forbidden lines with a wide range of ionization (Osterbrock and Miller 1975). The distribution of H α and [N II] lines also extends out from the nucleus to about $10''$ (Carilli et al., 1989).
- Ionized gas distributed in the central 5 kpc region appears to be rotating about an axis aligned close to the radio axis of Cygnus A (Simkin, 1977; Hargrave & Ryle, 1974). *This could be the gas which the black hole is accreting.*
- Although Cygnus A was originally classified as a NLRG due to detection of only narrow lines, broad Mg II emission lines (FWHM \sim

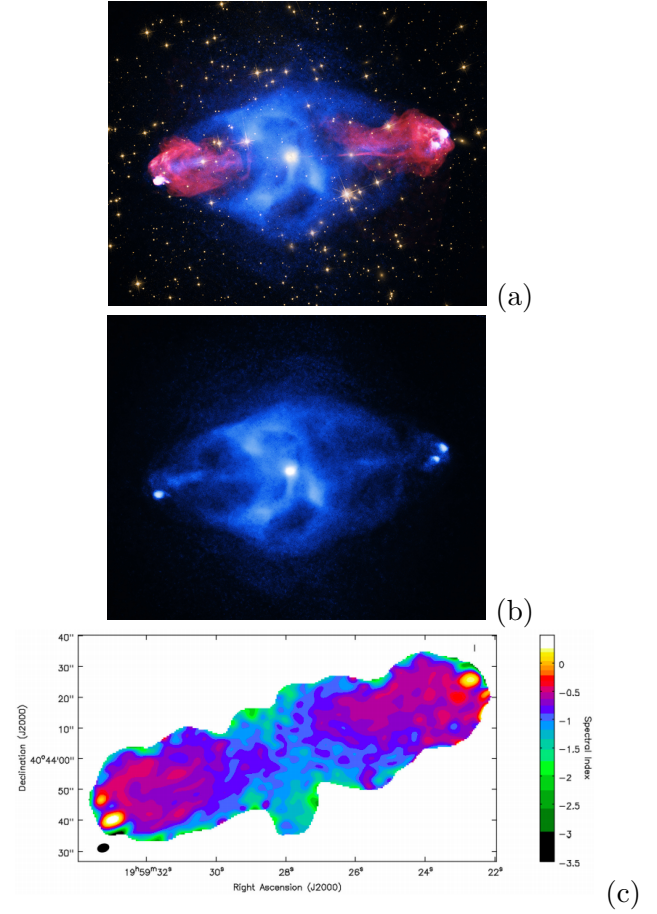


Figure 33: Multi-band image of FR II galaxy Cygnus A (a) and X-ray image of Cygnus A (b) downloaded from <http://chandra.harvard.edu/photo/2015/iyl/>. (a) Blue is X-ray data from Chandra telescope, red is radio data from VLA and yellow is optical data from the Hubble space telescope and DSS. The radio lobes and X-ray emission share a major axis and together define a oval cocoon although their distributions are anti-correlated. The hot spot forms at the periphery of the X-ray cocoon which is common for all FR II sources. (b) The X-ray image is shown to highlight the double-sided X-ray beams and their terminating pair of hotspots. The X-ray beam in the east seems to terminate above the hotspot. (c) Figure showing the distribution of spectral index between 109 and 183 MHz copied from McKean et al. (2016). Notice two pairs of hotspots - the bright hotspots A and D and another pair (north-east of D and south-west of A) which is not detected on total intensity maps. The plume is also clearly detected with a steep spectrum.

7500 kms^{-1}) have subsequently been detected (Antonucci et al., 1994). Broad Balmer lines ($\text{FWHM}(\text{H}\alpha) \sim 26000 \text{ kms}^{-1}$) have also been detected in polarised light from a bipolar region centred on the core which have been interpreted as line emission from the BLR scattered into our sightline by polar dust (Ogle et al., 1997).

- No optical line emission is detected from the radio lobes.
- The radio structure of Cygnus A consists of a core, two jets with one being considerably brighter than the other which when explained due to Doppler boosting indicate a jet velocity $> 0.45c$ and the angle made by the jets with the sightline $\theta < 63^\circ$ (Carilli et al., 1991a; Scheuer & Readhead, 1979), two lobes and two bright hotspots (Hargrave & Ryle, 1974). It is one of the brightest sources in the radio sky and has been studied across the electromagnetic spectrum.
- X-ray emission detected from the radio hotspots cannot be explained by the synchrotron process or thermal emission but well explains the observations if due to synchrotron self Compton process as was surmised from the hotspots in Cygnus A which were the first to be detected in X-ray bands (Harris et al., 1994).
- Figure 33(a) shows a superposed image of the extended radio and X-ray emission in Cygnus A. The radio and X-ray emission share a major axis and are of similar extent. However the X-ray emission is faint at the location of the radio lobes. *Cygnus A is the rare FR II which lies in a cluster of galaxies and is also the rare FR II wherein X-ray cavities are coincident with radio lobes.* Figure 33(b) shows only the X-ray emission which highlights the jet-like but laterally thick features which extend all the way from the core to the hotspots and appear to be coincident with the expected radio jet trajectories. We refer to these as X-ray beams to distinguish them from the radio jets which are significantly narrower. Interestingly, the X-ray beams do not terminate in the bright hotspots A (west) and D (east) but in distinct hotspots.
- High resolution images show that the two bright hotspots break up into two smaller distinct hotspots.
- Linear polarisation fractions which rise upto 70% are detected in the lobes (Carilli et al., 1989; Perley & Carilli, 1996).
- The linearly polarised emission from the jet shows that the magnetic field is aligned along the jet (Perley & Carilli, 1996).
- The spectral index map between 109 and 183 MHz (McKean et al., 2016) shows two distinct pairs of hotspots with each pair appearing collinear with the core (see Figure 33c). One of these pairs is coincident with the bright hotspots A (west hotspot) and D (east hotspot) detected in radio and X-ray images. The other pair of hotspots (south-west of A and north of D) which show up on the spectral index map are not clearly discernible in the radio and X-ray images indicating their radio/X-ray intensities are currently comparable to the lobes although the low radio frequency spectrum is getting flatter. Interestingly, it appears that the X-ray beams in Figure 33b terminate in this second pair of hotspots. *The radio jets should also terminate in this second pair of hotspots. The second pair of hotspots till which the X-ray beams extend seem to have just formed and should brighten over time. The bright hotspots A and D indicate the location of the older pair of hotspots and hence the previous jet position. Multiple pairs of hotspots are identified in most FR II and are characteristic of a precessing spin axis of the black hole.*
- Like Cygnus A, double X-ray beams have been detected in other FR II BLRG like Pictor A (see Figure 34) where a radio jet is barely detectable. The origin of the symmetric X-ray beams in Pictor A has been suggested to be synchrotron (Hardcastle et al., 2016). An offset is noted between the location of the radio and X-ray hotspots and temporal variability in the X-ray emission from hotspots has been noted over timescales of months to years which is inferred to be indicative of compact emitting regions (Hardcastle et al., 2016). Existence of multiple hotspots, offset radio and X-ray hotspots, variable hotspot emission, one-sided radio jets but two-sided X-ray beams, similar radio and X-ray extents appear to be common to several FR II sources. *As described in the previous sections, fast jets are composed of a positron-electron plasma and hence positron-electron annihilation will proceed at some rate along the entire radio jet, releasing soft γ -ray photons of energy $\sim 511 \text{ keV}$. These photons will be Compton-scattered by electrons to lower wavelengths thus explaining the X-ray beams which extend from the core to the hotspots. The two-sided X-ray*

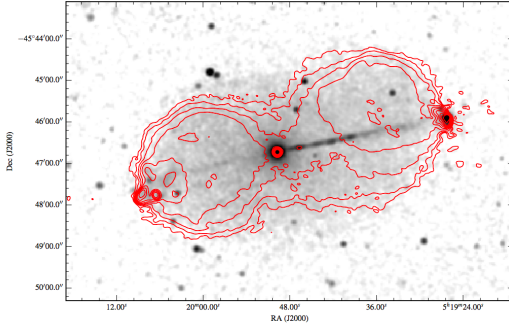


Figure 34: X-ray and radio image of FR II galaxy Pictor A copied from Hardcastle et al. (2016). Grey scale shows the X-ray image between 0.5-5 keV whereas the contours show the 5.5 GHz emission and their similar extents is striking. Double-sided X-ray beams are detected which extend from the core to the hotspots with the western one being brighter than the eastern beam. Radio jets are barely detectable. The X-ray and radio hotspots show an offset especially noticeable in the eastern lobe.

beams are detected since Doppler beaming is negligible unlike in radio jets.

- The spectrum of the core is curved and peaks near 30 GHz as shown in Figure 35a (Carilli et al., 1999). *The energy distribution of the electrons accelerated by the pulse of energy released in a thermonuclear outburst in the accreted matter on the polar pseudosurface of the black hole will be a normal distribution with a peak and dispersion determined by the expansion (escape) velocity and random motions respectively. Thus, such a peaked SED with the peak at high frequencies is the most probable distribution expected for the instantaneous injection of energy to a large number of particles.*
- The radio spectrum of the hotspot A (Figure 35b) and D is a steep power law between 10 GHz and 1000 GHz ($\alpha \sim 1$) but flattens at frequencies < 10 GHz (Carilli et al., 1999) and $\alpha = 0.34$ between 151 and 327 MHz (Carilli et al., 1991b). Low frequency LOFAR observations trace the turnover near 100 MHz in the hotspots A and D (McKean et al., 2016). This spectrum is very different from the core spectrum.
- Equipartition magnetic fields of 250 to 300 μG at the hotspots which decrease to $\sim 45\mu\text{G}$ near the core have been estimated (Carilli et al., 1991b).
- Radio variability in Cygnus A is low as noted from the data at 43 GHz which did not vary over a timescale of 1.3 years (Carilli et al., 1999).
- The jet opening angle is estimated to be $< 1.6^\circ$ on kpc scales (Carilli et al., 1996). A conical

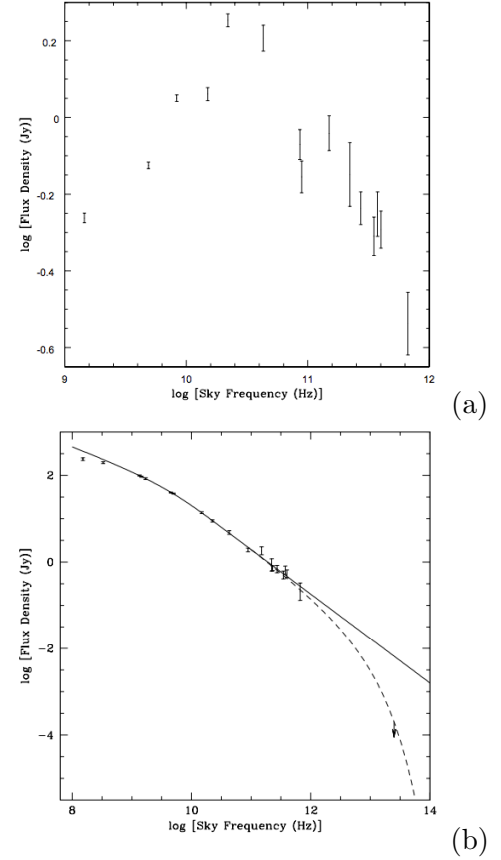


Figure 35: The spectra of the core (a) and hotspot A (b) in Cygnus A reproduced from Carilli et al. (1999). Notice the turnover of the core spectrum around 30 GHz whereas the hotspot spectrum shows a mild flattening below 10 GHz. On the other hand, the integrated spectrum of Cygnus A shown in Figure 2 shows a turnover below 20 MHz with a convex shaped spectrum at higher frequencies.

jet is not detected, instead the jet appears to be cylindrical at all scales - milliarcsec as shown in Boccardi et al. (2016) to arcseconds. *This could indicate the fairly small opening angle of the jets of FR II sources which hence remain laterally unresolved upto the hotspots.*

- The south-east radio lobe in Cygnus A which is formed by the backflow from the hotspot turns abruptly by an angle of $\sim 90^\circ$ near the core as can be seen in the images at frequencies below 1.5 GHz or so (e.g. Leahy et al., 1989; Lazio et al., 2006; McKean et al., 2016) and is often referred to as the ‘plume’ in literature. No lobe emission is detected near the core at 5 GHz (see Figure 33). *The nature of the bending is similar to X-shaped galaxies indicating that lobes bend in all FR II galaxies when they reach the core.*

Having summarised the observations, we try to understand the observational results on Cygnus A using the model described in the paper.

If the magnetic field in which the relativistic electrons emit synchrotron radiation giving rise to the core spectrum is $45 \mu\text{G}$, then the energy of the electrons emitting at the radio frequency of 30 GHz which is the peak of the SED (see Figure 35) would be 6.5 GeV ($\gamma = 1.2 \times 10^4$). The energy of electrons emitting synchrotron at a X-ray frequency of 10^{18} Hz would be $3.7 \times 10^4 \text{ GeV}$ i.e. 37 TeV ($\gamma = 7.3 \times 10^7$). The core spectrum is the best available representative of the injection spectrum of the relativistic electrons energised by the instantaneous energy released in the thermonuclear explosion. The observed core spectrum alongwith the estimated core magnetic field help infer that the energy distribution of relativistic electrons injected into the jets in Cygnus A peaks around 6.5 GeV . The peak energy could correspond to the escape velocity or likely higher velocity expulsion of positron-electron plasma from the poles of the pseudosurface. The peak energy of 6.5 GeV corresponds to a ultrarelativistic velocity of $0.9999c$ for the electrons. The observed energy distribution of all particles/cosmic rays should peak at same energies which could be 6.5 GeV in Cygnus A. This energy would correspond to peak velocities of about 36000 kms^{-1} for the proton distribution. If this velocity is equal to the escape velocity from the black hole then the line emitting matter will be ejected else it will remain trapped on the pseudosurface. Since launching of matter from the poles in FR II cores happens from within a few R_s of the black hole, it requires relativistic escape velocities. This suggests that protons ejected with a velocity of 36000 kms^{-1} might not be able to escape the black hole gravity and will fall back on the pseudosurface. However it should also be kept in mind that the peak energy estimates will be uncertain due to the core spectrum being measured away from the launch site and due to inaccuracies in the magnetic field estimates so that the actual peak injection energy could be much larger than what we record. Since emission line gas is observed to be distributed in a region of $10''$ around the nucleus, it indicates that there is a detectable fraction of line-forming gas that has been able to escape from the black hole. The large FR II radio structure indicates that the fast positron-electron plasma has been ejected in plenty from the polar pseudosurface.

The equipartition magnetic field in the hotspots has been estimated to be $300 \mu\text{G}$. In this field, the energy of electrons predominantly radiating at the turnover frequency of 100 MHz will be 0.14 GeV ($\gamma = 280$) whereas those radiating at 10 GHz where the spectrum shows a slight break will be 1.44 GeV ($\gamma = 2813$). Since we assume that the peak energy is indicative of the expansion velocity of matter, the

slowing down of the jet will be reflected in the declining peak energy. In other words, the number of particles that are moving forward with the high injection momentum keep declining along the jet. This would mean that the electrons which were injected into the jet with peak $\gamma \sim 1.2 \times 10^4$ has decelerated to peak $\gamma = 280$ at the hotspots where the jet is halted i.e. $\gamma \rightarrow 0$ and the plasma diffuses back. The integrated spectrum of Cygnus A shows a turnover at frequencies below 20 MHz and the slight break at 10 GHz is also discernible (see Figure 4). If this low frequency turnover is due to the spectrum of the lobes and if the magnetic field in the lobes is $45 \mu\text{G}$ then the electrons emitting at 20 MHz in the lobes are of energy 0.17 GeV which is similar to the peak electron energy in the hotspots. Since the forward motion of the jet is abruptly arrested at the hotspot, it is interesting to think about the change in the nature of the energy spectrum especially the peak energy. Since there is no forward motion, it should become centred on zero energy. However on the other hand, the abrupt stopping can also lead to the forward-directed energy being randomised with little change in the energy spectrum. The comparable peak energies for the hotspot and lobe electron populations argues for the latter wherein the electron energy spectrum remains the same after being stopped at the hotspot. *Thus, the same electron population that flowed from the core through the jets to the hotspots is flowing into the lobes i.e. there is no electron reacceleration in the hotspots.*

Narrow lines were first detected from Cygnus A and hence the emission line redshift was determined from the polar NLR which is generally detected at parsec and kiloparsec scales around active nuclei and is typically seen to show expansion of a few hundred kms^{-1} about the cosmological redshift. Thus, the redshift of Cygnus A ($z = 0.056$) likely does not contain any contribution from gravitational redshift unlike the broad lines from the BLR located close to the black hole. In fact, the redshift of Cygnus A lies towards the lower end of the redshift distribution of FR II type radio galaxies as shown in Figure 23. Since most FR II sources host a BLRG nucleus, the wide emission lines which are observed to appear at the highest redshifts in the spectrum and hence used to determine the cosmological redshift of the host galaxy, contain a non-zero contribution to the observed emission line redshift from a gravitational redshift component. The FR II sources hence appear at relatively higher redshifts than FR I sources which are predominantly NLRG.

As discussed earlier, the injection energy spectrum of electrons which will be launched along a jet will

be a gaussian distribution with a peak at an energy which is equal to or larger than the required escape velocity from the black hole and a dispersion indicating the random velocity component. The energy spectrum will evolve as the electrons proceed along the jet and lose energy - the forward velocity declines to a lower value so that the peak will move to lower energies and as the electrons radiate and suffer synchrotron losses, the high energy part of the energy spectrum will keep declining. In other words, the dispersion of the distribution will keep reducing i.e. the number of high energy particles will keep declining which will cause the energy distribution beyond the peak to get steeper. This, then explains the steepening of the observed radio spectrum. Adhering to the hypothesis that all electron acceleration occurs in the core and applying the above reasoning to the observed spectra of different components in Cygnus A tells us that the core spectrum is freshly injected into the jet and should peak at high radio frequencies as is observed (Figure 35). In FR II sources, the jet is surmised to expand relativistically till the hotspot so that the electron energy spectrum will continue to peak at relativistic energies although much lower than at the core. Due to synchrotron losses, the energy spectrum will steepen beyond the peak so that it is steeper than at the core. As seen in Figure 35, the radio spectrum of the hotspot A (and also hotspot D) shows a gentle break at 10 GHz and is steep beyond it but flattens at lower frequencies showing a turnover around 100 MHz. The spectrum is very different from the core spectrum which again argues against any fresh episode of reacceleration. The steep spectrum beyond 10 GHz in the hotspots can be easily explained by the aged electron population so that the high energy electrons have lost energy and the dispersion of the distribution has narrowed. The varying magnetic field in the lobes and hotspots translate to distinct peak radio frequencies of the spectrum (see Equation 2) even if the underlying electron energy distribution peaked at the same energy. If the core frequently ejects matter then it can lead to several energy distributions contributing to the observed radio spectrum which could result in a flat spectrum (Cotton et al., 1980) as has been observed in several active cores, especially if the peaks of the ejections are of similar intensity but varying energies.

The X-ray emission from the hotspots in Cygnus A has been explained by inverse Compton scattering of the radio photons generated in the synchrotron process by the same population of relativistic electrons i.e. synchrotron self-Compton (SSC). The frequency of the photons generated by the inverse Compton boosting of a low energy photon can be estimated

from Equation 5. In the hotspot where the magnetic field is estimated to be $300 \mu\text{G}$, electrons of energy 1.44 GeV ($\gamma \sim 2813$) will radiate at 10 GHz. In SSC, the 10 GHz photons will be inverse Compton-scattered to higher energies by the same population of relativistic electrons which emit the radio photons e.g. the 10 GHz photon can be inverse Compton-scattered to a photon of frequency 10^{17} Hz (X-ray photon of energy $\sim 1 \text{ keV}$) by electrons of energy $\gamma = 2813$. In this case, the energy losses in the hotspots below $\sim 10 \text{ GHz}$ will be predominantly due to the synchrotron process whereas above $\sim 10 \text{ GHz}$, the losses in the hotspots will be due to both synchrotron and inverse Compton processes which will steepen the spectrum faster as compared to synchrotron losses. While some of the relativistic plasma is trapped in the hotspots, most of it flows back and forms the lobes. The radio spectrum of the lobes of Cygnus A shows a break near 5 GHz (Carilli et al., 1991b). The synchrotron emission at this frequency would be due to electrons of energy 2.6 GeV ($\gamma = 5080$) radiating in the measured magnetic field $\sim 45 \mu\text{G}$.

The X-ray beams detected on either side of the core extending upto the hotspots (see Figure 33) i.e. $\sim 70 \text{ kpc}$ from the core, are difficult to explain due to the synchrotron process since that would require the existence of TeV electrons upto the hotspots. While TeV electrons are generated in the polar regions of the pseudosurface energised by the thermonuclear explosion, these would fade in 100-1000 years in the typical magnetic field of Cygnus A indicating that only the X-ray jet detected close to the core can be due to the synchrotron process. As suggested in the paper, the X-ray beams can be readily explained by the process of Compton scattering of the soft γ -ray photons generated in the positron-electron annihilation process to lower energies. The larger transverse extent of the X-ray beams compared to the radio jets indicates that the dense plasma around the jet might also be involved in the Compton-scattering process. Both the X-ray beams are detected since the effect of Doppler boosting is diminished. *To summarise: the X-ray beams are a direct result of Compton-scattering of the positron-electron annihilation photons, generated in the synchrotron jet, to lower energies. This process can remain active as long as the photons are emitted in a dense medium.*

The parsec scale jet-counterjet intensity ratio measured for Cygnus A is between 5 and 21 while the kiloparsec scale jet-counterjet intensity ratio is measured to be 2.6 ± 1 (Carilli et al., 1996). This ratio is typically large in FR II galaxies since the counterjet is seldom detected. The detection of a faint counter-

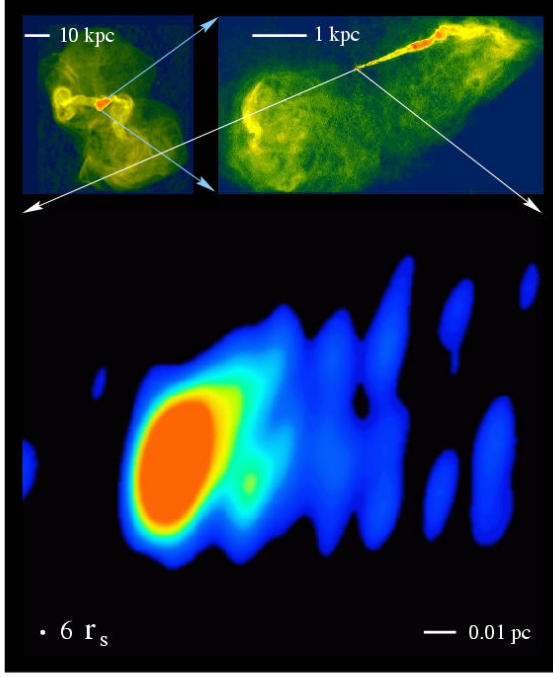


Figure 36: Radio images of M87 - the above two are with VLA while the lowermost highest resolution image is at 43 GHz with the VLBA from Junor et al. (1999). The image has been downloaded from <https://www.nrao.edu/pr/1999/m87/>. Notice how the conical jets are launched from the black hole as seen in the high resolution image. An opening angle of 60 degrees has been estimated near the core whereas the opening angle on kpc scale is much smaller. Notice how the triangular blob in the centre of the top left panel is resolved into a double-lobed single-conical jet structure which would have been difficult to surmise from the low resolution images.

jet in Cygnus A has provided strong support to the Doppler boosting hypothesis for the non-detection of the counterjet. It also provides strong support to the existence of a counterjet in all FR II radio galaxies even if not detected. The existence of the X-ray beams in Cygnus A which, as explained above, owe their existence to positron-electron annihilation along the radio jets also supports the presence of both jets in FR II galaxies. These are additional pieces of evidence - the existence of double lobes and pairs of hotspots on either side of the core have already provided strong proof to the existence of double-sided jets even if the counter-jet is not detected.

4.2.3.3 FR I galaxy - Virgo A :

Virgo A is the FR I radio source associated with the active nucleus of the elliptical galaxy M 87 which is the central galaxy of the Virgo cluster. For a distance of 16.7 Mpc to M 87, 1 arcmin corresponds

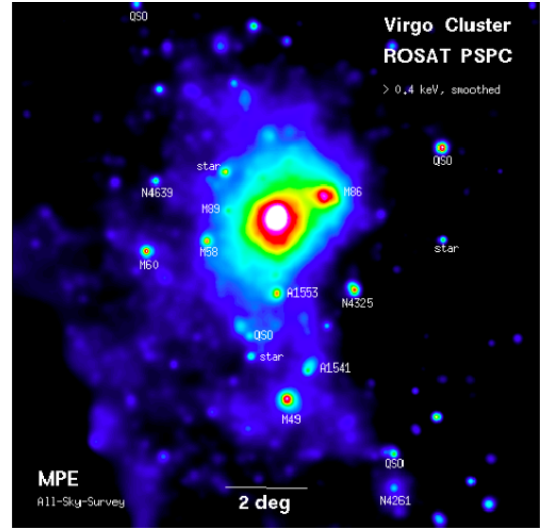
to about 4.95 kpc. This galaxy has been extensively studied across the electromagnetic spectrum and at angular resolutions ranging from single dish to VLBI (see Figure 36). Some of the observational results on this galaxy are summarised below:

- M 87 is a large cD galaxy which is the host of the active radio source Virgo A with the radio structure enclosing a region of size ~ 80 kpc.
- M 87 has more than 12000 associated globular clusters. About 2000 galaxies are believed to be members of the Virgo cluster.
- A bright conical radio jet detected upto kpc scales extends towards the north-west (Figure 36) while a faint counter-jet is detected close to the core as seen in VLBA images (Walker et al., 2018).
- Wiggles are noticeable in the radio jet in the north-west beyond a kpc or so after which the jet bends to the south and diffuses out to a wider structure like diffuse beams (see top left panel in Figure 36) and the conical nature of the jet is no longer distinguishable. *This would indicate that the jet remains ballistic upto a kpc or so till it bends, diffuses and loses its identity.* The counterjet in the east also seems to bend towards the south and diffuses.
- The distribution of diffuse X-ray emission in the 0.6 to 2 keV band is remarkably similar to the diffuse radio beams in Virgo A (Million et al., 2010). The X-ray emission from the beams is more intense than the X-rays from the extended halo emission i.e. is similar to the distribution of radio emission shown in the top left panel of Figure 36. The X-ray emission from the diffuse X-ray halo is brightest at 2 keV whereas the emission from the X-ray beams peaks at 1 keV and is barely detectable at 3 keV as can be surmised from the emission measure maps in Werner et al. (2010). This, then, could indicate that the X-ray emission coincident with the radio beams includes a contribution from another process in addition to the thermal emission. A collimated X-ray jet coincident with the inner radio jet in the north-west is also detected. The X-ray jet is distinct from the X-ray beams. *While the X-ray jet close to the core has a synchrotron origin like the radio jet, the X-ray beams which trace the diffuse radio beams will be due to Compton-scattering of the positron-electron annihilation photons generated in the radio jets/beams.* A prerequisite for this explanation is the coincidence of the radio

synchrotron features due to the positron-electron plasma and the X-ray features due to Compton scattering of soft γ -ray photons.

- A conical edge-brightened jet emerging with an opening angle of $\sim 60^\circ$ is detected on sub-parsec scales (Junor et al., 1999) (lowermost panel in Figure 36). The jet is observed to be collimated to less than 5° on the scale of hundreds of parsecs (Biretta et al., 1995) (see top right panel in Figure 36). Such observations which suggest that the jet is ejected in a cone of a large angle and is collimated to a cone of a smaller angle at large separations from the active core, have prompted theories which can explain such collimation. *Before the widely different conical angles of the jet near the core and far from it are taken to be indicative of the opening angle, possible effects on the sub-parsec jet morphology due to finite angular resolution should be examined. For example, such an effect is well demonstrated by the top panels in Figure 36. In the top left panel which is at a lower resolution than the top right panel, the entire radio structure of the top right panel is detected as a triangular region shown in orange. Large and asymmetric opening angles for the two jets would be surmised from the top left image. The higher resolution image of the central region shown in the top right panel is required to measure the conical angle of the jet. A similar angular resolution effect could be afflicting the jet opening angle in the bottom panel of Figure 36 which zooms in close to the core. It is important to obtain even higher resolution images before inferring different opening angles at the base of the jet and at large separations. In the model presented in the paper, the conical jet has to be ejected within a small angle which will remain constant as long as the jet remains ballistic. This is borne out by the jet with a constant conical angle from several parsecs to kpc scales as seen in the top right panel.*
- The base of the jet in Virgo A is resolved by interferometric observations at 230 GHz from which it is surmised that the emission which is fitted with a gaussian of FWHM $\sim 40\mu\text{arcsec}$, corresponds to a linear size of $5.5R_s$ (Doeleman et al., 2012) at 16.7 Mpc. This result indicates that the jet in Virgo A is launched from close to the black hole. The black hole mass in M 87 has been estimated to be $6.2 \times 10^9 M_\odot$ so that $R_s = 1.9 \times 10^{15}$ cm. *If $40\mu\text{arcsec}$ indicates the size of the pseudosurface i.e. the separation between the two poles from which jets are launched then the jets will be launched from a region separated from the black hole by $\sim 2.75R_s$. These jets have to be launched with a velocity $\geq 0.6c$ to be able to escape the gravity of the black hole. If we could detect emission lines from the matter at $2.75R_s$ then their redshift would be observed to be large due to the presence of an intrinsic component corresponding to a gravitational redshift of 0.18 and a Doppler component due to the expansion velocity of $0.6c$. Alternately, $40\mu\text{arcsec}$ could correspond to the size of a blob in the jet close to one of the poles in which its implications could be different.*
- The transverse extent of the optical jet is narrower than the radio jet so that it appears to be confined to the centre of the radio jet (Sparks et al., 1994) often referred to as the spine of the jet. The same is true for the X-ray jet and the correlation between the optical and X-ray jets is good (e.g. Marshall et al., 2002).
- Knots in Virgo A have been deduced to be expanding with velocities which are generally less than $0.5c$ although a few instances of superluminal expansion have also been reported (Biretta et al., 1995).
- The magnetic field lines are predominantly oriented along the jet as deduced from radio polarisation measurements. The percentage polarisation is typically 30% in the bright parts of the jet (i.e. spine) and 50% or more at the jet boundary (i.e. sheath) (Owen et al., 1989). The magnetic field in the jet is estimated to be 200-300 μG (Owen et al., 1989).
- The halo-like radio structure around M 87 is diffuse and amorphous and is commensurate to having been generated by a precessing jet (e.g. Rao, 1987).
- The spectrum between 25 MHz and 10 GHz of the central part of Virgo A is a power law with index 0.6 while for rest of the radio source the index is around 1.1 ($S \propto \nu^{-\alpha}$). Some steepening beyond 10 GHz is detectable from the diffuse regions (de Gasperin et al., 2012). They estimate equipartition magnetic fields which are on average 30 μG in the central part and 10 – 13 μG in the extended diffuse parts.
- The radio source has well defined boundaries so emission is detected from a region of the same extent at all radio frequencies.

- VHE γ -ray ($E > 100$ GeV) flares which last for only a day or so are detected from Virgo A and have been found to be accompanied by a rise in the flux density at high radio frequencies of the core or of a jet component like HST-1 (Abramowski et al., 2012).
- Optical filaments extending along the general direction of jets are detected in $H\alpha$ and forbidden lines. These filaments extend over about 3 kpc in the north-west and about 8 kpc in the south-east, are broader than the jets, patchy, show some lateral displacement from the jet and are kinematically perturbed (Boselli et al., 2018). Patchy dust is detected near the core and in patches around the core and in a broader region in the general direction of the jet (Boselli et al., 2018; Bellini et al., 2015). *All these signatures are typical of the NLR gas in Virgo A which is ejected from the black hole along with the relativistic plasma. Dust has formed in the dense clumps within the NLR. This explains why the distribution of dust and $H\alpha$ emitting gas are oriented along the jet.*
- VLBA images of Virgo A taken at regular intervals indicate jet ejections on timescales of weeks (Walker et al., 2018). *This means that sufficient matter is accreted on the polar regions of the pseudosurface and favourable physical conditions are established on timescales of weeks which triggers a thermonuclear outburst. A relativistically expanding positron-electron jet in addition to line forming gas are then ejected.*
- Diffuse soft X-ray emission is detected over a large region extending to several degrees and enclosing several member galaxies of the Virgo cluster (Böhringer et al., 1994). This emission shows peaks associated with several active galaxies with the brightest emission associated with the brightest cluster galaxy M 87 (see Figure 37). The disk galaxies within the X-ray halo show truncated gas disks (Chung et al., 2009) which has been interpreted as being due to the action of ram pressure on the interstellar medium of the galaxies. *The active nucleus in the central galaxy M 87 has led to the formation of a central mini-halo (around 80 kpc) like region which is detected in radio synchrotron and soft X-rays. The large scale X-ray emission (Figure 37) in Virgo cluster over about 12° region (linear extent of 3.5 Mpc) includes contributions from several active galaxies which have lost gas either through mass loss induced by a gravita-*



more complex and in addition to a precessing axis and episodic quasi-simultaneous ejections from the two poles, interaction with the intracluster medium needs to be invoked, which has rerouted the radio plasma.

High resolution VLBA radio images at 43 GHz have detected a faint radio feature close to the core which is attributed to the counter-jet (Walker et al., 2018). If the absence of the counter-jet was due to Doppler beaming then it would not have been detected on parsec scales where the bulk expansion velocities should be highly relativistic. If the detected feature is indeed the counter-jet then we have to search for reasons other than Doppler beaming for the non-detection of the counter-jet on kpc scales in Virgo A.

The entire radio structure in Virgo A is confined to a well-bounded region as is observed in several FR I sources (e.g. NGC 193). The extent of the emitting region in such sources is same at all radio frequencies and also comparable to the extent of the soft X-ray emission (e.g. NGC 193 and see Figure 27). Good correlation is observed between the radio and X-ray beams in Virgo A and supports a connection between the emission processes. In fact, the behaviour of such FR I sources is comparable to that of FR II sources like Cygnus A (see Figure 33) wherein, the soft X-ray and radio emissions share a major axis and the extent of the soft X-ray and radio emissions appear to be similar. All these argue for some connection between the radio synchrotron and thermal X-ray emissions in active galaxies. In NGC 193 and Cygnus A as in several other active galaxies, X-ray cavities are observed to be coincident with the radio lobes (NGC 193, Giacintucci et al., 2011). On a general note, it appears that the extremities of the radio emission in many FR I and FR II radio sources is determined by the thermal gas distribution associated with the galaxy. In fact, the radio morphology of NGC 193 suggests that the precessing jet is forming multiple hotspot-like features which trace the outermost boundary of the radio emission which is well-defined in the east and west. These hotspot-like features are identifiable on the spectral index image as the features where the spectrum is flatter (see Figure 27). In the eastern part, the X-ray and radio are of similar extent while in the west, the radio emission seems to extend further than the X-ray emission. In fact, it is interesting to note on comparing the second panel in (a) with (b) that in the eastern lobe, the hotspot-like features are confined to the outermost boundary while in the west, these cover the entire region where soft X-ray is missing from the lobe. This means that these hotspot-like features have formed at the edge

of the X-ray distribution again arguing for a connection. To recall, in FR II radio sources, the hotspots are formed just outside the soft X-ray distribution (e.g. Cygnus A in Figure 33) and the reason for the same has been explained earlier. The radio emission extended along the equatorial region has an especially steep spectrum and is coincident with faint soft X-ray emission.

The jet consists of both knots and uniform emission - if knots are ejected from the black hole than uniform emission might arise from ablation of the knots - an argument already used to explain the faint sheath observed around several bright jets. Moreover if ejections are frequent, knots might be too numerous to be resolved and could appear as uniform radiation. The radio movie at 43 GHz made from VLBA images showing the formation and expansion of jets from the core of Virgo A show the jet to be limb-brightened, dynamic and frequently replenished by plasma from the poles (Walker et al., 2018).

If for argument sake, we evolved the central active nucleus in FR I radio sources of M 87 and NGC 193 to future epochs when accretion has stopped so that no further radio ejections occurred from the source, then the jets and beams would diffuse and the large scale morphology of the fossil radio emission would resemble a radio halo/mini-halo often detected in centres of clusters. The extent and major axis of the soft X-ray and radio halo in clusters are comparable and relics are observed to form at the boundary of the soft X-ray emission. The similarity to the radio/X-ray sources associated with an active nucleus is uncanny and clearly argues for either a connection or similar physical processes being at work. This is discussed in the section on radio halos and relics.

4.2.3.4 Seyfert 1.5 - NGC 4151 : The main observational results on NGC 4151 are described below with comments included in italics.

- NGC 4151 is an almost face-on barred spiral galaxy of type Sab with HI distributed throughout the galaxy (Davies, 1973). The emission line redshift of NGC 4151 is 0.0033 ($\sim 960 \text{ kms}^{-1}$) which corresponds to a distance of $\sim 14 \text{ Mpc}$. At this distance, 1 arcsecond corresponds to a linear distance of 68 parsecs.
- The nuclear continuum emission is bright with the mean nuclear V band brightness being ~ 11.5 magnitudes (Liutyi, 1977). *This corresponds to a V band absolute magnitude of ~ -19.2 magnitudes for a distance of 14 Mpc.*
- The nuclear continuum emission in the ultraviolet bands consists of two components - a power

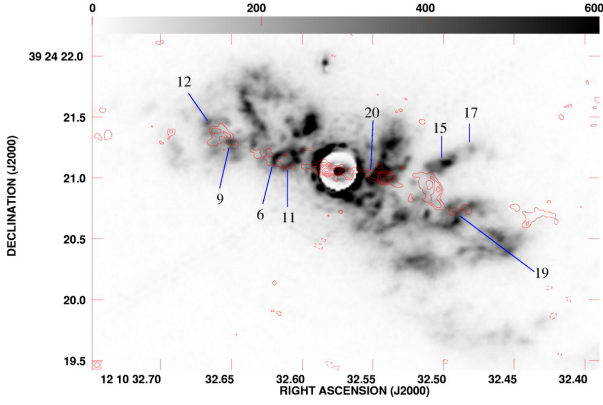


Figure 38: Figure showing the superposition of the [O III] line emitting gas (grey) and the radio continuum emission (contours) from the jets in NGC 4151, copied from Mundell et al. (2003). Notice the optical line emitting gas is distributed over a larger conical region than the radio jet.

law which fits wavelengths $> 2000\text{\AA}$ while wavelengths $< 2000\text{\AA}$ include excess emission over the power law (Penston et al., 1981). *The two dominant components will be the synchrotron component from the relativistic plasma at longer wavelengths and the black body emission from the hot pseudosurface dominating at shorter wavelengths.*

- The nuclear ultraviolet spectrum of NGC 4151 is characterised by wide-winged asymmetric emission lines ($\text{FWZM} \geq 10000 \text{ km s}^{-1}$) of He II, C IV, Mg II, Balmer lines etc which led to its original classification as a Seyfert 1 nucleus. Absorption lines are also detected which are blue-shifted wrt the emission lines. Absorption lines are detected at velocities ranging from 900 to -100 km s^{-1} (Penston et al., 1979, 1981). *The wide-winged emission lines arise in the BLR and the redshift contains a gravitational redshift component as can also be surmised from the detected absorption features which are blue-shifted wrt to the emission line redshift. This behaviour is typical of the broad spectral lines in quasar spectra although the magnitude of redshifts is much larger in quasars. These results on NGC 4151 demonstrate that the BLR in all active nuclei consist of emission and absorption line zones and the lines will be wide and include a detectable gravitational redshift component if the BLR forms sufficiently close to the black hole.*
- Correlated variability is detected in the continuum and the wide spectral lines. It is noted that

when the ultraviolet continuum is stronger, the broad emission lines are wider and stronger (e.g. Penston et al., 1981). For example, the FWZI of the C IV and Si IV lines were observed to vary from $\sim 30000 \text{ km s}^{-1}$ in May 1978 to less than 20000 km s^{-1} in January 1979 which was correlated with the dimming of the ultraviolet continuum (Penston et al., 1981). Depending on the continuum strength and linewidths, the source is in the ‘high’ or ‘low’ state. *The dominant continuum source at ultraviolet bands i.e. black body radiation from the hot pseudosurface is the photoionizing source for the BLR so that any change in the former leads to changes in the strength and width of the emission lines from the BLR. The correlated variability also supports the radiating pseudosurface and the relative location of the BLR and the pseudosurface. One of the original cause of variability could be the occasional thermonuclear outburst on the interface of pseudosurface/inner parts of the BLR.*

- Deep absorption components are detected within the broad C IV and Mg II emission lines (e.g. Ulrich et al., 1984).
- In NGC 4151, the high ionization emission and absorption lines of C IV, Si IV, He II are seen to vary with the ultraviolet continuum whereas the relatively narrow lines of C III], Si III] seem to remain unchanged (Penston et al., 1981). In the Seyfert 1 galaxy NGC 5548, comparable variability was recorded for C IV and C III] lines while the Mg II feature remained unchanged (Clavel et al., 1992). *Such a range of behaviour is expected due to the range of BLR properties such as separation from the black hole, extent, abundance, absorbing zone etc which will exist and be distinct for each active nucleus. Even in the same active nucleus, the observed BLR-related variability can show a range of properties.*
- The broad C IV and Si IV are the widest lines with FWZI reaching 30000 km s^{-1} followed by He I 5876 line observed to be in the range $12000 - 16000 \text{ km s}^{-1}$ and then Balmer lines whose widths are $\sim 8000 \text{ km s}^{-1}$ (Boksenberg et al., 1975). Broad Fe II lines are also detected from the nucleus of NGC 4151 (Boksenberg et al., 1975). NGC 4151 which was originally classified as a Seyfert 1 was later shifted to class 1.5 due to detection of the narrower Balmer features (Osterbrock & Koski, 1976).

- While most of the variability in X-ray and ultraviolet bands in NGC 4151 is well correlated

to within a few days, there exist the occasional ultraviolet flare which is not accompanied by an X-ray flare (Perola et al., 1986). A similar behaviour is also recorded between the ultraviolet (1350 Å) and X-ray (2-10 keV) emissions in NGC 5548 (Clavel et al., 1992). *This could be explained if the ultraviolet flare arises due to variability in the continuum from the BLR. The variability which arises on the hot pseudosurface will be detected in several wavebands including X-ray and ultraviolet bands but this might not be the case for the relatively cooler BLR.*

- NGC 4151 is variable in all wavebands ranging from the infrared to X-rays. Soft X-ray emission extended over a 2 kpc region about the active nucleus has been detected (Wang et al., 2010) which fills in the HI cavity. No X-ray emission that extends around the galaxy in a halo has been detected.
- The narrow line region in NGC 4151 has been inferred to extend by $\geq 6''$ (Ulrich, 1973).
- Radio jets, extending to scales of about $10''$ (680 pc), are observed to emerge from the active nucleus in NGC 4151 (Ulvestad et al., 1981; Johnston et al., 1982). The narrow line region detected in the optical and the radio jet are extended along similar directions (Ulvestad et al., 1981; Johnston et al., 1982; Ulrich, 1973). The optical line emitting gas is spread over a larger conical region of opening angle of 80° (Hutchings et al., 1998) than the radio jet (see Figure 38) and shows expansion with the north-east being redshifted and the southwest part being blueshifted (e.g. Johnston et al., 1982; Ulrich, 1973). *The differing transverse extent of the radio jet and NLR can be explained by a precessing spin axis of the black hole. The radio jet composed of relativistic positron-electron plasma traces the instantaneous position of the axis whereas the longer-living optical line emitting gas traces the entire precession cone indicating that the angle of the precession cone is close to 80° while the ejection in each epoch is over a conical angle determined from the radio jet.*
- Linearly polarised optical continuum emission with a position angle along the radio jet is also detected in NGC 4151 (Schmidt & Miller, 1980).
- The optical lines form a biconical outflow with expansion velocity of $\sim 350 \text{ kms}^{-1}$ and opening angle of 80° (Hutchings et al., 1998). From the line ratios, the authors infer that this narrow

line gas is photoionized by the central continuum source and they also infer a density gradient along the narrow line gas. The lines close to the core appear to be distributed along the radio axis and show higher expansion velocities as compared to the gas located farther from the core which is also patchy but appears to be displaced from the radio axis (see Figure 4 in Hutchings et al., 1998). *The photoionizing source for the NLR will be the ultraviolet photons from the hot polar pseudosurface from which it is ejected.*

- Reverberation studies have deduced that the C IV line arises in a region which is about 5 light days away from the continuum emitting region while the Mg II variability shows a lag of about 12 days wrt to the continuum from which it is determined that it is formed in a region about ~ 12 light days from the continuum emitting region (Gaskell & Sparke, 1986). Similar analysis with Balmer lines indicated that these lines arise in a region located about 10 times further than the region emitting C IV and He II lines (Ulrich et al., 1984). These results have led to the inference that the BLR is stratified into at least three emission line zones with varying ionization and densities (Ulrich et al., 1984). A black hole of mass $0.5 - 1 \times 10^8 M_\odot$ has been estimated in the centre of NGC 4151 from line variability studies (Ulrich et al., 1984). Another set of reverberation mapping of the broad emission lines has determined lags of about 3 days and hence radius of the broad line region to be 3 light days $\sim 0.0025 \text{ pc}$ and the mass of the central black hole to be $1.2 \times 10^7 M_\odot$ (Wandel et al., 1999). *Since the ionization structure of the BLR can be dynamic depending on the variation in the photoionizing source, the emitting zones will show radial shifts i.e. different lags.*
- Extended narrow line gas (ENLR) is detected around NGC 4151 such that the detected ratio $[\text{O III}] 5007/\text{H}\beta$ is lower than in the NLR and higher than in HII regions (Unger et al., 1987). The ENLR has dimensions of several kpc whereas the NLR is extended to a kpc or so. Moreover the linewidths from the ENLR ($\leq 45 \text{ kms}^{-1}$) are smaller than in NLR ($\sim 300 - 500 \text{ kms}^{-1}$) and the velocity variation along the ENLR of about 112 kms^{-1} suggests that the gas although extended along the inner milliarcsec ($\sim 2 \text{ pc}$) radio jet (and not the larger scale radio jet) follows disk-like rotation (Unger et al., 1987). *The ENLR could constitute the interstellar gas that has gotten channelled into the central*

parts of the galaxy and from which the black hole is accreting.

NGC 4151 which was originally classified as a Seyfert 1 was later shifted to class 1.5 due to detection of the narrower Balmer features (Osterbrock & Koski, 1976). From the range of widths of the broad emission lines that were observed and their ionization states, it was suggested by Ulrich et al. (1984) that the broad line region around NGC 4151 was stratified into three regions such that BLR1 where the broadest lines of C IV, Si IV, He II formed, was the closest line forming zone to the photoionizing source, had $n_e \geq 10^{10} \text{ cm}^{-3}$ and which recorded the highest line variabilities; BLR2 was the region where the narrower C IV, Mg II, He I formed and which also had similar densities as BLR1; BLR3 was the region where the narrower lower ionization lines of Mg II, C III], Balmer lines formed and densities were lower than 10^{10} cm^{-3} and variability was minimal. Balmer emission is faint or absent in BLR1 and BLR2 (Ulrich et al., 1984). Such a stratified behaviour of the BLR which lies immediately outside the pseudosurface is readily supported by the model presented in the paper. The hot pseudosurface is the source of the photoionizing photons which ionize and excite the BLR that is formed in the matter that is accreted on the pseudosurface. The BLR zones closest to the pseudosurface will show the highest ionization, will show the broadest lines due to the largest gravitational redshift component, will be the most dense of all the BLR zones and will show the highest correlated variability with the continuum from the pseudosurface. Beyond this there will be a gradation in the ionization, temperature and densities of the regions i.e. BLR2 and BLR3 zones. The stratified nature of the emission line region in the BLR into three zones based on the line widths is indicative of the differing separation of the respective zone from the pseudosurface of the black hole which provides the black body continuum and the photoionizing photons. Beyond the emission line zones in BLR, there can form absorption line zones. The gravitational redshift component in the emission lines will hence be larger than in the absorption lines which explains why the absorption lines are blueshifted wrt to the emission lines. If all the stratified layers of the BLR are of comparable linear thickness then the zones lying closer to the black hole will form broader lines due to enhanced gravitational broadening. The line widths can be used to estimate the fractional width of the line forming region.

A black hole of mass $0.5 - 1 \times 10^8 M_\odot$ has been estimated in the centre of NGC 4151 from line variability studies (Ulrich et al., 1984). If the pseudo-

surface in such a black hole has formed at a separation equal to R_s then it will need to be very hot to explain the observed V band absolute magnitude of -19.2 magnitudes which is comparable to the absolute magnitude of the quasar 3C 273. From Table 3, it can be deduced that the temperature will have to be $\gg 40000 \text{ K}$. On the other hand, the pseudosurface and BLR are expected to be located farther than R_s in Seyferts, as can be inferred from the significantly lower quanta of the intrinsic redshift component in the wide emission lines. The further the pseudosurface from the black hole, larger should be its surface area i.e. emitting surface which will bring down the requirement for an extremely high black body temperature.

We estimate a few typical physical parameters expected for the BLR which has formed in the non-polar regions of the supermassive black hole in NGC 4151. The galaxy (emission line) redshift is 0.0033 so that the intrinsic redshift due to gravitational redshift has to be ≤ 0.0033 . Lets assume the extreme case wherein the dominant contribution to the observed redshift is due to a gravitational redshift i.e. $z_g = 0.003$. Since $z_g = R_s/2R$, this photon will arise from a distance of about $167R_s$ from the black hole which gives a lower limit to the separation of the BLR from the black hole. If $z_g < 0.003$, then the photon will arise from a larger separation from the black hole. For a black hole of mass $10^8 M_\odot$, $R_s = 3 \times 10^{11} \text{ m}$ and hence $167R_s = 5 \times 10^{13} \text{ m} \sim 2 \text{ light days}$ which is the separation of the BLR from the black hole. Thus, the high ionization broad emission lines in NGC 4151 would arise at a distance of 2 light days or more from the black hole. For a gravitational width of 100Å for the C IV 1550Å line (i.e. 20000 kms^{-1}), the ratio of the thickness and radial separation of the line forming region will be $100/1550 = 2/31$ and the thickness of the line forming region at $167R_s$ will be $2/31(167R_s) = 10.8R_s$. These estimates indicate the shortest possible separation of the C IV zone in the BLR from the black hole and its thickness in NGC 4151 when the line is gravitationally broadened to 100Å. The C IV zone will be farther from the black hole if there is a smaller contribution from gravitational redshift while its thickness will be larger to allow for the required change in the gravitational potential in the line forming zone. *To summarise: the main source of ultraviolet photons is the hot pseudosurface which ionize and excite the BLR formed in the non-polar parts. Lines broadened and redshifted due to the influence of the strong gravitational potential of the black hole are formed in the BLR around NGC 4151. If the black hole is of mass $10^8 M_\odot$, then from the maximum possible grav-*

itational redshift, we can surmise that the C IV line forming zone will be located at a separation ≥ 2 light days and will form a line of width $100A$ if its thickness is $\geq 11R_s$.

The physical processes active in the accreted matter in the polar regions are different from those in the BLR as can be surmised from the presence of bipolar radio jets and narrow line regions and we now discuss the polar properties in NGC 4151. To recall, in a rotating black hole, matter will accrete on the polar pseudosurface over an area determined by the angular speed of the black hole and hence the covering factor of the BLR. A fast rotating black hole will collect matter over a smaller polar region than a slower black hole. The accreted matter at the poles will be compressed and heated. If the temperature in the bottom layer exceeds 10^8 K, it will ignite in a thermonuclear blast which will release energy depending on the mass that is ignited. This instantaneous release of energy will energise the accreted matter and in many cases eject it. This would lead to bipolar outflows but since the two poles are separated by the BLR, the ignition and ejection at the two poles should happen independently. This will lead to the detailed structure of the two radio jets and NLR being different. The thermonuclear burst would eject relativistic positron-electron plasma and heavier atoms/ions which would be ejected at high velocities from the black hole. This, then, will constitute the radio jets and the narrow line gas which is found distributed along the jet. Faint radio jets and optical line emitting gas have been detected in NGC 4151 (e.g. Mundell et al., 2003) (see Figure 38) with the optical gas being extended over a larger region compared to the radio jets. The slightly differing mean position angles of the radio jet axis and the axis over which the optical line forming gas is distributed appears to be due to precession of the black hole so that the narrow line gas is spread over the entire precession cone region while the radio jet is confined to the instantaneous position of the spin axis which currently seems to be located at one edge of the line forming gas distribution (see Figure 38). Over time, the spin axis should precess so that the radio jet will be displaced in the clockwise direction. The line region and radio jet are resolved into a knotty structure (see Figure 38) which supports the episodic ejection expected in an accretion dependent thermonuclear expulsion. The low expansion velocity of 350 km s^{-1} estimated for the narrow line gas indicates that the relativistic ejection from the poles of the black hole rapidly slows down. However it can be noticed from Figure 38 that the opening angle of the jet in NGC 4151 is large and hence indicates that the black hole rotation is slower and the cover-

ing factor of the BLR is smaller. The small radial extent of the jet and NLR indicate that the jet is not as energetically ejected as in FR I or FR II sources. Moreover the coexistence of the radio jet and optical line emitting gas makes it possible for the radio jet plasma to radiate in the magnetic field frozen in the line forming gas. As explained earlier, a conical flow is expected when matter is radially launched from a spherical region at the poles and the biconical NLR in NGC 4151 strongly supports this scenario. NGC 4151 is classified as a radio-quiet active nucleus due to the faint nature of the bipolar radio emission compared to its optical continuum emission. However it clearly hosts radio jets supporting ongoing accretion, compression, ignition and ejection from the poles.

To summarise: the observed properties are well explained by the model for active nuclei presented in the paper. The coexistence of the radio jet and optical line forming gas supports their ejection following a thermonuclear blast in the accreted gas at the poles.

4.2.4 A short summary

The main points of the model for active nuclei/galaxies can be summarised as follows:

- All active nuclei host an accreting supermassive rotating black hole. The density of the infalling matter increases as it nears the event horizon and at some separation, the high densities can push matter into the degenerate state. This will lead to layers of degenerate matter being deposited outside the event horizon in a quasi-stable configuration and forming the pseudosurface of the black hole.
- Subsequent to the formation of the pseudosurface, infalling matter accumulates on the pseudosurface with a latitude-dependent accretion rate. Matter accretes directly on the pseudosurface in the polar region and through an accretion disk in the non-polar regions of the rotating black hole. The matter accumulated on the non-polar parts of the pseudosurface forms the broad line region (BLR).
- The separation of the pseudosurface and BLR from the black hole determines the type of active nucleus i.e. observable properties. If the separation is $\sim R_s$, then the observed properties will be a bright compact continuum source, high emission line redshifts and multi-redshifted broad absorption lines (due to the effect of a large and varying gravitational redshift) resulting in objects we identify as quasars; if the separation is several tens of R_s then these objects

show a bright nucleus and broad emission lines in their spectra (shifted and broadened by smaller gravitational redshifts) and we refer to them as BLRG if in an elliptical host; for still larger separations but where the influence of the gravitational potential of the black hole is still active in terms of broadening the lines and enhancing the nuclear continuum, the active nuclei, if in spiral hosts, are referred to as Seyfert 1. When the separation between the black hole and the BLR is several hundred R_s , then the observable effects of gravitational redshift are negligible and the objects host a faint nucleus and narrow emission lines and are classed into a NLRG or Seyfert 2 nucleus. The increasing separation of the pseudosurface and BLR from the black hole leads to decreasing continuum strengths, decreasing variability, lower gravitational redshift contribution to the lines and narrower lines from the BLR, if at all. This, then, forms a continuum of BLR properties so that there exist quasars found in both elliptical and spiral hosts and there will exist nuclei between extremes of BLRG and NLRG in elliptical hosts in addition to between type 1 and 2 Seyferts in spiral hosts.

A fast spinning black hole forms a latitude-thick BLR with a large covering factor which will be detectable from most sightlines except directly polar while a slow spinning black hole forms a latitude-thin BLR with a small covering factor which will be detectable only from sightlines which intercept the equatorial regions, except in the odd case wherein the lines from the non-polar BLR are scattered into our sightline by polar dust.

It should be noted that narrow emission lines are observed in almost all active nuclei unlike broad lines. In most active galaxies these lines are believed to arise in the polar NLR but it is possible that a fraction of the lines do arise in the non-polar distant BLR. Thermonuclear explosions can occur in the inner parts of the BLR if sufficiently high temperatures are reached and this can lead to enrichment of matter but expulsion of matter might be rare due to the massive accretion disk that has formed outside the BLR. However radio synchrotron emission has been detected in the equatorial regions of some active nuclei indicating that some relativistic plasma might be able to escape.

- Matter is directly accreted on the pseudosurface at the poles of a rotating black hole. This matter will be compressed and heated which will even-

tually lead to a thermonuclear outburst. This explosion can energise and expel matter at relativistic speeds from the small region at the poles which lacks an accretion disk. This expelled matter will form the bipolar jets detectable from radio to X-ray wavelengths and the optical line emitting gas (NLR) distributed along the jets, where the narrow emission lines form. The frequency of such ejections would depend on the accretion rates. Thus large radio sources like FR I and FR II types would indicate a long duration of reasonably large accretion rates and frequent energetic expulsion of relativistic matter from the poles of the black hole. The radio-quiet nature of Seyfert nuclei would then indicate the short duration of accretion, lower accretion rates and infrequent and low energy expulsion of relativistic matter from the poles of the black hole. In the active nuclei, where frequent explosions occur but are not sufficiently energetic to expel matter, matter will fall back on the poles and can get enriched through nucleosynthesis in the thermonuclear outbursts - such active galaxies will lack large scale radio jets and optical line forming gas. The pre-dominant detection of iron lines in such radio-quiet active nuclei seems to suggest an origin at the poles and supports the importance of nucleosynthesis in the matter which has failed to be ejected.

4.3 Radio relics and halos in galaxy clusters

Steep spectrum radio emission and soft X-ray thermal emission are detected from a quasi-spherical region in the central parts of several galaxy clusters. These are referred to as the radio halo and X-ray halo respectively and appear to occupy comparable volumes with the X-ray emitting gas occupying a larger region, if at all. The radio halo is sometimes accompanied by steep spectrum radio arcs located on the outskirts of the X-ray halo and which are referred to as radio relics in literature. Deep, meticulous observations of several clusters have helped narrow down the range of observed properties of radio halos and relics but the origin of these features remains a matter of debate. Radio emission from the halos and relics require the presence of relativistic electrons and a magnetic field. A widely accepted model for their origin, in literature, concerns merging of two clusters that generates turbulence and shocks which accelerate the electrons in the halo and relic respectively to relativistic velocities enabling them to emit synchrotron radiation in the magnetic field frozen in the

thermal hot X-ray halo.

In the rest of the section, we summarise some observed properties of these enigmatic objects and then converge on a comprehensive model which observations and physics appear to dictate. This model supports the origin of magnetic field in the X-ray halo as has been suggested in literature, but argues against requiring acceleration of electrons due to turbulence or shocks.

4.3.1 Summary of observed features

- Most clusters of galaxies host an X-ray halo. Some of these clusters also host radio halos and relics and such clusters do not host a bright radio galaxy in their centre.
- A radio halo is more commonly detected in clusters compared to radio relics. The radio relics when detected are observed to be circumferential to the halo being either symmetrically located on diametrically opposite sides on the longer axis of the radio/X-ray halo or only a single relic on the outskirts of the X-ray halo is detected. Typical diameters of the X-ray and radio halos range from few hundred kpc to couple of Mpc. The length of radio relics is measured to be several hundred kpc to Mpc or so.
- Clusters hosting radio halo and relics are also non-cooling flow clusters which, observationally, are clusters which host a X-ray halo but lack a strong centrally located peak in X-ray emission. Cooling flow clusters generally host a bright radio galaxy in their centre and record peaked X-ray emission of lower hardness ratio in the central 100 kpc or so.
- The emission from the radio halo is unpolarised while that from the radio relics is highly polarised. This means the radio halo is threaded by a randomly oriented magnetic field whereas relics host a predominantly ordered magnetic field. The magnetic field in the relics is oriented along the length of the relic.
- Equipartition magnetic field in cluster halos and relics have been estimated to range from 0.1 μG to 10 μG (e.g. Feretti & Giovannini, 1996; van Weeren et al., 2019). More specifically, the equipartition magnetic fields estimated for halos appear to range from 0.1 to 1 μG whereas in relics it is slightly higher ranging from 0.5 to 2 μG (e.g. Govoni & Feretti, 2004). Moreover the magnetic field is not constant throughout the cluster but declines with the cluster radius (e.g. Govoni & Feretti, 2004).
- The spectra of many relics is well-fit by a single power law between ~ 100 MHz to about 5 GHz with a typical spectral index between 1 and 2 ($S \propto \nu^{-\alpha}$). The radio spectrum of the radio halos is also similarly steep. At frequencies below 100 MHz or so, the radio spectrum has been occasionally observed to flatten while above ~ 5 GHz, the spectrum is observed to steepen. *This behaviour is reminiscent of the radio spectra of hotspots in FR II sources.*
- In the Toothbrush relic, the spectral index is constant along the length of the relic but shows a gradation along the minor axis of the relic (Figure 39b) (van Weeren et al., 2012b). The spectrum is flattest ($\alpha \sim 0.6$) at the outer edge of the relic and is observed to steepen towards the cluster centre ($\alpha \sim 2$) (van Weeren et al., 2012b). Such behaviour is typical of radio relics which are resolved along their minor axis.
- In the Toothbrush relic, 60% polarisation is recorded at 5 GHz which declines at lower frequencies indicating Faraday depolarisation and an equipartition magnetic field of about $7 - 9 \mu\text{G}$ has been estimated (van Weeren et al., 2012b).
- The Toothbrush and Sausage relics show a spectral break near 2.5 GHz such that the spectrum below 2.5 GHz has $\alpha \sim -0.9$ while between 2.5 GHz to 30 GHz, the spectrum is steeper with $\alpha \sim -1.7$ (Stroe et al., 2016).
- The emission mechanism responsible for the X-rays from the cluster halo has been deduced to be mainly thermal brehmstrahlung from hot gas (Felten et al., 1966) which is further supported from the observation of a blend of highly ionized iron lines near 7 keV which are detected from the intracluster gas. This gas also has solar-like abundance of iron which is inferred to suggest a stellar origin.
- Giovannini et al. (2009) find that $\sim 30\%$ of the clusters in their sample host both a halo and a relic radio source. The radio size and power are correlated for both small and giant radio halos while the cluster X-ray luminosity (indicative of cluster mass) is correlated with the radio halo power (Giovannini et al., 2009). *The correlation between the X-ray luminosity and radio halo power is reminiscent of the observed correlation between the luminosity of the optical line emitting gas that forms the NLR and radio power of*

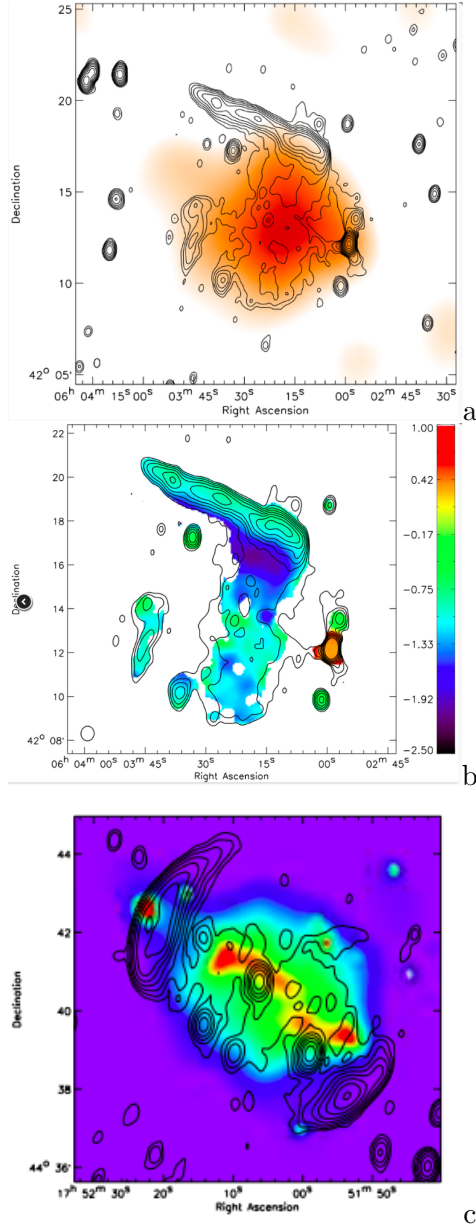


Figure 39: Figure panels (a) and (b) reproduced from van Weeren et al. (2012b). The figures show the X-ray and radio emission in a cluster at redshift 0.225 which hosts the large relic referred to as the Toothbrush relic. (a) The radio emission in the band 1.2 – 1.8 GHz from WSRT is in contours while the X-ray emission from ROSAT is in orange. The ~ 1.5 Mpc long northern Toothbrush relic skirts the X-ray halo in the north. The radio halo emission is of similar extent as the X-ray halo. (b) The spectral index distribution between 147 MHz and 2273 MHz made from maps with a resolution of $35''$ is shown in blue. Notice the extremely steep spectrum on the lower part of the Toothbrush relic and in the region where it meets the halo. (c) Figure showing the X-ray halo (colour) and radio relics, halo (contours) in the cluster MACS J1752.0+4440 at $z = 0.366$ copied from van Weeren et al. (2012a). Double relics are detected at the edge of the X-ray halo. The radio halo and X-ray halo are coincident and share a major axis at the end of which relics are detected and this kind of structure is commonly observed in clusters.

jets in radio galaxies. The radio jet and NLR have a common energy source in the thermonuclear energy.

- Radio power at 1.4 GHz ranges from 10^{23} to 10^{26} W Hz $^{-1}$ whereas X-ray luminosity typically is in the range of few times 10^{43} erg s $^{-1}$ to few times 10^{45} erg s $^{-1}$ (e.g. van Weeren et al., 2019). *The X-ray energy released from the halo in a year will be $\sim 3 \times 10^{52}$ erg. while over a billion years, about 3×10^{61} ergs will be released in the soft X-ray component.*
- Mini-radio halos which are smaller in size than radio halos have been identified in clusters (e.g. Feretti & Giovannini, 1996) with the current number being about 10 mini-halos of size ranging from 50 to 300 kpc (e.g. Giacintucci et al., 2014). Unlike halos, mini-halos are detected in cool core clusters which host a central radio galaxy like the Perseus cluster. Mini-halos also show a quasi-spherical symmetry like halos but show more small scale asymmetries than halos. *An evolutionary sequence seems to emerge on collating the properties of halos, mini-halos, central radio galaxy in clusters. Central radio galaxy to a radio mini-halo to a radio halo. The first two commonly coexist in clusters while there seem to be clusters in which the last two are seen to co-exist. However clusters in which a halo and central radio galaxy coexist are rare. The connection is chronological so that when a radio halo is formed, the central radio galaxy has exhausted its fuel and entered a quiescent phase. This can be inferred to argue for an evolutionary connection between the three features.*
- It is noted that in several radio galaxies, groups and clusters, cavities in the diffuse X-ray emission coincide with extended radio emission like lobes. The first such radio lobe - X-ray cavity correlation was noted in the Perseus cluster by Boehringer et al. (1993) (see Figure 40c). Perseus cluster has a central radio galaxy (NGC 1275 i.e. 3C 84), a radio mini-halo of ~ 300 kpc extent (Pedlar et al., 1990) in addition to a X-ray halo with cavities (Boehringer et al., 1993). Such correlations between X-ray cavities and radio emission have been widely observed. *Such correlations tend to argue for some connection between the radio and X-ray processes. Since the radio plasma radiates in the magnetic field frozen in the X-ray emitting intracuster medium, the presence of radio lobes at the X-ray cavities indicate the existence of magnetised thermal gas*

although X-ray emission is significantly fainter. The non-detection could be due to scattering of soft X-rays to different energies.

4.3.2 A comprehensive explanation

The widely accepted model in literature used to explain the presence of relativistic electrons in the radio halo and relics invokes a cluster-cluster merger which leads to turbulence in the central parts and sets up outwardly expanding shocks along the merger axis. Turbulence and shocks are believed to be the processes contributing to particle acceleration in the radio halo and relics respectively. In other words, the existence of radio halos and/or relics in a cluster is considered to be an indicator of two clusters undergoing a merger. The observational results on such clusters consist of an ellipsoidal distribution of the X-ray and radio halos, presence of relics at the edges of the major axis of the halos and the detection of some concentration of galaxies along the major axis of the halo. These observations have been interpreted to mean that two clusters of galaxies are approaching along the major axis of the halos and merging. The merger sets up turbulence in the central region of the cluster explaining the radio halo while shocks propagate outwards on either side which are believed to result in the relic emission. Reacceleration is believed to be required since the assumed large energy losses that the relativistic electrons suffer means their lifetimes are fairly small.

We searched for an origin which is commensurate with one of the main results of this paper and Kantharia (2017) that the dominant mechanism accelerating electrons to relativistic velocities is an explosive thermonuclear outburst on a compact object (supermassive black hole in this case) before the accelerated electrons are launched into space. Any further acceleration as in Compton process that occurs post-ejection leads to only a trivial increase in their velocities, if at all. Since the radio halo is quasi-symmetric over the centre of the cluster which has to host an active core although not accreting any more, it appears possible to start with the assumption that the relativistic electrons which populate the radio halo and relics were originally energised in this active nucleus when it was in its accreting radio galaxy phase. It is possible that this pool of electrons is supplemented by electrons accelerated in other nearby radio galaxies within the cluster but this cannot be the dominant contribution due to the central location of the halo. This means that we look for an explanation for formation of halos and relics with the implicit understanding that the resident relativistic electron population has been energised in a thermonuclear blast

and ejected along bipolar jets from the pseudosurface of a rotating accreting supermassive black hole located in the galaxy at the centre of the halo. Thermonuclear energy released in simultaneous ignition of a large mass of fuel is a source of enormous energy in a hydrogen-dominated universe - recall that simultaneous ignition of half a solar mass of fuel can release energy of 10^{51} ergs within 100s of seconds. Since the clusters hosting a radio halo and relic lack a powerful radio galaxy at the centre, it can mean that the active nucleus in the parent galaxy has long stopped accreting and ejecting relativistic material. Whatever it ejected during its active phase has expanded along jets and diffused out to encompass a large volume around the galaxy. Soon after the bipolar ejections from the central source stopped, the jets would have lost their identity as the last bursts of plasma lost its ballistic nature and expanded into lobes. This is not far-fetched as can be seen from the morphology of the extended radio emission around Virgo A at the centre of the Virgo cluster and the halo-like radio emission in NGC 193 (see Figures 36,27). If the jets were extinguished in both these galaxies, then the extended radio emission would resemble a elliptical radio halo. The fossil plasma will continue to diffuse around the central black hole till the component electrons exhausted their energy and faded into oblivion. If there was no ambient magnetic field i.e. no extended thermal gas in which the field was frozen then the electrons will suffer only kinetic losses and if a magnetic field was available in the extended thermal gas, then the positron-electron plasma would radiate synchrotron emission and explain the existence of the radio halo. We examine the validity of this hypothesis on the basis of observational results, electron lifetimes etc. Since direct signatures of inverse Compton scattering which can contribute to rapid draining of electron energies are yet to be observed, it is not included in estimating the electron lifetimes.

First of all, it is significant that the radio spectral index of the halo and relic emission are similar and steep at $\alpha \geq 1$. Since the estimated magnetic fields in the two regions differ by only a factor of few, it appears safe to assume that similar energy electrons are radiating at a given frequency in both objects. In this case, the similar spectral indices argue for a common parent population of relativistic electrons and since we suggest that the halo electrons arise from the central black hole, the relic electrons also have the same origin. The second line of support for the origin of the relativistic plasma in the central supermassive black hole during its active phase comes from the current large scale morphology of some FR I sources like Virgo A (top left panel in Figure 36) and NGC 193

(Figure 27) as mentioned above. If we were to null out the central radio galaxy, jets and structure traceable to recent activity, then we would be left with diffuse elliptical structure whose major axis of about 80 kpc or so is similar to that of the soft X-ray emission and a radio mini-halo. Literature often refers to the extended radio emission around Virgo A as a mini-halo and there appears little doubt that this extended emission is fed by the central black hole and the observed sub-structure would also include structure in the magnetic field. In other words, the electron population of the mini-halo around Virgo A is certainly energised in the active nucleus. In fact, the sharp boundary of radio emission observed at all radio frequencies in several such radio galaxies is likely indicative of the drop in magnetic field intensity i.e. lack of X-ray emitting gas beyond the observed radio emission. In fact a physical process similar to one responsible for hotspots is likely to be operational here but at a lower level so that radiation pressure also contributes to confining the thermal and radio plasma within the sharp boundary. The X-ray gas is likely to slowly expand and encompass an ever-increasing volume in which the positron-electron plasma will radiate in a declining magnetic field so that the radio mini-halo will keep expanding and the radio and X-ray sizes will remain comparable. The timescales over which the plasma (both positron-electron and thermal X-ray emitting proton-electron plasma) diffuse to occupy a spherical region of radius 1 Mpc which is typical of a radio halo will depend on the diffusion velocities, region over which the jet retained some of its forward propelling velocity etc. However the paucity of clusters which host both a radio halo and a central radio galaxy indicates that by the time a large Mpc-scale radio halo is detected the supermassive black hole has stopped accreting gas and entered a quiescent state. It is also possible that the positron-electron plasma has diffused beyond the X-ray halo but is not emitting synchrotron radiation due to the absence of an appropriate magnetic field. The positron-electron plasma in this region will suffer lower energy losses and hence enjoy longer lifetimes. There also exist other radio galaxies which show radio structures which are several hundred kpc across and are unambiguously created by the central active nucleus such as Hydra A. This provides further support to the positron-electron plasma succeeding in etching out such large structures before fading.

The origin of the hot thermal X-ray emitting gas in ejections from the central source is supported by the estimated equipartition magnetic fields. In active radio galaxies, the magnetic fields range from several tens of μG in the jets and lobes to few hundred μG

in the hotspots while in radio halos and relics, the magnetic fields are estimated to be of the order of a μG . This kind of behaviour of the magnetic field is expected if the field is frozen in the plasma ejected by the central source. As the plasma keeps diffusing over larger regions, the constant magnetic flux ($BA = \text{constant}$; where B is magnetic field and A is the area through which the magnetic field is threaded) condition ensures that the magnetic field frozen in that plasma keeps declining as the area it covers keeps increasing. New ejections will modify the magnetic field in the overlapping regions. We do not know the field strength close to the black hole from where matter is launched into space at relativistic velocities although we do know that in the lobes of active galaxies, typical magnetic fields of few tens of μG are estimated. These fields are frozen in the ionized thermal gas component i.e. either optical line forming gas or the X-ray emitting gas. If we assume that the field threading a spherical surface of radius 100 kpc around the active galaxy is $20 \mu\text{G}$ then the magnetic flux will be $BA = 4\pi \times 20 \times (100^2) = 8\pi \times 10^5 \mu\text{G-kpc}^2$. For a spherical radio halo of radius 1 Mpc, such a flux would result in a magnetic field of $B = 8\pi \times 10^5 / (4\pi \times (1000^2)) = 0.2 \mu\text{G}$. In the extended radio halos in clusters, typical magnetic fields have been estimated to range from 0.1 to few μG with earlier studies systematically having determined lower fields (e.g. Feretti & Giovannini, 1996) as compared to more recent studies. This simple calculation demonstrates that the magnetic field pervading the halo is the same as the field in which jets and lobes associated with the central radio galaxy radiate and the simplest explanation is as above wherein the field is frozen in the matter ejected from the active nucleus of the galaxy at the centre of the cluster and keeps declining as the matter occupies an ever-increasing region.

Radio galaxies span a large range in size from parsecs in FR 0 sources to few kpc in GPS, CSS sources to several tens to hundred kpc in FR I sources to several hundred kpc to Mpc in FR II sources. This tells us that the radio plasma energised and ejected from some active cores is capable of traversing distances upto Mpc or so before fading i.e. electrons energised in the central engine and emitting predominantly in the radio bands can survive upto a Mpc or so from the central core when traversing along the jet wherein the typical magnetic field can be upto a few tens of μG . It also tells us that the reason for the existence of small to large radio sources is the plasma energetics i.e. the quantity of matter that is simultaneously ignited in the thermonuclear burst is varied in different active nuclei leading to differences in the released energy and quantity of matter ener-

gised, ejected and detected. If the mean magnetic field along the jets is assumed to average to about $10 \mu\text{G}$ then the lifetime of the 1.4 GHz emitting electron will be about 28 million years and it can traverse a distance of $\sim 5.3 \times 10^{22} \text{ m} = 1.7 \text{ Mpc}$ at a bulk velocity of $0.2c$ before fading. If the mean magnetic field in which the electrons radiate synchrotron emission is $2 \mu\text{G}$, then the lifetime of electrons dominantly emitting at 1.4 GHz will be 3.2×10^8 years and these can travel a distance of $6 \times 10^{23} \text{ m}$ at an average bulk velocity of $0.2c (= 60000 \text{ kms}^{-1})$ i.e. $\sim 20 \text{ Mpc}$! At larger bulk velocities as in FR II sources, the electrons can traverse even longer distances. For comparison, the electrons predominantly emitting at 1.4 GHz in a field of $0.1 \mu\text{G}$ can survive for about 28×10^9 years. The high energy electrons which lose energy will move to lower energies and can contribute to the low radio frequency emissions. All this discussion is aimed at showing that the synchrotron lifetimes of electrons are sufficiently long to explain the population in radio halos and relics. In a radio galaxy, the electrons along the jets can travel ballistically to long separations which can be covered in shorter times. However the electrons that make up the lobes can take longer to cover the same distances since they are no longer moving ballistically at relativistic velocities but diffusing at much lower velocities. If diffusion of the positron-electron plasma from the jets is occurring at a velocity of about 1000 kms^{-1} , then in a billion years, the plasma can diffuse over a distance of 1 Mpc . The electrons which started with high energies will move to progressively lower energies so that the emission at high radio frequencies will fade. Since other processes which shorten the electron lifetime like inverse Compton, although postulated, have not been unequivocally inferred from observations, these are not included. In future if other processes are found, the estimates can be revised. It should be pointed out that instead of losses, the annihilation photons near 511 keV are likely to be continuously generated in the positron-electron plasma and if these are Compton scattered to X-ray wavelengths by the relativistic electrons throughout the halo then it can result in small energy boosts to the electrons. An important reason for both relics and halos being detectable inspite of low magnetic fields is likely to be their enhanced synchrotron emissivity due to the long pathlengths in the cluster over which the relativistic plasma is distributed. Since relics are formed at the outer edge of the radio halo in clusters, the population of electrons therein can also be explained with an origin in the central black hole and there should be no lifetime problem. The steep spectra that are observed for both these and the absence of

high energy electrons as witnessed from the absence of synchrotron emission at even high radio frequencies argues for an aged electron population. The rest of the observable properties of relics are distinct from the radio halo and hence require a separate discussion. *Here we limit ourselves to making the statement that the electron population that was generated in the active nucleus of the central radio galaxy can indeed survive in the low magnetic fields of the radio halo and explain synchrotron emission from the radio halo and relics and there is no need to invoke an extensive reacceleration mechanism.*

We now discuss the origin of radio relics in clusters. The different observed properties of radio halos and relics in clusters indicate the distinct physical processes that the plasma and magnetic field are subject to in the two features. Since the relics, when detected in a pair, are located on diametrically opposite sides of the centre of the cluster, subtend a small angle there and are along the major axis of the halo, we suggest that the axis connecting the relics tell us about the path followed by the jets when the central nucleus was actively expelling matter. The conical region defined by connecting the relic edges to the centre of the cluster defines the region over which the jet launched from the black hole would have traversed. While the low magnetic field in the radio halo region would have allowed electrons to survive longer, another reason also exists for longer lives for at least a fraction of the electron population in the jets. Along the jet, there would always be a fraction of electrons which do not suffer synchrotron losses due to their dominant relativistic random motion being along the magnetic field. The bulk motion of the positron-electron plasma is ballistic and radially outwards from the launch site. However over and above this, all particles have a random velocity component which for the jet plasma is relativistic and all electrons which have a velocity component which is not along the magnetic field will execute circular motion about the field lines which is responsible for the synchrotron emission whereas their bulk forward velocity will lead to the motion about the magnetic field lines being helical. Once the random velocity component becomes aligned to the radial magnetic field then no Lorentz force will act on the particle and the particle will stop radiating synchrotron emission till it regains a velocity component which is not along the magnetic field. Such electrons along the field will only suffer kinetic energy losses as they expand away from the active nucleus and it means that the lifetimes of such electrons can be enhanced so that they can traverse longer distances from the parent black hole. In reality the random velocity component of

the relativistic electrons will define a range of pitch angles with the magnetic field and hence experience different synchrotron losses with maximum loss being experienced by the electron moving perpendicular to the field to minimum losses by the electron moving along the field. Quantifying this further, an electron with a pitch angle of 10° will suffer 3% of the losses suffered by an electron moving perpendicular to the magnetic field.

The detection of strong polarised emission from relics (unlike halos) from which magnetic field lines stretched along the relic are surmised, gives strong evidence to the enhancement of ordered magnetic fields at the periphery of the halo emission in clusters. The relic and field lines in the relics are extended circumferential to the X-ray halo i.e. perpendicular to the direction in which the jet would have traversed outwards from the central active nucleus and their morphology is strongly indicative of having been subjected to compression. The magnetic field orientation in the relics facilitates synchrotron emission from the electrons which had a random velocity component which was predominantly along the field lines in the jet i.e. lower pitch angles and hence suffered lower synchrotron losses after being ejected from the central black hole. In fact, there is similarity in the observational properties of the radio relics, which appear to signify the edge of the fossil jets launched from the central FR I galaxy and radio hotspots observed at the end of jets in FR II sources except that the linear scales and hence radio intensities involved are very different. We, hence, explore if the formation scenarios could be due to a similar physical process. To recall, we pointed out that the formation of hotspots can be attributed to radiation pressure exerted on the plasmas by the positron-electron annihilation photons near 511 keV, formed beyond the extended X-ray emission. If the axis connecting the relics does indicate the orientation of the historical jet including the precession cone then after the positron-electron plasma of the halo leaves the X-ray emitting halo then the mean free path of the annihilation photons will increase which will lengthen their lifetimes. These photons can exert radiation pressure back on the plasmas. This can result in further expansion of the plasma being stopped and the plasma at the edge being compressed. The magnetic field frozen in the thermal plasma will be enhanced and ordered due to the radial compression. Thus it appears that the formation of relics can also be explained by the action of radiation pressure on the plasma. The radio spectrum of some relics is observed to show flattening at frequencies around 100 MHz which would indicate the peak of the normal distribution of the parent elec-

tron population which has aged since it was ejected from the black hole. For a magnetic field of $5 \mu\text{G}$ in the relics, this indicates the peak of the aged electron energy distribution is about 1 GeV.

This explanation is comprehensive in that it explains the formation of radio halos, radio relics and accounts for the location of relics at the periphery of the X-ray halo of the cluster without invoking any exotic processes. The explanation starts with the same population of positrons-electrons injected along the jets in an active nucleus and follows their evolution. In principle, such enhanced relic-like emission can surround the entire radio halo since the positron-electron plasma will continuously diffuse outwards and if it expands beyond the X-ray halo, the positron-electron annihilation photons can exert radiation pressure on the halo plasma. It is easier to envisage this if the positron-electron plasma has a net outward motion which is larger than that of the thermal plasma and hence it is easier to expect this along jets.

We list properties of hotspots and relics in Table 6 since both occur in the transition zone from a dense to tenuous medium. Properties of the radio halo are also included for completion. There are several similarities between the hotspot and relic properties such as their location at the extremum of radio emission and X-ray halo, high polarisation fractions, magnetic field orientation, steep spectrum and their frequent occurrence in symmetric pairs about the central source. The radio spectrum in both hotspots and relics is observed to be flattest at the lowest observed radio frequencies (10-100 MHz), steepens at higher radio frequencies (upto 5 GHz) and steepens further beyond radio frequencies of 5 GHz or so. There is also similarity in the magnetic field behaviour. The magnetic field which had been predominantly along the jet changes orientation and becomes perpendicular to the jets at the hotspots in addition to being enhanced. The magnetic field in the radio halo which is predominantly randomly oriented becomes highly ordered and along the relics in addition to being enhanced. *To summarise: the physical process responsible for the formation of hotspots at the end of radio jets in FR II sources and radio relics at the periphery of the X-ray halo in clusters which would have hosted a powerful FR I radio source in the past are the same. Positron-electron plasma fills up the radio halo and at least in clusters which host relics, it has continued to move along the jets long after the matter ejection episodes from the central active nucleus have been quenched. This plasma will continue to generate the annihilation photons at some rate which will be scattered/absorbed by the thermal electrons. How-*

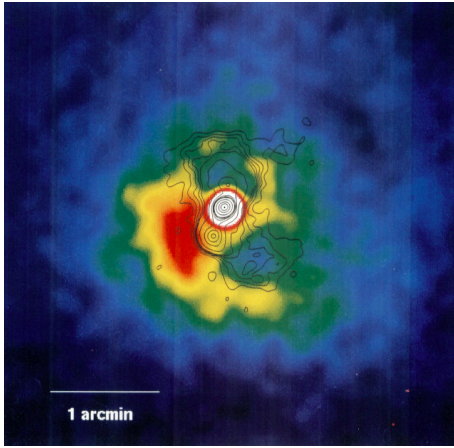


Figure 40: NGC 1275/3C 84 from Boehringer et al. (1993). Notice how the radio (in contours) lobes are located in X-ray (in colour scale) cavities.

ever the photons generated beyond the X-ray emitting thermal gas will survive longer and can exert radiation pressure back on the thermal and non-thermal plasma. This will result in compression of both the plasma - i.e. enhancement of magnetic field in thermal plasma and enhancement of relativistic electron density in the non-thermal plasma. Both these factors can enhance the radio brightness and we identify these regions as relics in clusters.

An important detection criterion for relic emission appears to be its location i.e. the angle it makes with the sightline. All relics which have been detected are the ones whose long axis is in the sky plane and hence perpendicular to the sightline i.e. magnetic field is predominantly perpendicular to the sightline which facilitates the synchrotron cones being directed towards us. It might be that radio relics in the outskirts of the X-ray halo, exist in all clusters which host a radio halo, but due to the highly ordered magnetic field in the relic, the detection of relic emission is sightline-dependent. On the other hand, the magnetic field in the radio halo is randomly oriented indicating that it should be detectable along all sightlines. Radio halos are detected in only about 10% of clusters while a soft X-ray halo is detected in almost all clusters. It is interesting to note that radio-loud active nuclei are surmised to constitute about 10% of the entire population of active galaxies. It could be inferred from this that only about 10% of the population of active galaxies are successful in launching detectable long-lived fast radio jets. The similar fraction of radio-loud active nuclei and radio halos lends support to the direct connection between them. Detection of synchrotron radio halos should be more common than detection of radio relics which is in line with the detection of a relic source in about 30% of the clusters which host a radio halo (Giovannini

et al., 2009).

The ‘Toothbrush’ relic (van Weeren et al., 2012b) is located to the north of a ~ 2 Mpc large radio halo which is coincident with the X-ray emission from the cluster 1RXS J0603.3+4214 (see Figure 39a). The spectral index is flattest (~ 0.6) on the outer edge with a gradient along the minor axis so that the steepest spectrum is where the inner parts of the relic which might be due to a backflow meets the radio halo (≥ 2). For the same parent electron population, the steepening could indicate a varying magnetic field along the minor axis of the relic such that it is maximum at the outer edge and decreases towards the halo. This is what we could expect from the field that is enhanced due to compression of gas at the periphery. The magnetic field gradient means relatively higher energy electrons will emit on the inner edge as compared to the outer edge. For a normal distribution of energies, this could indicate that electrons near the peak energies emit at the outer edge and hence the spectrum is relatively flatter. The Faraday depolarisation in the relic supports the mixing of the X-ray emitting gas which provides the magnetic field for the positron-electron plasma.

Another interesting relic-halo cluster is MACS J1752.0+4440 which hosts a double relic of spectral index ~ -1.1 and lengths of 0.9 and 1.3 Mpc in addition to a radio halo with an extent of 1.6 Mpc (van Weeren et al., 2012a). The relics are located outside and along the major axis of the X-ray halo emission (see Figure 39c). The radio emission is highly polarised and the morphology of the relics and magnetic field argue for a compression event.

While the dominant contribution of relativistic electrons to the radio halo in clusters should be from the central active source which is often a massive cD galaxy believed to have grown by mergers, other radio galaxies in the vicinity are also likely to contribute relativistic plasma and/or thermal plasma to the halos as is the case for the cluster-scale X-ray halo in Virgo cluster (see Figure 37).

If the origin of the relativistic plasma populating the radio jets, lobes, mini-halos, halos and relics and the thermal plasma which initially emits optical emission lines and graduates to emitting thermal X-rays, lie in the ejected accreted gas around a black hole following a thermonuclear explosion then a correlation between the radio power of mini-halos, halos and X-ray luminosity should be observed. The radio power of active galaxies has been found to be correlated with the optical line power and the radio power of halos is found to be correlated with the X-ray luminosity which supports the above connection. The cases wherein the X-ray emission is from several dif-

Table 6: Comparison of observed properties of hotspots in FR II galaxies with relics and halos in clusters of galaxies. The observed properties are listed on the top and some inferences that are drawn in the paper are listed at the bottom.

| Property | Hotspot | Relic | Halo |
|--|---|--|--|
| Separation from centre in kpc | ≥ 100 | ~ 1000 | centered |
| Location | Edge of radio jets/X-ray | Edge of radio/X-ray halo | centred |
| Radio polarisation | $\sim 60\%$ | $\sim 70 - 80 \%$ | unpolarised |
| Magnetic field direction | \perp to jet | \perp to cluster radius | random |
| Magnetic field strength | $\geq 100\mu\text{G}$ | few μG | $\leq \mu\text{G}$ |
| Spectral index α ($S \propto \nu^\alpha$) | ~ -1 at $\nu \geq 10$ GHz | ≤ -1 | ≤ -1 |
| Spectral turnover ν | ~ 100 MHz | ~ 100 MHz | ? |
| Symmetry | diametric double | single or diametric double | roughly spherical |
| Multi-band emission | yes | only radio | only radio |
| Some inferences | | | |
| Magnetic field B | $B_{\text{ordered}} \uparrow$ | $B_{\text{random}} \rightarrow B_{\text{ordered}}$ | $B_{\text{ordered}} \rightarrow B_{\text{random}}$ |
| Plasma expansion velocity | $v_{\text{jet}} \rightarrow -v_{\text{random}}$ | $v_{\text{jet}} \rightarrow -v_{\text{random}}$ | $v_{\text{diffusion}}$ |
| External pressure | yes | yes | no |

‘ \uparrow ’ means an increase in amplitude of the quantity.

‘ \rightarrow ’ means that the left hand side quantity is converted to the right hand side quantity.

ferent galaxies while the mini-halo is from the central galaxy, no correlation between the radio and X-ray luminosities can be expected.

To summarise the discussion in this section, the relativistic electron population in radio halos and relics in clusters has its origin in the energetic ejections from the supermassive black hole in the central active galaxy which has since been quenched. The halo is formed by diffusion of the plasma over a large region, similar to supernova remnants which distribute relativistic plasma throughout spiral galaxies. Support for this comes from several active radio galaxies like Virgo A, Perseus A which already show the existence of a radio mini-halo. It appears that ejections from the active nucleus in the central galaxy of the cluster leads to the formation of radio mini-halo and radio halo as the relativistic positron-electron plasma diffuse outwards and surround the entire region around the central galaxy. The optical line emitting gas ejected alongwith the relativistic plasma leads to the formation of the tenuous hot X-ray emitting thermal gas. The relics are formed at the edge of the X-ray halo and require a compression from the outside to explain their shape, magnetic field orientation, high polarisation and spectral index gradient. It is suggested that this compression is provided by radiation pressure.

5 Formation of soft X-ray halos

Gas at a million degrees which predominantly emits thermal brehmstrahlung and highly ionized spectral lines is detected from several objects ranging from stars to clusters of galaxies. For example, the sun is

a strong soft X-ray emitter with enhanced emission often associated with solar flares and other activity, X-ray emission is detected from the hot ionized component of the interstellar medium while clusters of galaxies are regularly identified from the presence of a large X-ray halo which encompasses several galaxy members of the cluster. The X-ray emitting hot ($10^6 - 10^8$ K) magnetised intracluster medium typically of mass $\sim 10^{13} - 10^{14} M_\odot$ constitutes a significant fraction of the cluster mass of $\sim 10^{15} M_\odot$. The typical electron densities of the thermal intracluster medium are estimated to be $\sim 10^{-3} - 10^{-4} \text{ cm}^{-3}$. X-ray emission is also detected from a halo of hot gas of temperatures of 10 million degrees K surrounding luminous early type galaxies ($M_B < -19$ magnitudes) and can extend upto radial distances of 100 kpc from the centre of the galaxy with gas mass in the X-ray halo being estimated to range from a few times $10^9 M_\odot$ to a few times $10^{10} M_\odot$ i.e. upto $\sim 7\%$ of the stellar mass in the galaxy (Forman et al., 1985) and active galaxies (see Figure 33). Early studies which detected hot halo gas around normal ellipticals in the Virgo cluster with X-ray luminosities of $0.5 - 7 \times 10^{40} \text{ ergs s}^{-1}$ prompted the inference that the hot gas in the intracluster medium is the material lost by member galaxies (Forman et al., 1979). Subsequent inferences have also suggested an external accretion origin for the hot X-ray gas especially on galactic scales. All these observations point at thermal X-ray emission being common to several widely different extended astronomical systems indicating the ubiquity of low density thermal plasma at temperatures in excess of million degrees. The origin of this important component of the universe is still debated. Once the low

density hot medium is formed, it is likely to be long-lived with small energy inputs balancing the radiative losses. Here, we try to understand the origin of this hot gas on galactic and cluster levels.

On a general note, it is possible to imagine that a large fraction of the diffuse low density thermal free-free X-ray emitting gas around galaxies and in clusters can be generated due to a process analogous to evaporation at the interface between high density and low density regions like evaporation of water from the surface of a water body into air as water vapour. The water vapour has a lower density than water and higher kinetic energy. The same can occur on a galaxy level wherein the cold dense gas is slowly evaporated and eventually forms hot tenuous gas. For an ideal gas $PV = nRT$ where P is the pressure, V is the volume, n is the molar density, R is the gas constant and T is the temperature of the pressured gas. Most of the gas in galaxies except in self-gravitating molecular cores can be assumed to be ideal due to their low densities. Since the gas mass is surrounded by low density gas, the gas will expand i.e. V will increase and n will decrease. If the expanding gas takes away some energy from the cold gas mass then it can increase its kinetic energy i.e. temperature. Since pressure of interstellar atomic gas and hot million degrees gas is observed to be nearly constant in a disk galaxy, this can mean that the temperature of the gas increases according to the ideal gas law (i.e. $V_1/V_2 = n_1 T_1/(n_2 T_2)$). It is significant that the galaxies which are surrounded by a hot gas halo seldom host large quantities of interstellar gas within the galaxy whereas the galaxies which are not surrounded by a massive hot gas halo contain significant amount of cooler interstellar matter within the galaxy. This provides strong support to the origin of the soft X-ray emitting halo gas being the interstellar medium of the galaxy itself and enhances the efficacy of processes like evaporation. This scenario is opposite to the case wherein the density of matter keeps increasing in a gravitational collapse so that eventually the atoms are stripped of their electrons and degenerate matter is formed as seen in compact objects.

Three distinct mechanisms for the formation of soft X-ray halo around galaxies and in the central parts of clusters appear to be operational as can be surmised from observations: (1) The gaseous interstellar medium of disk galaxies is lost due to the effect of a gravitational torque exerted by the passage of another galaxy. If the ideal gas expands isobarically, the densities decrease and the temperature increases as the gas occupies an ever-increasing volume around the galaxy. The galaxy will be depleted of its gas and

evolve to a gas-poor elliptical with the formation of a thermal soft X-ray halo. (2) The gaseous interstellar medium in disk galaxies is channelled inwards towards the supermassive black hole as a result of the gravitational torque exerted by the passage of another galaxy. The gas drives the black hole into the active regime so that it repeatedly ejects matter from its poles leading to the formation of a large radio double structure and optical line emission gas distributed around it and the galaxy evolves to a gas-poor elliptical. The continued expansion of the optical line emitting gas especially if isobaric can drive it into a low density phase such that its temperature increases and the gas evolves into a soft X-ray emitting thermal plasma. (3) The third mechanism involves the annihilation photons near 511 keV that will be continuously generated in the relativistic positron-electron plasma ejected by the black hole. Compton scattering of these photons to X-ray energies might result in a X-ray halo like structure around the galaxy but it remains difficult to ascertain this. However this mechanism can be frequently identified with the thick X-ray beams that are coincident with the radio jets in radio galaxies.

We cite some examples of galaxies which appear to provide clues to the formation mechanism for the X-ray halo observed around them. NGC 6482 is an elliptical galaxy surrounded by a hot X-ray halo which hosts a weak active nucleus in its centre and no extended double radio source is associated with it NGC 4555 is another such case of an isolated elliptical galaxy with a X-ray halo (O'Sullivan & Ponman, 2004), no active nucleus and no extended radio structure associated with the central black hole. NGC 4382, an S0 in the Virgo cluster shows a X-ray halo (Sansom et al., 2006), is devoid of HI (Hibbard & Sansom, 2003), hosts no active nucleus and no extended radio double structure is associated with it. In all these galaxies, it appears that the galaxy has lost its interstellar medium which has subsequently formed a low density soft X-ray emitting halo around it while the galaxy has evolved from a gas-rich to a gas-poor galaxy. The nuclear black hole in these galaxies remain underfed and hence lack or host at most a faint active nucleus. In the pair NGC 7626 and NGC 7619, both of which are classified as elliptical galaxies and have comparable optical sizes, a more extended X-ray halo is detected around NGC 7619 in which radio emission is confined to the nucleus whereas the diffuse X-ray emission around NGC 7626 is relatively compact but it shows bright radio jets and lobes extending to several tens of kpc beyond the optical galaxy and the X-ray halo indicating the presence of a vigorous active nucleus (Randall et al.,

2009). A cloud of gas of temperature of about 0.75 keV seems to be associated with both the galaxies while the hot thermal gas that is observed to pervade the space beyond the galaxies shows higher temperatures (Randall et al., 2009). These observation can be used to infer the X-ray halo around NGC 7619 is formed when the galaxy lost most of its gas which evaporated into the hot tenuous thermal gas and only a small amount of the interstellar gas was channelled inwards to the supermassive black hole so that it hosts a low-activity nucleus which has not resulted in a large radio structure. On the other hand, in NGC 7626 which hosts a large double radio source but a smaller X-ray halo than NGC 7619, it could be that most of its interstellar medium was channelled inwards and fed the central black hole which in turn has ejected a large fraction of this in the form of positron-electron jets and optical line emitting gas. The observed X-ray halo in this galaxy might have formed from the galaxy losing some of its interstellar medium or it could have formed from isobaric expansion of the optical line emitting gas into hot tenuous X-ray emitting gas. From the widely different sizes of the soft X-ray halo around NGC 7626 and the radio double, it appears more likely that the current X-ray halo is formed from the interstellar medium and contribution from the ejected matter from the black hole is yet to append to it. The X-ray halo around the host galaxy of the FR II galaxy Cygnus A whose extent is similar to the radio extent would have formed from isobaric expansion of the optical line forming gas ejected from the active nucleus. This means that the host galaxy has channelled most of its gas to its centre which has fuelled the black hole. In the process the galaxy has evolved to a gas-poor state. The accreting black hole has resulted in a vigorous active nucleus which has experienced several episodes of mass ejections forming a large double radio source and a matched X-ray halo. It appears that this galaxy would not have formed a X-ray halo around it prior to its active nucleus phase. These examples, although few, seem to support the suggestion that galaxies are often subjected to a gravitational torque that changes their angular momentum which is primarily mediated through the interstellar medium. The change in the angular momentum results in changing the gas distribution in the galaxy so that in some cases, most of the gas is gently ejected either as stellar winds or in form of rings which forms ring galaxies (whose main stellar body is often observed to be gas-poor) as was suggested by Kantharia (2016b). In other cases, most of the gas in the galaxies is channelled inwards fueling the supermassive black hole in the nucleus triggering

repeated polar ejections and extended radio bright structures. The galaxies which lose most of their gas can at most harbour a weak active nucleus while the galaxies which channel most of their gas inwards can harbour a vigorously active nucleus. This, then, also provides us with a prescription for the formation of early type galaxies wherein the gas is depleted in either of the ways mentioned above.

The third mechanism which can result in soft X-ray emitting gas is the Compton scattering of the positron annihilation photons near 511 keV that are continuously generated in the positron-electron plasma that emits the radio emission in jets and lobes in active galaxies. The soft γ -ray photons are down-converted to X-ray energies which can contribute to the observed X-ray emission. The examples which almost certainly point to the existence of this process are (1) the double-sided thick X-ray beams detected along radio jets in FR II galaxies like Cygnus A and Pictor A and (2) the X-ray emission which is coincident with the thick radio features extending on either side of the core in Virgo A in the general direction of the compact radio jets.

To summarise: The X-ray halo often observed surrounding gas-poor early type galaxies is formed from the interstellar medium that is lost by the originally gas-rich galaxy. The X-ray halo often observed around gas-poor active galaxies with extended radio double structure with comparable radio and X-ray extents argue for an origin in the ejections from the active nucleus. In the first case, interstellar gas is lost due to expansion out of the stellar body of the galaxy whereas in the second case, interstellar gas is used up in fuelling the central supermassive black hole. There could also be some contribution from the Compton scattering of positron-electron annihilation photons to lower energy X-rays.

6 Resolving outstanding problems; creating new ones

We briefly summarise some of the outstanding questions that the work in this paper has been able to address within the ambit of known physics and observational constraints. The questions that working on this paper has raised or not explained and which need to be resolved with the help of solid observational evidence and physics are also mentioned.

- *Formation of S0/ellipticals and active nuclei:* Since we are not in possession of any data that support the contrary, it appears appropriate to assume that all galaxies are formed with a central supermassive black hole surrounded by

gaseous matter. In fact existing observations wherein gaseous matter is detected either within or around galaxies, support this initial condition for all galaxies. Star formation would have been triggered in the gaseous matter using up a large fraction of the gas with the leftover gas forming the interstellar medium of the galaxy. Taking a cue from the present day disk galaxies, the leftover gas mass would have been at least $10^9 - 10^{10} M_{\odot}$. This gas, which would be spread across the galaxy can be assumed to behave like a fluid and hence should be able to change its global properties when a strong gravitational torque is exerted by the passage of another massive galaxy. (Under other circumstances this gas can also be considered to be ideal due to their extremely low densities. The situation is somewhat like the wave-particle duality of quantum particles so that the interstellar gas behaves like a fluid in some events and like an ideal collisionless gas for other events. On the other hand, the stellar distribution is always a collisionless system.) The torque will change the angular momentum of the galaxy which can be reflected in the gas component either as a change in its radial distribution or its kinetic properties as was described in Kantharia (2016b) i.e. $\text{torque} = dL/dt = d(I\omega)/dt$ where L is the angular momentum, I is the moment of inertia and ω is the angular speed. If we limit this discussion to the torque-induced radial rearrangement of the gaseous component, then it can be inferred that the gas can either move outwards or inwards towards the centre of the galaxy. It should also be possible for both processes to occur depending on the details of the gravitational interaction(s). This means that the gas distributed over the entire galaxy is gradually channeled inwards towards the black hole providing fuel to drive it into the active state and/or channeled outwards forming a ring around the galaxy. The galaxies which channel most of their gas inwards should trigger intense activity in their nuclei and large radio doubles whereas the galaxies which lose most of their gas can only host weak short-lived active nuclei with faint radio structure, if at all. The observed results that most large radio double sources are hosted by a gas-poor elliptical galaxies, most ring (and polar ring) galaxies are gas-poor lenticular galaxies and most gas-rich spiral galaxies are seldom hosts to strong double radio sources and are seldom observed as ring galaxies strongly support the above explanation wherein the dominant source of fuel for the central black hole and

the gas in ring galaxies is from the host galaxy itself and there exist more than one outcome for the evolution of this gas. This, then supports the present day elliptical and lenticulars as the first galaxies which were born as gas-rich disk galaxies.

- *Origin of large emission line redshifts of quasars:* Quasars are active nuclei with the largest emission line redshifts. Since in literature, these emission line redshifts are considered to be cosmological in origin, quasars have been placed at very large distances, their luminosities have been estimated to be enormous and their radio jets have been observed to expand with superluminal velocities. However the study by Kantharia (2016a) pointed out the irrefutable evidence that exists in the redshift data of spectral lines towards quasars which support a finite and large contribution from gravitational (intrinsic) redshift in the observed broad emission and absorption line redshifts. In their recipe, the lowest absorption line redshift detected in a quasar spectrum is the cosmological redshift of the quasar so that the difference redshift for the emission line provides an estimate of the largest intrinsic redshift present in the quasar spectrum. Once this intrinsic component is removed from the emission line redshift of quasars then they seem to occupy a redshift space comparable to other active nuclei, have comparable luminosities and their radio jets expand subluminally. The large component of gravitational redshift in the wide spectral lines from quasars tell us that the broad line region is located close to the event horizon of the black hole. In quasars, the emission lines are formed within $30R_s$ of the black hole and in more than half the quasars, the broad lines are formed within a separation of $2R_s$ from the black hole. The largest gravitational redshift component in other active nuclei is smaller i.e. the emission lines are formed farther from the black hole. In fact, this is physical property which is responsible for the extreme nature of quasars compared to other active nuclei.
- *Origin of multiply redshifted spectral lines in quasars:* The multiple redshifts commonly detected in a quasar spectrum are due to the contribution of a varying gravitational redshift component in the wide spectral lines of different species and ionizations, which arise in the BLR from a range of separations from the black hole. Such behaviour but with redshifts of lower amplitude has also been observed in lower redshift

active nuclei.

- *Source of transient energy in nova, supernovae, active nuclei:* The source of the energy burst in all these transients can be traced to a thermonuclear outburst. This origin can explain both the timescales and energy released in these events. Moreover this means that all three objects should emit γ -rays generated in the thermonuclear reaction - with energies ranging from tens of MeV to several hundred MeV depending on whether the photons generated in the reaction escape unchanged or are inverse Compton boosted to higher energies by relativistic electrons. It appears that thermonuclear reaction is the source of energy which dominates transient events in the universe in addition to powering the steady stellar radiative output. This should continue to be the case till the universe becomes iron-dominated when thermonuclear reactions will cease to generate energy. It could be that the transient sky will become quiet in the iron-dominated era and the universe will enter a quiescent phase of evolution.
- *Origin of a conical, collimated radio jet:* Radio jets and optical line forming gas are launched from the polar regions of the quasi-spherical pseudosurface around a black hole due to the energy input from a thermonuclear explosion in the accreted gas. Since matter radially launched from a small spherical surface has to be confined to a conical region with its apex at the centre of the sphere, the jet and optical line forming gas describe a conical flow as they expand away from the core. The conical angle (jet opening angle) is determined by the extent of the launch region which in turn will be determined by the black hole spin. In other words, the observed conical structure of the radio jets lends strong support to their being radially launched from a spherical surface i.e. pseudosurface of the black hole. If the jet is launched from close to the black hole which requires highly relativistic velocities to escape, then the jet can remain ballistic for long distances and hence collimated.
- *Radio structure in active galaxies:* The differences in the size of the radio structure associated with active nuclei in elliptical and spiral hosts is trivially explained by the active nucleus having switched on much earlier in the elliptical galaxy than in the spiral galaxy i.e. accretion by the black hole would have commenced much earlier in elliptical than in spiral galaxies. Since accretion by the black hole is an important sink for gas

depletion, the gas-poor active ellipticals which host extended radio double sources have channeled most of its gaseous component inwards and consistently fuelled the nuclear black hole. On the other hand, as indicated by the copious quantities of gas in spiral galaxies, the nuclear black hole is yet to accrete a significant amount of gas and subsequently eject it along radio jets explaining the lack of extended radio doubles in spiral hosts.

Another contributory factor to the weak radio structure of active nuclei in spiral hosts could be the lower spin of the black holes in spiral hosts which leads to large jet opening angles and hence the jets will lose their identity at short separations from the black hole. In the fast rotating black holes in elliptical hosts, the jet opening angles are small and the jets launched from close to the black hole are launched with relativistic ejection velocities which ensures collimation upto a long distance.

The question remains as to why the black hole in elliptical hosts rotate faster than in spiral hosts.

- *Most FR II are BLRG while most FR I are NLRG:* FR II radio sources are formed when the jet opening angle is extremely small and the BLR covers most of the pseudosurface - both of which occur for fast-spinning black holes. If the emission zone of the BLR lies close to the black hole due to the diminished non-polar accretion rates then lines will include a larger contribution from gravitational broadening and broader emission lines will be more frequently detected from such objects along most sightlines explaining the connection between BLRG and FR II radio sources.

In FR I sources, the black hole spin is relatively lower, the jet opening angle relatively larger and the covering factor of BLR smaller than in FR II nuclei. For the same infalling matter densities and hence comparable polar accretion rates in the FR I and FR II cores, the accretion rates at a given latitude in FR I cores can be larger than in FR II cores due to different centrifugal contributions. This can cause the non-polar pseudosurface in FR I cores to thicken and the BLR can form progressively farther from the black hole and hence the detected emission lines are likely to be more frequently narrower due to the smaller gravitational broadening and the galaxy will be classified as NLRG. The smaller covering factor of the BLR in FR I cores can also make detection of lines from the BLR orientation-dependent.

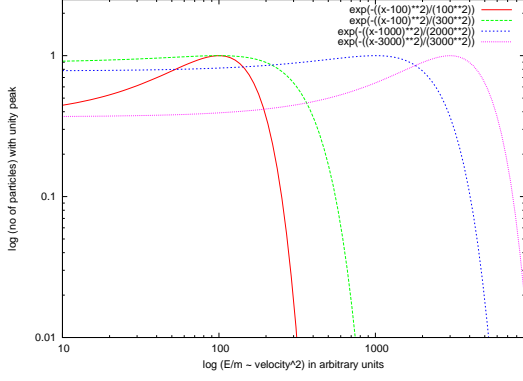


Figure 41: The expected energy distribution for particles energised in an explosive fast event like a thermonuclear outburst is shown on log-log. Energy distributions expected for four different mass particles is shown with the peak normalised to unity and the E/m in arbitrary units. Neutrinos with their lowest mass will have a distribution centred at the highest velocities followed by electrons/positrons, protons and heavy ions. The dispersion of the distributions will be as shown in the plot. Neutrinos have the highest dispersion followed by electrons/positrons, protons and heavy ions. The energy distribution for protons and heavy ions is shown to peak at the same velocities and the difference in the distributions are due to distinct dispersions.

- *Energy distribution of cosmic rays:* The energy input in supernovae and active nuclei which launches matter is from an explosive thermonuclear outburst which instantaneously energises a large quantity of matter. This statistical event has to result in normal/gaussian distribution of energies for all species of particles ranging from neutrinos to electrons/positrons to protons and heavy cosmic rays. The distributions can be assumed to be centred on similar energies and can have different dispersions which depend on the mass of the particle. Thus if E/m is plotted as in Figure 41, neutrinos, due to their negligible mass, will show the distribution at the highest E/m followed by electrons/positrons. The distribution of protons and heavy ions are shown to peak at the same E/m in Figure 41. These plots are only indicative but these already reproduce the observed particle energy distributions fairly well. The distribution beyond the peak in all cases can be approximated by power laws. If the dispersion of the distribution is small then the curve will show a convex shape whereas if the dispersion is large, the curve will show a large

flat part at lower energies. Thus all particles should be injected with such a energy spectrum which can be modified due to several physical processes after they leave the system. Thus, a fraction of the ejected cosmic rays will quickly leave the system and is detected by us. Another fraction of the cosmic rays especially protons and heavy ions can undergo collisions which leads to thermalising of the plasma.

- *Composition of radio jets is positron-electron plasma:* Several observations seem to point to a positron-electron plasma in the fast radio jets. These are detection of the annihilation line from microquasars, detection of radio emission in two distinct phases in supernovae namely the prompt radio emission which can be explained if attributed to a fast positron-electron plasma and the delayed supernova remnant emission which can be attributed to a relativistic electron-proton plasma mixed with the thermal plasma. The formation of X-ray beams detected along radio jets and hotspots in several FR II sources are readily explained by a positron-electron plasma in the jet which emits positron-annihilation photons near 511 keV along the jet which are Compton-scattered to X-ray energies or exert a radiation pressure.

Is there a relativistic electron-proton plasma that is mixed with the optical line forming gas i.e. thermal gas? Are there any radio signatures which can distinctly be associated with synchrotron emission from the proton-electron plasma? Or is it that the fast proton-dominated plasma also rushes out with the positron-electron plasma and provides the magnetic field along the jet? Since observations of the prompt radio emission in supernovae strongly suggest that the magnetic field is not frozen in the positron-electron plasma, we assume this is true for other astrophysical systems as well. Thus, we assume that in radio jets, the emitting plasma is positron-electron but the magnetic field is provided by the proton-dominated plasma. This is also supported by the comparable spatial extent of the radio plasma (relativistic particles) and the thermal X-ray emitting or optical line emitting plasma (magnetic field).

- *Origin of the centrally located radio and X-ray halo in clusters:* The origin of a large fraction of both the radio and X-ray halos detected in the centres of clusters is likely to be due to energetic ejections from the active nucleus of the central

galaxy over long timescales. If several galaxies have either merged with the central galaxy or lost their interstellar medium to the central galaxy in repeated encounters, then a large fraction of this matter can fuel the central black hole and a large fraction can be ejected following thermonuclear explosions at the poles. The ejected matter will be composed of two main detectable components: positron-electron plasma which gives rise to radio synchrotron emission and the proton(ion)-electron plasma which gives rise to the thermal free-free emission at X-ray wavelengths and provides the magnetic field for the positron-electron plasma.

Other contributions to the radio and X-ray halo can include similar ejections from other active galaxies in the cluster. The X-ray halo can also include contributions from galaxies which are losing their gas content via rings and stellar winds. For example, Virgo cluster is good example of a X-ray halo which contains both a halo formed by the central active galaxy M 87 and X-ray emission contributed by other galaxies in the cluster as is obvious from the multiple peaks in the non-spherical X-ray distribution (see Figure 37).

It is noticed that the X-ray luminosities of elliptical galaxies with the same optical luminosity span more than an order of magnitude (Sarazin, 1997). This could indicate the existence of two distinct origins for the thermal plasma namely in the gas that is gently lost by the galaxy and in the gas that is accreted onto the pseudosurface of the central black hole and then episodically ejected. Both the gas isobarically expand around the galaxy to more than million degrees K. The two different origins might be related to the formation of cavities in the X-ray distribution that is observed to be associated with radio lobes in several low power FR I radio galaxies especially in groups and clusters. In other words, the galaxy might have formed a X-ray halo as it gently lost gas before the black hole entered its active phase and started ejecting matter along polar jets which formed the radio lobes.

- *Formation of hotspots and relics at the edge of the X-ray halo; formation of thick X-ray beams along radio jets:* In literature, formation of hotspots is understood as being due to a reverse/termination shock whereas formation of relics is attributed to shocks set up by the merging of two clusters. These explanations are incomplete and vague leaving them open to misin-

terpretation - for example, it is not clear in this scenario which physical process abruptly halts the still relativistic jet in FR II sources at the hotspots nor is it clear how such intense emission of hotspots can result from the jet encountering the lower density intergalactic medium? In case of relics, the shock scenario fails to explain the formation of relics at the edge of the X-ray halo. Since such crucial points lack clarity in the widely accepted models, they are interpreted by astronomers in a variety of ways. Concrete physical reasons can be identified for the formation of hotspots and relics as described in the paper.

The morphology and physical properties (e.g. magnetic field orientation) of both the hotspots and relics argue for a halting mechanism like ram pressure or radiation pressure both of which are found to be widely effective in the universe. Since the medium beyond the hotspot is more tenuous than the medium in which the jet has already propagated, ram pressure can be ruled out. We hence examine the feasibility of radiation pressure being responsible for hotspots and relics. Interestingly, both hotspots and relics are formed on the outskirts of the diffuse extended thermal free-free X-ray emission. For radiation pressure to explain hotspots and relics, a source of hard photons beyond the hotspots and relics is required. The pair annihilation photons near 511 keV generated along the entire positron-electron jet can be the photons which can exert a radiation pressure. These photons will be promptly scattered or absorbed by the dense gas around the jet and Compton scattering of these photons to X-ray wavelengths explains the thick X-ray beams detected along radio jets. However when the radio jet travels beyond the dense gas defined by the soft X-ray emission the annihilation photons near 511 keV can survive longer. and a fraction of these can exert radiation pressure on the matter at the periphery of the X-ray emission - both radio plasma and thermal plasma. This pressure can compress the thermal gas which enhances the magnetic field and orients it perpendicular to the jet direction. The radiation pressure can also redirect a large fraction of the positron-electron plasma. The main requirement for these being that the plasmas are optically thick to the photons. This explains the formation of hotspot at the periphery of the X-ray distribution and no reacceleration of electrons at the hotspots is required. The same population of electrons ejected from the active nucleus can explain the hotspot emission. This also implies

that deep observations might detect the annihilation line from the region immediately beyond the hotspots. Since no radio synchrotron emission is detected beyond the hotspots although some of the positron-electron plasma is certainly escaping beyond the hotspots supports the freezing of the magnetic field in the thermal hot gas and is hence not available beyond the thermal gas boundary.

It is possible to think that relics are formed from a similar process on the outskirts of the X-ray halo in clusters. The X-ray emission is from the thermal proton-electron plasma whereas the radio emission is from the relativistic positron-electron plasma that radiates in the magnetic field frozen in the thermal plasma. The dominant source of both these plasma was the central active galaxy. The plasma in the radio halo co-exists with the X-ray halo and hence the annihilation photons are rapidly absorbed or Compton scattered. However beyond the X-ray halo, matter densities are extremely low and the 511 keV photons can survive longer. These photons can exert a radiation pressure on the relativistic plasma and the thermal plasma. If the axis, which is generally the major axis of the radio and X-ray halos, at the end of which relics are detected defines the original direction of the jets from the nucleus of the central galaxy when it was in its active phase then it is possible that the positron-electron plasma still retains a finite outward motion. When this plasma exits the dense region of the X-ray halo, the annihilation photons can survive longer and exert radiation pressure which can compress the plasma in the interface region which compresses the thermal gas and enhances magnetic fields which will be oriented perpendicular to the radial axis of the halo. The compression of radio plasma and enhanced magnetic field can result in enhanced radio emission i.e. relics. The relic is seen to be spread over a large linear region which when joined to the centre defines a larger opening angle than observed for hotspots. This is not surprising since the central nucleus in its active phase would have been a FR I source with a larger jet opening angle which would be increased by a precessing spin axis of the black hole. This explanation hence appears to be plausible and is consistent with rest of the discussion on active nuclei. However it needs to be further investigated and specific observations that would provide targetted results need to be conducted.

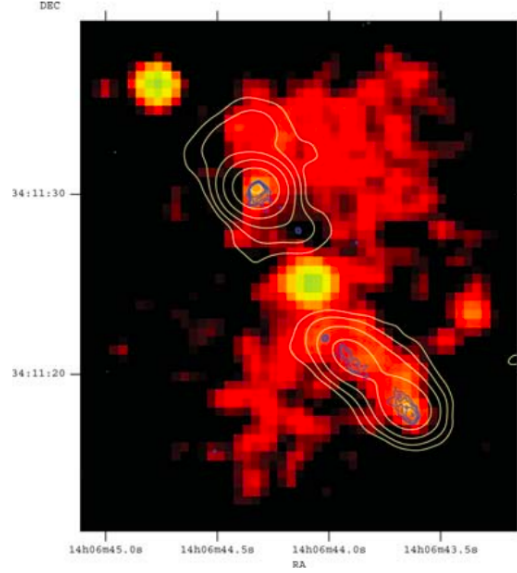


Figure 42: The X-ray emission between 0.5-3 keV in colour overlaid with contours of radio emission at 8.46 GHz (higher resolution) and 1.425 GHz (lower resolution) of 3C 294 copied from Erlund et al. (2006). Notice the biconical morphology traced by the X-rays with the radio jets being confined to one edge of the X-ray emission which is reminiscent of the ionization bicones often imaged in forbidden lines of oxygen centred on the active core - for example, in the Seyfert galaxy Circinus as in Figure 24.

- *Evolution from radio galaxy to minihalo to halo*
? A correlation between the presence of a central X-ray peak which is inferred to indicate a cooling flow in a cluster and the presence of a central radio galaxy has been noted. On the other hand, it is observed that the clusters which host both a radio and X-ray halo often lack a radio galaxy at its centre. This can be understood as follows. The centrally located radio and X-ray halo in the cluster has an origin in the energetic ejections from the active nucleus as discussed in the paper and hence has evolved from the nuclear (R_s) scales to galactic (several 10s kpc) scales to cluster (several 100s kpc) scales. In other words, the ejections from the central nucleus can lead to double radio structure which evolves to a minihalo and then a radio halo. Similarly the ejections will lead to a galaxy-size X-ray halo which evolves to a mini-halo and halo-sized X-ray emissions. It has been observed that a central radio galaxy and mini-halo co-exist in several clusters while in some clusters structures which can be dissociated into a radio mini-halo and halo have been observed. Such observations justify an evolutionary connection. It would also mean that by the time a uniform centralised cluster-level halo

is formed, the active nucleus has exhausted its fuel and is no longer launching jets.

- *X-ray cavities and radio lobes:* In several radio galaxies and groups/clusters of galaxies, bright radio emission of the lobes is coincident with faint emission in X-rays which is often referred to as X-ray cavities since these regions appear dark as compared to rest of the X-ray halo. Literature suggests that these cavities are a result of pressure differences between the X-ray emitting gas and the synchrotron emitting plasma so that the latter has displaced X-rays. While this might be possible, since the positron-electron plasma radiates in the magnetic field frozen in the thermal plasma which when at lower temperatures is characterised by optical emission lines and when at higher temperature emits X-rays, it is possible that there is a transient stage when both the plasma are mixed in the regions which emit synchrotron radiation e.g. lobes. This, then argues, against any displacement of the thermal gas. Optical line emitting gas i.e. thermal proton-electron gas is ejected alongwith the positron-electron plasma and is likely to eventually isobarically expand to a million degrees gas and contribute to X-ray emission. Cases such as the one in Figure 42 wherein the X-ray distribution shows a biconical structure like optical line emitting gas lends support to this scenario. There, then, exists the possibility that the X-ray cavities indicate the transition regions wherein the cooler 10^4 K gas is mixed with the hotter $> 10^6$ K gas so that the resultant temperature of the gas is between 10^4 and 10^6 K and does not emit X-rays.

There also exists another possible explanation for the X-ray cavities which is opposite of the above. The relativistic electrons in the lobes might inverse Compton scatter the existing X-ray photons to higher energies so that the lobes appear fainter in the low energy X-ray photons. Observations should be used to disentangle the two possible origins of the cavities. The X-ray emission from most FR II lobes are well explained by inverse Compton scattering of lower energy photons to X-ray energies. Literature often supports the inverse Compton scattering of the CMB photons as the source of the X-ray emission from the FR II lobes. However, it is also possible that inverse Compton scattering of the optical photons emitted by the 10^4 K gas which was ejected alongwith the radio plasma from the black hole and should be flooding the

lobes is responsible for the X-ray photons. Relativistic electrons of energy $\gamma \sim 100$ or so can scatter the optical photons to X-ray energies. In analogy to this, if the X-ray photons (instead of or alongwith optical photons) already present in the FR I lobes are inverse Compton scattered to higher energies then the lobes would shine at very high energies - hard X-ray or soft γ -ray energies and be faint at soft X-ray energies as is observed in several such sources.

It should be of relevance that diffuse X-ray halos are more often detected around FR I sources compared to FR II sources. A possible explanation might lie in the manner in which the host galaxy has lost its interstellar gas. If in FR I sources, the host galaxy has lost its gas through both formation of external structures like rings and by channelling fraction of gas inwards to the black hole, it could lead to the formation of a soft X-ray halo around FR I hosts from the thermal gas evaporated from the ring by the time the central black hole in its vigorous active phase, ejects and distributes radio plasma along bipolar jets and lobes. On the other hand, it is possible that in FR II hosts most of the gas is channelled inwards towards the black hole and hence no soft X-ray halo is formed around the galaxy prior to nuclear activity distributing radio plasma along jets and lobes. This can consistently account for the distinct nature of the diffuse X-ray emission around FR I and FR II sources, their distinct power regimes and the distinct observed nature of the X-ray emission from lobes of FR I and FR II sources. However it needs to be verified or ruled out by detailed examination of observations such as evolution of ring galaxies into FR I sources and non-ring galaxies into FR II sources. For example, the observation that FR I structures are commonly formed in cluster-like environs while FR II structures are commonly formed in isolated environs does lend support to the above scenario.

- *X-shaped radio galaxies:* There exist radio galaxies which show a pair of intense active lobes along the radio axis and a pair of diffuse lobes (often referred to as wings in literature) along an axis which is often displaced from the radio axis by an angle close to 90° , thus lending the radio structure a X-shaped morphology. These galaxies are referred to as X-shaped radio galaxies in literature (see Figures 43,44). The active radio lobes in many of these galaxies terminate in a hotspot and hence most of these galaxies have

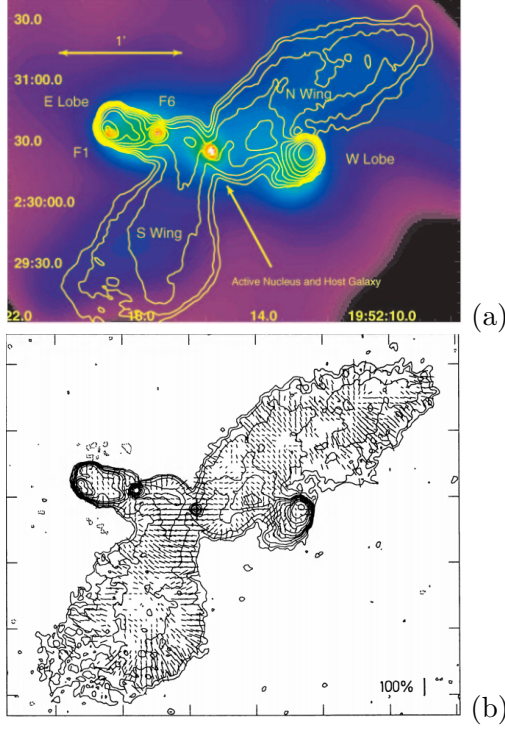


Figure 43: The X-shaped radio galaxy 3C 403. (a) Figure reproduced from Kraft et al. (2005). The contours denote the radio emission at 8.3 GHz overlaid on the X-ray emission between 0.5 and 2 keV. Notice how the X-ray and radio lobes are coincident and the lobes are bent by right angles near the core. (b) Figure reproduced from (Black et al., 1992). The contours depict the total intensity at 8.3 GHz whereas the dashes denote the polarisation vectors. Notice the enhanced polarised emission at the edge of the wing near the core and indicates a magnetic field oriented along the length of the wing. It is suggested that such wings are formed due to the backflow being stopped and diverted by the accretion disk of the black hole.

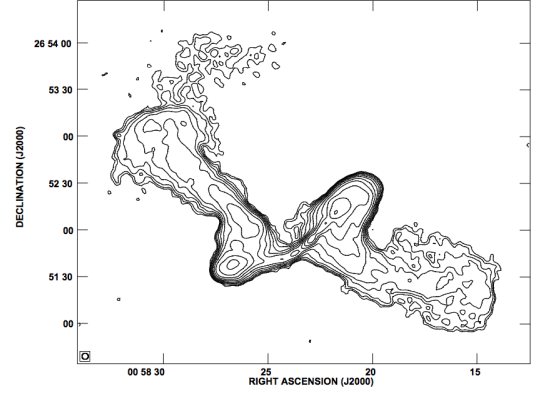


Figure 44: The X-shaped radio galaxy NGC 326 at 1.4 GHz. Figure copied from Murgia et al. (2001). Notice how the wings are bent at right angles near the core. The dimension of the linear side of the wing which continues would indicate the size of the accretion disk around the supermassive black hole.

been classified as FR II type sources although their radio power is generally estimated to be between the FR I and FR II types. The formation of the X-shaped radio structure in such galaxies has been a subject of debate in literature.

A few inferences derived for X-shaped radio galaxies from a statistical study (Saripalli & Subrahmanyan, 2009) are (1) The orientation of the radio axis in X-shaped sources is within $\sim 50^\circ$ of the major axis of the host galaxy whereas wings are oriented within 40° of the minor axis of the host galaxy. (2) The linear size of radio galaxies in which the radio axis is oriented along the host minor axis, is larger than when the radio axis is closer to the host major axis with the latter more often showing wings and other distortions. They find that the largest linear dimension of the X-shaped galaxies is smaller than of linear FR I and FR II sources. It was suggested that the X-shaped morphology could be explained if the backflow in FR II sources was deflected. One of the deflecting agents is considered to be the thermal X-ray emitting halo around the host galaxy (Saripalli & Subrahmanyan, 2009). Other origin scenarios for X-shaped radio galaxies in literature involve a change in the jet axis either due to precession or due to dual black holes in the active galaxy. Magnetic field in the edge of the wings of X-shaped radio galaxies is observed to be parallel to the length of the wings (see Figure 43b). Such persisting nature of the ordered magnetic field in the jets and wings can be inferred to indicate a net flow direction for the gas in which it is frozen.

The backflow explanation seems to well explain the observed morphology of X-shaped radio sources. As pointed out in the paper, the hotspots and backflow are due to the action of radiation pressure exerted by the pair annihilation photons at 511 keV on the plasmas so that these are redirected towards the core. In X-shaped radio galaxies, the backflow near the core is bent at right angles to the radio axis before the plasma diffuses out to form the wing-like structure (see Figures 43,44). This behaviour argues for a restraining medium/structure near the core which is oriented perpendicular to the radio axis which first halts and then deflects the plasma away from the core such that the plasma does not cross the core towards the other jet. In other words, both the positron-electron and thermal proton(ion)-electron plasma appear to be ramming into a dense medium near the core which deflects them. The location and nature of the observed effect, especially the bending of the backflow by 90 degrees strongly supports bending by the equatorial accretion disk that has formed around the central supermassive black hole. The accretion disk will be formed close to the core and be perpendicular to the bipolar jets. If a line through the core is drawn perpendicular to the radio axis, then the wings generally skirt this line in X-shaped sources. This line would represent the location of the accretion disk. If precession of the jet axis is included then the rest of the X-shaped sources wherein the wings seem to flow a bit onto the other side can also be accounted for. This then suggests that the accretion disk can extend to several kpc around the fast rotating supermassive black hole as it keeps accreting matter over billions of years. The especially low non-polar accretion rates in the fast rotating black hole in FR II sources will lead to the formation of a radially extended accretion disk. Winged sources appear to be more common when the radio axis is oriented closer to the major axis instead of the minor axis (Saripalli & Subrahmanyan, 2009). This could simply be an effect of the larger resistance provided to the polar ejections from the black hole by the galaxy when the jet is oriented closer to its major axis so that the plasma turns back sooner and hence encounters the accretion disk more frequently. In the cases when the jet is along the minor axis, the jets extend much further before turning back. This means the timescales required by the backflow to encounter the accretion disk and be deflected are much longer.

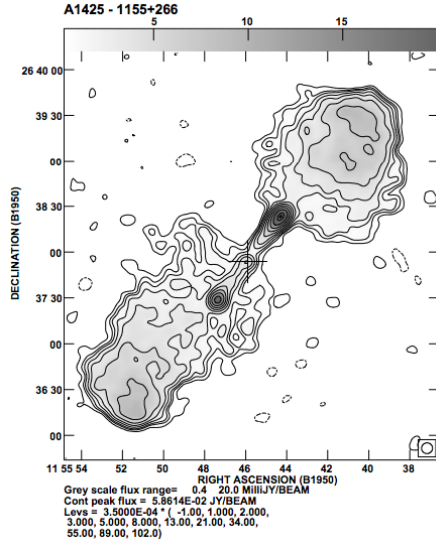
The backflows on either side of the core in X-shaped galaxies are observed to be bent in opposite directions giving it the appearance of a dual pair of lobes. There also exist sources in which the backflows on either side of the core are bent on the same side instead of opposite sides

FR II radio galaxies which are believed to have restarted from the existence of an inner pair of hotspots like A1425 (Owen & Ledlow, 1997) (see Figure 45a) and J0116-473 (Saripalli et al., 2002), although not X-shaped show an abrupt turning of the backflow at right angles to the radio axis in one of the lobes. The physical process at work is likely to be similar to X-shaped galaxies except that the backflow on the opposite side is yet to reach the core. The morphology of the two radio galaxies is remarkably similar and the spin axis of the black hole appears to be precessing as can be surmised from the displaced positions of the pairs of hotspots which are collinear with the core. Another interesting inference that follows from the discussion so far is that the new radio axis determined by connecting the new pair of hotspots has to be displaced from the previous one such that the thermal gas along the new direction is confined to a smaller region around the core thus enabling the formation of the new pair of hotspots. This means the new pair of jets and hotspots are only projected on the old pair of lobes, but occupy an independent region of space along the sightline if the explanation for the formation of hotspots presented in the paper is valid which requires relatively empty space beyond the hotspots.

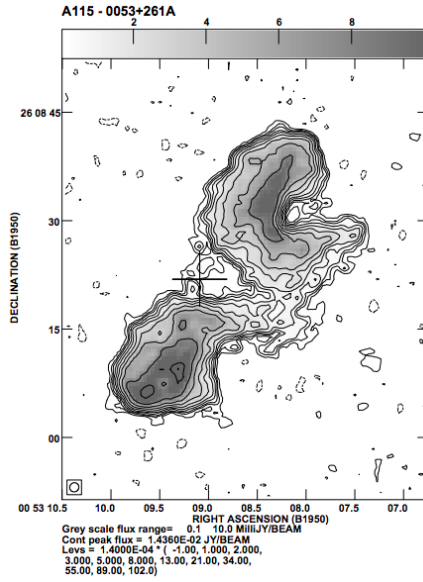
The galaxy 0053+261A in Abell 115 is a variant of a X-shaped radio galaxy wherein both the lobes formed by the backflow from the hotspots are deflected towards the same side of the jet axis by the accretion disk (see Figure 45b). If the lobes had been deflected towards opposite sides of the jet axis, the galaxy would have been classified as a X-shaped galaxy.

In summary, X-shaped sources are FR II sources wherein the backflow on both sides have encountered the accretion disk around the central black hole and hence deflected by 90°. The extent of the perpendicular wing can be used to obtain the radial extent of the accretion disk. In principle, all FR II sources will form X-shaped sources when the plasma in the backflow reaches the core i.e. accretion disk.

- *Explaining radio spectra of blazars:* The typical radio spectrum of a blazar (i.e. an active



(a)



(b)

Figure 45: Figures showing two examples of radio galaxies wherein lobe(s) are bent by right angles near the core. Figures reproduced from Owen & Ledlow (1997). In (a), the galaxy 1155+266 in Abell 1425 is shown wherein the backflow in the south appears to have rammed into the accretion disk which has confined it to the same side as the lobe, bending it by 90° to the jet axis as defined by the new pair of hotspots detected within the older lobes. In (b), the galaxy 0053+261A in Abell 115 is shown wherein lobes formed by backflows on either side of the core have reached the accretion disk around the black hole and have been deflected and confined to the same side as the corresponding lobe. In this case the deflection for both lobes is towards the same side - if the lobes were deflected towards opposite sides, it would have been classified as a X-shaped galaxy. The formation mechanism appears to be the same.

nucleus which is viewed along or close to its polar axis) is flat over a large radio frequency range and shows a convex curvature at low radio frequencies. This can be understood from the discussion in the paper as follows. Blazars are all radio-loud indicating repeated ejection of radio-emitting plasma, each with a normal energy distribution. It is possible that the peak of the energy distribution in the different ejection episodes are at differing energies so that emission from several such plasma blobs located along the sightline results in a flat spectrum. This composite spectrum will curve at the lowest radio frequencies - this could be postulated to arise from the radio plasma which is closest to us along the sightline and hence has aged the most. This explanation is similar to that given by Cotton et al. (1980) to explain flat radio spectra of active nuclei and only appends it with a physical reason which explains the spectral turnover.

Several Fermi LAT γ -ray emitting sources have been found to be blazars. This supports the thermonuclear origin for the explosion which emits γ -ray photons in addition to energising and ejecting relativistic plasma as jets. Since we view these objects along their polar axis, all the emission will be Doppler-enhanced.

- *Origin of γ -ray bursts and their afterglow:* Episodic thermonuclear ignition of accreted matter at the poles on the pseudosurface of a black hole will release γ -rays and energy. The thermonuclear explosion in which a large mass of fuel is ignited on the poles of a faint accreting black hole can release energy that can heat the entire pseudosurface due to the high conductivity of degenerate matter which forms the pseudosurface. A large number of γ -ray photons upto energies of 25 MeV or so will be released and can be inverse Compton-scattered to the higher energies that we detect. This burst of γ -ray photons can explain γ -ray bursts. It is also possible that the γ -ray burst is due to the γ -rays released in the thermonuclear explosion of a supernova which signals the formation of a black hole/neutron star or the annihilation of white dwarfs. The afterglow signatures for the two origins will be distinct due to the different nature of the two physical systems. The typical afterglow signatures of a GRB consists of kilonova emission which can be explained by black body radiation, multi-band jet emission consistent with a synchrotron process and spectral lines which can be narrow or wide, often multi-redshifted similar to the lines

from the BLR in an active nucleus. Most supernova explosions are spherically symmetric and hence will not result in jet-like structures giving rise to synchrotron emission. Hence the GRBs in which afterglow signatures include a synchrotron jet cannot be associated with a supernova explosion and instead have to be associated with an accreting rotating black hole. It does appear easier to explain the afterglow signatures for an accreting black hole. The thermonuclear explosion in the accreted matter at the poles will heat and hence brighten the entire pseudosurface due to the enhanced black body radiation which explains the enhanced ultraviolet-optical emission which is often referred to as kilonova emission in literature. The emergence of hard photons from the heated pseudosurface in the kilonova phase can excite the non-polar BLR lying dormant next to it so that wide lines become detectable in the spectra of the afterglow emission. As the pseudosurface radiatively cools, the emission known as kilonova will fade and the broad lines will disappear. The matter ejected at the poles will consist of relativistic positron-electron plasma which explains the synchrotron emission observed from X-rays to radio bands and the narrow optical line emitting gas i.e. thermal proton(ion)-electron plasma. These plasmas will keep expanding along the jet so that jets are detectable till the emission fades below sensitivity limits. GRB 170817A which was extensively observed demonstrated several of the above properties - a γ -ray pulse followed by kilonova emission and synchrotron emission along jets. These would indicate that the burst was associated with an accreting rotating black hole. A range of observational signatures are possible. For example, the actual γ -ray burst could be missed but afterglow signatures could be noted else a fraction of the afterglow signatures are detected alongwith the GRB.

Thus, it appears that GRBs can be explained by transient events on an accreting rotating black hole or supernovae.

- *Single or double-peaked light curves of supernovae:* The light curves of type Ia supernova show a single peak especially in B and V bands and the typical t_2 i.e. time over which the peak magnitude drops by 2, is noted to be around 20 days. The light curves of the SN Ia at infrared and red bands often show a second peak. On the other hand, light curves of type II supernovae are characterised by double peaks or plateaus

and the typical t_2 is longer. As pointed out for novae (Kantharia, 2017), the pre-maximum halt and final rise of light curve to maximum in addition to the post-maximum plateau observed in light curves of some novae could be understood as being due to light contribution from a hot central source like the white dwarf. This contribution could be in form of radiation or it could also lead to change in the temperature of the ejecta and hence its emission properties. A similar explanation could explain the double peaks or plateau which are normally observed in supernovae of type II. The absence of double peaks and plateaus in the light curves of type Ia supernovae in which the central object is believed to be destroyed lends support to the above model. Since dust will be formed in the ejecta of supernovae in a way similar to novae (Kantharia, 2017), the second peak, often observed in the red and infrared lightcurves of SN Ia would signal the inclusion of radiation from newly formed dust.

- *Origin of the optical transient AT2018cow:* This transient was first recorded on 16 June 2018 with an apparent magnitude of ~ 14.76 magnitudes in ATLAS o-band with its position being inside the galaxy CGCG 137-068 (distance of 60 Mpc) but displaced from its centre (Smartt et al., 2018). At the distance to the galaxy, the maximum optical luminosity was -19.9 magnitudes while the peak bolometric luminosity was estimated to be $\sim 4 \times 10^{44}$ erg s $^{-1}$. The transient showed predominantly blue colours and a rapid rise followed by a rapid decay of the light curve with no secondary peaks (Perley et al., 2018; Margutti et al., 2018b). The line spectrum was initially featureless but the spectra taken between days 4 and 8 showed the presence of a very wide feature which was interpreted as an absorption feature of full width 1500 Å centred around 4600 Å arising in gas expanding with velocities $> 0.1c$ (Perley et al., 2018). Alongwith this feature, radio and sub-mm continuum emission also became detectable while narrower (few thousand kms $^{-1}$), redshifted (~ 3000 kms $^{-1}$) asymmetric emission lines of hydrogen and helium appeared in the spectra after 10 days (Perley et al., 2018; Margutti et al., 2018b). The transient, first detected in the ultraviolet-optical-infrared bands was detected from radio to X-ray bands. The ultraviolet-optical spectrum is well fit with a black body spectrum whose temperature decreases from 30000 K to 15000 K while the infrared and radio emission can be explained by a

power law component (Perley et al., 2018). Two possible origins are suggested for the transient - supernova or a tidal disruption event by an intermediate mass black hole but both are found to be inadequate in explaining all the observations (Perley et al., 2018). The V band light curve of AT2018cow drops by 2 magnitudes in ≤ 7 days as can be surmised from Figure 2 in Perley et al. (2018). Long-lived soft X-ray emission and transient hard X-ray emission (between days 8 and 17) are detected from AT2018cow (Margutti et al., 2018b). It is inferred that less than $0.5 M_{\odot}$ of matter was ejected in the explosion of AT2018cow with the observed ejecta velocities between 0.05 to 0.1c and the energy radiated in the optical/ultraviolet bands was $10^{50.5} - 10^{51.5}$ ergs (Margutti et al., 2018b). While the above estimates are model-dependent, it is useful to mention that an energy of 10^{51} ergs can be released in a short timescale from simultaneous thermonuclear ignition of about $0.5 M_{\odot}$ which is typical of supernova explosions and explosions which eject matter in active nuclei.

The well-known and widely observed objects in which highly energetic transient events are most certainly powered by a thermonuclear outburst are: nova outbursts, supernova explosions, jet launching in microquasars (X-ray binaries) and active nuclei. γ -ray bursts can also be explained by the inverse Compton boosted γ -rays generated in a thermonuclear explosion. In fact, it appears that most transient energetic events in the universe are connected to a thermonuclear explosion. It, hence, appears most reasonable to assume that AT2018cow is also a result of the energy pulse from a thermonuclear outburst either in a supernova or in a microquasar located in the galaxy CGCG 137-068. AT2018cow cannot be associated with the centre of the galaxy since its position is displaced. The black body emission is reminiscent of a hot pseudosurface around the black hole, the absorption/emission lines can arise in the BLR or NLR while the radio emission can be associated with polar jets launched from the pseudosurface. Only if the observational data has fundamental problems with this simple explanation then other possible physical scenarios need to be explored.

- *A possible origin of fast radio bursts (FRB):* Fast radio bursts are energetic, isolated, highly dispersed radio pulses of millisecond duration. The DM estimated from FRB signals appears to have a mean of about $1000 \text{ cm}^{-3}\text{pc}$ with the range

being $200\text{-}2600 \text{ cm}^{-3}\text{pc}$ with no dependence on Galactic latitude (Figure 2 in Lorimer, 2018). This feature has prompted an extragalactic origin for FRBs (Lorimer et al., 2007). It is interesting to note that detection of highly dispersed pulses between 430 and 1420 MHz had been reported from the core of M 87 in 1980 (Linscott & Erkes, 1980) which were not confirmed by further observations (Hankins et al., 1981; Taylor et al., 1981; McCulloch et al., 1981). Energetic, highly-dispersed radio bursts had also been reported from the directions of Sgr A* and MXB1730-335 (Linscott et al., 1978). Several radio bursts from the frequent X-ray burster MXB1730-335 were reported at a frequency of 4.1 GHz (Calla et al., 1979, 1980a,b) but no radio bursts were detected at 327 MHz (Rao & Venugopal, 1980). These radio detections were considered suspect since they were erratic and often not repeatable. However now with the detection of several highly dispersed FRBs from which only a single highly dispersed millisecond duration pulse is often detected at GHz frequencies, it appears that the early observations could have detected the same population of sources. The earlier targetted observations associate the origin of FRBs with accreting black holes i.e. active nuclei or microquasars (X-ray binaries).

About 60 FRBs have now been detected out of which only one has been observed to be repetitive - FRB 121102 which is localised to within a dwarf galaxy at a redshift of ~ 0.192 (Tendulkar et al., 2017) for which a luminosity distance of 900 Mpc has been estimated. The number of theories put forward to explain FRBs exceeds the number of FRBs that have been detected. While this indicates the high level of interest amongst astronomers in the intriguing signals, it also warns us against letting free-wheeling imagination triumph over well-constrained imagination working within the confines of known physics and astrophysics. Free-wheeling imagination can make it almost impossible to ever understand the origin of FRB signals since we cannot unequivocally verify or rule out so many models. One can take the easy way out and say that each FRB is due to a different physical process but this is obviously an incorrect inference made to justify our favourite model which in the larger scheme of research has no relevance beyond our individual frame of reference.

For the repeating FRB 121102, isotropic energies of individual radio pulses have been estimated to be between 10^{37} and 10^{40} ergs (Lorimer, 2018,

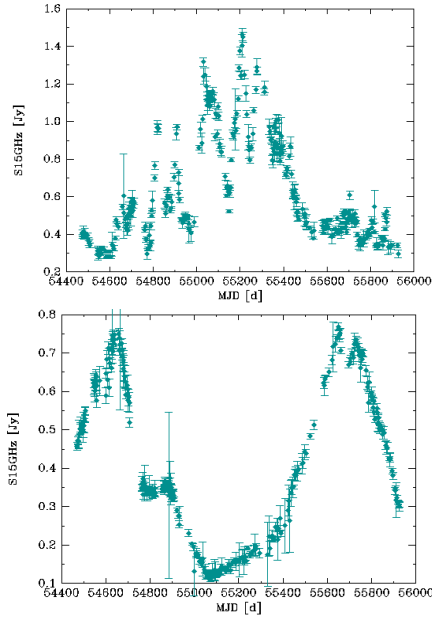


Figure 46: Figure showing the 15 GHz light curves of blazars copied from Richards et al. (2014). Notice the amplitude and timescales of variability. (a) The blazar CGRaBS J0128+4901 has an emission line redshift of 0.067 whereas in (b) the FSRQ CGRaBS J0225+1846 has an emission line redshift of 2.69.

and references therein). For comparison the solar luminosity is $3.8 \times 10^{33} \text{ erg s}^{-1}$ so that the energy released in radio bands in FRB 121102 is equivalent to the energy that the sun releases over a week or so. If FRBs are confined to a jet then the energy released in each event will be reduced. For example, if the energy is released within an angular area of 25 square degrees then only 0.02% of the energy will suffice i.e. $2 \times 10^{33} - 10^{36}$ ergs. The energy released in FRBs is small compared to supernovae ($\sim 10^{50}$ ergs), active nuclei (total energy $\gg 10^{50}$ ergs) and transient events like γ -ray bursts ($\geq 10^{50}$ ergs). The short timescales over which FRBs are detected have helped infer that the size of the emitting region is less than a few thousand kms.

As demonstrated in the paper, thermonuclear outbursts which ignite a large mass of fuel can release a huge quantity of energy in a short timescale and can successfully explain the energetic transients. We, hence, examine if the source of energy in FRBs can be thermonuclear and are associated with explosive ejection of radio plasma from stellar mass accreting rotating black holes in microquasars or supermassive accreting rotating black holes in centres of galaxies. Large DM are measured for most FRBs which have been predominantly detected

at GHz frequencies. Only recently, detection of a few FRBs at frequencies between 400 and 800 MHz with CHIME have been reported (Boyle & Chime/Frb Collaboration, 2018). The radio emission from the repeating FRB 121102 shows varying high linear polarisation and extremely high rotation measures ($10^4 - 10^5 \text{ radians m}^{-2}$) at 4.5 GHz (Michilli et al., 2018). The polarisation behaviour appears similar to that noted in the vicinity of the supermassive black holes in the centres of galaxies. For example, the linearly polarised emission from Sagittarius A* is detected at frequencies above 100 GHz (Aitken et al., 2000) and is found to vary over timescales of hours. High rotation measures ($\geq 10^5 \text{ radians m}^{-2}$) have been measured for Sagittarius A* at sub-mm wavelengths (Marrone et al., 2007). High rotation measures have also been measured for pulsars located close to the Galactic centre (e.g. Eatough et al., 2013). High rotation measures of few thousand radians- m^{-2} are commonly measured at centimetre wavelengths and $\sim \text{mas}$ resolution towards the core component of active nuclei which drops to a hundred or so radians- m^{-2} over a few mas from the core and a possible origin for such high rotation measures is suggested to be the strong magnetic fields in the NLR (e.g. Taylor et al., 1998; Hovatta et al., 2012). Even higher $\text{RM} > 10^5 \text{ radians-}\text{m}^{-2}$ are recorded at mm and sub-mm wavelengths from the cores of radio galaxies and a possible origin is suggested to be the accretion flow onto the black hole e.g. 3C 84 (Plambeck et al., 2014), M 87 (Kuo et al., 2014). Thus, the polarisation properties measured for the repeating FRB support an origin close to the supermassive black hole in galaxies.

It is relevant to note that several BL Lac objects show variability of 100% or more so that their radio flux densities double or halve or vary by various factors over hours to days as shown for a couple blazars in Figure 46 taken from Richards et al. (2014). In Figure 46, the intensity of the blazar in the top panel varies by a factor of four whereas the one at the bottom varies by a factor of eight and the change is observed to occur over timescales ranging from what appears to be a day to several tens of days. This behaviour is typical of blazars which are known for their high variability quotient. The observed radio flux densities of BL Lacs range from sub-Jy to few Jys which is also the typical range in which FRB pulses are detected thus prompting us to suggest a possible association with BL

Lac-like active nuclei i.e. nuclei whose polar axis is along the sightline. FRBs can also arise in microquasars whose radio axis is directed along the sightline. The rapid quenching of the radio signal from FRBs is intriguing and needs further investigation. It is possible that FRBs are predominantly detected in radio-faint accreting black holes.

- *Events referred to as TDE:* A tidal disruption event (TDE) signifies an event in which a main sequence star is fragmented due to its close approach to a black hole such that half of it falls into the black hole and other half escapes from the black hole. In literature, TDEs are observationally identified with sources which show enhanced short-term brightening in the ultraviolet/blue bands which is well fit with a black body spectrum, wide emission lines of helium and/or hydrogen which show correlated changes with the ultraviolet continuum (e.g. Gezari et al., 2012), a constant black body temperature, lack of optical colour evolution and the events are not observed to repeat over the monitored timescales of few hundred days. This range of transient observational signatures that have been postulated to arise in a TDE near a black hole are similar to the observed signatures of microquasars, active nuclei and kilonova/afterglow signals of a γ -ray burst which do not necessarily require a major accretion event. For example, sudden brightening, especially in the ultraviolet bands of an apparently blank region, many times coincident with the centres of galaxies and occasionally accompanied by brightening in the X-ray and radio bands is attributed to a TDE. Wide emission lines especially of hydrogen and helium with FWZM of several thousand kms^{-1} (Arcavi et al., 2014; Brown et al., 2017) are detected in several of the events labelled as TDE, which evolve with the ultraviolet continuum such that the wide lines fade as the continuum fades. The same observations could also be associated with the afterglow signatures of a γ -ray burst or variability in the non-polar pseudosurface and BLR of a Seyfert 1/BLRG/quasar nucleus. Reverberation studies are concerned with the correlation between the ultraviolet continuum and wide lines from the BLR in Seyfert 1 nuclei. This means that there seems to exist some subjectivity in interpreting similar observational results. It would be useful if the observational results are explicitly shown to not be commensurate with, for example, emission from the structure associated with a uniformly accreting black hole such

as the hot pseudosurface and BLR before it is attributed to alternate explanations like a TDE. Since few candidate TDEs have been detected in radio bands (e.g. Arcavi et al., 2014) which can be inferred to mean that the variability identified as TDEs seldom launch radio plasma along jets, it might suggest that TDEs trace variability in the non-polar regions around the accreting black hole.

The debris of a TDE event can lead to enhancing the infall densities which can increase the accretion rates at the poles and accretion rates onto the accretion disk in the non-polar regions of the black hole, but obviously require special circumstances to explain the ultraviolet brightening and occurrence of wide lines in the source which are, on the other hand, common signatures of the hot pseudosurface and BLR around the accreting black hole. This is further supported by the detection of variability in the broad lines which is correlated with the ultraviolet continuum emission. This means the transient signatures attributed to a TDE can be explained by short-term variability (thermonuclear blast?) in the already present non-polar BLR and pseudosurface. This needs to be investigated further and concretised by examining observational data on individual TDEs.

- *Double-peaked optical lines from active nuclei:* Double-peaked optical lines are expected from the ionized line forming gas that is ejected by the active nucleus alongwith the radio jets and which we identify as the NLR. Early investigations of resolved radio galaxies often detected Lyman α line emission extended along the bipolar radio jets which were blueshifted and redshifted wrt to the galaxy redshift on the two sides. Such lines would appear as double-peaked lines in case of distant and unresolved radio galaxies about the galaxy redshift and need not signify the presence of double active nuclei.
- *More questions:* Is the pseudosurface formed around all accreting black holes or does it require minimum infalling matter densities ?

The predominant source of synchrotron emission in radio galaxies appears to be the positron-electron plasma - is there any synchrotron contribution from the proton-electron plasma in radio galaxies and cluster radio halos and can it be distinguished from synchrotron emission due to the positron-electron plasma ? The magnetic field is observed to remain oriented along the straight

jet as long as the radio jet appears to remain ballistic i.e. forward momentum far exceeds the lateral momentum. Since the field is provided by the proton-electron plasma, does this mean that this plasma remains ballistic till the hotspots in FR II radio sources and the positron-electron plasma which can have random relativistic motions comparable to the forward bulk motion is merely dragged along the field lines and hence appears to be ballistic? Is it that if the field was removed, the positron-electron plasma would diffuse in all directions i.e. the perceived confinement of radio plasma in jets or in lobes is provided by the field frozen in the proton-electron plasma?

Are the forbidden emission lines which are detected at redshifts similar to broad lines in the spectra of some quasars formed in low density pockets of the BLR or in the NLR just ejected from the black hole?

What causes the spin axis of the supermassive black holes to precess? If due to an external gravitational torque, does it mean that the black hole does exchange gravitational information with the outside world? How does the infalling matter external to the black hole surmise that the black hole is rotating and its rotational speed? In other words, how does information regarding the rotation state of the black hole leave the event horizon and influence the external infalling matter i.e. how does the space-time outside the Schwarzschild radius get appropriately distorted and reflect the spin of the black hole?

The extent of the event horizon is determined by the mass of the black hole while the gravitational potential which gravitationally redshifts a photon, the escape velocity that a particle requires to leave the black hole etc are dependent on the separation from the event horizon (or black hole if it is assumed to be a point source at the centre of a sphere of radius equal to the Schwarzschild radius). Recall that no matter or electromagnetic radiation can leave from within the event horizon since they require velocities in excess of light then how is the above information passed on to the world outside the event horizon? Is it that the black hole can exchange gravitational information with the outside world? This can be inferred to mean that the graviton, which if believed to be the mediator of the gravitational interaction, travels with a speed which exceeds the speed of light so that it can effortlessly escape the event horizon of the black hole and transmit the

gravitational information from within the event horizon to the outside world. Can there be any other explanation?

7 Summary and Conclusions

This paper has attempted to comprehensively explain observations of radio synchrotron objects within the framework of known physics. It has also pointed out reasons for the observed shapes of cosmic ray energy spectra, in particular the relativistic electron energy spectra and the observed radio spectra of synchrotron sources. The observed energy distribution adheres to what we would expect from thermodynamics and statistical physics. Thermonuclear energy has emerged as the source of transient explosive energy which is released in a myriad of phenomena near black holes and in supernovae. While conditions conducive for triggering thermonuclear outbursts rapidly converge due to the immense gravity near black holes, the actual source of energy is thermonuclear and is adiabatically transferred to matter in a short time. Jets and narrow line emitting gas in active galaxies, owe their existence to episodic radial eruptions from the polar regions of the quasi-spherical pseudosurface close to the event horizon of the rotating black hole following a thermonuclear outburst. Observations favour a positron-electron composition for the fast radio synchrotron jets.

The study can be summarised as follows:

- The observed cosmic ray energy spectrum and observed radio spectra which are approximate power laws at the high energy/frequency end are observed to be convex-shaped at the lower energy/frequency side. The matter is energised in energetic transient events. Once it is appreciated that the instantaneous energising of a large number of particles is statistical in nature, it follows that it will lead to a normal/gaussian (log-normal) distribution of energies with a centroid and a finite dispersion which is the largest entropy distribution and it follows that the observed nature of the energy spectra is no longer a mystery. If the energetic event which energises and expels matter (such as supernova explosions) adiabatically imparts comparable quanta of energy to each particle (neutrinos, electrons, protons, ions etc) which if predominantly kinetic in nature i.e. $E = mv^2/2$ would lead to the centroid of the resulting energy distribution for all particles being located at the energy equal to or larger than the escape velocity from the system. The centroid energy will primarily be

determined by the heavier particles that escape. This naturally accounts for the peak of the cosmic ray distribution which is observed to be near 1 GeV for various particle species. The dispersion of the E/m distribution for each particle species will determine the random velocity component for the species which will be largest for the lightest particles. This will result in highly relativistic velocities for neutrinos and electrons.

As the forward bulk motion of the ejected matter declines, the centroid of the particle energy distributions should move to progressively lower energies. As the electrons suffer synchrotron losses, the dispersion of their energy distribution will keep reducing so that the post-peak distribution which we always approximate by a power law of index p related to the radio spectral index α by $p = 2\alpha + 1$ will appear to steepen.

- It appears beyond doubt that the composition of the fast radio synchrotron jet in accreting black holes (i.e. microquasars and active nuclei) and of the plasma giving rise to the prompt radio synchrotron emission in supernovae consists of positrons and electrons.
- A supernova explosion of type II involves implosion of the core of a massive star and thermonuclear explosion of half a solar mass or so of the surrounding gas which releases more than 10^{51} ergs within seconds and explosively ejects the outer parts of the star. Supernova explosions of type Ia have been explained by a thermonuclear explosion triggered when the mass of a white dwarf exceeds the $1.4 M_{\odot}$ limit. Observations support the ejection of a fast light positron-electron plasma which is responsible for the prompt radio emission from the supernova whereas the massive ejecta i.e. proton(ion)-plasma, which slows down soon after expulsion, eventually forms the supernova remnant and is responsible for the prompt optical light curve, delayed radio emission and the long-lasting spectral line emission i.e. it consists of a thermal plasma mixed with a non-thermal relativistic plasma. The same injected energy spectrum of the relativistic electrons results in the synchrotron emission in the prompt supernova phase and delayed remnant phase although it might be possible for the two phases to contain relativistic electrons from different energy bins.

Radio observations including polarisation studies indicate that the prompt synchrotron emission due to the fast positron-electron plasma requires an ambient magnetic field whereas the

synchrotron emission from the supernova remnant is due to the magnetic field frozen in the plasma. This, then, supports freezing of the stellar magnetic field in the heavy plasma.

- Hard X-ray emitting rims have been detected around the main body of several supernova remnants like Kepler, Tycho, Cas A. Most of these supernova remnants (except Cas A) are explosions classified as type Ia from which prompt radio or X-ray emission has never been detected and in literature this has been attributed to the lack of a dense circumstellar medium. While this study also supports this general explanation, the reasons are different. Since relativistic plasmas are ejected in all supernova explosions, the reason for the lack of prompt radio synchrotron in type Ia is the absence of an appropriate magnetic field due to the lack of a circumstellar medium in which it would be frozen. In the absence of the field, the ejected positron-electron plasma will expand with only kinetic losses and hence can survive longer. When this plasma encounters an appropriate magnetic field, it will start radiating synchrotron emission. This, then can explain the presence of hard X-ray synchrotron emitting rings that are detected mostly around supernova remnants of type Ia. The magnetic field configuration is predominantly radial within young remnants and shows a distinct structure outside the main remnant extent when radio and/or hard X-ray synchrotron emitting circumferential rings are detected. On the other hand, there is no difference in the synchrotron properties of the supernova remnant of types I and II and in both cases, the remnant consisting of thermal and non-thermal plasma should become detectable once the thermal plasma becomes optically thin to radio synchrotron emission as was the case with SN 1986J.
- Observations of type II SN 1987A support the fast propagation of a positron-electron plasma ($\sim 25000 \text{ kms}^{-1}$ till the equatorial ring) and relatively slow propagation of a thermal proton(ion)-electron plasma ($\sim 2000 \text{ kms}^{-1}$). The presence of a mixed non-thermal proton-electron plasma is not yet clear. The rapid detection and quenching of prompt radio emission from SN 1987A can be understood as being due to paucity of distributed ambient matter and magnetic field due to episodic mass loss by the progenitor so that most of the circumstellar matter is concentrated in the triple ring system. The origin of the triple ring system can be under-

stood if the progenitor of SN 1987A was in a loose binary system and experienced episodes of rapid ejection of matter from its equatorial regions at high velocities from three distinct locations in the orbit.

The brightening of the inner equatorial ring in optical would have happened when the fast positron-electron plasma exited it, in the radio when sufficient positron-electron plasma started radiating synchrotron emission in the magnetic field of the ring. The optical/infrared source that has become visible at the centre of the inner ring should be the heavy ejecta i.e. supernova remnant which was spherically symmetric in 1994 and has now evolved into a faint elliptical shell detected in spectral lines and dust emission. Radio synchrotron emission has not been detected from this central remnant till now.

- In general, accretion by a black hole should be spherical due to the small sizes of the black holes as compared to either a binary companion or the scale height of the interstellar medium in centres of galaxies. Non-spherical accretion, if found to be the case for a subset of black holes, can be studied as special cases. Irrespective of the black hole mass, accretion of matter by a rotating black hole should lead to formation of similar physical structures around the black hole. This should consist of (1) a hot quasi-spherical layer of degenerate matter that forms a pseudosurface of the black hole and emits black body radiation; (2) a broad line region formed from the matter deposited on the non-polar pseudosurface wherein broadening of emission and absorption lines is dominated by the changing gravitational potential within the region; (3) bipolar conical radio synchrotron jets and optical line emitting gas which is the accreted matter that is episodically ejected into space following energy input from thermonuclear outbursts in the hot accreted matter at the poles and (4) an accretion disk in the non-polar regions which is formed beyond the broad line region due to the accumulation of the excess infalling matter that is yet to be accreted due to the lower equatorial accretion rates for a rotating black hole. Accreting black holes can show all or a subset of the above properties since their detection will depend on the distinct physical parameters of each system and this can account for the observed variety in the properties of active nuclei/galaxies and microquasars.
- Observational results on microquasars can be

understood with the above. The Galactic microquasar SS 433 which is believed to have formed from the supernova explosion which resulted in the remnant W 50, shows blueshifted and redshifted optical emission lines with changing frequencies ($\sim 0.26c$ about a mean redshift of about 0.04) and helical twisting of the radio jet, both with a period of about 167 days. These are consistently explained by precession of the black hole spin axis in literature and hence can be identified with the thermal proton(ion)-electron and non-thermal positron-electron plasmas which are launched at escape velocities ($\sim 0.26c$) from the polar pseudosurface of the rotating black hole following a thermonuclear explosion in the accreted matter. The launching site has to be separated from the black hole by about 14.8 Schwarzschild radii so that it needs to be accelerated to at least $0.26c$ to escape the gravity of the black hole. The gravitational redshift component in the spectral lines emerging from this location will be about 0.034 (intrinsic redshift would be 0.035) which is comparable to the mean redshift over which the velocity of the spectral lines are observed to oscillate (about 0.04) lending further support to the model. The occasional disappearance of the moving lines would support episodic ejection of matter and/or indicate dust formation and obscuration in the ejected optical line forming gas. Thus several observations of SS 433 are consistently explained. The radio and γ -ray flares observed from microquasars would be due to thermonuclear energising and ejection of matter from the poles whereas the detection of the positron annihilation line near 511 keV supports the positron-electron composition of the radio jets. Positrons can be generated in the thermonuclear blast.

- GRB 170817A (and several other GRBs) can be explained by the γ -ray photons released in a thermonuclear explosion in the accreted matter deposited on the polar pseudosurface of the black hole in a microquasar located in the galaxy NGC 4993. These γ -rays could be inverse Compton scattered to the higher energies by the relativistic electrons energised in the same explosion. The width of the γ -ray pulse could be indicative of duration of the thermonuclear outburst. Observationally, GRB 170817A was characterised by the γ -ray pulse, thermal ultraviolet/optical emission and synchrotron emission. The energy released in the thermonuclear outburst heats the entire pseudosurface of the black hole which enhances its black body emis-

sion at ultraviolet and optical bands i.e. the kilonova emission. The outburst also energises and launches relativistic plasma from the poles i.e. bipolar jets which emit multi-band synchrotron radiation referred to as the afterglow. These emissions fade as the effect of the explosion wears off. In general, it appears that a large fraction of GRBs can be explained with an origin in energetic thermonuclear outbursts in supernovae, microquasars and active nuclei. Broad emission/absorption lines arising in the BLR have been detected in several GRBs supporting their origin in active nuclei.

- The spin of the accreting black hole appears to be the most important parameter determining the observable characteristics of active nuclei. High spin massive black holes result in radio galaxies and high spin massive stellar mass black holes result in microquasars. The spin of the black hole determines the latitude coverage of the centrifugal barrier which in turn determines the magnitude of the jet opening angles and the latitude thickness of the broad line region and accretion disk. FR II radio sources appear to host the fastest spinning black holes in the universe and hence should have the smallest jet opening angles, ballistic and collimated jets upto the largest distances, a broad line region with the largest covering factor and an accretion disk with the largest radial extent.
- The observed broad-band continuum emission from active nuclei which is known in literature to consist of three emission components can be explained as follows: a black body component from the pseudosurface, a thermal continuum from the non-polar broad emission line region and a synchrotron component from the relativistic positron-electron plasma ejected along the poles. The relativistic plasma is energised by the explosion energy before ejection. The spectra of active nuclei consists of broad permitted emission and absorption lines from the non-polar broad line region (BLR) and narrow permitted plus forbidden emission lines from the polar narrow line region (NLR). Narrow lines from a distant BLR could contribute lines to the spectra of type 2 active nuclei.
- The observed emission line redshifts of active nuclei especially quasars are large due to the inclusion of a significant gravitational redshift component and hence distances to quasars have been overestimated in literature. The gravitational redshift component needs to be removed

before using the redshift to estimate the distances to quasars. This is demonstrated for the FR II quasar 3C 273 whose distance is changed to about 20 Mpc and it is shown that this correction results in several observations converging on similar physical parameters. For example, the expected area of the emitting black body of temperature 26000 K (temperature taken from literature) is comparable to the area of a spherical pseudosurface for Schwarzschild radius of a billion solar mass black hole which is the black hole mass that has been inferred for 3C 273 in literature, indicating that the major source of the black body emission is indeed the pseudosurface formed at the event horizon of the black hole; the expected V band absolute magnitude estimated from the Stephen-Boltzmann luminosity matches the observed V band luminosity estimated for the corrected distance indicating that the major source of the V-band emission in 3C 273 is the hot pseudosurface and finally the jet expansion speeds become subluminal for the corrected distance.

- In the FR II galaxy Cygnus A, thick X-ray beams are seen to extend from the core to the hotspots along the finer radio synchrotron jets. Even if the radio jets are single-sided, the X-ray beams are observed to be two-sided. These X-ray photons could be from the Compton scattering of the higher energy pair annihilation photons near 511 keV generated along the positron-electron jets and are not subject to any Doppler effects explaining their two-sidedness. A similar origin is suggested for the thick X-ray beams observed in Pictor A, Virgo A, 3C 294 and 3C 432 along the radio jets/lobes. This origin follows once the composition of the jets is narrowed down to positrons and electrons. Conversely the observed X-ray beams support a positron-electron composition of the jets.
- A more concrete origin for the hotspots in FR II radio sources emerges from the positron-electron composition of the radio jets. Most of the pair annihilation photons near 511 keV are likely to be Compton scattered/absorbed by the thermal gas along the radio jet. Once the pair plasma jet expands beyond the periphery of the thermal gas and enters the highly tenuous intergalactic medium, the annihilation photons will have longer mean free paths (and lifetimes) and hence can exert radiation pressure back on the dense thermal plasma, halting it, compressing it and enhancing the ordered magnetic field. The syn-

chrotron jet will fade beyond the periphery of the thermal plasma due to lack of a magnetic field. However the pair annihilation photons can exert a radiation pressure on the thermal and relativistic plasma pushing them back towards the active nucleus explaining the formation of hotspots where the jet is turning back, the backflow and formation of radio lobes in FR II sources. If the backflow extends to the core then it can be stopped and deflected by the radially extended, thick accretion disk around the supermassive black hole, thus forming X-shaped or winged radio sources.

- Multi-band variability in microquasars and active nuclei can be explained by temporal variations in the structure and accreted gas located close to the black hole. Thermonuclear outbursts which launch matter from the poles can account for the frequent radio and γ -ray flares in blazars and microquasars, FRBs and also the enormous instantaneous energy released in extreme events like GRBs. The proximity of the accreted matter to the event horizon of the black hole makes it inherently quasi-stable in nature so, for example, any change in the temperature or thickness of the non-polar pseudosurface and BLR can explain the variability in thermal continuum and broad lines from the active nuclei.
- The aged relativistic plasma in radio halos and relics in clusters is commensurate with an origin in the polar ejections from the pseudosurface of the supermassive black hole in the central massive FR I galaxy which has long exhausted its gas supply and entered a quiescent phase. Both, the low μJy to sub- μJy magnetic fields in the halos and the subset of electrons which have their relativistic motion along the field lines and hence suffer low losses ensure longer lives for a large pool of electrons so that the relativistic plasma can expand and survive so far from the black hole and diffuse forming a halo. Such low magnetic fields are expected from flux conservation if they were originally frozen in the NLR which has expanded to halo dimensions. The existence of double relics which are located on diametrically opposite sides of the cluster centre indicates the orientation of the jet axis when the central black hole was active and along which the positron-electron plasma flowed outwards. The relics are always detected beyond the thermal X-ray halo (similar to hotspots in FR II sources which are formed beyond the thermal X-ray gas). It is hence suggested that the relics are formed due

to the radiation pressure exerted by pair annihilation photons near 511 keV generated beyond the thermal gas. The radiation pressure compresses the thermal plasma and circumferentially enhances the ordered magnetic field as observed in relics.

- Diffuse soft X-ray emitting gas is ubiquitous - it forms the hot ionized medium in spiral galaxies, a halo around elliptical galaxies and active galaxies and a centrally located halo in clusters of galaxies. The kinematic and spatial correlation observed between the optical line emitting gas and the X-ray emitting gas in active galaxies supports the evaporation of the optical gas which is originally ejected from the poles of the active nucleus to the higher temperature tenuous X-ray gas. The presence of a X-ray halo around normal elliptical galaxies argues for an origin in a gentler process such as through the formation of a ring around the galaxy due to the action of a gravitational torque and eventual evaporation of the gaseous component to X-ray densities and temperatures as it expands. The X-ray halo in clusters could be a combination of both the above as can be discerned in case of the Virgo cluster.

Acknowledgements

I gratefully acknowledge using ADS abstracts, arXiv e-prints, AAVSO data, gnuplot, LaTeX, Wikipedia, NASA Extragalactic Database, ViZier database and Google search engines enabled by the internet and the world wide web, in this research. **If you happen to use any of the figures copied from literature, please credit the original reference since I have only used these to better demonstrate a point.** Although no effort is spared in studying literature, this paper addresses popular fields of research so that literature is vast and it is practically impossible to study all of it - this again underlines the need to be choosy in publishing our results to prevent ourselves from getting lost in trivia. This work has benefitted from wide-ranging discussions with Prasad Subramanian.

References

- Abbott, B. P., Abbott, R., Abbott, T. D., Acernese, F., Ackley, K., Adams, C., Adams, T., Addesso, P., Adhikari, R. X., Adya, V. B., & et al. 2017a, ApJ, 848, L13

- . 2017b, *ApJ*, 848, L12
- Abell, G. O. & Margon, B. 1979, *Nature*, 279, 701
- Abramowski, A., Acero, F., Aharonian, F., Akhperjanian, A. G., Anton, G., Balzer, A., Barnacka, A., Barres de Almeida, U., Becherini, Y., Becker, J., & et al. 2012, *ApJ*, 746, 151
- Aitken, D. K., Greaves, J., Chrysostomou, A., Jenness, T., Holland, W., Hough, J. H., Pierce-Price, D., & Richer, J. 2000, *ApJ*, 534, L173
- Alfvén, H. & Herlofson, N. 1950, *Physical Review*, 78, 616
- Alloin, D., Pelat, D., Phillips, M., & Whittle, M. 1985, *ApJ*, 288, 205
- Alloin, D., Pelat, D., Phillips, M. M., Fosbury, R. A. E., & Freeman, K. 1986, *ApJ*, 308, 23
- Anderson, M. C. & Rudnick, L. 1996, *ApJ*, 456, 234
- Angel, J. R. P., Stockman, H. S., Woolf, N. J., Beaver, E. A., & Martin, P. G. 1976, *ApJ*, 206, L5
- Annibali, F., Bressan, A., Rampazzo, R., Zeilinger, W. W., Vega, O., & Panuzzo, P. 2010, *A&A*, 519, A40
- Antonucci, R., Hurt, T., & Kinney, A. 1994, *Nature*, 371, 313
- Antonucci, R. R. J. 1983, *Nature*, 303, 158
- Antonucci, R. R. J. & Miller, J. S. 1985, *ApJ*, 297, 621
- Arcavi, I., Gal-Yam, A., Sullivan, M., Pan, Y.-C., Cenko, S. B., Horesh, A., Ofek, E. O., De Cia, A., Yan, L., Yang, C.-W., Howell, D. A., Tal, D., Kulkarni, S. R., Tendulkar, S. P., Tang, S., Xu, D., Sternberg, A., Cohen, J. G., Bloom, J. S., Nugent, P. E., Kasliwal, M. M., Perley, D. A., Quimby, R. M., Miller, A. A., Theissen, C. A., & Laher, R. R. 2014, *ApJ*, 793, 38
- Axon, D. J., Capetti, A., Fanti, R., Morganti, R., Robinson, A., & Spencer, R. 2000, *AJ*, 120, 2284
- Baade, W. & Minkowski, R. 1954a, *ApJ*, 119, 206
- . 1954b, *ApJ*, 119, 215
- Baars, J. W. M., Genzel, R., Pauliny-Toth, I. I. K., & Witzel, A. 1977, *A&A*, 61, 99
- Bahcall, J. N., Kirhakos, S., Schneider, D. P., Davis, R. J., Muxlow, T. W. B., Garrington, S. T., Conway, R. G., & Unwin, S. C. 1995, *ApJ*, 452, L91
- Bahcall, J. N., Kozlovsky, B.-Z., & Salpeter, E. E. 1972, *ApJ*, 171, 467
- Baldi, R. D., Capetti, A., & Giovannini, G. 2019, *MNRAS*, 482, 2294
- Ball, L., Campbell-Wilson, D., Crawford, D. F., & Turtle, A. J. 1995, *ApJ*, 453, 864
- Bartel, N., Bietenholz, M. F., Rupen, M. P., Beasley, A. J., Graham, D. A., Altunin, V. I., Venturi, T., Umana, G., Cannon, W. H., & Conway, J. E. 2002, *ApJ*, 581, 404
- Bartel, N., Rupen, M. R., & Shapiro, I. I. 1989, *ApJ*, 337, L85
- Baum, S. A. & Heckman, T. 1989a, *ApJ*, 336, 681
- . 1989b, *ApJ*, 336, 702
- Baum, S. A., Heckman, T. M., Bridle, A., van Breugel, W. J. M., & Miley, G. K. 1988, *ApJS*, 68, 643
- Baum, S. A., Zirbel, E. L., & O’Dea, C. P. 1995, *ApJ*, 451, 88
- Begelman, M. C., Rees, M. J., & Blandford, R. D. 1979, *Nature*, 279, 770
- Bell, A. R. 1978, *MNRAS*, 182, 147
- Bellini, A., Renzini, A., Anderson, J., Bedin, L. R., Piotto, G., Soto, M., Brown, T. M., Milone, A. P., Sohn, S. T., & Sweigart, A. V. 2015, *ApJ*, 805, 178
- Bethe, H. A. 1939, *Physical Review*, 55, 434
- Beuermann, K., Brandt, S., & Pietsch, W. 1994, *A&A*, 281, L45
- Bevan, A., Barlow, M. J., & Milisavljevic, D. 2017, *MNRAS*, 465, 4044
- Bietenholz, M., Bartel, N., Rupen, M. P., Dwarkadas, V. V., Beasley, A. J., Graham, D. A., Venturi, T., Umana, G., Cannon, W., & Conway, J. 2010a, in 10th European VLBI Network Symposium and EVN Users Meeting: VLBI and the New Generation of Radio Arrays, 57
- Bietenholz, M. F. & Bartel, N. 2017a, *ApJ*, 839, 10
- . 2017b, *ApJ*, 851, 7

- Bietenholz, M. F., Bartel, N., & Rupen, M. P. 2002, *ApJ*, 581, 1132
- . 2003, *ApJ*, 597, 374
- . 2010b, *ApJ*, 712, 1057
- Bionta, R. M., Blewitt, G., Bratton, C. B., Casper, D., Ciocio, A., Claus, R., Cortez, B., Crouch, M., Dye, S. T., Errede, S., Foster, G. W., Gajewski, W., Ganezer, K. S., Goldhaber, M., Haines, T. J., Jones, T. W., Kielczewska, D., Kropp, W. R., Learned, J. G., Losecco, J. M., Matthews, J., Miller, R., Mudan, M. S., Park, H. S., Price, L. R., Reines, F., Schultz, J., Seidel, S., Shumard, E., Sinclair, D., Sobel, H. W., Stone, J. L., Sulak, L. R., Svoboda, R., Thornton, G., van der Velde, J. C., & Wuest, C. 1987, *Physical Review Letters*, 58, 1494
- Biretta, J. A., Zhou, F., & Owen, F. N. 1995, *ApJ*, 447, 582
- Black, A. R. S., Baum, S. A., Leahy, J. P., Perley, R. A., Riley, J. M., & Scheuer, P. A. G. 1992, *MNRAS*, 256, 186
- Blanco, W. M., Gregory, B., Hamuy, M., Heathcote, S. R., Phillips, M. M., Phillips, N. B., Suntzeff, N. B., Terndrup, D. M., Walker, A. R., Williams, R. E., Pastoriza, M. G., Storchi-Bergmann, T., & Matthews, J. 1987, *ApJ*, 320, 589
- Blandford, R. D. 1976, *MNRAS*, 176, 465
- Blandford, R. D. & McKee, C. F. 1982, *ApJ*, 255, 419
- Boccardi, B., Krichbaum, T. P., Bach, U., Mertens, F., Ros, E., Alef, W., & Zensus, J. A. 2016, *A&A*, 585, A33
- Boehringer, H., Voges, W., Fabian, A. C., Edge, A. C., & Neumann, D. M. 1993, *MNRAS*, 264, L25
- Böhringer, H., Briel, U. G., Schwarz, R. A., Voges, W., Hartner, G., & Trümper, J. 1994, *Nature*, 368, 828
- Boksenberg, A., Shortridge, K., Allen, D. A., Fosbury, R. A. E., Penston, M. V., & Savage, A. 1975, *MNRAS*, 173, 381
- Borisov, N. V. & Fabrika, S. N. 1987, *Soviet Astronomy Letters*, 13, 200
- Borkowski, K. J., Reynolds, S. P., Hwang, U., Green, D. A., Petre, R., Krishnamurthy, K., & Willett, R. 2013, *ApJ*, 771, L9
- Boroson, T. A. & Oke, J. B. 1984, *ApJ*, 281, 535
- Boroson, T. A., Persson, S. E., & Oke, J. B. 1985, *ApJ*, 293, 120
- Boselli, A., Fossati, M., Longobardi, A., Consolandi, G., Amram, P., Sun, M., Andreani, P., Boquien, M., Braine, J., Combes, F., Cote, P., Cuillandre, J. C., Duc, P. A., Emsellem, E., Ferrarese, L., Gavazzi, G., Gwyn, S., Hensler, G., Peng, E. W., Plana, H., Roediger, J., Sanchez-Janssen, R., Sarzi, M., Serra, P., & Trinchieri, G. 2018, *ArXiv e-prints*
- Bouchet, L., Mandrou, P., Roques, J. P., Vedrenne, G., Cordier, B., Goldwurm, A., Lebrun, F., Paul, J., Sunyaev, R., Churazov, E., Gilfanov, M., Pavlinsky, M., Grebenev, S., Babalyan, G., Dekhanov, I., & Khavenson, N. 1991, *ApJ*, 383, L45
- Boyle, P. C. & Chime/Frb Collaboration. 2018, *The Astronomer's Telegram*, 11901
- Bridle, A. H. in , *IAU Symposium*, Vol. 97, *Extragalactic Radio Sources*, ed. D. S. Heeschen C. M. Wade, 121–128
- Bridle, A. H., Hough, D. H., Lonsdale, C. J., Burns, J. O., & Laing, R. A. 1994, *AJ*, 108, 766
- Bridle, A. H. & Perley, R. A. 1984, *ARA&A*, 22, 319
- Brinkmann, W., Aschenbach, B., & Kawai, N. 1996, *A&A*, 312, 306
- Broderick, J. W., Fender, R. P., Miller-Jones, J. C. A., Trushkin, S. A., Stewart, A. J., Anderson, G. E., Staley, T. D., Blundell, K. M., Pietka, M., Markoff, S., Rowlinson, A., Swinbank, J. D., van der Horst, A. J., Bell, M. E., Breton, R. P., Carbone, D., Corbel, S., Eisloffel, J., Falcke, H., Griesmeier, J.-M., Hessels, J. W. T., Kondratiev, V. I., Law, C. J., Molenaar, G. J., Serylak, M., Stappers, B. W., van Leeuwen, J., Wijers, R. A. M. J., Wijnands, R., Wise, M. W., & Zarka, P. 2018, *ArXiv e-prints* 1802.03406, <https://arxiv.org/abs/1802.03406>
- Brown, J. S., Holoien, T. W.-S., Auchettl, K., Stanek, K. Z., Kochanek, C. S., Shappee, B. J., Prieto, J. L., & Grupe, D. 2017, *MNRAS*, 466, 4904
- Brunetti, G., Comastri, A., Setti, G., & Feretti, L. 1999, *A&A*, 342, 57
- Burrows, C. J., Krist, J., Hester, J. J., Sahai, R., Trauger, J. T., Stapelfeldt, K. R., Gallagher, III, J. S., Ballester, G. E., Casertano, S., Clarke, J. T., Crisp, D., Evans, R. W., Griffiths, R. E., Hoessel,

- J. G., Holtzman, J. A., Mould, J. R., Scowen, P. A., Watson, A. M., & Westphal, J. A. 1995, *ApJ*, 452, 680
- Burrows, D. N., Michael, E., Hwang, U., McCray, R., Chevalier, R. A., Petre, R., Garmire, G. P., Holt, S. S., & Nousek, J. A. 2000, *ApJ*, 543, L149
- Caldwell, N. 1984, *PASP*, 96, 287
- Calla, O. P. N., Barathy, S., Snagal, A. K., Bhandar, S. M., Deshpande, M. R., & Vyas, H. O. 1980a, *IAU Circ.*, 3458
- Calla, O. P. N., Bhandari, S. M., Deshpande, M. R., & Vats Hari, O. M. 1979, *IAU Circ.*, 3347
- Calla, O. P. N., Sangal, A. K., & Barathy, S. 1980b, *IAU Circ.*, 3467
- Cannon, R. D., Penston, M. V., & Brett, R. A. 1971, *MNRAS*, 152, 79
- Carilli, C., Perley, R., Bartel, N., & Dreher, J. The jets in Cygnus A: from pc- to kpc-scales, ed. , C. L. CarilliD. E. Harris, 76
- Carilli, C. L., Bartel, N., & Linfield, R. P. 1991a, *AJ*, 102, 1691
- Carilli, C. L., Dreher, J. W., Conner, S., & Perley, R. A. 1989, *AJ*, 98, 513
- Carilli, C. L., Kurk, J. D., van der Werf, P. P., Perley, R. A., & Miley, G. K. 1999, *AJ*, 118, 2581
- Carilli, C. L., Perley, R. A., Dreher, J. W., & Leahy, J. P. 1991b, *ApJ*, 383, 554
- Casadio, C., Gómez, J. L., Grandi, P., Jorstad, S. G., Marscher, A. P., Lister, M. L., Kovalev, Y. Y., Savolainen, T., & Pushkarev, A. B. 2015, *ApJ*, 808, 162
- Chakrabarti, S. K., Anandarao, B. G., Pal, S., Mondal, S., Nandi, A., Bhattacharyya, A., Mandal, S., Sagar, R., Pandey, J. C., Pati, A., & Saha, S. K. 2005, *MNRAS*, 362, 957
- Cheung, C. C. & Loh, A. 2016, *The Astronomer's Telegram*, 9502
- Chevalier, R. A. 1987, *Nature*, 329, 611
- Chung, A., van Gorkom, J. H., Kenney, J. D. P., Crowl, H., & Vollmer, B. 2009, *AJ*, 138, 1741
- Clark, D. H. & Murdin, P. 1978, *Nature*, 276, 44
- Clavel, J., Nandra, K., Makino, F., Pounds, K. A., Reichert, G. A., Urry, C. M., Wamsteker, W., Peracaula-Bosch, M., Stewart, G. C., & Otani, C. 1992, *ApJ*, 393, 113
- Cohen, M. H., Ogle, P. M., Tran, H. D., Goodrich, R. W., & Miller, J. S. 1999, *AJ*, 118, 1963
- Compton, A. H. 1923, *Physical Review*, 21, 483
- Condon, J. J. & Dressel, L. L. 1978, *ApJ*, 221, 456
- Cotton, W. D., Wittels, J. J., Shapiro, I. I., Marcaide, J., Owen, F. N., Spangler, S. R., Rius, A., Angulo, C., Clark, T. A., & Knight, C. A. 1980, *ApJ*, 238, L123
- Coulter, D. A., Foley, R. J., Kilpatrick, C. D., Drout, M. R., Piro, A. L., Shappee, B. J., Siebert, M. R., Simon, J. D., Ulloa, N., Kasen, D., Madore, B. F., Murguia-Berthier, A., Pan, Y.-C., Prochaska, J. X., Ramirez-Ruiz, E., Rest, A., & Rojas-Bravo, C. 2017, *Science*, 358, 1556
- Crampton, D., Cowley, A. P., & Hutchings, J. B. 1980, *ApJ*, 235, L131
- Crotts, A. P. S., Kunkel, W. E., & McCarthy, P. J. 1989, *ApJ*, 347, L61
- Davies, R. D. 1973, *MNRAS*, 161, 25P
- Davis, T. A., Alatalo, K., Sarzi, M., Bureau, M., Young, L. M., Blitz, L., Serra, P., Crocker, A. F., Krajnović, D., McDermid, R. M., Bois, M., Bournaud, F., Cappellari, M., Davies, R. L., Duc, P.-A., de Zeeuw, P. T., Emsellem, E., Khochfar, S., Kuntschner, H., Lablanche, P.-Y., Morganti, R., Naab, T., Oosterloo, T., Scott, N., & Weijmans, A.-M. 2011, *MNRAS*, 417, 882
- de Bruyn, A. G. & Wilson, A. S. 1978, *A&A*, 64, 433
- de Gasperin, F., Orrú, E., Murgia, M., Merloni, A., Falcke, H., Beck, R., Beswick, R., Birzan, L., Bonafede, A., Brüggen, M., Brunetti, G., Chyży, K., Conway, J., Croston, J. H., Enßlin, T., Ferrari, C., Heald, G., Heidenreich, S., Jackson, N., Macario, G., McKean, J., Miley, G., Morganti, R., Offringa, A., Pizzo, R., Rafferty, D., Röttgering, H., Shulevski, A., Steinmetz, M., Tasse, C., van der Tol, S., van Driel, W., van Weeren, R. J., van Zwieten, J. E., Alexov, A., Anderson, J., Asgekar, A., Avruch, M., Bell, M., Bell, M. R., Bentum, M., Bernardi, G., Best, P., Breitling, F., Broderick, J. W., Butcher, A., Ciardi, B., Dettmar, R. J., Eisloffel, J., Frieswijk, W., Gankema, H., Garrett, M., Gerbers, M., Griessmeier, J. M., Gunst, A. W.,

- Hassall, T. E., Hessels, J., Hoeft, M., Horneffer, A., Karastergiou, A., Köhler, J., Koopman, Y., Kuniyoshi, M., Kuper, G., Maat, P., Mann, G., Mevius, M., Mulcahy, D. D., Munk, H., Nijboer, R., Noordam, J., Paas, H., Pandey, M., Pandey, V. N., Polatidis, A., Reich, W., Schoenmakers, A. P., Sluman, J., Smirnov, O., Sobey, C., Stappers, B., Swinbank, J., Tagger, M., Tang, Y., van Bemmelen, I., van Cappellen, W., van Duin, A. P., van Haarlem, M., van Leeuwen, J., Vermeulen, R., Vocks, C., White, S., Wise, M., Wucknitz, O., & Zarka, P. 2012, *A&A*, 547, A56
- Dhawan, V., Mirabel, I. F., & Rodríguez, L. F. 2000, *ApJ*, 543, 373
- Dickel, J. R. & Milne, D. K. 1976, *Australian Journal of Physics*, 29, 435
- Doeleman, S. S., Fish, V. L., Schenck, D. E., Beaudoin, C., Blundell, R., Bower, G. C., Broderick, A. E., Chamberlin, R., Freund, R., Friberg, P., Gurwell, M. A., Ho, P. T. P., Honma, M., Inoue, M., Krichbaum, T. P., Lamb, J., Loeb, A., Lonsdale, C., Marrone, D. P., Moran, J. M., Oyama, T., Plambeck, R., Primiani, R. A., Rogers, A. E. E., Smythe, D. L., SooHoo, J., Strittmatter, P., Tilanus, R. P. J., Titus, M., Weintroub, J., Wright, M., Young, K. H., & Ziurys, L. M. 2012, *Science*, 338, 355
- Eatough, R. P., Falcke, H., Karuppusamy, R., Lee, K. J., Champion, D. J., Keane, E. F., Desvignes, G., Schnitzeler, D. H. F. M., Spitler, L. G., Kramer, M., Klein, B., Bassa, C., Bower, G. C., Brunthaler, A., Cognard, I., Deller, A. T., Demorest, P. B., Freire, P. C. C., Kraus, A., Lyne, A. G., Noutsos, A., Stappers, B., & Wex, N. 2013, *Nature*, 501, 391
- Edelson, R. A. 1987, *ApJ*, 313, 651
- Ekers, R. D. 1974, in *IAU Symposium*, Vol. 58, *The Formation and Dynamics of Galaxies*, ed. J. R. Shakeshaft, 257–277
- Erlund, M. C., Fabian, A. C., Blundell, K. M., Celotti, A., & Crawford, C. S. 2006, *MNRAS*, 371, 29
- Fabian, A. C. & Rees, M. J. 1979, *MNRAS*, 187, 13P
- Fanaroff, B. L. & Riley, J. M. 1974, *MNRAS*, 167, 31P
- Feigelson, E. D., Laurent-Muehleisen, S. A., Kollgaard, R. I., & Fomalont, E. B. 1995, *ApJ*, 449, L149
- Felten, J. E., Gould, R. J., Stein, W. A., & Woolf, N. J. 1966, *ApJ*, 146, 955
- Feretti, L. & Giovannini, G. *IAU Symposium*, Vol. 175, , *Extragalactic Radio Sources*, ed. R. D. Ekers, C. Fanti & L. Padrielli, 333
- Fermi, E. 1949, *Physical Review*, 75, 1169
- Fomalont, E. B., Geldzahler, B. J., & Bradshaw, C. F. 2001, *ApJ*, 553, L27
- Forman, W., Jones, C., & Tucker, W. 1985, *ApJ*, 293, 102
- Forman, W., Schwarz, J., Jones, C., Liller, W., & Fabian, A. C. 1979, *ApJ*, 234, L27
- Fowler, R. H. 1926, *MNRAS*, 87, 114
- Frank, K. A., Zhekov, S. A., Park, S., McCray, R., Dwek, E., & Burrows, D. N. 2016, *ApJ*, 829, 40
- Fransson, C., Cassatella, A., Gilmozzi, R., Kirshner, R. P., Panagia, N., Sonneborn, G., & Wamsteker, W. 1989, *ApJ*, 336, 429
- Fransson, C., Larsson, J., Migotto, K., Pesce, D., Challis, P., Chevalier, R. A., France, K., Kirshner, R. P., Leibundgut, B., Lundqvist, P., McCray, R., Spyromilio, J., Taddia, F., Jerkstrand, A., Mattila, S., Smith, N., Sollerman, J., Wheeler, J. C., Crotts, A., Garnavich, P., Heng, K., Lawrence, S. S., Panagia, N., Pun, C. S. J., Sonneborn, G., & Sugerman, B. 2015, *ApJ*, 806, L19
- Gaensler, B. M., Manchester, R. N., Staveley-Smith, L., Tzioumis, A. K., Reynolds, J. E., & Kesteven, M. J. 1997, *ApJ*, 479, 845
- Garnavich, P. & Kirshner, R. 1996, *IAU Circ.*, 6368
- Gaskell, C. M. 1982, *ApJ*, 263, 79
- Gaskell, C. M. & Sparke, L. S. 1986, *ApJ*, 305, 175
- Gelderman, R. 1995, *PASP*, 107, 205
- Gelderman, R. & Whittle, M. 1994, *ApJS*, 91, 491
- Gezari, S., Chornock, R., Rest, A., Huber, M. E., Forster, K., Berger, E., Challis, P. J., Neill, J. D., Martin, D. C., Heckman, T., Lawrence, A., Norman, C., Narayan, G., Foley, R. J., Marion, G. H., Scolnic, D., Chomiuk, L., Soderberg, A., Smith, K., Kirshner, R. P., Riess, A. G., Smartt, S. J., Stubbs, C. W., Tonry, J. L., Wood-Vasey, W. M., Burgett, W. S., Chambers, K. C., Grav, T., Heasley, J. N., Kaiser, N., Kudritzki, R.-P., Magnier, E. A., Morgan, J. S., & Price, P. A. 2012, *Nature*, 485, 217

- Giacintucci, S., Markevitch, M., Venturi, T., Clarke, T. E., Cassano, R., & Mazzotta, P. 2014, *ApJ*, 781, 9
- Giacintucci, S., O’Sullivan, E., Vrtilek, J., David, L. P., Raychaudhury, S., Venturi, T., Athreya, R. M., Clarke, T. E., Murgia, M., Mazzotta, P., Gitti, M., Ponman, T., Ishwara-Chandra, C. H., Jones, C., & Forman, W. R. 2011, *ApJ*, 732, 95
- Giommi, P., Capalbi, M., Fiacchi, M., Memola, E., Perri, M., Piranomonte, S., Rebecchi, S., & Massaro, E. *Blazar Astrophysics with BeppoSAX and Other Observatories*, ed. , P. Giommi, E. Massaro & G. Palumbo, 63
- Giovannini, G., Bonafede, A., Feretti, L., Govoni, F., Murgia, M., Ferrari, F., & Monti, G. 2009, *A&A*, 507, 1257
- Goldwurm, A., Ballet, J., Cordier, B., Paul, J., Bouchet, L., Roques, J. P., Barret, D., Mandrou, P., Sunyaev, R., Churazov, E., Gilfanov, M., Dyachkov, A., Khavenson, N., Kovtunenkov, V., Kremnev, R., & Sukhanov, K. 1992, *ApJ*, 389, L79
- Gotthelf, E. V., Koralesky, B., Rudnick, L., Jones, T. W., Hwang, U., & Petre, R. 2001, *ApJ*, 552, L39
- Goudfrooij, P., Hansen, L., Jorgensen, H. E., & Norgaard-Nielsen, H. U. 1994, *A&AS*, 105, 341
- Govoni, F. & Feretti, L. 2004, *International Journal of Modern Physics D*, 13, 1549
- Grandi, P., Guainazzi, M., Maraschi, L., Morganti, R., Fusco-Femiano, R., Fiacchi, M., Ballo, L., & Tavecchio, F. 2003, *ApJ*, 586, 123
- Grandi, P., Torresi, E., & on behalf of the FERMI-LAT collaboration. 2012a, *ArXiv e-prints*
- Grandi, P., Torresi, E., & Stanghellini, C. 2012b, *ApJ*, 751, L3
- Green, D. A., Reynolds, S. P., Borkowski, K. J., Hwang, U., Harrus, I., & Petre, R. 2008, *MNRAS*, 387, L54
- Greenstein, J. L. & Schmidt, M. 1964, *ApJ*, 140, 1
- Guberman, D., Cortina, J., de Oña Wilhelmi, E., Galindo, D., Moralejo, A., & for the MAGIC collaboration. 2017, *ArXiv e-prints* 1709.00280
- Hada, K., Kino, M., Doi, A., Nagai, H., Honma, M., Akiyama, K., Tazaki, F., Lico, R., Giroletti, M., Giovannini, G., Orienti, M., & Hagiwara, Y. 2016, *ApJ*, 817, 131
- Hankins, T. H., Campbell, D. B., Davis, M. M., Ferguson, D. C., Sieber, W., Neidhoefer, J., Wright, G. A. E., Ekers, R., & Osullivan, J. 1981, *ApJ*, 244, L61
- Hardcastle, M. J. & Croston, J. H. 2005, *MNRAS*, 363, 649
- Hardcastle, M. J., Lenc, E., Birkinshaw, M., Croston, J. H., Goodger, J. L., Marshall, H. L., Perlman, E. S., Siemiginowska, A., Stawarz, L., & Worrall, D. M. 2016, *MNRAS*, 455, 3526
- Hargrave, P. J. & Ryle, M. 1974, *MNRAS*, 166, 305
- Harris, D. E., Carilli, C. L., & Perley, R. A. 1994, *Nature*, 367, 713
- HAWC Collaboration, Abeysekara, A. U., Albert, A., Alfaro, R., Alvarez, C., Álvarez, J. D., Arceo, R., Arteaga-Velázquez, J. C., Avila Rojas, D., Ayala Solares, H. A., Belmont-Moreno, E., BenZvi, S. Y., Brisbois, C., Caballero-Mora, K. S., Capistrán, T., Carramiñana, A., Casanova, S., Castillo, M., Cotti, U., Cotzomi, J., Coutiño de León, S., De León, C., De la Fuente, E., Díaz-Vélez, J. C., Dichiaro, S., Dingus, B. L., DuVernois, M. A., Ellsworth, R. W., Engel, K., Espinoza, C., Fang, K., Fleischhack, H., Fraija, N., Galván-Gómez, A., García-González, J. A., Garfias, F., González Muñoz, A., González, M. M., Goodman, J. A., Hampel-Arias, Z., Harding, J. P., Hernandez, S., Hinton, J., Hona, B., Hueyotl-Zahuantitla, F., Hui, C. M., Hüntemeyer, P., Iriarte, A., Jardin-Blicq, A., Joshi, V., Kaufmann, S., Kar, P., Kunde, G. J., Lauer, R. J., Lee, W. H., León Vargas, H., Li, H., Linnemann, J. T., Longinotti, A. L., Luis-Raya, G., López-Coto, R., Malone, K., Marinelli, S. S., Martinez, O., Martinez- Castellanos, I., Martínez-Castro, J., Matthews, J. A., Miranda-Romagnoli, P., Moreno, E., Mostafá, M., Nayerhoda, A., Nellen, L., Newbold, M., Nisa, M. U., Noriega-Papaqui, R., Pérez-Pérez, E. G., Pretz, J., Ren, Z., Rho, C. D., Rivière, C., Rosa-González, D., Rosenberg, M., Ruiz-Velasco, E., Salesa Greus, F., Sandoval, A., Schneider, M., Schoorlemmer, H., Seglar Arroyo, M., Sinnis, G., Smith, A. J., Springer, R. W., Surabali, P., Taboada, I., Tibolla, O., Tollefson, K., Torres, I., Vianello, G., Villaseñor, L., Weisgarber, T., Werner, F., Westerhoff, S., Wood, J., Yapici, T., Yodh, G., Zepeda, A., Zhang, H., & Zhou, H. 2018, *ArXiv e-prints*, arXiv:1810.01892
- Heckman, T. M. 1980, *A&A*, 87, 152
- Hibbard, J. E. & Sansom, A. E. 2003, *AJ*, 125, 667

- Hirata, K., Kajita, T., Koshiha, M., Nakahata, M., Oyama, Y., Sato, N., Suzuki, A., Takita, M., Tot-suka, Y., Kifune, T., Suda, T., Takahashi, K., Tan-imori, T., Miyano, K., Yamada, M., Beier, E. W., Feldscher, L. R., Kim, S. B., Mann, A. K., New-comer, F. M., van, R., Zhang, W., & Cortez, B. G. 1987, *Physical Review Letters*, 58, 1490
- Hjellming, R. M. & Johnston, K. J. 1981, *ApJ*, 246, L141
- Hönig, S. F., Kishimoto, M., Antonucci, R., Marconi, A., Prieto, M. A., Tristram, K., & Weigelt, G. 2012, *ApJ*, 755, 149
- Hönig, S. F., Kishimoto, M., Tristram, K. R. W., Prieto, M. A., Gandhi, P., Asmus, D., Antonucci, R., Burtscher, L., Duschl, W. J., & Weigelt, G. 2013, *ApJ*, 771, 87
- Houck, J. C. in , *X-Ray and Radio Connections*, ed. L. O. Sjouwerman K. K. Dyer, 4.06
- Hovatta, T., Lister, M. L., Aller, M. F., Aller, H. D., Homan, D. C., Kovalev, Y. Y., Pushkarev, A. B., & Savolainen, T. 2012, *AJ*, 144, 105
- Howard, III, W. E., Dennis, T. R., Maran, S. P., & Aller, H. D. 1965, *ApJS*, 10, 331
- Hoyle, F. & Fowler, W. A. 1960, *ApJ*, 132, 565
- Hummel, E. 1980, *A&A*, 89, L1
- Hummel, E. IAU Symposium, Vol. 94, , *Origin of Cosmic Rays*, ed. G. Setti G. Spada & A. W. Wolfendale, 167
- Hutchings, J. B., Crenshaw, D. M., Kaiser, M. E., Kraemer, S. B., Weistrop, D., Baum, S., Bowers, C. W., Feinberg, L. D., Green, R. F., Gull, T. R., Hartig, G. F., Hill, G., & Lindler, D. J. 1998, *ApJ*, 492, L115
- Hwang, U., Laming, J. M., Badenes, C., Berendse, F., Blondin, J., Cioffi, D., DeLaney, T., Dewey, D., Fesen, R., Flanagan, K. A., Fryer, C. L., Ghavamian, P., Hughes, J. P., Morse, J. A., Plucinsky, P. P., Petre, R., Pohl, M., Rudnick, L., Sankrit, R., Slane, P. O., Smith, R. K., Vink, J., & Warren, J. S. 2004, *ApJ*, 615, L117
- IceCube, T., Fermi-LAT, MAGIC, AGILE, ASAS-SN, HAWC, S. H. E. S., INTEGRAL, Kanata, Kiso, Kapteyn, telescope, L., Subaru, Swift/NuSTAR, VERITAS, & VLA/17B-403 teams. 2018, *ArXiv e-prints*; <https://arxiv.org/abs/1807.08816>
- Indebetouw, R., Matsuura, M., Dwek, E., Zanardo, G., Barlow, M. J., Baes, M., Bouchet, P., Burrows, D. N., Chevalier, R., Clayton, G. C., Fransson, C., Gaensler, B., Kirshner, R., Lakićević, M., Long, K. S., Lundqvist, P., Martí-Vidal, I., Marcaide, J., McCray, R., Meixner, M., Ng, C.-Y., Park, S., Sonneborn, G., Staveley-Smith, L., Vlahakis, C., & van Loon, J. 2014, *ApJ*, 782, L2
- Isobe, N., Makishima, K., Tashiro, M., & Hong, S. 2005, *ApJ*, 632, 781
- Isobe, N., Tashiro, M., Makishima, K., Iyomoto, N., Suzuki, M., Murakami, M. M., Mori, M., & Abe, K. 2002, *ApJ*, 580, L111
- Jansky, K. G. 1933, *Nature*, 132, 66
- Johnston, K. J., Elvis, M., Kjer, D., & Shen, B. S. P. 1982, *ApJ*, 262, 61
- Junor, W., Biretta, J. A., & Livio, M. 1999, *Nature*, 401, 891
- Jura, M., Kim, D. W., Knapp, G. R., & Guhathakurta, P. 1987, *ApJ*, 312, L11
- Kaneda, H., Tashiro, M., Ikebe, Y., Ishisaki, Y., Kubo, H., Makshima, K., Ohashi, T., Saito, Y., Tabara, H., & Takahashi, T. 1995, *ApJ*, 453, L13
- Kantharia, N. 2017, *ArXiv e-prints* 1709.09400, <https://arxiv.org/pdf/1709.09400>
- Kantharia, N. G. 2016a, *ArXiv e-prints* 1609.01593 <https://arxiv.org/pdf/1609.01593>
- . 2016b, *ArXiv e-prints* 1606.04242, <https://arxiv.org/abs/1606.04242>
- Kassim, N. E. 1989, *ApJ*, 347, 915
- Kassim, N. E., Perley, R. A., Dwarakanath, K. S., & Erickson, W. C. 1995, *ApJ*, 455, L59
- Katz-Stone, D. M. & Rudnick, L. 1994, *ApJ*, 426, 116
- Katz-Stone, D. M., Rudnick, L., Buten hoff, C., & O'Donoghue, A. A. 1999, *ApJ*, 516, 716
- Khachikian, E. Y. & Weedman, D. W. 1974, *ApJ*, 192, 581
- Kinney, A. L., Schmitt, H. R., Clarke, C. J., Pringle, J. E., Ulvestad, J. S., & Antonucci, R. R. J. 2000, *ApJ*, 537, 152
- Koski, A. T. 1978, *ApJ*, 223, 56

- Kotilainen, J., Falomo, R., Bettoni, D., Karhunen, K., & Uslenghi, M. 2013, ArXiv e-prints
- Kraft, R. P., Hardcastle, M. J., Worrall, D. M., & Murray, S. S. 2005, *ApJ*, 622, 149
- Krawczynski, H., Coppi, P. S., & Aharonian, F. 2002, *MNRAS*, 336, 721
- Krichbaum, T. P., Witzel, A., Booth, R. S., Kus, A. J., Ronnang, B. O., Witzel, A., Graham, D. A., Pauliny-Toth, I. I. K., Quirrenbach, A., Hummel, C. A., Alberdi, A., Zensus, J. A., Johnston, K. J., Spencer, J. H., Rogers, A. E. E., Lawrence, C. R., Readhead, A. C. S., Hirabayashi, H., Inoue, M., Morimoto, M., Dhawan, V., Bartel, N., Shapiro, I. I., Burke, B. F., & Marcaide, J. M. 1990, *A&A*, 237, 3
- Kuo, C. Y., Asada, K., Rao, R., Nakamura, M., Algaba, J. C., Liu, H. B., Inoue, M., Koch, P. M., Ho, P. T. P., Matsushita, S., Pu, H.-Y., Akiyama, K., Nishioka, H., & Pradel, N. 2014, *ApJ*, 783, L33
- La Parola, V., Burderi, L., Guainazzi, M., & Robba, N. R. 1999, *Astrophysical Letters and Communications*, 39, 125
- Laing, R. in , *Lecture Notes in Physics*, Berlin Springer Verlag, Vol. 327, *Hot Spots in Extragalactic Radio Sources*, ed. K. Meisenheimer H.-J. Roeser, 27–43
- Laing, R. A. 1995, *Proceedings of the National Academy of Science*, 92, 11413
- Laing, R. A., Bridle, A. H., Parma, P., Feretti, L., Giovannini, G., Murgia, M., & Perley, R. A. 2008, *MNRAS*, 386, 657
- Laing, R. A., Guidetti, D., Bridle, A. H., Parma, P., & Bondi, M. 2011, *MNRAS*, 417, 2789
- Laing, R. A., Riley, J. M., & Longair, M. S. 1983, *MNRAS*, 204, 151
- Landau, R., Golisch, B., Jones, T. J., Jones, T. W., Pedelty, J., Rudnick, L., Sitko, M. L., Kenney, J., Roellig, T., Salonen, E., Urpo, S., Schmidt, G., Neugebauer, G., Matthews, K., Elias, J. H., Impey, C., Clegg, P., & Harris, S. 1986, *ApJ*, 308, 78
- Larsson, J., Fransson, C., Östlin, G., Gröningson, P., Jerkstrand, A., Kozma, C., Sollerman, J., Chalis, P., Kirshner, R. P., Chevalier, R. A., Heng, K., McCray, R., Suntzeff, N. B., Bouchet, P., Crofts, A., Danziger, J., Dwek, E., France, K., Garnavich, P. M., Lawrence, S. S., Leibundgut, B., Lundqvist, P., Panagia, N., Pun, C. S. J., Smith, N., Sonneborn, G., Wang, L., & Wheeler, J. C. 2011, *Nature*, 474, 484
- Lazio, T. J. W., Cohen, A. S., Kassim, N. E., Perley, R. A., Erickson, W. C., Carilli, C. L., & Crane, P. C. 2006, *ApJ*, 642, L33
- Leahy, J. P., Muxlow, T. W. B., & Stephens, P. W. 1989, *MNRAS*, 239, 401
- Leibundgut, B., Kirshner, R. P., Pinto, P. A., Rupen, M. P., Smith, R. C., Gunn, J. E., & Schneider, D. P. 1991, *ApJ*, 372, 531
- Lico, R., Giroletti, M., Orienti, M., Costamante, L., Pavlidou, V., D’Ammando, F., & Tavecchio, F. 2017, *A&A*, 606, A138
- Ling, J. C. & Wheaton, W. A. 1989, *ApJ*, 343, L57
- Linscott, I. R. & Erkes, J. W. 1980, *ApJ*, 236, L109
- Linscott, I. R., Erkes, J. W., Powell, N. R., & Irwin, J. 1978, in *BAAS*, Vol. 10, *Bulletin of the American Astronomical Society*, 657
- Lipovetsky, V. A., Neizvestny, S. I., & Neizvestnaya, O. M. 1988, *Soobshcheniya Spetsial’noj Astrofizicheskoy Observatorii*, 55, 5
- Liutyi, V. M. 1977, *Soviet Ast.*, 21, 655
- López-Gonzaga, N., Jaffe, W., Burtscher, L., Tristram, K. R. W., & Meisenheimer, K. 2014, *A&A*, 565, A71
- Lorimer, D. R. 2018, *Nature Astronomy*, 2, 860
- Lorimer, D. R., Bailes, M., McLaughlin, M. A., Narkevic, D. J., & Crawford, F. 2007, *Science*, 318, 777
- Lynden-Bell, D. 1969, *Nature*, 223, 690
- Lynden-Bell, D. & Rees, M. J. 1971, *MNRAS*, 152, 461
- Malkan, M. A. & Sargent, W. L. W. 1982, *ApJ*, 254, 22
- Manchester, R. N., Gaensler, B. M., Wheaton, V. C., Staveley-Smith, L., Tzioumis, A. K., Bizunok, N. S., Kesteven, M. J., & Reynolds, J. E. 2002, *PASA*, 19, 207
- Marconi, A., Moorwood, A. F. M., Origlia, L., & Oliva, E. 1994, *The Messenger*, 78, 20
- Margon, B. 1984, *ARA&A*, 22, 507

- Margon, B., Anderson, S. F., Aller, L. H., Downes, R. A., & Keyes, C. D. 1984, *ApJ*, 281, 313
- Margon, B., Ford, H. C., Grandi, S. A., & Stone, R. P. S. 1979a, *ApJ*, 233, L63
- Margon, B., Ford, H. C., Katz, J. I., Kwitter, K. B., Ulrich, R. K., Stone, R. P. S., & Klemola, A. 1979b, *ApJ*, 230, L41
- Margutti, R., Alexander, K. D., Xie, X., Sironi, L., Metzger, B. D., Kathirgamaraju, A., Fong, W., Blanchard, P. K., Berger, E., MacFadyen, A., Giannios, D., Guidorzi, C., Hajela, A., Chornock, R., Cowperthwaite, P. S., Eftekhari, T., Nicholl, M., Villar, V. A., Williams, P. K. G., & Zrake, J. 2018a, *ApJ*, 856, L18
- Margutti, R., Metzger, B. D., Chornock, R., Vurm, I., Roth, N., Grefenstette, B. W., Savchenko, V., Cartier, R., Steiner, J. F., Terreran, G., Migliori, G., Milisavljevic, D., Alexander, K. D., Bietenholz, M., Blanchard, P. K., Bozzo, E., Brethauer, D., Chilingarian, I. V., Coppejans, D. L., Ducci, L., Ferrigno, C., Fong, W., Götz, D., Guidorzi, C., Hajela, A., Hurley, K., Kuulkers, E., Laurent, P., Mereghetti, S., Nicholl, M., Patnaude, D., Ubertini, P., Banovetz, J., Bartel, N., Berger, E., Coughlin, E. R., Eftekhari, T., Frederiks, D. D., Kozlova, A. V., Laskar, T., Svinkin, D. S., Drout, M. R., Macfadyen, A., & Paterson, K. 2018b, *arXiv e-prints*, arXiv:1810.10720
- Marrone, D. P., Moran, J. M., Zhao, J.-H., & Rao, R. 2007, *ApJ*, 654, L57
- Marshall, H. L., Miller, B. P., Davis, D. S., Perlman, E. S., Wise, M., Canizares, C. R., & Harris, D. E. 2002, *ApJ*, 564, 683
- Massaro, E., Perri, M., Giommi, P., & Nesci, R. 2004, *A&A*, 413, 489
- Matheson, T., Filippenko, A. V., Barth, A. J., Ho, L. C., Leonard, D. C., Bershad, M. A., Davis, M., Finley, D. S., Fisher, D., González, R. A., Hawley, S. L., Koo, D. C., Li, W., Lonsdale, C. J., Schlegel, D., Smith, H. E., Spinrad, H., & Wirth, G. D. 2000, *AJ*, 120, 1487
- Matthews, T. A., Morgan, W. W., & Schmidt, M. 1964, *ApJ*, 140, 35
- McCarthy, P. J., Spinrad, H., & van Breugel, W. 1995, *ApJS*, 99, 27
- McCarthy, P. J., Spinrad, H., van Breugel, W., Liebert, J., Dickinson, M., Djorgovski, S., & Eisenhardt, P. 1990, *ApJ*, 365, 487
- McCulloch, P. M., Ellis, G. R. A., Gowland, G. A., & Roberts, J. A. 1981, *ApJ*, 245, L99
- McKean, J. P., Godfrey, L. E. H., Vegetti, S., Wise, M. W., Morganti, R., Hardcastle, M. J., Rafferty, D., Anderson, J., Avruch, I. M., Beck, R., Bell, M. E., van Bemmell, I., Bentum, M. J., Bernardi, G., Best, P., Blaauw, R., Bonafede, A., Breitling, F., Broderick, J. W., Brüggem, M., Cerrigone, L., Ciardi, B., de Gasperin, F., Deller, A., Duscha, S., Engels, D., Falcke, H., Fallows, R. A., Frieswijk, W., Garrett, M. A., Griebmeier, J. M., van Haarlem, M. P., Heald, G., Hoeft, M., Horst, A. J. v. d., Iacobelli, M., Intema, H., Juette, E., Karastergiou, A., Kondratiev, V. I., Koopmans, L. V. E., Kuniyoshi, M., Kuper, G., van Leeuwen, J., Maat, P., Mann, G., Markoff, S., McFadden, R., McKay-Bukowski, D., Mulcahy, D. D., Munk, H., Nelles, A., Orru, E., Paas, H., Pandey-Pommier, M., Pietka, M., Pizzo, R., Polatidis, A. G., Reich, W., Röttgering, H. J. A., Rowlinson, A., Scaife, A. M. M., Serylak, M., Shulevski, A., Sluman, J., Smirnov, O., Steinmetz, M., Stewart, A., Swinbank, J., Tagger, M., Thoudam, S., Toribio, M. C., Vermeulen, R., Vocks, C., van Weeren, R. J., Wucknitz, O., Yatawatta, S., & Zarka, P. 2016, *MNRAS*, 463, 3143
- Meisenheimer, K. & Roeser, H.-J. 1986, *Nature*, 319, 459
- Mestel, L. 1965, *Stellar Structure - Stars and Stellar Systems*, 8, 297
- Michilli, D., Seymour, A., Hessels, J. W. T., Spitler, L. G., Gajjar, V., Archibald, A. M., Bower, G. C., Chatterjee, S., Cordes, J. M., Gourdji, K., Heald, G. H., Kaspi, V. M., Law, C. J., Sobey, C., Adams, E. A. K., Bassa, C. G., Bogdanov, S., Brinkman, C., Demorest, P., Fernandez, F., Hellbourg, G., Lazio, T. J. W., Lynch, R. S., Maddox, N., Marcote, B., McLaughlin, M. A., Paragi, Z., Ransom, S. M., Scholz, P., Siemion, A. P. V., Tendulkar, S. P., van Rooy, P., Wharton, R. S., & Whitlow, D. 2018, *Nature*, 553, 182
- Miley, G. 1980, *ARA&A*, 18, 165
- Miley, G. K., Heckman, T. M., Butcher, H. R., & van Breugel, W. J. M. 1981, *ApJ*, 247, L5
- Miley, G. K. & Miller, J. S. 1979, *ApJ*, 228, L55
- Milgrom, M. 1979, *A&A*, 76, L3
- Milisavljevic, D. & Fesen, R. A. 2017, *ArXiv e-prints*

- Milisavljevic, D., Fesen, R. A., Leibundgut, B., & Kirshner, R. P. 2008, *ApJ*, 684, 1170
- Million, E. T., Werner, N., Simionescu, A., Allen, S. W., Nulsen, P. E. J., Fabian, A. C., Böhringer, H., & Sanders, J. S. 2010, *MNRAS*, 407, 2046
- Minkowski, R. 1941, *PASP*, 53, 224
- Mirabel, I. F. 1994, *ApJS*, 92, 369
- . 2012, *ArXiv e-prints* 1206.1041, <https://arxiv.org/abs/1206.1041>
- Mirabel, I. F. & Rodríguez, L. F. 1994, *Nature*, 371, 46
- Mirabel, I. F., Rodríguez, L. F., Cordier, B., Paul, J., & Lebrun, F. 1992, *Nature*, 358, 215
- Molnar, L. A., Reid, M. J., & Grindlay, J. E. 1988, *ApJ*, 331, 494
- Morganti, R. & Oosterloo, T. 2018, *arXiv e-prints*, [arXiv:1807.01475](https://arxiv.org/abs/1807.01475)
- Mundell, C. G., Wrobel, J. M., Pedlar, A., & Galimore, J. F. 2003, *ApJ*, 583, 192
- Murgia, M., Parma, P., de Ruiter, H. R., Bondi, M., Ekers, R. D., Fanti, R., & Fomalont, E. B. 2001, *A&A*, 380, 102
- Nulsen, P. E. J. 1982, *MNRAS*, 198, 1007
- O’Dea, C. P. 1998, *PASP*, 110, 493
- O’Dea, C. P. & Owen, F. N. 1986, *ApJ*, 301, 841
- Ogle, P. M., Cohen, M. H., Miller, J. S., Tran, H. D., Fosbury, R. A. E., & Goodrich, R. W. 1997, *ApJ*, 482, L37
- Olivares, V., Salomé, P., Combes, F., Hamer, S., Guillard, P., Lehnert, M. D., Polles, F., Beckmann, R. S., Dubois, Y., Donahue, M., Edge, A., Fabian, A. C., McNamara, B., Rose, T., Russell, H., Tremblay, G., Vantyghem, A., Canning, R. E. A., Ferland, G., Godard, B., Hogan, M., Peirani, S., & Pineau des Forets, G. 2019, *arXiv e-prints*, [arXiv:1902.09164](https://arxiv.org/abs/1902.09164)
- Osterbrock, D. E. 1960, *ApJ*, 132, 325
- . 1977, *ApJ*, 215, 733
- . 1989, *Astrophysics of gaseous nebulae and active galactic nuclei*
- Osterbrock, D. E. & Koski, A. T. 1976, *MNRAS*, 176, 61P
- O’Sullivan, E., Kolokythas, K., Raychaudhury, S., Vrtilek, J., & Kantharia, N. 2014, in *Astronomical Society of India Conference Series*, Vol. 13, *Astronomical Society of India Conference Series*, 259–262
- O’Sullivan, E. & Ponman, T. J. 2004, *MNRAS*, 354, 935
- Owen, F. N., Hardee, P. E., & Cornwell, T. J. 1989, *ApJ*, 340, 698
- Owen, F. N. & Ledlow, M. J. 1997, *ApJS*, 108, 41
- Owen, F. N., Ledlow, M. J., Morrison, G. E., & Hill, J. M. 1997, *ApJ*, 488, L15
- Paczynski, B. 1978, *Acta Astron.*, 28, 91
- Pancoast, A., Barth, A. J., Horne, K., Treu, T., Brewer, B. J., Bennert, V. N., Canalizo, G., Gates, E. L., Li, W., Malkan, M. A., Sand, D., Schmidt, T., Valenti, S., Woo, J.-H., Clubb, K. I., Cooper, M. C., Crawford, S. M., Hönig, S. F., Joner, M. D., Kandrashoff, M. T., Lazaro, M., Nierenberg, A. M., Romero-Colmenero, E., Son, D., Tollerud, E., Walsh, J. L., & Winkler, H. 2018, *ApJ*, 856, 108
- Paragi, Z., Vermeulen, R. C., Fejes, I., Schilizzi, R. T., Spencer, R. E., & Stirling, A. M. 1999, *New A Rev.*, 43, 553
- Pauliny-Toth, I. I. K. & Kellermann, K. I. 1966, *ApJ*, 146, 634
- Pearson, T., Unwin, S., Cohen, M., Linfield, R., Readhead, A., Seielstad, G., Simon, R., & Walker, R. in , *IAU Symposium*, Vol. 97, *Extragalactic Radio Sources*, ed. D. S. Heeschen C. M. Wade, 355
- Pearson, T. J., Unwin, S. C., Cohen, M. H., Linfield, R. P., Readhead, A. C. S., Seielstad, G. A., Simon, R. S., & Walker, R. C. 1981, *Nature*, 290, 365
- Pedlar, A., Ghataure, H. S., Davies, R. D., Harrison, B. A., Perley, R., Crane, P. C., & Unger, S. W. 1990, *MNRAS*, 246, 477
- Penston, M. V., Boksenberg, A., Bromage, G. E., Clavel, J., Elvius, A., Gondhalekar, P. M., Jordan, C., Lind, J., Lindegren, L., Perola, G. C., Pettini, M., Sniijders, M. A. J., Tanzi, E. G., Tarenghi, M., & Ulrich, M. H. 1981, *MNRAS*, 196, 857
- Penston, M. V. & Cannon, R. D. 1969, *Communications of the Konkoly Observatory Hungary*, 65, 485

- Penston, M. V., Clavel, J., Snijders, M. A. J., Boksenberg, A., & Fosbury, R. A. E. 1979, *MNRAS*, 189, 45P
- Perley, D. A., Mazzali, P. A., Yan, L., Cenko, S. B., Gezari, S., Taggart, K., Blagorodnova, N., Fremming, C., Mockler, B., Singh, A., Tominaga, N., Tanaka, M., Watson, A. M., Ahumada, T., Anupama, G. C., Ashall, C., Becerra, R. L., Bersier, D., Bhalerao, V., Bloom, J. S., Butler, N. R., Copperwheat, C., Coughlin, M. W., De, K., Drake, A. J., Duev, D. A., Frederick, S., Jesús González, J., Goobar, A., Heida, M., Ho, A. Y. Q., Horst, J., Hung, T., Itoh, R., Jencson, J. E., Kasliwal, M. M., Kawai, N., Kulkarni, S. R., Kumar, B., Kumar, H., Kuttyrev, A. S., Khanam, T., Lee, W. H., Maeda, K., Mahabal, A., Murata, K. L., Neill, J. D., Ngeow, C.-C., Penprase, B., Pian, E., Quimby, R., Ramirez-Ruiz, E., Richer, M., Román-Zúñiga, C. G., Srivastava, S., Socia, Q., Sollerman, J., Tachibana, Y., Taddia, F., Tinyanont, K., Troja, E., Ward, C., & Wee, J. 2018, *ArXiv e-prints*
- Perley, R. A. & Carilli, C. L. The structure and polarization of Cygnus A at λ 3.6cm, ed. , C. L. Carilli D. E. Harris, 168
- Perley, R. A. & Meisenheimer, K. 2017, *A&A*, 601, A35
- Perley, R. A., Roser, H.-J., & Meisenheimer, K. 1997, *A&A*, 328, 12
- Perola, G. C., Piro, L., Altamore, A., Fiore, F., Boksenberg, A., Penston, M. V., Snijders, M. A. J., Bromage, G. E., Clavel, J., Elvius, A., & Ulrich, M. H. 1986, *ApJ*, 306, 508
- Peterson, B. M. & Horne, K. in , *Planets to Cosmology: Essential Science in the Final Years of the Hubble Space Telescope*, ed. M. Livio S. Casertano, Vol. 18, 89
- Phillips, M. M. 1978, *ApJS*, 38, 187
- Phillips, M. M., Heathcote, S. R., Hamuy, M., & Navarrete, M. 1988, *AJ*, 95, 1087
- Phillips, M. M., Jenkins, C. R., Dopita, M. A., Sadler, E. M., & Binette, L. 1986, *AJ*, 91, 1062
- Piro, L., Matt, G., & Ricci, R. 1997, *A&AS*, 126, 525
- Plambeck, R. L., Bower, G. C., Rao, R., Marrone, D. P., Jorstad, S. G., Marscher, A. P., Doeleman, S. S., Fish, V. L., & Johnson, M. D. 2014, *ApJ*, 797, 66
- Prestwich, A. H., Galache, J. L., Linden, T., Kalogera, V., Zezas, A., Roberts, T. P., Kilgard, R., Wolter, A., & Trinchieri, G. 2012, *ApJ*, 747, 150
- Pringle, J. E. 1981, *ARA&A*, 19, 137
- Pushkarev, A. B., Kovalev, Y. Y., Lister, M. L., & Savolainen, T. 2009, *A&A*, 507, L33
- Randall, S. W., Jones, C., Kraft, R., Forman, W. R., & O'Sullivan, E. 2009, *ApJ*, 696, 1431
- Rao, A. P. 1987, *Proceedings of NRAO Workshop on 'Radio Continuum Processes in Clusters of Galaxies'*, ed. C. P. O'Dea and J. M. Uson, 16, 79
- Rao, A. P. & Venugopal, V. R. 1980, *Bulletin of the Astronomical Society of India*, 8, 41
- Reynolds, S. P., Borkowski, K. J., Green, D. A., Hwang, U., Harrus, I., & Petre, R. 2008, *ApJ*, 680, L41
- Reynolds, S. P. & Keohane, J. W. 1999, *ApJ*, 525, 368
- Richards, J. L., Hovatta, T., Max-Moerbeck, W., Pavlidou, V., Pearson, T. J., & Readhead, A. C. S. 2014, *MNRAS*, 438, 3058
- Richardson, D., Branch, D., Casebeer, D., Millard, J., Thomas, R. C., & Baron, E. 2002, *AJ*, 123, 745
- Ripero, J., Garcia, F., Rodriguez, D., Pujol, P., Filippenko, A. V., Treffers, R. R., Paik, Y., Davis, M., Schlegel, D., Hartwick, F. D. A., Balam, D. D., Zurek, D., Robb, R. M., Garnavich, P., & Hong, B. A. 1993, *IAU Circ.*, 5731
- Robinson, A., Binette, L., Fosbury, R. A. E., & Tadhunter, C. N. 1987, *MNRAS*, 227, 97
- Rogstad, D. H. & Ekers, R. D. 1969, *ApJ*, 157, 481
- Rudnick, L. & Katz-Stone, D. M. *Astronomical Society of the Pacific Conference Series*, Vol. 100, , *Energy Transport in Radio Galaxies and Quasars*, ed. P. E. Hardee A. H. Bridle & J. A. Zensus, 233
- Rupen, M. P., van Gorkom, J. H., Knapp, G. R., Gunn, J. E., & Schneider, D. P. 1987, *AJ*, 94, 61
- Ryle, M., Caswell, J. L., Hine, G., & Shakeshaft, J. 1978, *Nature*, 276, 571
- Sansom, A. E., O'Sullivan, E., Forbes, D. A., Proctor, R. N., & Davis, D. S. 2006, *MNRAS*, 370, 1541

- Sarazin, C. L. *Astronomical Society of the Pacific Conference Series*, Vol. 116, , *The Nature of Elliptical Galaxies*; 2nd Stromlo Symposium, ed. M. Arnaboldi G. S. Da Costa & P. Saha, 375
- Saripalli, L. & Subrahmanyan, R. 2009, *ApJ*, 695, 156
- Saripalli, L., Subrahmanyan, R., & Udaya Shankar, N. 2002, *ApJ*, 565, 256
- Scheuer, P. A. G. & Readhead, A. C. S. 1979, *Nature*, 277, 182
- Schilizzi, R. T., Romney, J. D., & Spencer, R. E. *IAU Symposium*, Vol. 110, , *VLBI and Compact Radio Sources*, ed. R. Fanti K. I. Kellermann & G. Setti, 289
- Schmidt, G. D. & Miller, J. S. 1980, *ApJ*, 240, 759
- Schmidt, M. 1963, *Nature*, 197, 1040
- Schmitt, H. R., Ulvestad, J. S., Antonucci, R. R. J., & Kinney, A. L. 2001, *ApJS*, 132, 199
- Schneider, D. P., Richards, G. T., Hall, P. B., Strauss, M. A., Anderson, S. F., Boroson, T. A., Ross, N. P., Shen, Y., Brandt, W. N., Fan, X., Inada, N., Jester, S., Knapp, G. R., Krawczyk, C. M., Thakar, A. R., Vanden Berk, D. E., Voges, W., Yanny, B., York, D. G., Bahcall, N. A., Bizyaev, D., Blanton, M. R., Brewington, H., Brinkmann, J., Eisenstein, D., Frieman, J. A., Fukugita, M., Gray, J., Gunn, J. E., Hibon, P., Ivezić, Ž., Kent, S. M., Kron, R. G., Lee, M. G., Lupton, R. H., Malanushenko, E., Malanushenko, V., Oravetz, D., Pan, K., Pier, J. R., Price, III, T. N., Saxe, D. H., Schlegel, D. J., Simmons, A., Snedden, S. A., SubbaRao, M. U., Szalay, A. S., & Weinberg, D. H. 2010, *AJ*, 139, 2360
- Seaquist, E. R., Garrison, R. F., Gregory, P. C., Taylor, A. R., & Crane, P. C. 1979, *AJ*, 84, 1037
- Seaquist, E. R., Gilmore, W. S., Johnston, K. J., & Grindlay, J. E. 1982, *ApJ*, 260, 220
- Seward, F., Grindlay, J., Seaquist, E., & Gilmore, W. 1980, *Nature*, 287, 806
- Seyffert, E. N., Cooksey, K. L., Simcoe, R. A., O'Meara, J. M., Kao, M. M., & Prochaska, J. X. 2013, *ApJ*, 779, 161
- Shakura, N. I. & Sunyaev, R. A. 1973, *A&A*, 24, 337
- Share, G. H., Murphy, R. J., Smith, D. M., Schwartz, R. A., & Lin, R. P. 2004, *ApJ*, 615, L169
- Siegert, T., Diehl, R., Greiner, J., Krause, M. G. H., Beloborodov, A. M., Bel, M. C., Guglielmetti, F., Rodriguez, J., Strong, A. W., & Zhang, X. 2016, *Nature*, 531, 341
- Simkin, S. M. 1977, *ApJ*, 217, 45
- . 1978, *ApJ*, 222, L55
- Slane, P., Gaensler, B. M., Dame, T. M., Hughes, J. P., Plucinsky, P. P., & Green, A. 1999, *ApJ*, 525, 357
- Slane, P., Hughes, J. P., Edgar, R. J., Plucinsky, P. P., Miyata, E., Tsunemi, H., & Aschenbach, B. 2001, *ApJ*, 548, 814
- Slingo, A. 1974, *MNRAS*, 168, 307
- Smartt, S. J., Clark, P., Smith, K. W., McBrien, O., Maguire, K., O'Neil, D., Fulton, M., Magee, M., Prentice, S., Colin, C., Tonry, J., Denneau, L., Stalder, B., Heinze, A., Weiland, H., Flewelling, H., & Rest, A. 2018, *The Astronomer's Telegram*, 11727
- Smith, N., Hinkle, K. H., & Ryde, N. 2009, *AJ*, 137, 3558
- Spangler, S. R. 1979, *ApJ*, 232, L7
- Sparks, W. B., Biretta, J. A., & Macchetto, F. 1994, *ApJS*, 90, 909
- Spencer, R., de La Force, C., & Stirling, A. 2001, in *IAU Symposium*, Vol. 205, *Galaxies and their Constituents at the Highest Angular Resolutions*, ed. R. T. Schilizzi, 264
- Staveley-Smith, L., Manchester, R. N., Gaensler, B. M., Kesteven, M. J., Tziournis, A. K., Bizunok, N. S., & Wheaton, V. C. in , *IAU Colloq. 192: Cosmic Explosions, On the 10th Anniversary of SN1993J*, ed. J.-M. Marcaide K. W. Weiler, 89
- Staveley-Smith, L., Manchester, R. N., Kesteven, M. J., Reynolds, J. E., Tziournis, A. K., Killeen, N. E. B., Jauncey, D. L., Campbell-Wilson, D., Crawford, D. F., & Turtle, A. J. 1992, *Nature*, 355, 147
- Staveley-Smith, L., Manchester, R. N., Kesteven, M. J., Tziournis, A. K., & Reynolds, J. E. R. 1993, *Proceedings of the Astronomical Society of Australia*, 10, 331
- Staveley-Smith, L., Potter, T. M., Zanzardo, G., Gaensler, B. M., & Ng, C.-Y. in , *IAU Symposium*, Vol. 296, *Supernova Environmental Impacts*, ed. A. Ray and R. A. McCray, 15–22

- Stewart, R. T., Caswell, J. L., Haynes, R. F., & Nelson, G. J. 1993, *MNRAS*, 261, 593
- Stockton, A. & MacKenty, J. W. 1987, *ApJ*, 316, 584
- Stroe, A., Shimwell, T., Rumsey, C., van Weeren, R., Kierdorf, M., Donnert, J., Jones, T. W., Röttgering, H. J. A., Hoeft, M., Rodríguez-Gonzálvez, C., Harwood, J. J., & Saunders, R. D. E. 2016, *MNRAS*, 455, 2402
- Subramanian, P., Becker, P. A., & Kafatos, M. 1996, *ApJ*, 469, 784
- Subramanian, P., Becker, P. A., & Kazanas, D. 1999, *ApJ*, 523, 203
- Sunyaev, R., Churazov, E., Gilfanov, M., Dyachkov, A., Khavenson, N., Grebenev, S., Kremnev, R., Sukhanov, K., Goldwurm, A., Ballet, J., Cordier, B., Paul, J., Denis, M., Vedrenne, G., Niel, M., & Jourdain, E. 1992, *ApJ*, 389, L75
- Sunyaev, R., Churazov, E., Gilfanov, M., Pavlinsky, M., Grebenev, S., Babalyan, G., Dekhanov, I., Khavenson, N., Bouchet, L., Mandrou, P., Roques, J. P., Vedrenne, G., Cordier, B., Goldwurm, A., Lebrun, F., & Paul, J. 1991, *ApJ*, 383, L49
- Taylor, G. B., Venturi, T., & Udomprasert, P. S. *Astronomical Society of the Pacific Conference Series*, Vol. 144, , IAU Colloq. 164: Radio Emission from Galactic and Extragalactic Compact Sources, ed. J. A. Zensus G. B. Taylor & J. M. Wrobel, 113
- Taylor, J. H., Backus, P. R., & Damashek, M. 1981, *ApJ*, 244, L65
- Tendulkar, S. P., Bassa, C. G., Cordes, J. M., Bower, G. C., Law, C. J., Chatterjee, S., Adams, E. A. K., Bogdanov, S., Burke-Spolaor, S., Butler, B. J., Demorest, P., Hessels, J. W. T., Kaspi, V. M., Lazio, T. J. W., Maddox, N., Marcote, B., McLaughlin, M. A., Paragi, Z., Ransom, S. M., Scholz, P., Seymour, A., Spitler, L. G., van Langevelde, H. J., & Wharton, R. S. 2017, *ApJ*, 834, L7
- Thomson, R. C., Mackay, C. D., & Wright, A. E. 1993, *Nature*, 365, 133
- Tinyanont, S., Kasliwal, M. M., Fox, O. D., Lau, R., Smith, N., Williams, R., Jencson, J., Perley, D., Dykhoff, D., Gehrz, R., Johansson, J., Van Dyk, S. D., Masci, F., Cody, A. M., & Prince, T. 2016, *ApJ*, 833, 231
- Tripp, T. M., Jenkins, E. B., Williger, G. M., Heap, S. R., Bowers, C. W., Danks, A. C., Davé, R., Green, R. F., Gull, T. R., Joseph, C. L., Kaiser, M. E., Lindler, D., Weymann, R. J., & Woodgate, B. E. 2002, *ApJ*, 575, 697
- Tristram, K. R. W., Burtscher, L., Jaffe, W., Meisenheimer, K., Hönig, S. F., Kishimoto, M., Schartmann, M., & Weigelt, G. 2014, *A&A*, 563, A82
- Troja, E., van Eerten, H., Ryan, G., Ricci, R., Burgess, J. M., Wieringa, M., Piro, L., Cenko, S. B., & Sakamoto, T. 2018, *ArXiv e-prints*
- Trushkin, S. A., Nizhelskij, N. A., & Tsybulev, P. G. 2014, *The Astronomer's Telegram*, 6492
- Trushkin, S. A., Nizhelskij, N. A., Tsybulev, P. G., & Zhekanis, G. V. 2016a, *The Astronomer's Telegram*, 9481
- . 2016b, *The Astronomer's Telegram*, 9444
- . 2016c, *The Astronomer's Telegram*, 9501
- Trushkin, S. A., Nizhelskij, N. A., Tsybulev, P. G., & Zhekanis, G. V. *Stars: From Collapse to Collapse*, ed. , Y. Y. Balega D. O. Kudryavtsev I. I. Romanyuk & I. A. Yakunin, 492
- . 2017b, *The Astronomer's Telegram*, 10126
- Tuffs, R. J., Chini, R., & Kreysa, E. 1989, in *ESA Special Publication*, Vol. 290, *Infrared Spectroscopy in Astronomy*, ed. E. Böhm-Vitense
- Turner, T. J. & Pounds, K. A. 1989, *MNRAS*, 240, 833
- Turtle, A. J., Campbell-Wilson, D., Bunton, J. D., Jauncey, D. L., Kesteven, M. J., Manchester, R. N., Norris, R. P., Storey, M. C., & Reynolds, J. E. 1987, *Nature*, 327, 38
- Tyson, J. A., Crane, P., & Saslaw, W. C. 1977, *A&A*, 59, L15
- Ulrich, M.-H. 1973, *ApJ*, 181, 51
- Ulrich, M. H., Boksenberg, A., Bromage, G. E., Clavel, J., Elvius, A., Penston, M. V., Perola, G. C., Pettini, M., Snijders, M. A. J., Tanzi, E. G., & Tarengi, M. 1984, *MNRAS*, 206, 221
- Ulvstad, J. S., Wilson, A. S., & Sramek, R. A. 1981, *ApJ*, 247, 419
- Unger, S. W., Pedlar, A., Axon, D. J., Whittle, M., Meurs, E. J. A., & Ward, M. J. 1987, *MNRAS*, 228, 671
- Urry, C. M. & Padovani, P. 1995, *PASP*, 107, 803

- van Breugel, W., Miley, G., Heckman, T., Butcher, H., & Bridle, A. 1985, *ApJ*, 290, 496
- van der Kruit, P. C. 1973, *A&A*, 29, 263
- van Driel, W., Yoshida, S., Nakada, Y., Aoki, T., Soyano, T., Tarusawa, K., Ichikawa, T., Kakehashi, T., Nomoto, K., & Wakamatsu, K. 1993, *PASJ*, 45, L59
- van Gorkom, J., Rupen, M., Knapp, G., Gunn, J., Neugebauer, G., & Matthews, K. 1986, *IAU Circ.*, 4248
- van Weeren, R. J., Bonafede, A., Ebeling, H., Edge, A. C., Brüggen, M., Giovannini, G., Hoeft, M., & Röttgering, H. J. A. 2012a, *MNRAS*, 425, L36
- van Weeren, R. J., de Gasperin, F., Akamatsu, H., Brüggen, M., Feretti, L., Kang, H., Stroe, A., & Zandanel, F. 2019, *arXiv e-prints*, [arXiv:1901.04496](https://arxiv.org/abs/1901.04496)
- van Weeren, R. J., Röttgering, H. J. A., Intema, H. T., Rudnick, L., Brüggen, M., Hoeft, M., & Oonk, J. B. R. 2012b, *A&A*, 546, A124
- Vink, J. & Laming, J. M. 2003, *ApJ*, 584, 758
- Walker, R. C., Hardee, P. E., Davies, F. B., Ly, C., & Junor, W. 2018, *ApJ*, 855, 128
- Waltman, E. B., Fiedler, R. L., Johnston, K. J., & Ghigo, F. D. 1994, *AJ*, 108, 179
- Wampler, E. J. & Richichi, A. 1989, *A&A*, 217, 31
- Wampler, E. J., Wang, L., Baade, D., Banse, K., D’Odorico, S., Gouiffes, C., & Tarengi, M. 1990, *ApJ*, 362, L13
- Wandel, A., Peterson, B. M., & Malkan, M. A. 1999, *ApJ*, 526, 579
- Wang, J., Fabbiano, G., Risaliti, G., Elvis, M., Mundell, C. G., Dumas, G., Schinnerer, E., & Zezas, A. 2010, *ApJ*, 719, L208
- Wardle, J. F. C. & Aaron, S. E. 1997, *MNRAS*, 286, 425
- Watson, M. G., Willingale, R., Grindlay, J. E., & Seward, F. D. 1983, *ApJ*, 273, 688
- Webber, W. R. 2015, *ArXiv e-prints* 1508.01542, <https://arxiv.org/abs/1508.01542>
- Weiler, K. W., Panagia, N., Montes, M. J., & Sramek, R. A. 2002, *ARA&A*, 40, 387
- Weiler, K. W., Panagia, N., & Sramek, R. A. 1990, *ApJ*, 364, 611
- Weiler, K. W., Williams, C. L., Panagia, N., Stockdale, C. J., Kelley, M. T., Sramek, R. A., Van Dyk, S. D., & Marcaide, J. M. 2007, *ApJ*, 671, 1959
- Werner, N., Simionescu, A., Million, E. T., Allen, S. W., Nulsen, P. E. J., von der Linden, A., Hansen, S. M., Böhringer, H., Churazov, E., Fabian, A. C., Forman, W. R., Jones, C., Sanders, J. S., & Taylor, G. B. 2010, *MNRAS*, 407, 2063
- Whittle, M., Haniff, C. A., Ward, M. J., Meurs, E. J. A., Pedlar, A., Unger, S. W., Axon, D. J., & Harrison, B. A. 1986, *MNRAS*, 222, 189
- Wilson, A. S. & Willis, A. G. 1980, *ApJ*, 240, 429
- Wolter, A. & Trinchieri, G. 2004, *A&A*, 426, 787
- Woo, J.-H. & Urry, C. M. 2002, *ApJ*, 579, 530
- Wright, M., Dickel, J., Koralesky, B., & Rudnick, L. 1999, *ApJ*, 518, 284
- Young, A., Rudnick, L., Katz-Stone, D. M., & Giovannini, G. 2000, in *Bulletin of the American Astronomical Society*, Vol. 32, American Astronomical Society Meeting Abstracts, 1523
- Young, A. J., Wilson, A. S., & Shopbell, P. L. 2001, *ApJ*, 556, 6
- Zanardo, G., Staveley-Smith, L., Ball, L., Gaensler, B. M., Kesteven, M. J., Manchester, R. N., Ng, C.-Y., Tzioumis, A. K., & Potter, T. M. 2010, *ApJ*, 710, 1515